7-7-2020

Vibration Control of Bridge Stay Cables Using Negative Stiffness Dampers

Majd Javanbakht
University of Windsor

Vibration Control of Bridge Stay Cables Using Negative Stiffness Dampers

By

Majd Javanbakht

A Dissertation
Submitted to the Faculty of Graduate Studies
through the Department of Civil and Environmental Engineering
in Partial Fulfillment of the Requirements for
the Degree of Doctor of Philosophy
at the University of Windsor

Windsor, Ontario, Canada

2020

Vibration Control of Bridge Stay Cables Using Negative Stiffness Dampers

By

Majd Javanbakht

APPROVED BY:

Y. Fujino, External Examiner
Josai University

B. Minaker
Department of Mechanical, Automotive & Materials Engineering

N. Van Engelen
Department of Civil and Environmental Engineering

S. Bhattacharjee
Department of Civil and Environmental Engineering

S. Cheng, Advisor
Department of Civil and Environmental Engineering

F. Ghrib, Co-Advisor
Department of Civil and Environmental Engineering

May 14, 2020

Declaration of Co-authorship/Previous Publication

I. Co-Authorship

I hereby declare that this dissertation incorporates material that is result of joint research undertaken with my advisors, Dr. Shaohong Cheng and Dr. Faouzi Ghrib of the University of Windsor. In all cases, the key ideas, primary contributions, experimental designs, data analysis, interpretation, and writing were performed by the author, and the contribution of co-authors was primarily through the provision of the study and suggesting possible directions. Results related to this research are reported in Chapters 3 through 8, inclusive.

I am aware of the University of Windsor Senate Policy on Authorship and I certify that I have properly acknowledged the contribution of other researchers to my dissertation, and have obtained written permission from each of the co-author(s) to include the above material(s) in my dissertation.

I certify that, with the above qualification, this dissertation, and the research to which it refers, is the product of my own work.

II. Previous Publication

This dissertation includes 5 original papers that have been previously published/submitted for publication in peer reviewed journals, as follows:

Dissertation Chapter	Full Citation	Publication Status
Chapters 3 and 6	Javanbakht M., Cheng S., Ghrib F. (2018), "Refined design formulas for a cable equipped with positive or negative stiffness dampers", *Structural Control and Health Monitoring*, 25(10), e2236. DOI:10.1002/stc.2236.	Published
Chapter 4	Javanbakht M., Cheng S., Ghrib F. (2019), "Control-oriented model for the dynamic response of a damped cable", *Journal of Sound and Vibration*, 442, 249-267. DOI: 10.1016/j.jsv.2018.10.036.	Published
Chapter 3	Javanbakht M., Cheng S., Ghrib F. (2017), "Design of negative stiffness dampers for bridge stay cable vibration control", *International Symposium on the Dynamics and Aerodynamics of Cables ISDAC2017*, October 30-31, Porto, Portugal.	Published
Chapter 6	Javanbakht M., Cheng S., Ghrib F. (2020), "Impact of support stiffness on the performance of negative stiffness dampers". *Structural Control and Health Monitoring*.	Under revision
Chapters 5 and 7	Javanbakht M., Cheng S., Ghrib F. (2020), "Multimode vibration control of stay cables using optimized negative stiffness damper". *Structural Control and Health Monitoring,* 27(4). DOI: 10.1002/stc.2503.	Published

I certify that I have obtained a written permission from the copyright owner(s) to include the above published material(s) in my thesis. I certify that the above material describes work completed during my registration as a graduate student at the University of Windsor.

III. General

I declare that, to the best of my knowledge, my dissertation does not infringe upon anyone's copyright nor violate any proprietary rights and that any ideas, techniques, quotations, or any other material from the work of other people included in my dissertation,

published or otherwise, are fully acknowledged in accordance with the standard referencing practices. Furthermore, to the extent that I have included copyrighted material that surpasses the bounds of fair dealing within the meaning of the Canada Copyright Act, I certify that I have obtained a written permission from the copyright owner(s) to include such material(s) in my dissertation.

I declare that this is a true copy of my dissertation, including any final revisions, as approved by my dissertation committee and the Graduate Studies office, and that this dissertation has not been submitted for a higher degree to any other University or Institution.

Abstract

Stay cables are one of the main structural elements in a cable-stayed bridge. Due to their high lateral flexibility and low inherent damping, cables are susceptible to large-amplitude vibrations that can adversely affect bridge safety and serviceability. As a practical measure, passive viscous dampers are installed transversely near the cable-deck anchorage. However, such devices can only provide a limited amount of damping. In recent years, the need for an effective yet simple control technique has led to the development of high-performance passive negative stiffness dampers (NSD). The present dissertation aims to study the behaviour of NSDs, enable their design for mitigating excessive bridge stay cable vibrations and evaluate their control effectiveness in comparison with other alternative schemes. To investigate the behaviour of NSDs, an analytical study has been conducted to obtain the in-plane free-vibration response of a shallow-flexural damped cable. The effect of damper stiffness was modeled as a linear spring aligned in parallel with a linear viscous dashpot. As a refinement to the existing damper design formulas, a unified design equation has been developed for the idealized fixed-fixed and hinged-hinged cable boundary conditions. The design procedure is based on an asymptotic solution to the modal damping ratio of the cable-damper system. The mode superposition method (MSM) has been adopted to numerically simulate the dynamic response of a controlled shallow-flexural cable subjected to arbitrary dynamic excitations. The numerical efficiency of the MSM was improved by including the cable static displacement caused by an arbitrary point load at the damper location as a correction term in the shape function vector and modifying the conventional sinusoidal shape functions to satisfy the boundary conditions. Results showed that the refined design formula yielded a slightly conservative estimation and therefore safe

damper design. Also, the enhanced MSM-based numerical framework was found to substantially reduce the computational cost for designing cable vibration control schemes. Using the aforementioned analytical and numerical tools, the control performance of a NSD has been evaluated. The superior control effectiveness of a NSD compared to the positive- and zero-stiffness dampers was justified by employing the force generation mechanism of a viscous damper with linear stiffness. Theoretical and practical limits of the negative damper stiffness have been identified to ensure the stability of NSD and avoid unsafe design. An innovative NSD design procedure for mitigating both the single-mode and the multi-mode stay cable vibrations has been proposed. Analytical design relationships have been developed to determine NSD parameters for achieving the desired damping ratio in target mode(s). The impact of damper support flexibility on the NSD control performance has been studied to determine the optimum combination of NSD parameters and damper support stiffness. Results showed that the performance of a NSD designed/optimized based on the proposed methods was comparable to that of an optimal active controller. Furthermore, it has been found that optimizing NSD for a flexible damper support would result in a cost-efficient NSD design and inhibit additional NSD-induced cable displacement. The outcomes yielded from this dissertation extend the current knowledge associated with the dynamic behaviour of NSD-equipped bridge stay cables. The developed analytical/numerical tools and optimization methods contribute to the bridge industry by enabling accurate, efficient and reliable design of cable-NSD systems either in the preliminary design stage or during the rehabilitation process of cable-stayed bridges. The findings of this study will assist infrastructure management and improve the global economy by extending the life-span of cable-stayed bridges.

To my wonderful parents, Khalil and Fatemeh

and beloved wife, Negar

Acknowledgements

I would like to express my deepest gratitude to my research advisors, Dr. Shaohong Cheng and Dr. Faouzi Ghrib, for their continuous patience, enlightening guidance, and kind support during my Ph.D. program. This research would not have been possible without their insightful supervision and instructive contribution.

I would like to thank my doctoral committee members, Dr. Minaker, Dr. Van Engelen, and Dr. Bhattacharjee, for their guidance. I must thank Professor Fujino for his valuable suggestions and comments as the external reviewer of this dissertation.

I wish to thank my friends Ashkan and Sima who have been supporting me since the very first day I arrived at Windsor. I am deeply grateful to my older brother and mentor, Pirooz, for his valuable support, friendship and encouragement. I would like to express my appreciation to my incredible parents for inspiring me to become my possible best and always believing in me.

Finally, I would like to thank my lovely wife, Negar, for her endless help, tireless support, and exceptional patience. Without her unconditional love, this journey would not have come true.

Table of Contents

List of Tables

List of Figures

Chapter 1 Introduction

1.1. Background

The original idea of cable-stayed bridges coincided with the development of suspended bridges in Europe in the early 19th century. However, the concept was abandoned for a long time after the collapse of the first built examples in England and Germany due to a lack of proper understanding of their structural behaviour [1]. Prior to the emergence of modern cable-stayed bridges in the 20th century, several hybrid bridges were built using stay cables as stiffening elements in suspension bridges. An outstanding example of this type is the Brooklyn Bridge in New York, designed by J. A. Roebling in 1869 and opened in 1883 [2]. The era of modern cable-stayed bridges began after the World War II in the early 1950s with the construction of the Strömsund Bridge in Sweden (1956) and the Düsseldorf triple bridge family in Germany (1957, 1969 and 1976) [3]. The economic efficiency, aesthetic aspect, ease of construction, and adaptability to poor soil conditions have greatly contributed to the worldwide popularity of cable-stayed bridges [4]. Consequently, the feasible span of cable-stayed bridges has increased rapidly in the recent decade due to the advances in materials and construction methods. Examples of super-long cable-stayed bridges include the Russky bridge (Russia-2012) with a record span of 1104 m, the Sutong Bridge (China-2008) with a span of 1088 m, and the Stonecutters Bridge (China-2009) with a span of 1018 m [5].

Stay cables are one of the main load-carrying structural elements in a cable-stayed bridge. The length of the cables depends directly on the free span of the bridge, and as it increases, the lateral flexibility of the cables would also increase. Moreover, in order to maintain the static equilibrium of the cables, large tension is applied during installation, which significantly reduces their intrinsic damping ratio [6]. According to the field measurements, the majority of stay cables have an intrinsic damping ratio less than 0.3% [7]. Hence, due to their low inherent damping and high lateral flexibility, stay cables are prone to large-amplitude vibrations when subjected to dynamic excitation such as environmental and traffic loads [8]. This problem has been well documented and addressed in recent decades. One of the earliest reports was the high-amplitude cable vibrations at the Brotonne Bridge (France) in 1977 [9]. With the rapid growth of cable-stayed bridges in the 1980s, numerous cable vibration incidences were reported particularly with the presence of wind, rain, snow, ice and a combination thereof [10]; these include the 2 m peak-to-peak vibrations on the Tempozan Bridge (Japan) [11], 1 m peak-to-peak vibrations on the Fred Hartman Bridge (United States) [12], an estimated 2.5 m peak-to-peak vibrations on the Dubrovnik Bridge (Croatia) [13], and 0.7 m peak-to-peak vibrations on the Dongting Lake Bridge (China) [14]. Regardless of the origin of the vibration mechanisms (i.e. rain-wind-induced vibration (RWIV), buffeting, galloping, vortex-induced vibration, parametric excitation, etc.), recurring large-amplitude cable oscillations would accelerate fatigue and can seriously damage the cable protection system, the cable-deck and cable-pylon anchorages, and the control devices attached to the cable [13] and thus adversely affects the life-span of both the stay cables and the bridge itself [15]. Besides, excessive vibration also has a negative impact on the public's confidence on bridge safety. Therefore, preventing the occurrence

of severe cable vibrations and controlling their amplitude to allowable limits are of great importance during the construction and operation of cable-stayed bridges.

Extensive studies on various mechanisms associated with cable vibration have assisted engineers to find effective solutions to mitigate excessive vibrations. Practical approaches for controlling cable vibrations include aerodynamic and mechanical measures [16]. In the former, the common practice is to modify the aerodynamic properties of the cables by applying modifications to the surface of cable protective sheath in the form of helical fillets [17], longitudinal ribs [18] and patterned dimples [19]. These modifications are mainly designed to prevent the formation of longitudinal water rivulets on the cable surface, which is believed to be responsible for rain-wind-induced vibration of stay cables [20]. One of the major limitations of this approach is its inability to effectively control cable vibrations due to mechanisms other than rain-wind-induced vibration. Also, surface modification is difficult to implement on existing stay cables on site and helical fillets have been reported to increase the drag on longer cables [9]. Nevertheless, cable surface treatment has become a standard component in the cable manufacturing industry during the past decades [21]. Mechanical type vibration controlling methods, on the other hand, tend to improve the dynamic behaviour of a stay cable by modifying its stiffness and/or damping properties. To improve the in-plane stiffness of a stay cable, transverse cross-tie(s) can be used to connect adjacent cables. Cross-ties can effectively suppress cable vibrations due to different mechanisms by increasing the in-plane frequency of interconnected cables [22] and redistributing the kinetic energy in the system [23], increasing modal mass of the cables [10], enhancing cable damping [24], and reducing sag variation among the connected cables [2]. The main drawbacks of applying cable networks include the generation of a

large number of closely spaced local modes, the inability to control out-of-plane vibrations, and the impact of cross-ties on bridge aesthetics [25]. Cross-ties have been successfully applied to a number of cable-stayed bridges [1,26–28] and research is ongoing to further develop this method [29–35].

As an alternative effective mechanical measure, the low structural damping of stay cables can be increased by providing additional energy-dissipating devices. Passive dampers have been extensively installed on stay cables both externally or internally [21]. In the external configuration, transverse viscous dampers [36–39] can be mounted near the cable-deck anchorage, usually at 2 to 5% of the cable length to the anchorage, and tuned mass dampers [40] can be installed along the cable. In the internal configuration, friction dampers [41] and high damping rubber (HDR) dampers [42] can be placed inside the cable-deck anchorage block. It has been shown through analytical studies that the performance of transverse viscous dampers is compromised when the effects of cable sag [43], cable bending stiffness [44], damper support stiffness [45,46] and positive damper stiffness [39,47] are not negligible. In addition, these dampers may become inadequate in the case of longer stay cables where the damper installation location is relatively closer to the cable end. Moreover, viscous dampers may not be able to suppress multi-mode cable vibrations since they are often optimized to control a specific mode [48]. Field observations indicate that cable vibrations are often dominated by multiple modes, especially in the case of RWIV [10,38,49]. On the other hand, the dominant modes of a cable vibration incident depend on the excitation source and are subjected to change. Hence, optimizing the performance of a passive viscous damper for a specific single-mode may result in suboptimal damper performance for other cable modes. In such cases, more efficient

control tools such as active [50–52] and semi-active [53,54] devices need to be used. An important feature of these control methods is their adaptability to unforeseen loading conditions. As a widely used semi-active control device, magneto-rheological (MR) dampers have been installed on a number of cable-stayed bridges [55,56].

The application of active control schemes has been limited by their high demand on a power source and stability concerns. On the other hand, semi-active dampers require real-time measurement of cable response as well as pre-designed controllers and computer-based calculations to generate the control action [57]. Although these tools typically require less power and are inherently stable, their design and implementation are more challenging and costly than the conventional passive dampers. Therefore, the development of a passive system capable of achieving control effectiveness at the level of active/semi-active control schemes has been of interest to researchers in recent decades. The crucial need of more efficient, robust and cost-effective passive control techniques has led to the recent development of negative stiffness dampers (NSD). The idea of NSD emerged when the negative-stiffness behaviour in the force-deformation response of optimally-controlled active dampers was found to improve their control performance [58]. As a result, it was attempted to artificially introduce the negative stiffness mechanism in control systems designed for seismically-excited buildings [59], cable-stayed bridges [60], and stay cables [61,62]. In parallel, the efficiency of several NSD specimens has been experimentally studied in stay cable vibration control [63–65]. Recent experimental [66] and numerical [67] studies have shown that NSD provide a significantly improved control performance compared to conventional viscous dampers and mitigates cable vibration comparable to optimal active controllers [68].

1.2. Motivation

Application of passive discrete dampers has been a classical solution for mitigating stay cable vibrations since its first implementation on the Brotonne Bridge (France) [69]. External transverse dampers are typically placed near the lower cable anchorage at a distance of about 2% of the cable length. Design tools are available for selecting optimum viscous dampers to control cable vibrations under a specific mode [39,43,44,70–72]. However, the existing approaches do not consider the effects of damper stiffness, damper support stiffness, cable sag, and cable bending stiffness in the analytical formulation. Due to the possible interaction of these factors to influence the damper performance, a comprehensive analytical model is needed to take into account all the above factors. In addition, the effect of damper stiffness can be explicitly investigated to address the design of three categories of dampers, namely the positive stiffness damper (PSD), the zero-stiffness damper (ZSD), and the negative stiffness damper (NSD). Access to such a model is particularly essential for a better understanding of the dynamic behaviour of the cable-NSD system and the development of design and optimization tools for NSDs.

In addition to analytical solutions, numerical methods such as the finite difference method (FDM) [73] and the mode superposition method (MSM) [69,74] have been adopted to study the dynamic behaviour of undamped and damped stay cables. In these methods, the governing equation of a cable motion is solved numerically and the control performance is evaluated by calculating the modal damping ratio of the damped cable. Application of MSM has led to the presentation of a widely used universal curve for designing viscous dampers [69]. In order to design semi-active control systems, the MSM has been improved by adding the static correction to enhance its accuracy and computational efficiency [57].

However, the existing numerical models do not consider the effects of cable stiffness and cable sag, though both effects would have impact on the dynamic behaviour of a damped cable. On the other hand, assumptions have been made to obtain asymptotic design relationships which yield a more conservative damper design. It is necessary to evaluate the error associated to these assumptions and specify the permissible range of design parameters that ensure a safe design.

As an efficient tool to control the wind-induced cable vibrations, NSD has received much attention in recent years. Experimental [64–66], analytical [61], and numerical [67,68] studies have been performed to investigate its dynamic behaviour. In these studies, a simplified cable model (i.e. taut cable), along with a rigid damper support, was considered. Two issues were reported for the NSD-equipped cables including the instability of the cable-damper system for large amounts of negative stiffness in the NSD [61] and the increased cable displacement around the damper installation location [67]. To address the first issue, an allowable limit for the negative stiffness of NSD was proposed to ensure system stability [67]. In order to portray a more accurate picture of the NSD functionality and stability, the effects of cable sag and cable bending stiffness must be included in the model. Besides, a few studies have shown that damper support stiffness may also have a considerable influence on the performance of a viscous damper [45–47,71]. Since dampers are likely to be supported by a flexible structure, neglecting the damper support stiffness may result in inaccurate NSD design. The aforementioned issues regarding the NSD design can be addressed by developing comprehensive models that incorporate the effects of cable sag, cable bending stiffness, damper stiffness, and damper support stiffness. This will allow for accurate NSD design and facilitates its practical application on cable-stayed bridges.

On-site records have shown that wind-induced cable vibrations may be governed by more than one mode. Also, even in the case a single-mode dominates, the excitation source would dictate which mode is to be considered. The majority of the existing methods for designing passive dampers target at a specific mode of cable vibration. Due to the passive nature of this type of damper, such methods would result in a suboptimal damper performance in the case of multi-mode cable vibration and unforeseen wind loads. A number of studies investigated the problem of optimizing passive [48,75], nonlinear [76], and semi-active [77] dampers for multi-mode cable vibration control. However, in these studies, the damper is not designed to achieve a specific damping ratio in the target modes and the effects of cable sag, cable bending stiffness, and damper support stiffness are not considered. Cost-efficient passive systems are generally preferable for semi-active control schemes because of their simplicity. The design of passive systems does not need real-time measurements. Recently, NSD has emerged as a good candidate for controlling multi-mode cable vibrations due to its remarkable damping capacity. However, existing NSD design tools only address single-mode cable vibration control and it is of the utmost importance to study the potential application of NSD in mitigating multi-mode cable vibrations and extend the current design/optimization approaches for NSD.

1.3 Objectives

This research aims at proposing new approaches for controlling harmful cable vibrations by means of efficient passive dampers such as NSD by improving the existing analytical and numerical dynamic models of a damped cable. The objectives of the current study are as follows:

1. Develop a comprehensive analytical model for the dynamic response of a damped stay cable by including the effects of cable sag, cable bending stiffness, damper stiffness, and damper support stiffness and considering different cable boundary conditions. (Chapter 3, Section 3.2)
2. Obtain asymptotic solutions for the modal damping ratio of a damped cable based on the comprehensive analytical model (Step 1) and propose a damper design tool applicable to NSD, PSD and ZSD. Provide easy-to-use design curves to facilitate the design process of a passive damper. (Chapter 3, Section 3.3)
3. Establish a numerical model for the dynamic response of a damped stay cable based on the mode superposition method and improve the accuracy and computational efficiency of this model by applying a static correction technique. (Chapter 4)
4. Study the action mechanism and stability requirements of NSD and propose design formulas for optimizing NSD to control single-mode cable vibrations. Provide a more accurate stability criterion for NSD design. (Chapter 5)
5. Investigate the effect of damper support stiffness on the dynamic behaviour and controlling performance of NSD. In case the flexible support is beneficial, optimize the damper support stiffness. (Chapter 6)
6. Formulate NSD design equations to achieve target damping ratio in two or more dominant modes under multi-mode cable vibration. Conduct numerical studies to verify the applicability of the proposed design equations to full-size stay cables under wind excitation. (Chapter 7)

Chapter 2 Literature Review

2.1. Introduction

In this chapter, reference studies and recent findings in the field of vibration control of bridge stay cables are reviewed. The classical linear theory of cable dynamics is first described. Then, existing analytical and numerical methods for the dynamic analysis of a damped cable are explained and conventional passive approaches for controlling stay cable vibrations are presented. Next, the literature that has focused on the characteristics of high-performance passive negative stiffness dampers (NSD) as well as their application in cable vibration control is surveyed. In addition, studies that have investigated the role of damper support stiffness on control performance are discussed. Finally, current passive and semi-active approaches for mitigating multi-mode cable vibrations are discussed. The purpose of this chapter is to portray existing solutions for stay cable vibration control and identify the urgent problems that require further attention.

2.2. Linear theory of cable dynamics

2.2.1. Undamped cables

The linear theory of free vibrations of a suspended undamped cable was developed by Irvine and Caughey [78]. Figure 2-1 shows the mechanical model of a horizontally suspended uniform cable with a unit mass per length of m, a length of L, and an axial stiffness of EA. The horizontal component of the cable tension is denoted by H. The x-axis is taken along the cable chord direction and the y-axis is in the vertical in-plane direction.

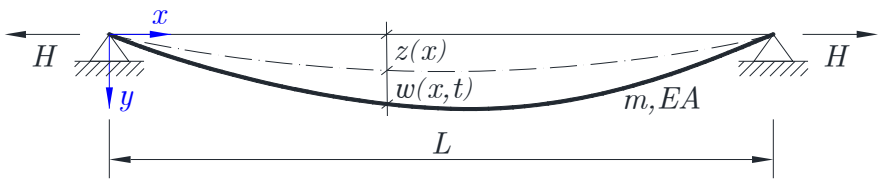

Fig. 2-1. Dynamic response of a suspended undamped cable (after Irvine and Caughey [78]).

In this figure, $z(x)$ and $w(x,t)$ represent the static displacement of the cable under its own weight and the dynamic in-plane displacement of the cable, respectively. If the cable sag is less than one-eighth of the span, i.e. $d = z(0.5L) \leq L/8$, the static profile of the cable can be approximated as parabolic and described as:

$$z(x) = \frac{mgL^2}{2H}\left[\frac{x}{L} - \left(\frac{x}{L}\right)^2\right] \tag{2-1}$$

Accordingly, the in-plane motion of the cable free vibration can be described by a 2nd order partial differential equation expressed as:

$$m\frac{\partial^2 w}{\partial t^2} - H\frac{\partial^2 w}{\partial x^2} - h\frac{dz^2}{dx^2} = 0 \tag{2-2}$$

where $h(t)$ is the horizontal component of the additional cable tension due to cable motion and is only a function of time. It should be noted that the effects of cable bending stiffness and cable inherent damping have been ignored in Eq. (2-2). A linearized equation is obtained for $h(t)$ based on the geometric and elastic compatibility of an infinitesimal cable element subjected to external and internal loads [79]. It can be expressed as:

$$h(t) = \frac{mgEA}{HL_e}\int_0^L w(x,t)dx \tag{2-3}$$

where $L_e = \int_0^L [1 + (dz/dx)^2]^{3/2} \approx L[1 + 8(d/L)^2]$ is the effective cable length and $d = mgL^2/(8H)$ is the cable sag. For antisymmetric in-plane modes of vibration, the integral term on the right-hand side of Eq. (2-3) is equal to zero and hence, $h(t) = 0$.

In this case, the natural frequencies are given by:

$$\omega_n = \frac{2n\pi}{L}\sqrt{H/m} \quad (n = 1,2,3, \dots) \tag{2-4}$$

The symmetric in-plane modes are affected by the cable sag and their corresponding natural frequencies are governed by the following transcendental equation:

$$\tan\left(\tfrac{1}{2}\beta_n L\right) = \left(\tfrac{1}{2}\beta_n L\right) - (4/\lambda^2)\left(\tfrac{1}{2}\beta_n L\right)^3 \quad (n = 1,2,3, \dots) \tag{2-5}$$

where $\beta_n = \omega_n\sqrt{m/H}$ and $\lambda^2 = (8d/L)^2\, L/[HL_e/(EA)]$ is the Irvine's sag-extensibility parameter. Equation (2-5) can be solved numerically to determine the modal frequencies of in-plane symmetric modes of a flat-sag suspended cable. Figure 2-2 illustrates the relation between the first four natural frequencies of a flat-sag suspended cable and the sag-extensibility parameter λ^2 provided by Irvine [79]. As shown in the figure, for $\lambda^2 > 4\pi^2$, the frequency of the first mode is greater than that of the second mode. This will cause the first symmetric modal component to have two internal nodes (i.e. locations with zero displacements) along the span. Also, for $4\pi^2 < \lambda^2 < 16\pi^2$, both the first and the second symmetric modes have two internal nodes. This phenomenon is known as the modal cross-over. The above equations have been extensively used in the studies of cable dynamics and the parameter λ^2 has been identified as a key factor in explaining the behaviour of cables. However, the main limitation of Irvine's solution is that the effect of cable flexural stiffness is excluded in the formulation.

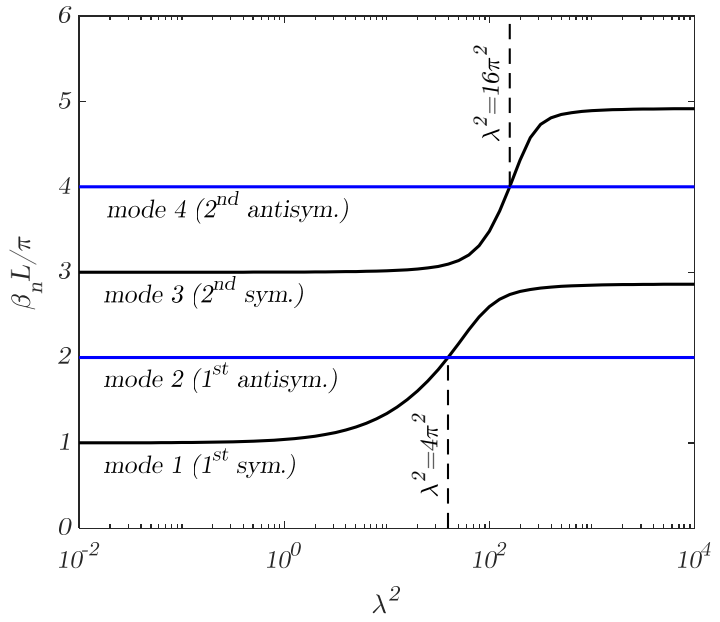

Fig. 2-2. Variation of the first four modal frequencies of a flat-sag suspended cable with Irvine's sag-extensibility parameter (modal cross-over phenomenon) (after Irvine [79]).

Shimada [80] proposed a method for estimating the tension of an undamped cable from ambient vibrations by using an exact solution of the cable motion. By considering the effects of cable flexural rigidity, cable sag, and inclination of the cable, the equation of motion can be expressed as:

$$m\frac{\partial^2 w}{\partial t^2} + EI\frac{\partial^4 w}{\partial x^4} - H\frac{\partial^2 w}{\partial x^2} - h\frac{dz^2}{dx^2} = 0 \tag{2-6}$$

where EI is the flexural rigidity of the cable. The exact solution of Eq. (2-6) results in the following characteristic equation for the cable tension:

$$\Phi\frac{L_e H}{EA} - \left(\frac{8d}{L}\right)^2 \frac{1}{(m_2 L)^2}(Q + R + L\Phi) = 0 \tag{2-7}$$

where Φ, Q, R and m_2 are functions of the cable properties, i.e. mass, length, tension, and axial and flexural rigidity; $d = mgL^2\cos\theta/(8H)$ is the sag of an inclined cable; and θ is

the inclination angle. The frequency of higher modes of cable vibration is obtained by applying microtremor measurement methods to estimate the ambient cable vibrations on-site. Then the cable tension is calculated by solving Eq. (2-7) using iterative numerical methods. In order to facilitate these calculations, approximate relationships have been proposed by Zui et al. [81] for calculating the cable tension based on the frequency of the first, second, or higher modes.

Mehrabi and Tabatabai [73] developed a finite difference (FD) formulation for evaluating the dynamic response of a damped cable by taking both the cable sag and cable bending stiffness effects into consideration. For a discretized cable with n internal nodes, the free vibration response of node i is assumed to take the form of $w_i(t) = u_i e^{pt}$. By substituting w_i into Eq. (2-6), the eigenvalue problem that governs the discretized cable can be expressed in a matrix form as:

$$(p^2\boldsymbol{M} + p\boldsymbol{C} + \boldsymbol{K})\{u\} = \{0\} \tag{2-8}$$

where $p = -\xi\omega_n \pm i\omega_n\sqrt{1-\xi^2}$ is the complex eigenvalue pair and $\{u\}_{n\times 1}$ is the corresponding eigenvector. By assuming a parabolic self-weight profile and utilizing the central finite difference formulation, the stiffness matrix $\boldsymbol{K}$ becomes:

$$\boldsymbol{K} = \begin{bmatrix} \tilde{Q} & U & W & & & 0 \\ & S & U & W & & \\ & & S & U & & \\ & & & S & \cdots & \\ & \text{sym} & & \vdots & \ddots & \\ & & & & & \tilde{Q} \end{bmatrix}_{n\times n} + \frac{\lambda^2 H l^2}{L^3}\boldsymbol{J} \tag{2-9}$$

where $\tilde{Q} = 7EI/l^3 + 2H/l$ for the fixed-fixed cable and $\tilde{Q} = 5EI/l^3 + 2H/l$ for the hinged-hinged cable; $U = -4EI/l^3 - H/l$; $W = EI/l^3$; $S = 6EI/l^3 + 2H/l$; $l = L/(n+$

1) and $\boldsymbol{J} = [1]_{n\times n}$ is the all-ones matrix. The mass and damping matrices are defined as $\boldsymbol{M} = (m_i l)\boldsymbol{I}_n$ and $\boldsymbol{C} = (c_i l)\boldsymbol{I}_n$, respectively, where m_i is the nodal mass, c_i is the nodal damping and $\boldsymbol{I}_n$ is the identity matrix. Equation (2-8) can be solved numerically to estimate the modal frequencies of a cable using the provided FD matrices. Both the accuracy and the computational cost of the FD model are closely related to the spatial and temporal discretization. A more efficient numerical approach for analyzing dynamic response of cable systems is to apply the mode superposition technique, which will be reviewed in the next section.

2.2.2. Damped cables

As mentioned in Chapter 1, a practical measure to suppress harmful cable vibrations is to attach a transverse passive viscous damper near the cable end. To better understand the behaviour of a cable-damper system, Carne [82] studied the dynamic behaviour of a damped guy cable and proposed an analytical expression for the first modal damping ratio. Based on this asymptotic formula, the optimum damper size and the corresponding maximum damping ratio can be determined. Figure 2-3 shows the mechanical model of a taut cable attached with a transverse viscous damper at the position $x = x_d$ from the left cable end. The term "taut" means both the effects of cable bending stiffness, EI, and cable axial stiffness, EA, are ignored. For this system, the equation of motion can be expressed as:

$$m\frac{\partial^2 w}{\partial t^2} - H\frac{\partial^2 w}{\partial x^2} = -c_d \dot{w}(x_d, t)\delta(x - x_d) \tag{2-10}$$

where c_d is the damper size and $\delta(\cdot)$ is the Dirac delta function. The term "$h(dz^2/dx^2)$" observed in the left-hand side of Eq. (2-2) has been dropped as a result of taut cable

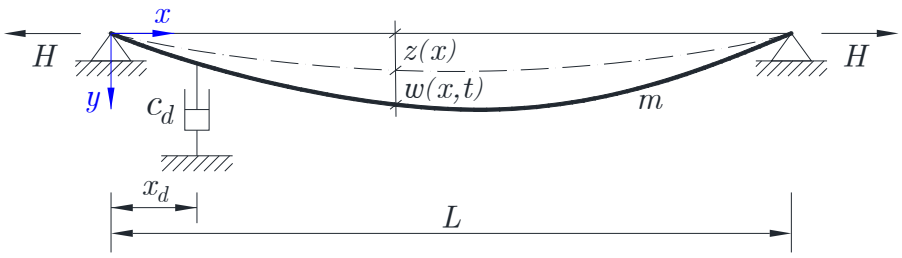

Fig. 2-3. Mechanical model of a damped taut cable (after Carne [82]).

assumption. By considering the boundary and compatibility conditions at the damper installation location and using the separation of variables technique, the exact solution of Eq. (2-10) leads to the following transcendental equation for the complex system eigenfrequencies:

$$\frac{L^*}{x_d}\frac{\tan\beta L^*}{\beta L^*} + i^* c \tan\beta L^* + 1 = 0 \tag{2-11}$$

where $L^* = L - x_d$, $c = c_d/\sqrt{Hm}$, and $i^* = \sqrt{-1}$. Equation (2-11) can be solved approximately to find an asymptotic expression for the damping ratio of the first mode, which is given by:

$$\frac{\zeta_1}{x_d/L} = \frac{\pi(x_d/L)c}{1 + [\pi(x_d/L)c]^2} \tag{2-12}$$

Equation (2-12) reveals that the damping ratio becomes zero either at $c = 0$ or $c \to \infty$ and it is maximum for an intermediate value of c_d. The optimum damper size and the corresponding maximum damping ratio can be expressed as:

$$\zeta_{1,max} = \frac{x_d/L}{2} \; at \; c_{d,opt} = \frac{\sqrt{Hm}}{\pi(x_d/L)} \tag{2-13}$$

Pacheco et al. [69] adopted the mode superposition method (MSM) to obtain the modal damping ratios of a damped cable by calculating the system complex eigenvalues using standard numerical methods. In this approach, the in-plane dynamic cable displacement is approximated by the following finite series:

$$w(x,t) = \sum_{i=0}^{n} \phi_i(x)\, q_i(t) \tag{2-14}$$

where n is the number of included modes, $\phi_i(x)$ is the i^{th} modal shape function that satisfies all the kinematic boundary conditions, and $q_i(t)$ is the generalized coordinate of the i^{th} mode. Sinusoidal shape functions defined as $\phi_i(x) = \sin(i\pi x/L)$ are considered. By substituting Eq. (2-14) into (2-10), multiplying by $\phi_j(x)$ and integrating over the cable length, the matrix form of the equation of motion can be expressed as:

$$\boldsymbol{M}\{\ddot{q}\} + \boldsymbol{C}\{\dot{q}\} + \boldsymbol{K}\{q\} = \{0\} \tag{2-15}$$

where $\boldsymbol{M}_{ij} = \delta_{ij}$ is the normalized mass matrix, $\boldsymbol{C}_{ij} = 2\,[c_d/(\pi\sqrt{Hm})]\sin(i\pi x_d/L)\sin(j\pi x_d/L)$ is the normalized damping matrix, $\boldsymbol{K}_{ij} = i^2\delta_{ij}$ is the normalized stiffness matrix and δ_{ij} is the Kronecker delta. After constructing mass, damping and stiffness matrices, standard numerical methods are applied to calculate the complex eigenvalues of the system from which the modal damping ratios are determined. Figure 2-4 represents graphically the results in the form of a universal curve for estimating modal damping ratio of a damped taut cable [69]. In this figure, i is the mode number and $\omega_{01} = (\pi/L)\sqrt{H/m}$ is the undamped natural frequency of the 1st mode. It was suggested to consider the effect of cable sag in order to obtain more accurate estimation of the damping ratio, especially for longer cables.

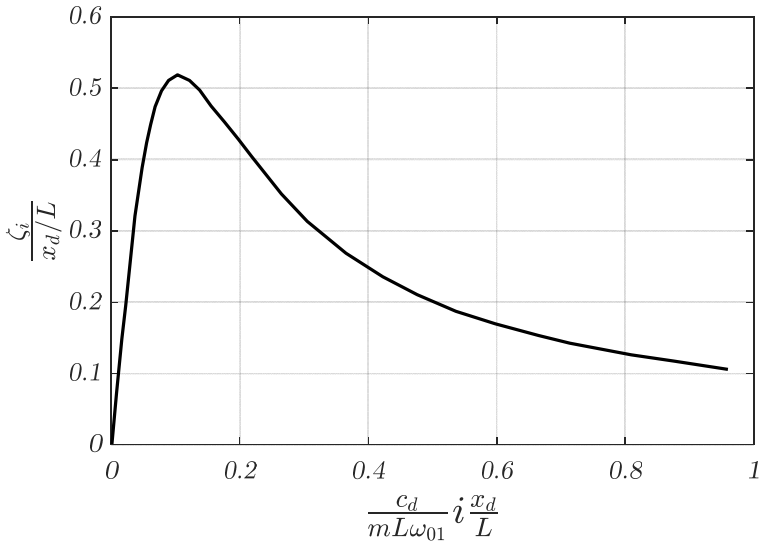

Fig. 2-4. Universal curve for estimating modal damping ratio of taut cables attached with a viscous damper (after Pacheco et al. [69]).

Krenk [70] conducted an analytical study to address the damping ratio of higher modes by assuming $x_d/L \ll 1$. In this study, the asymptotic damping ratio formula originally introduced by Carne [82] was extended to cover higher modes and expressed as:

$$\frac{\zeta_i}{x_d/L} = \frac{i\pi(x_d/L)c}{1 + [i\pi(x_d/L)c]^2} \tag{2-16}$$

where i is the mode number. The maximum damping ratio and the corresponding optimal damper size are given by $\zeta_{i,max} = (x_d/L)/2$ and $c_{d,opt} = \sqrt{Hm}/[i\pi(x_d/L)]$. This equation governs the universal damper design curve proposed by Pacheco et al. [69]. An iterative procedure was also provided to accurately estimate the modal damping ratio when $x_d/L \geq 0.05$. To investigate the effect of cable sag on the damping ratio of a cable-damper system, Krenk and Nielsen [43] included the effect of cable sag by considering the following equation of motion for the symmetric modes of a shallow cable equipped with a transverse viscous damper:

$$m\frac{\partial^2 w}{\partial t^2} - H\frac{\partial^2 w}{\partial x^2} - h\frac{d^2 z}{dx^2} = -c_d \dot{w}(x_d, t)\delta(x - x_d) \tag{2-17}$$

An asymptotic solution for the modal damping ratio was derived as:

$$\frac{\zeta_i}{x_d/L} = R_{si}\frac{i\pi\eta_{si}(x_d/L)c}{1 + [i\pi\eta_{si}(x_d/L)c]^2} \tag{2-18}$$

where η_{si} and R_{si} represent the effect of cable sag and are given respectively by $\eta_{si} = 2\psi/(i\pi)$ and $R_{si} = [\tan(\psi) - (x_d/L)\psi]^2/[\tan^2(\psi) + (12/\lambda^2)\psi^2]$, $\psi = 0.5\beta_{0i}^s L$, and β_{0i}^s is the wave number of a shallow undamped cable given by the solution of $\tan(\psi) = \psi - (4/\lambda^2)\psi^3$. The antisymmetric modes are not affected by the effect of cable sag and their corresponding damping ratio is still governed by Eq. (2-16). Consequently, the maximum damping ratio and the corresponding optimal damper size are given by $\zeta_{i,max} = R_{si}\,(x_d/L)/2$ and $c_{d,opt} = \sqrt{Hm}/[i\pi\eta_{si}(x_d/L)]$.

Following the approach developed in [69], Johnson et al. [57] proposed a control-oriented MSM-based model for analyzing the dynamic response of a damped shallow cable, where the computational efficiency of the MSM was substantially improved by applying the static correction technique [83]. In this study, the approximate static profile of a shallow cable subjected to a concentrated load at the damper location was selected as one of the shape function terms in the MSM. This term reflected the impact of damper presence on the vibrational shape of the cable and was expressed as:

$$\phi_1(x) = \frac{12+\lambda^2}{12+\lambda^2-3\lambda^2\bar{x}_d(1-\bar{x}_d)}\left[\frac{x}{x_d}+\left(1-\frac{x}{x_d}\right)\frac{H(x-x_d)}{1-\bar{x}_d} - \frac{3\lambda^2}{12+\lambda^2}\bar{x}(1-\bar{x})\right] \tag{2-19}$$

where $\bar{x} = x/L$ and $\bar{x}_d = x_d/L$. Sinusoidal functions were selected for the remaining terms. As a result, the total number of terms required to reach an acceptable accuracy is substantially reduced and the numerical model can be used for designing semi-active and active control systems. However, the correction term given by Eq. (2-19) does not represent the exact static displacement profile of the cable and excludes the effect of cable bending stiffness.

Krenk and Høgsberg [39] conducted an analytical study to examine the effects of damper stiffness and damper mass on the modal damping of a shallow cable equipped with a viscous damper. As shown in Fig. 2-5, the damper consists of a linear spring and a viscous dashpot aligned in parallel and a concentrated mass. It was shown that the effect of the damper stiffness is equivalent to a reduced damper installation location. Hence, the presence of damper stiffness will reduce damper effectiveness. The reduced damper installation location is expressed as:

$$x_d^* = \frac{x_d}{1+x_d k_d/H} \tag{2-20}$$

Also, the concentrated mass would act out-of-phase of the damper force and thus tends to increase the damper efficiency. The combined effects of the damper stiffness and mass can be approximated by the reduced stiffness $k_d^* = k_d - \omega_n^2 m_d$ in Eq. (2-20) provided that $\omega_n^2 < 2k_d/m_d$, where ω_n is the natural frequency of the cable.

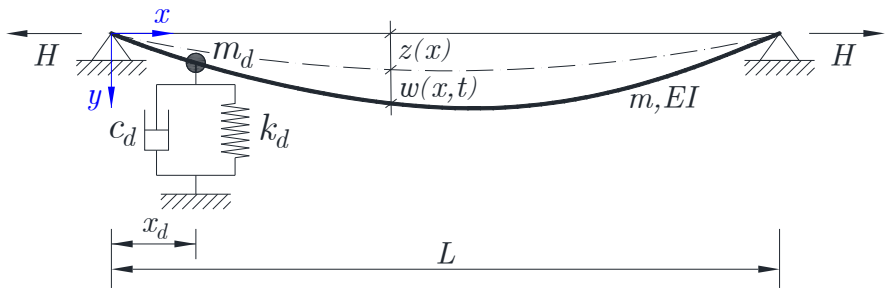

Fig. 2-5. Mechanical model of a damped shallow cable (after Krenk and Høgsberg [39]).

Hoang and Fujino [44] studied the effect of cable bending stiffness on the performance of a viscous damper attached to a fixed-fixed non-sag cable and obtained an exact analytical solution for the following equation of motion:

$$m\frac{\partial^2 w}{\partial t^2} + EI\frac{\partial^4 w}{\partial x^4} - H\frac{\partial^2 w}{\partial x^2} = -c_d\dot{w}(x_d,t)\delta(x-x_d) \tag{2-21}$$

A transcendental equation that governs the complex natural frequencies of the damped cable is derived based on the analytical solution of Eq. (2-21), which can be solved numerically to determine the damped modal frequencies and damping ratios. The following asymptotic expression for the modal damping ratio can be obtained by simplifying the transcendental equation for small values of cable bending stiffness parameter $\varepsilon = EI/(HL)^2$ and $4\varepsilon\beta^2L^2 \ll 1$:

$$\frac{\zeta_i}{x_d/L} = R_f\frac{i\pi\eta_f(x_d/L)c}{1+\left[i\pi\eta_f(x_d/L)c\right]^2} \tag{2-22}$$

where η_f and R_f represent the effect of cable bending stiffness and are defined as $\eta_f = 1-q-0.5rq^2$ and $R_f = (1-q)^2/(1-q-0.5rq^2)$, respectively; $q = (1-e^{-r})/r$ and $r = (x_d/L)/\sqrt{\varepsilon}$. It is shown that the cable flexural rigidity may reduce the maximum

achievable damping ratio up to 20% while it would increase the optimal damper size. The maximum damping ratio and the corresponding optimal damper size are governed by $\zeta_{i,max} = R_f\,(x_d/L)/2$ and $c_{d,opt} = \sqrt{Hm}/[i\pi\eta_f(x_d/L)]$.

Fujino and Hoang [71] proposed a comprehensive formula for the design of viscous dampers based on an analytical study on a damped inclined cable fixed at both ends. The combined effects of cable sag, cable bending stiffness and damper support flexibility were considered. As depicted in Fig. 2-6, the effect of damper support flexibility was modeled by a linear spring attached in series with the dashpot. In this case, an asymptotic formula for the damping ratio can be expressed as:

$$\frac{\zeta_i}{x_d/L} = R_k R_f R_{si} \frac{\eta_k \eta_{si} \eta_i}{1 + (\eta_k \eta_{si} \eta_i)^2} \tag{2-23}$$

where η_k and R_k represent the effect of damper support stiffness and are defined as $\eta_k = \eta_f + 1/\bar{k}_s$ and $R_k = \eta_f/(\eta_f + 1/\bar{k}_s)$, respectively; $\bar{k}_s = k_s x_d/H$ is the nondimensional damper support stiffness; and $\eta_i = i\pi(x_d/L)c_d/\sqrt{Hm}$ is the nondimensional damper size.

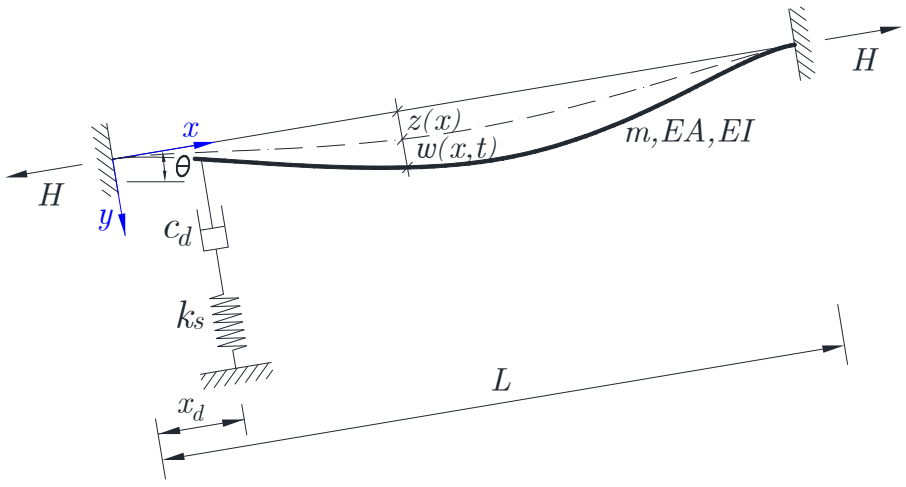

Fig. 2-6. Mechanical model of a damped shallow-flexural cable (after Fujino and Hoang [71]).

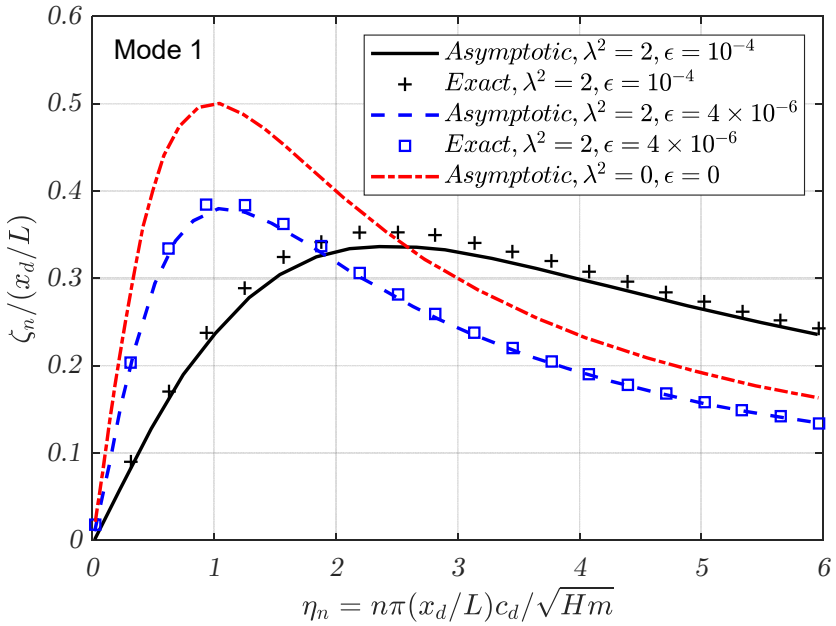

Fig. 2-7. Combined effects of cable sag and flexural rigidity on modal damping ratio in cable with viscous damper (after Fujino and Hoang [71]).

Therefore, the most general form for the maximum achievable damping ratio and the optimal damper size of the cable-damper system shown in Fig. 2-6 can be found as $\zeta_{i,max} = R_k R_f R_{si}\,(x_d/L)/2$ and $c_{d,opt} = \sqrt{Hm}/[i\pi\eta_k\eta_{si}(x_d/L)]$. It was shown that the damper support stiffness reduces the damper performance by up to 12% for $\varepsilon = 10^{-4}$ and $\bar{k}_s = 20$. Figure 2-7 compares the exact and the asymptotic 1st modal damping ratio of a typical cable attached with a viscous damper at $x_d/L = 0.02$. It can be seen that the asymptotic solution (Eq. (2-23)) is slightly conservative as it gives smaller values for the damping ratio compared to the exact numerical solution of the governing transcendental model.

2.3. Negative stiffness dampers and their application

The concept of "negative stiffness" was first used to develop zero-gravity testbeds for spacecraft experiments [84]. It was subsequently adopted to manufacture low-frequency

vibration isolators for vibration-sensitive equipment such as electron microscopes [85] and installed in vehicle seat suspension for improving driver vibration isolation [86]. In the field of structural vibration control, the usage of negative stiffness damper in controlling cable vibrations emerged when the apparent negative stiffness phase in the force-deformation response of an optimally-controlled active damper was observed to be beneficial for the control performance [58]. As an attempt to artificially introduce the negative stiffness mechanism in control systems, Iemura and Pradono [87] proposed a semi-active control algorithm to produce a pseudo-negative stiffness hysteresis loop for variable-orifice dampers installed on a seismically-excited cable-stayed bridge. The pseudo-negative stiffness behaviour helped to achieve a nearly-rigid perfectly-plastic force-deformation curve with a large damping ratio. The performance of the variable damper with pseudo-negative stiffness was compared with a conventional linear damper and showed better control performance. The variable-orifice damper with pseudo-negative stiffness was observed to generate less control force for providing the same amount of damping. In parallel, negative stiffness elements were implemented as a yield mechanism in seismic control of buildings [88]. The commercial application of negative stiffness systems is still limited due to the lack of reliable design tools, the possible need for an additional re-centering mechanism in the control device, and the risk of instability in the controlled system if designed improperly.

Li et al. [61] studied the role of negative stiffness in the behaviour of active and semi-active control schemes for stay cable vibration reduction. The authors considered a taut cable model and conducted analytical and MSM-based numerical analysis by introducing a

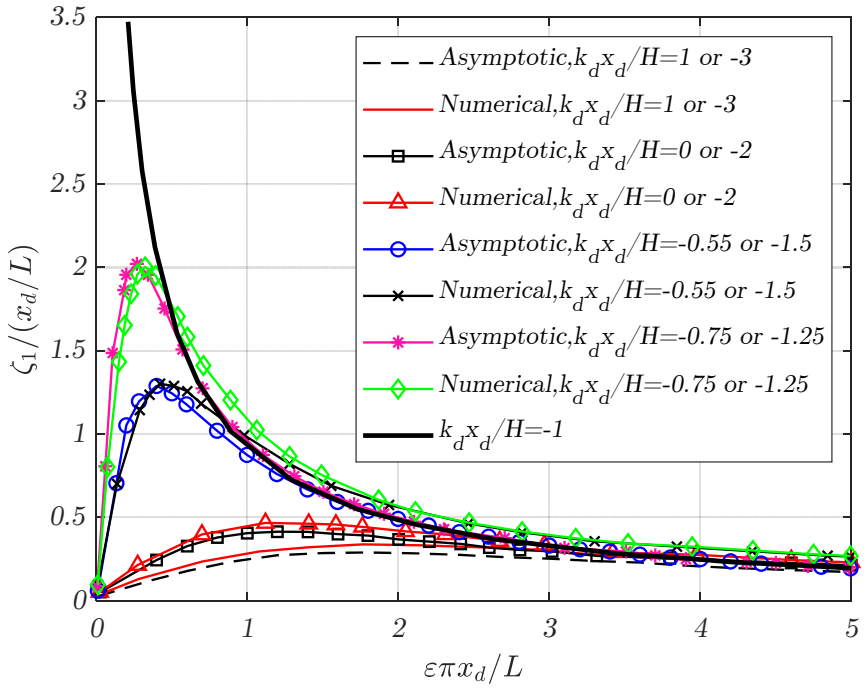

Fig. 2-8. Comparison of first modal damping ratio for various damper stiffness between asymptotic solution and complex numerical eigenvalue analysis ($\varepsilon = c_d/\sqrt{Hm}$) (after Li et al. [61]).

pseudo-viscoelastic (P-VE) damper to replace the active/semi-active device in the analysis. The damping ratio of P-VE with positive or negative stiffness, k_d, is governed by:

$$\frac{\zeta_i}{x_d/L} = \frac{i\pi(x_d/L)c}{(1 + k_d x_d/H)^2 + [i\pi(x_d/L)c]^2} \tag{2-24}$$

It is reported that a sufficiently large negative stiffness in P-VE can cause instability by producing an infinite damping ratio and zero natural frequency in the cable-damper system. To prevent instability, the negative stiffness should satisfy the following condition:

$$\frac{k_d x_d}{H} < -1 \tag{2-25}$$

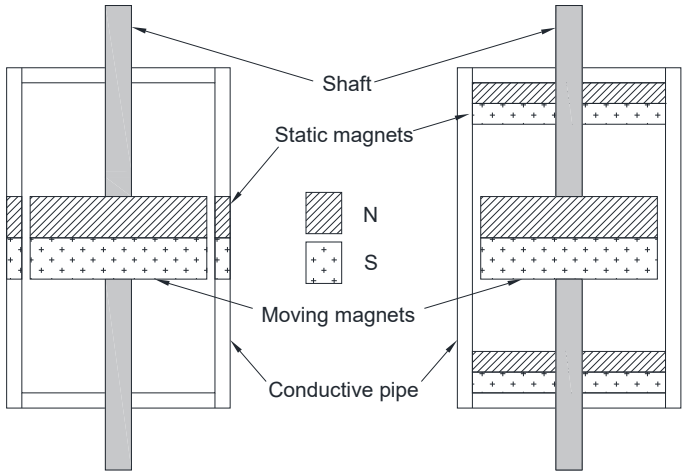

Fig. 2-9. Configuration of magnetic negative stiffness damper (MNSD) (after Shi and Zhu [63]).

Figure 2-8 illustrates the damping performance of P-VE with different values of negative stiffness in the first mode. It can be seen the P-VE with negative stiffness demonstrates considerably better performance compared to the zero or positive stiffness cases.

Weber and Boston [62] developed an optimized clipped viscous damper with negative-stiffness (VD&NS) control strategy for suppressing cable vibration. In contrast with optimal linear-quadratic regulator (LQR) control, the proposed scheme does not require full state feedback and is suitable for practical implementation. Also, its implementation does not use real-time estimation of the damper displacement which is required for semi-active controllers. The performance of VD&NS was validated experimentally for a stay cable equipped with a magneto-rheological (MR) damper at 4% cable length. It was shown that the proposed control algorithm with negative-stiffness is able to provide twice as much cable damping as experimentally optimized viscous damping. Weber and Distl [77] approximated the control force characteristics of a semi-active clipped linear-quadratic

regulator (LQR) by using collocated viscous damping with negative stiffness for controlling multi-mode cable vibration. This system provides superior damping ratio as compared to optimized viscous dampers (1.87 to 2.33 times more cable damping) in both single-mode and multi-mode cable vibrations. An advantageous feature of the proposed semi-active controller is its independency of the excitation frequency in the case of single-mode vibration.

On the other hand, NSD prototypes have been proposed and experimentally tested to further demonstrate their effectiveness. Shi and Zhu [63] introduced innovative configurations of passive magnetic NSD consisting of static and moving magnets arranged in a conductive pipe (Fig. 2-9). The negative-stiffness behaviour (i.e. force in the direction of motion) is generated between the magnets and the damping effect is realized by eddy-current in the conductive pipe. Both specimens provide symmetrical negative stiffness with a compact design that facilitates their practical use on stay cables. In a subsequent study, Shi et al. [67] evaluated the performance of a passive NSD in controlling vibrations of a taut stay cable using analytical and numerical approaches. Results showed that the asymptotic solution can provide accurate estimation of damping for either positive or moderate negative stiffness. However, the accuracy of the solution would be affected if significant negative stiffness exists in the damper. The NSD stability limit was revisited and it was found that the NSD tends to amplify local displacement at the damper location. Shi et al. [68] compared the performance of passive NSD with active LQR control for stay cable vibration control. It was shown that NSD could provide a high damping ratio in a specific vibration mode while the LQR could effectively mitigate several modes at the same time. In this case, NSD tended to reduce the frequency of the target mode, whereas

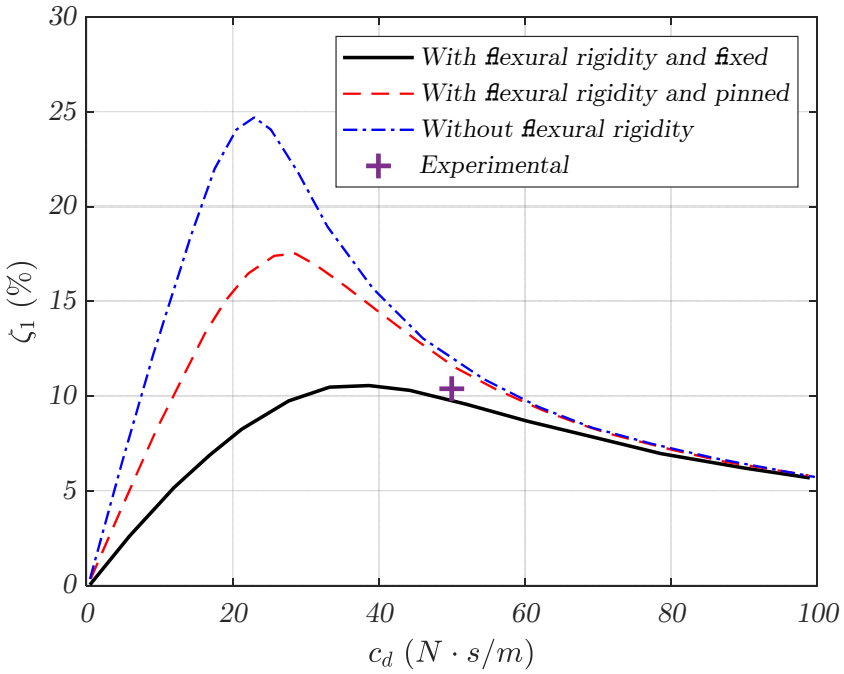

Fig. 2-10. Comparison between experimental and simulated damping ratios (after Shi et al. [66]).

the active LQR slightly increased the modal frequencies of the damped cable. Besides, the control performance improved with an increasing number of state feedbacks. However, access to all states of the system, as required by the LQR controller, would be a major challenge in practice.

Shi et al. [66] conducted an experimental study to verify the superiority of NSD for stay cable vibration control as suggested by analytical and numerical results. NSD was found to be four times as effective as the optimal viscous dampers in providing damping in a cable-damper system under different loading conditions. The effect of cable bending stiffness and boundary conditions on the predicted NSD performance was found to be significant. It was reported that the experimental results were more agreeable with the case of a flexural cable with fixed-fixed ends (Fig. 2-10). Therefore, the application of a taut cable model would result in an overestimated damping ratio and lead to unsafe design.

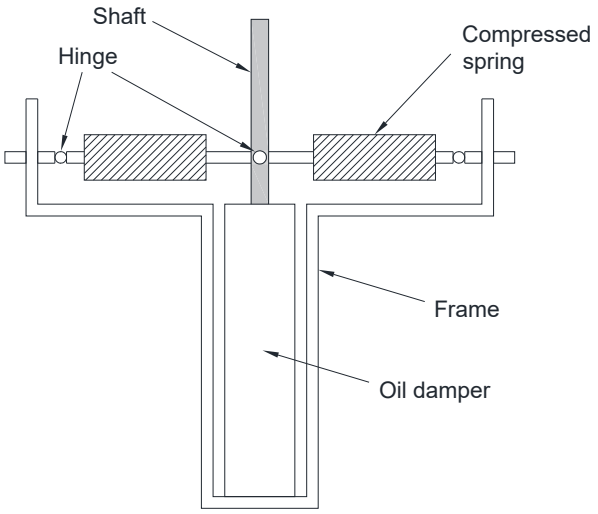

Fig. 2-11. Schematic of a NSD device fabricated by attaching two compressed springs to the oil damper (after Zhou and Li [51]).

Zhou and Li [64] proposed a passive NSD prototype by adding two compressed springs perpendicular to an oil damper (Fig. 2-11). A mechanical model for the NSD was established. Numerical simulations and experimental tests were conducted to evaluate the damper performance in suppressing single-mode and multi-mode stay cable vibrations. Results confirmed the superior NSD performance for cable vibration mitigation as compared to the oil damper alone. More recently, Liu et al. [65] attached pre-compressed springs to a superelastic shape memory alloy (SMA) damper to obtain a novel self-centering NSD (SCNSD) damper. Experimental and numerical studies were conducted to investigate the performance of SCNSD in controlling a single degree of freedom (SDOF) system. It was observed that SCNSD is highly effective in controlling SDOF vibrations and reducing peak acceleration and displacement.

2.4. Effect of damper support stiffness

The damper support flexibility can adversely affect the control performance of passive viscous dampers. It has been shown experimentally and analytically that mounting viscous dampers on a flexible support would reduce the achievable damping ratio. In some cases, dampers installed on cable-stayed bridges are mounted on a support structure. Hence, it is necessary to consider the effect of damper support stiffness. Huang and Jones [45] studied the effect of damper support stiffness on the damper effectiveness of a cable-damper system by assuming a taut cable model and considering a linear elastic support in series with the damper. Two types of damper were investigated, namely linear viscous damper and friction damper. Exact analytical solutions of the system motion and approximate expressions for the modal damping ratio and the maximum force between the damper and the support spring were derived. A family of universal curves were proposed that indicated that the damper support flexibility would reduce the performance of both the viscous and friction dampers.

The impact of damper stiffness and damper support stiffness on the performance of a linear viscous damper was studied by Fournier and Cheng [46] through experimental tests and numerical simulations. Empirical design formulas for selecting the optimum damper size and predicting the maximum achievable system modal damping were proposed, which took into account the effect of damper stiffness and damper support stiffness. Results showed a good agreement between the predicted maximum damping ratio using the proposed equations and other existing methods (Fig. 2-12). It was postulated that the efficiency of a linear viscous damper in mitigating stay cable vibrations would be maximized when the damper stiffness is negligible and the damper support is nearly rigid.

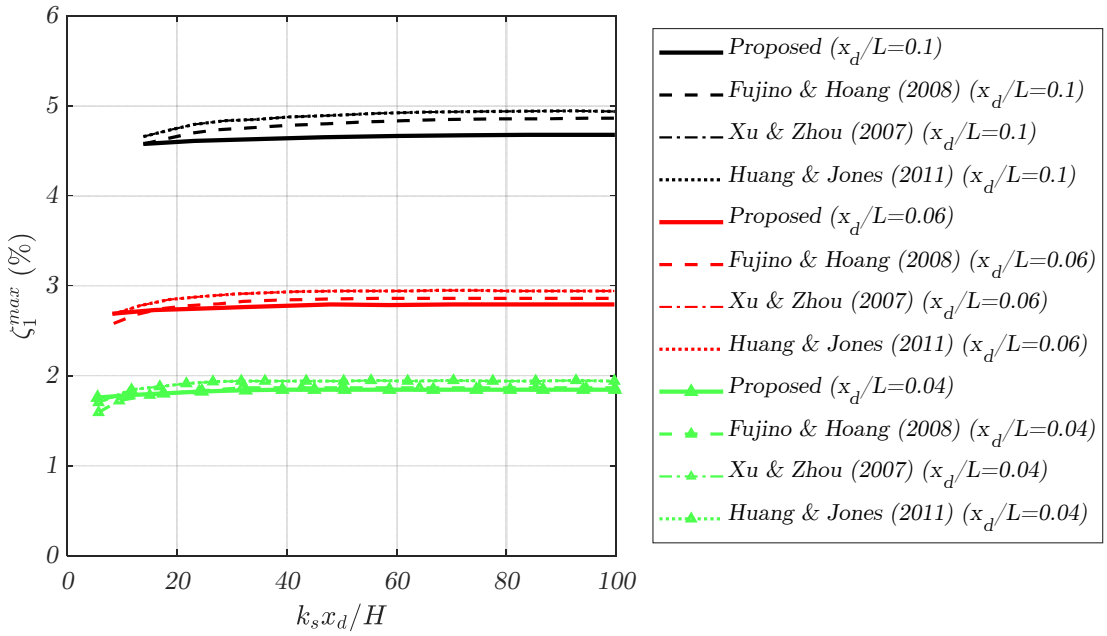

Fig. 2-12. Comparison of maximum achievable damping ratio estimations for zero damper stiffness (after Fournier and Cheng [46]).

2.5. Multi-mode cable vibration control

The existing methods for optimizing the design of passive viscous dampers generally focus on the control cable vibration dominated by a specific mode. However, on-site records indicate that the first few cable modes are often excited simultaneously in the case of RWIV [10,38,49]. On the other hand, the dominant cable modes during a vibration incidence highly depend on the excitation source and may vary. Hence, using single-mode-based approaches to optimize passive viscous damper design, including NSDs, may result in suboptimal damper performance. In order to address this concern, multi-mode vibration control techniques have been studied by a number of researchers for both passive and semi-active dampers of a linear or nonlinear nature.

Wang et al. [75] proposed a method to optimize the performance of viscous dampers in mitigating multi-mode cable vibrations. The optimal damper size was obtained by

minimizing the difference between the optimal gain of an idealized active actuator and the achievable gain of a practical viscous damper. Weber et al. [48] developed an analytical method for the optimization of linear viscous dampers. It could supply a sufficient amount of damping to multiple modes simultaneously and also allows the damper to be positioned as close as possible to the end of the cable. This systematic approach provides equal damping ratio to the lowest and the highest target modes, whereas a higher damping ratio for the intermediate modes is obtained. However, a target damping ratio can be addressed directly. Hoang and Fujino [76] studied the behaviour of nonlinear dampers and obtained an equivalent damping ratio by using energy-based arguments. Results showed that a nonlinear damper could effectively suppress cable motion containing a wide range of modes and was, therefore, more advantageous than linear dampers in multi-mode vibration control. Weber and Distl [77] introduced a semi-active control scheme for multi-mode cable vibration mitigation. It is based on the approximate collocated solution of a clipped negative-stiffness viscous damper optimized by the linear quadratic regulator (LQR) method and requires real-time measurement of the damper stroke and force. In this regard, linear passive devices would be a better choice for designing a less-complicated measurement-free controller. Izzi et al. [89] studied the application of nonlinear Targeted-Energy-Transfer (TET) devices to control stay cable vibration. The TET device was modelled as a dashpot with a viscous damper in parallel with a power-law nonlinear elastic spring element and a lumped mass restrained to one end. By considering the effects of the nonlinear elastic damper stiffness, the lumped mass and the support flexibility, a new set of "universal design curves" for the TET devices were derived. It was found that the peak regions of these amplitude-dependent design curves were flatter than that of the

conventional viscous dampers and thus the TET devices would be more effective in multi-mode vibration control of cables.

The recently emerged NSD devices have shown high damping capability which is comparable to smart semi-active systems. Nonetheless, since existing NSD design tools only address single-mode cable vibration control, it is of the utmost importance to study the potential of NSD in mitigating multi-mode cable vibrations.

2.6. Summary

The above literature review has identified the need for an analytical model that can address the combined effects of cable sag, cable bending stiffness, damper stiffness, and damper support stiffness, on the behaviour of a damped cable. It is essential to develop such comprehensive analytical model to predict the control performance of positive- and negative stiffness dampers more accurately and to better understand the dynamic behaviour of a cable equipped with these control devices (Chapter 3). The asymptotic relationships derived to predict the damping ratio were shown to involve conservative approximations. To evaluate the effect of such approximations on the damper design, a high-precision numerical model is also needed to simulate the dynamic response of a damped cable and verify the damping ratio predicted by the asymptotic formulas. However, the existing numerical models do not take into account the combined effects of cable sag and flexural rigidity. Therefore, the next objective of this research is to develop an accurate and computationally efficient and numerical model for analyzing the dynamic response of a damped cable (Chapter 4).

In addition, the majority of existing studies focused on NSDs and their control function have used simple analytical models based on the taut cable assumption. By using the

comprehensive analytical and numerical models developed in Chapters 3 and 4, the control performance of negative stiffness dampers and their stability issues will be investigated in detail (Chapter 5). Due to the very limited studies on the effect of damper support stiffness on the performance of passive dampers, especially NSD, it is necessary to devote a separate chapter to this effect and propose analytical methods to optimize the damper support flexibility (Chapter 6). Besides, the high potential of NSD makes it a good candidate for multi-mode vibration control of stay cables. So far, no studies have been conducted on NSD optimization for multi-mode vibration control of stay cables. By adopting the analytical model developed in Chapter 3, a new method will be proposed to optimize NSD for suppressing cable vibrations dominated by two or more cable modes. This topic will be discussed in more detail in Chapter 7 of this dissertation.

Chapter 3 Analytical Study on the Modal Damping of a Cable-damper System

3.1. Introduction

In this chapter, an analytical model will be developed for predicting the dynamic response of cable-damper systems by including the effect of the damper stiffness. The objective is to further extend the existing analytical model developed by Fujino and Hoang [71], in which the influence of cable sag, cable flexural stiffness, and damper support stiffness have been considered. The equation of motion of a damped cable equipped with a passive viscous damper is formulated. Both the fixed-fixed and hinged-hinged boundary conditions are studied. The damper stiffness and the damper support stiffness are modeled as linear springs in the damper mechanical model. The free vibration response is expressed in the form of a transcendental equation for the modal frequencies of the system. Besides seeking a numerical solution for the governing transcendental equation, an asymptotic solution is also derived, which, as a refinement of the existing damper design tool by Fujino and Hoang [71], accounts for the effect of the damper stiffness in terms of a reduction factor and a modification factor to the maximum achievable system damping.

3.2. Analytical model for the free vibration response of a cable-damper system

3.2.1. Fixed-fixed cable

Consider a sagged inclined cable with a transverse damper placed at a distance $x = x_d$ from the lower end, as shown in Fig. 3-1. The cable is fixed at both ends and its orientation

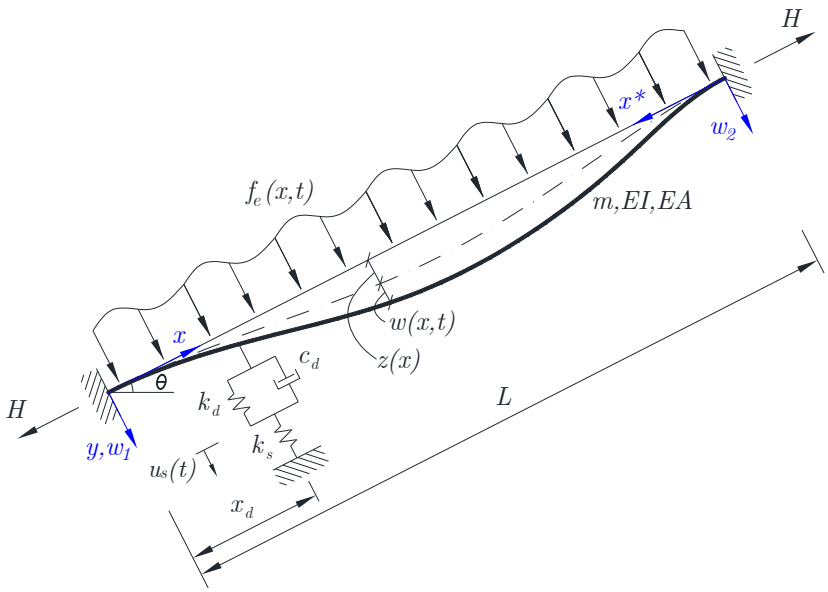

Fig. 3-1. Mechanical model of a shallow-flexural cable equipped with a transverse viscous damper.

is described by an angle θ between the cable chord and the horizontal direction. The coordinate system is defined such that the x-axis is along the cable chord and the y-axis is along the transverse in-plane direction. By considering the effects of cable sag and cable flexural stiffness, the in-plane motion of the studied cable-damper system under the effect of an external distributed load is governed by:

$$m\frac{\partial^2 w}{\partial t^2} + EI\frac{\partial^4 w}{\partial x^4} - H\frac{\partial^2 w}{\partial x^2} - h\frac{d^2 z}{dx^2} = f_e(x,t) - F_d(t)\delta(x - x_d) \qquad (3\text{-}1)$$

where $w(x,t)$ is the transverse in-plane displacement of the cable; $z(x)$ is the static cable displacement due to its self-weight; H is the chord tension, m is the mass per unit length, EI is the flexural rigidity, and EA is the axial rigidity of the cable; $F_d(t)$ is the concentrated damper force; $f_e(x,t)$ is the in-plane distributed load; $\delta(\cdot)$ is the Dirac delta function; and $h(t)$ is the additional chord tension due to the cable motion. By assuming a parabolic distribution for the static cable displacement under its self-weight defined as $z(x) =$

$(4dx/L)(1 - x/L)$ with the cable sag given by $d = mgL^2 \cos\theta\,/(8H)$, the dynamic cable tension $h(t)$ can be expressed as:

$$\frac{h(t)L_e}{EA} = \frac{8d}{L^2}\int_0^L w(x,t)dx \tag{3-2}$$

where $L_e \approx L[1 + 8(d/L)^2]$ is the effective cable length in static equilibrium state.

Under free vibration, the cable transverse displacement, the damper force and the additional chord tension can be respectively expressed as $w(x,t) = \tilde{w}(x)e^{i\omega t}$, $F_d(t) = \tilde{F}_d e^{i\omega t}$ and $h(t) = \tilde{h}e^{i\omega t}$, where ω is the natural frequency of motion and $i^2 = -1$. By substituting these expressions into the homogeneous form of Eq. (3-1), it can be reduced to the following 4th order ordinary differential equation:

$$\frac{d^4\tilde{w}}{dx^4} - \left(\frac{1}{\varepsilon L^2}\right)\frac{d^2\tilde{w}}{dx^2} - \left(\frac{\beta^2}{\varepsilon L^2}\right)\tilde{w} = -\frac{8d}{\varepsilon L^4}\frac{\tilde{h}}{H} \tag{3-3}$$

where $\beta = \omega\sqrt{m/H}$ is the wave number and $\varepsilon = EI/(HL^2)$ is the nondimensional cable bending stiffness parameter.

By dividing the cable into two segments on the left and right side of the damper installation location, the cable displacement can be expressed for each side as $w_L(x,t) = \tilde{w}_L(x)e^{i\omega t}$ and $w_R(x^*,t) = \tilde{w}_R(x^*)e^{i\omega t}$, respectively, where x^* is the chord direction from the top of the cable.

Equation (3-3) can be explicitly solved for $\tilde{w}_L(x)$ and $\tilde{w}_R(x^*)$ to obtain:

$$\widetilde{w}_L(x) = A_1 \sin(\gamma_b x) + B_1 \cos(\gamma_b x) + C_1 \sin h(\gamma_a x) + D_1 \cosh(\gamma_a x) + \frac{8d}{(\beta L)^2}\frac{\tilde{h}}{H} \qquad 0 < x < x_d \tag{3-4}$$

$$\widetilde{w}_R(x^*) = A_2 \sin(\gamma_b x^*) + B_2 \cos(\gamma_b x^*) + C_2 \sin h(\gamma_a x^*) + D_2 \cosh(\gamma_a x^*) + \frac{8d}{(\beta L)^2}\frac{\tilde{h}}{H} \qquad 0 < x^* < L - x_d \tag{3-5}$$

where $\gamma_{a,b}^2 = [1/(2\varepsilon L^2)](\sqrt{1 + 4\varepsilon\beta^2 L^2} \pm 1)$. Equations (3-4) and (3-5) consist of 9 unknowns in total, including 8 coefficients $A_1 \sim D_1$ and $A_2 \sim D_2$, and $\tilde{h}$. These unknowns can be determined by applying the boundary conditions at the cable ends and the continuity conditions at the damper location, including $\widetilde{w}_L(0) = \widetilde{w}_L'(0) = 0$, $\widetilde{w}_R(0) = \widetilde{w}_R'(0) = 0$, $\widetilde{w}_L(x_d) = \widetilde{w}_R(x_d^*)$, $\widetilde{w}_L'(x_d) = \widetilde{w}_R'(x_d^*)$, $\widetilde{w}_L''(x_d) = \widetilde{w}_R''(x_d^*)$, and $EI[\widetilde{w}_L'''(x_d) - \widetilde{w}_R'''(x_d^*)] = \tilde{F}_d$ with $x_d^* = L - x_d$; and by satisfying the complex form of Eq. (3-2), i.e. $\tilde{h} = (8d/L^2)(EA/L_e)[\int_0^{x_d} \widetilde{w}_L(x)dx + \int_0^{x_d^*} \widetilde{w}_R(x^*)dx^*]$. After specifying the unknown coefficients and $\tilde{h}$, the explicit form of $\widetilde{w}_L(x)$ and $\widetilde{w}_R(x^*)$ can be obtained. Considering the expression of $\widetilde{w}_L(x)$ at the damper installation location, namely $\widetilde{w}_L(x_d)$, a transcendental equation is formed that relates the damper force, $\tilde{F}_d$, to the natural frequency of the cable-damper system. This equation can be expressed as:

$$\frac{(f_1 - \alpha f_2)}{f_3 - f_4 + \alpha f_5} = \frac{\tilde{F}_d}{\widetilde{w}_d EI} \tag{3-6a}$$

where

$$f_1 = 2\gamma_a\gamma_b(\gamma_a^2 + \gamma_b^2)[\gamma_a z_2(1 - z_3) + \gamma_b z_1(1 - z_4)] \tag{3-6b}$$

$$f_2 = (\gamma_a^2 - \gamma_b^2)z_1 z_2 + 2\gamma_a\gamma_b(1 - z_3 z_4) \tag{3-6c}$$

$$f_3 = 2\gamma_b^2 z_1[\bar{z}_2 - z_2 + \sinh(\gamma_a x_d^*)] - 2\gamma_a^2 z_2[\bar{z}_1 - z_1 + \sin(\gamma_b x_d^*)] \tag{3-6d}$$

$$\begin{aligned} f_4 = \gamma_a\gamma_b\{2[&\cos(\gamma_b x_d^*)(\bar{z}_4 - z_4 + 1 - \cosh(\gamma_a x_d^*)) \\ &+ \cosh(\gamma_a x_d^*)(\bar{z}_3 - z_3 + 1) - (\bar{z}_4 - 1)(\bar{z}_3 - 1)] \\ &+ (z_3 - 1)\cosh(\gamma_a(x_d^* - x_d)) + (z_4 - 1)\cos(\gamma_b(x_d^* \\ &- x_d)) - z_3(2\bar{z}_4 + 1) - z_4(2\bar{z}_3 - 4z_3 + 1)\} \end{aligned} \tag{3-6e}$$

$$\begin{aligned} f_5 = \{&(\gamma_a^2 + \gamma_b^2)[\gamma_a z_2 \cos(\gamma_b(x_d^* - x_d)) - \gamma_b z_1 \cosh(\gamma_a(x_d^* - x_d))] \\ &+ 4\gamma_a\gamma_b[\gamma_a(\bar{z}_4\bar{z}_1 + \cosh(\gamma_a(x_d^* - x_d))\sin(\gamma_b(x_d^* \\ &- x_d))) - \gamma_b(\bar{z}_3\bar{z}_2 + \cos(\gamma_b x_d^*)\sinh(\gamma_a(x_d^* - x_d)))] \\ &- \gamma_a z_3 z_2(\gamma_a^2 - 3\gamma_b^2) - \gamma_b z_4 z_1(3\gamma_a^2 - \gamma_b^2)\}/(2\gamma_a\gamma_b(\gamma_a^2 \\ &+ \gamma_b^2)) \end{aligned} \tag{3-6f}$$

and $\alpha = \gamma_a^2\gamma_b^2 L[1 - \beta^2 L^2/\lambda^2]$; $z_1 = \sin(\gamma_b L)$; $z_2 = \sinh(\gamma_a L)$; $z_3 = \cos(\gamma_b L)$; $z_4 = \cosh(\gamma_a L)$; $\bar{z}_1 = \sin(\gamma_b x_d)$; $\bar{z}_2 = \sinh(\gamma_a x_d)$; $\bar{z}_3 = \cos(\gamma_b x_d)$; $\bar{z}_4 = \cosh(\gamma_a x_d)$; $\lambda^2 = (8d/L)^2[LEA/(HL_e)]$ is the Irvine's sag-extensibility parameter ; and $\widetilde{w}_d = \widetilde{w}_L(x_d) = \widetilde{w}_R(x_d^*)$.

The mechanical model of a transverse damper and its support is shown in Fig. 3-1. In this model, the damper consists of a linear dashpot with size c_d and a linear spring with stiffness k_d connected in parallel. The damper support is modeled as a linear spring with stiffness k_s connected to the damper in series. Based on this model, the time-dependent force generated by the damper can be expressed as:

$$F_d(t) = k_s u_s(t) = k_d[w(x_d,t) - u_s(t)] + c_d[\dot{w}(x_d,t) - \dot{u}_s(t)] \tag{3-7}$$

where $w(x_d,t)$ is the transverse cable displacement at the damper location and $u_s(t)$ is the displacement at the top of the damper support spring. Substitute $w(x_d,t) = \tilde{w}_d e^{i\omega t}$ and $u_s(t) = \tilde{u}_s e^{i\omega t}$ into equation (3-7), it yields:

$$\tilde{u}_s = \frac{(k_d + ic_d\omega)\tilde{w}_d}{(k_s + k_d + ic_d\omega)} \tag{3-8}$$

Next, the damper force amplitude can be obtained as:

$$\begin{aligned} \tilde{F}_d = k_s\tilde{u}_s &= \frac{k_s(k_d + ic_d\omega)}{(k_s + k_d + ic_d\omega)}\tilde{w}_d \\ &= \frac{k_s(k_d + ic_d\omega)(k_s + k_d - ic_d\omega)}{(k_s + k_d)^2 + (c_d\omega)^2}\tilde{w}_d \end{aligned} \tag{3-9}$$

By substituting $\tilde{F}_d/\tilde{w}_d$ from Eq. (3-9) into Eq. (3-6a) and replacing ω with $\beta\sqrt{H/m}$, the transcendental equation can be solved for the complex wave number β using standard numerical methods, based on which the modal damping ratio of the cable-damper system can be calculated as:

$$\zeta_n = \frac{\mathrm{Im}[\beta_n]}{|\beta_n|} \tag{3-10}$$

where Im[·] and |·| denote the imaginary part and the magnitude of a complex number, respectively, and n is the mode number.

3.2.2. Hinged-hinged cable

The fixed-fixed support conditions assumed in Section 3.2.1 may not accurately reflect the behaviour of stay cables that are not rigidly connected to the deck. Also, it has been shown

that the response of very long stays, where the effect of cable bending stiffness is negligible, is better represented by hinged-hinged boundary conditions [90]. Therefore, it is necessary to provide an analytical model that can determine the damping ratio of such cables where a hinged-hinged end condition is more realistic. In order to extend the applicability of the aforementioned numerical approach for obtaining the natural frequency and modal damping ratio of the cable-damping system, the hinged-hinged cable boundary condition is considered in this section. In this case, the boundary conditions $\widetilde{w}_L^{'}(0) = 0$ and $\widetilde{w}_R^{'}(0) = 0$ which restrain the cable rotation at both ends should be replaced with $\widetilde{w}_L^{''}(0) = 0$ and $\widetilde{w}_R^{''}(0) = 0$. As a result, the transcendental equation of the cable displacement at the damper location becomes:

$$\frac{EI\widetilde{w}_d}{\tilde{F}_d} = g_1 - \frac{g_2 \times g_3}{g_4 - \alpha g_5} \tag{3-11a}$$

where

$$g_1 = \frac{[z_1 \bar{z}_2 \gamma_b \sinh(\gamma_a x_d^*) - z_2 \bar{z}_1 \gamma_a \sin(\gamma_b x_d^*)]}{[z_1 z_2 \gamma_a \gamma_b (\gamma_a^2 + \gamma_b^2)]} \tag{3-11b}$$

$$g_2 = z_2 \gamma_a^2 [\bar{z}_1 - z_1 + \sin(\gamma_b x_d^*)] + z_1 \gamma_b^2 [\bar{z}_2 - z_2 + \sinh(\gamma_a x_d^*)] \tag{3-11c}$$

$$g_3 = z_2 \gamma_a^2 [z_1(1 - \bar{z}_3) - \bar{z}_1(1 - z_3)] + z_1 \gamma_b^2 [z_2(1 - \bar{z}_4) - \bar{z}_2(1 - z_4)] \tag{3-11d}$$

$$g_4 = 2 z_1 z_2 \gamma_a \gamma_b (\gamma_a^2 + \gamma_b^2)[z_2 \gamma_a^3 (1 - z_3) - z_1 \gamma_b^3 (1 - z_4)] \tag{3-11e}$$

$$g_5 = [z_1 z_2 (\gamma_a^2 + \gamma_b^2)]^2 \tag{3-11f}$$

By substituting $\tilde{F}_d / \widetilde{w}_d$ from Eq. (3-9) into Eq. (3-11a) and solving the transcendental equation for the complex wave number β, the modal damping ratio of the cable-damper system can be calculated from Eq. (3-10).

3.3. Asymptotic solution for the modal damping ratio

3.3.1. Fixed-fixed cable

An asymptotic solution to Eq. (3-6) for predicting the modal damping ratio of a stay cable equipped with a transverse viscous damper has been developed by Fujino and Hoang [71]. Consider that the damper installation will cause a minimal perturbation in the wave number defined as $\Delta\beta_n = \beta_n - \beta_{0n}^s \ll \beta_{0n}^s$, where β_n is the n^{th} modal wave number of the damped flexural-extensible cable and β_{0n}^s is the basic wave number of an undamped non-flexural extensible cable, which is governed by Eqs. (2-4) and (2-5). For small values of cable bending stiffness factor, i.e. $4\varepsilon\beta^2 L^2 \ll 1$, the following approximations can be made: $\gamma_a \cong 1/\sqrt{\varepsilon L^2}$; $\gamma_b \cong \beta$; $z_2 \cong z_4 \gg 1$ and $\sinh(\gamma_a x_d^*) \cong \cosh(\gamma_a x_d^*) \cong e^{-r} z_4$. By applying these terms to Eq. (3-6), simplifying and substituting into Eq. (3-10), it yields:

$$\frac{\zeta_n}{x_d/L} \cong R_{sn} \times Im\left[\frac{2/r + (x_d \tilde{F}_d/\tilde{w}_d H)(1 + 2e^{-r}/r - 2q/r)}{1 + (x_d \tilde{F}_d/\tilde{w}_d H)(1 - q - 0.5rq^2)}\right] \qquad (3\text{-}12)$$

where $r = (x_d/L)/\sqrt{\varepsilon}$ and $q = (1 - e^{-r})/r$ are the auxiliary bending stiffness coefficients, and $R_{sn} = [\tan(\psi) - (x_d/L)\psi]^2/[\tan^2(\psi) + (12/\lambda^2)\psi^2]$ with $\psi = 0.5\beta_{0n}^s L$ is a factor that reflects the effect of cable sag. Substituting Eq. (3-9) into Eq. (3-12) and computing the imaginary part gives:

$$\frac{\zeta_n}{x_d/L} \cong R_{sn} \times \left[\frac{\kappa\bar{b}(1-q)^2}{[1 + (1-\kappa)\bar{k}_s\eta_f]^2 + (\eta_f + 1/\bar{k}_s)^2\bar{b}^2}\right] \qquad (3\text{-}13)$$

where $\bar{b} = \kappa c_d \omega_n x_d/H$; $\kappa = 1/(1 + \bar{k}_d/\bar{k}_s)$; $\eta_f = 1 - q - 0.5rq^2$; and $\bar{k}_d = x_d k_d/H$ and $\bar{k}_s = x_d k_s/H$ are the normalized damper stiffness and damper support stiffness parameters. Equation (3-13) can be further simplified to:

$$\frac{\zeta_n}{x_d/L} \cong C_k R_{sn} \times \left[\frac{C_k b(1-q)^2}{1+[C_k(\eta_f + 1/\bar{k}_s)b]^2}\right] \tag{3-14}$$

where $C_k = 1/[1 + \bar{k}_d(\eta_f + 1/\bar{k}_s)]$ is the integrated stiffness coefficient and $b = c_d\omega_n x_d/H$. By using the approximation $\omega_n \cong \beta_{0n}^s\sqrt{H/m}$ and adopting the reduction and modification factors defined by Fujino and Hoang [71], Eq. (3-4) can be reduced to the following refined design formula:

$$\frac{\zeta_n}{x_d/L} = \bar{R}_k R_f R_{sn} \frac{\bar{\eta}_k \eta_{sn} \eta_n}{1+(\bar{\eta}_k \eta_{sn} \eta_n)^2} \tag{3-15}$$

where $\eta_n = n\pi(x_d/L)c_d/\sqrt{Hm}$ is the dimensionless damping parameter; $\eta_{sn} = \beta_{0n}^s L/(n\pi)$ is the modification factor for η_n due to the influence of cable sag; $\bar{\eta}_k = C_k\eta_k = C_k(\eta_f + 1/\bar{k}_s)$ is the modification factor for η_n due to combined effect of cable flexural rigidity, damper stiffness and damper support stiffness; and η_f is the modification factors for η_n due to the influence of cable flexural rigidity. Also, R_{sn}, $R_f = (1-q)^2/\eta_f$ and $\bar{R}_k = C_k R_k = C_k[\eta_f/(\eta_f + 1/\bar{k}_s)]$ are the reduction factors for the maximum damping ratio due to the influence of cable sag, cable flexural rigidity and the combined stiffness effects of the cable, the damper and its support, respectively. Figure 3-2 provides the values of $(\eta_{sn} - R_{sn})$ factors for practical ranges of λ^2 and x_d/L. Similarly, Fig. 3-3 illustrates the variation of $(\eta_f - R_f)$ factors with respect to the ε and x_d/L. It should be noted that η_{sn} and R_{sn} factors are equal to 1 for the antisymmetric modes with $n = 2,4,$ ..., and as can be observed in Fig. 3-2, are almost equal to 1 for the higher order symmetric modes, namely modes 3, 5, etc.

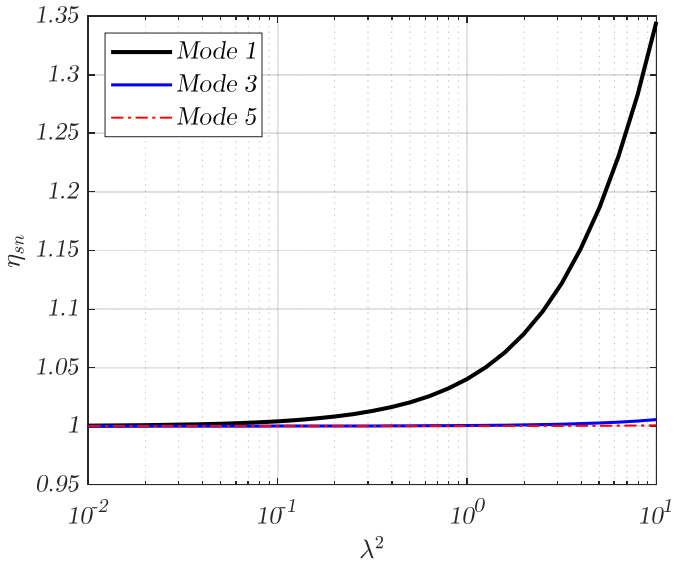

(a)

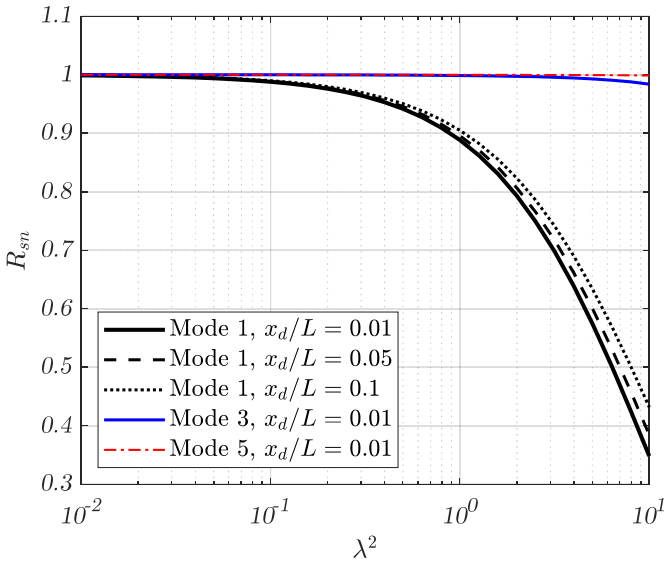

(b)

Fig. 3-2. Modification and reduction factors for the modal damping ratio due to the effect of cable sag.

For a given damper location, the maximum achievable cable damping ratio of the n^{th} mode can then be identified by differentiating ξ_n with respect to η_n in Eq. (3-15), i.e.

$$\frac{\zeta_n^{max}}{x_d/L} = 0.5\bar{R}_k R_f R_{sn} \;\; at \;\; \eta_n^{opt} = \frac{1}{\bar{\eta}_k \eta_{\mathrm{sn}}} \tag{3-16}$$

Equation (3-16) can be used to design a cable-damper system when the damper has either zero, positive or negative stiffness. This expression is analogous to the design formula proposed by Fujino and Hoang [71], except for the proposed refined coefficients $\bar{R}_k$ and $\bar{\eta}_k$ which include the effect of damper stiffness through the integrated stiffness coefficient C_k. The maximum achievable damping ratio of a transverse passive damper with zero

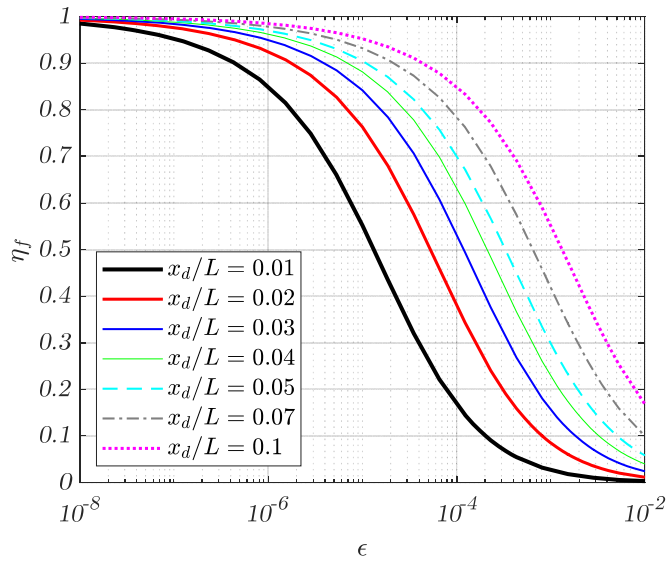

(a)

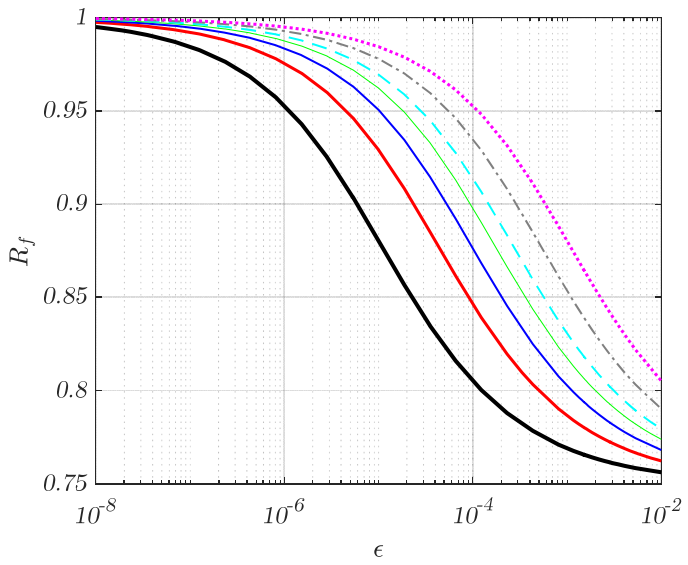

(b)

Fig. 3-3. Modification and reduction factors for the modal damping ratio due to the effect of cable bending stiffness.

stiffness and rigid support attached to an ideal taut cable is given by $\zeta_n^{max}/(x_d/L) = 0.5$ [70]. According to Eq. (3-16), this ideal value is decreased by three reduction coefficients which respectively reflect the effects of cable sag (R_{sn}), cable bending stiffness (R_f), and damper stiffness and support stiffness ($\bar{R}_k$).

The integrated stiffness coefficient C_k represents the combined influences of the damper support stiffness, the damper stiffness and the cable bending stiffness on the damping property of a damped cable and can be expressed as:

$$C_k = 1 - \frac{1}{1+\Psi} = 1 - \frac{1}{1 + (\bar{k}_s/\bar{k}_d)/(1+\bar{k}_s\eta_f)} \tag{3-17}$$

where $\Psi = (\bar{k}_s/\bar{k}_d)/(1+\bar{k}_s\eta_f) = 1/(\bar{k}_d\eta_k)$ is an auxiliary parameter. The value of the normalized damper stiffness $\bar{k}_d$ can be selected either positive or negative. In the case of zero damper stiffness, Ψ approaches infinity and based on Eq. (3-17), the integrated stiffness coefficient becomes 1. Figure 3-4 shows the variation of the integrated stiffness coefficient C_k against Ψ for both PSD and NSD. It can be seen from the figure that based on the definition of Ψ and its value, the viscous damper can be classified as PSD ($\Psi > 0$) and NSD ($\Psi < 0$); whereas $\Psi = 0$ corresponds to the scenario where the damper stiffness is much larger than the support stiffness ($\bar{k}_d \gg \bar{k}_s$), which, in an extreme case, leads to the condition of rigid damper stiffness and/or zero support stiffness ($\bar{k}_d \to \infty,\ \bar{k}_s = 0$). Therefore, when the cable vibrates, the rigid stiffness of the damper would constrain the motion of the damper dashpot and thus the amount of the provided damping. Also, since no constraint would be provided by the damper support, the damper would play the role of an additional attached mass during cable vibration rather than dissipating energy. As

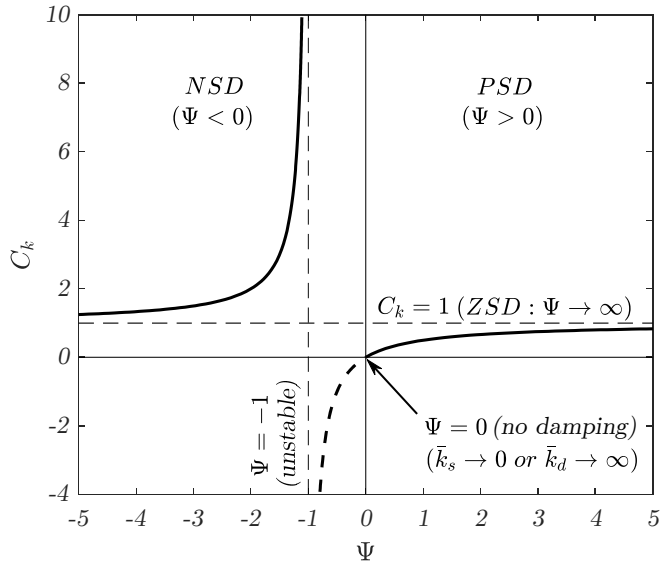

Fig. 3-4. Variation of the integrated stiffness coefficient C_k as a function of Ψ for NSD and PSD.

reflected in Fig. 3-4, the integrated stiffness coefficient C_k becomes zero when $\Psi = 0$. According to Eq. (3-15), in this case the damper provides no damping and $\xi_n = 0$.

In the case of PSD, the damper has a positive stiffness which gives $\Psi > 0$. Based on Eq. (3-17), it results in $0 < C_k < 1$ and implies a lower damping ratio than the ZSD case. This phenomenon is in agreement with the existing experience [46,47,67,91] indicating that the presence of positive damper stiffness would have an adverse effect on the damper efficiency. Nevertheless, it was found that the impact of a positive stiffness was minor and could be neglected in the analysis and design [46,92]. Besides, if the positive stiffness of the damper becomes negligible ($\bar{k}_d \to 0^+$), Ψ would approach to infinity ($\Psi \to +\infty$) and Eq. (3-17) would give $C_k = 1$. In this case, Eq. (3-15) would have the same form as the design formula developed by Fujino and Hoang [71].

In Fig. 3-4, two distinct regions separated by the line $\Psi = -1$ can be observed from the NSD zone where the damper stiffness is negative. It can be seen from the figure that for $\Psi < -1$, the integrated stiffness coefficient C_k is always greater than 1, which, according to Eq. (3-16), would give a maximum damping ratio higher than that of the ZSD case. This implies that NSD is more effective in vibration control than ZSD and PSD and should be designed in the region of $\Psi < -1$. As Ψ approaches to $-\infty$ ($\bar{k}_d \to 0^-$), C_k becomes 1 and Eq. (3-15) again reduces to the same form as the design formula by Fujino and Hoang [71]. In addition, it is interesting to note that as Ψ gradually increases and approaches to -1, the integrated stiffness coefficient would approach to infinity ($C_k \to +\infty$), and the NSD would thus lose its stability. The requirement to ensure stable performance of NSD will be further discussed in the next section. The second region corresponds to $0 < \Psi < -1$, within which C_k becomes negative and highly sensitive to the variation of Ψ. Even a slight decrease of the Ψ value could cause a drastic reduction of C_k and thus a considerable impact on the damper performance. Therefore, it is recommended to avoid this region in designing NSD.

To verify Eq. (3-15), a special case of rigid damper support and taut cable, which has been studied by Shi et al. [67], is considered. By assuming a rigid damper support, the following simplifications can be made:

$$\lim_{\bar{k}_s \to \infty} C_k = \lim_{\bar{k}_s \to \infty} \left(1 - \frac{1}{1 + (\bar{k}_s / \bar{k}_d)/(1 + \bar{k}_s \eta_f)} \right) = \frac{1}{1 + \bar{k}_d \eta_f} \tag{3-18}$$

$$\lim_{\bar{k}_s \to \infty} \bar{\eta}_k = C_k \eta_f \tag{3-19}$$

$$\lim_{\bar{k}_s \to \infty} \bar{R}_k = C_k \tag{3-20}$$

Therefore, in this case, Eqs. (3-16) and (3-17) can respectively be written as:

$$\frac{\zeta_n}{x_c/L} = C_k R_f R_{sn} \frac{C_k \eta_f \eta_{sn} \eta_n}{1 + (C_k \eta_f \eta_{sn} \eta_n)^2} \tag{3-21}$$

$$\frac{\zeta_n^{max}}{x_d/L} = 0.5 C_k R_f R_{sn} \ \ at \ \ \eta_n^{opt} = \frac{1}{C_k \eta_f \eta_{\mathrm{sn}}} \tag{3-22}$$

In the case of a taut non-flexural cable, i.e. $\lambda^2 \to 0$ and $\varepsilon \ll 1$, the modification and reduction factors corresponding to the cable sag and bending stiffness effects would all become 1. Thus, the above equations can be reduced to:

$$C_k = \frac{1}{1 + \bar{k}_d} \tag{3-23}$$

$$\frac{\zeta_n}{x_d/L} = C_k \frac{C_k \eta_n}{1 + (C_k \eta_n)^2} = \frac{\eta_n}{1/{C_k}^2 + (\eta_n)^2} \tag{3-24}$$

$$\frac{\zeta_n^{max}}{x_d/L} = 0.5 C_k \ \ at \ \ \eta_n^{opt} = \frac{1}{C_k} \tag{3-25}$$

which are equivalent to the design formulas proposed by Shi et al. [67]. Therefore, the validity of the integrated stiffness coefficient formulated in Eq. (3-17), and the damping property of the damped cable predicted by Eqs. (3-15) and (3-16) are verified for the special case of a taut non-flexural cable with rigid damper support.

3.3.2. Hinged-hinged cable

In the case of a hinged-hinged cable, a similar approach is followed to obtain the design equation. An asymptotic solution to Eq. (3-11) can be derived for small values of cable bending stiffness, i.e. $4\varepsilon\beta_n^2 L^2 \ll 1$. In this case, the following approximations can be made [71]:

$$\gamma_a \cong \frac{r}{x_d} \;\; ; \;\; \gamma_b \cong \beta_n \;\; ; \;\; \gamma_a^2 + \gamma_b^2 \cong \left(\frac{r}{x_d}\right)^2 \;\; ;$$

$$\sinh(\gamma_a L) \cong \cosh(\gamma_a L) \gg 1 \;\; ; \tag{3-26}$$

$$\sinh(\gamma_a \bar{x}_d) \cong \cosh(\gamma_a \bar{x}_d) \cong e^{-r} \sinh(\gamma_a L)$$

After applying these approximations and dropping negligible terms of $\beta_n x_d / r^3$, Eq. (3-11) can be simplified to:

$$\frac{\widetilde{w}_d H}{\tilde{F}_d x_d} \cong \frac{\beta_n x_d \left[\tan\left(\frac{\beta_n L}{2}\right) - \tan\left(\frac{\beta_n x_d}{2}\right)\right]^2}{2[\tan\left(\frac{\beta_n L}{2}\right) - \frac{\beta_n L}{2} + \left(\frac{4}{\lambda^2}\right)\left(\frac{\beta_n L}{2}\right)^3} + \frac{1 - e^{-2r}}{2r} - 1 \tag{3-27}$$

Following the perturbation approach introduced by Krenk [70] and extended by Krenk and Nielsen [43], the wave number β_n of the damped cable can be assumed as:

$$\beta_n = \beta_{0n}^S + \Delta\beta_n \tag{3-28}$$

where $\Delta\beta_n$ is a small wave number perturbation due to the damper installation; and β_{0n}^S is the real-valued wave number of the undampe cable. In the case of small damper distance from the cable end, i.e. $x_d/L \ll 1$, the following approximations are valid for symmetric modes ($n = 1,3, \ldots$):

$$\begin{aligned} &\tan\left(\frac{\beta_n L}{2}\right) - \left[\frac{\beta_n L}{2} - \left(\frac{4}{\lambda^2}\right)\left(\frac{\beta_n L}{2}\right)^3\right] \\ &\qquad \cong \left[\tan^2\left(\frac{\beta_{0n}^S L}{2}\right) + \left(\frac{12}{\lambda^2}\right)\left(\frac{\beta_{0n}^S L}{2}\right)^2\right]\frac{\Delta\beta_n L}{2} \end{aligned} \tag{3-29}$$

$$\tan\left(\frac{\beta_n L}{2}\right) - \tan\left(\frac{\beta_n x_d}{2}\right) \cong \tan\left(\frac{\beta_{0n}^s L}{2}\right) - \frac{\beta_{0n}^s x_d}{2}$$

By substituting these expressions into Eq. (3-27) and simplifying, it yields:

$$\frac{\Delta\beta_n}{\beta_{0n}^s} \cong \frac{x_d}{L}\left(\frac{R_{sn}}{\frac{\widetilde{w}_d H}{\tilde{F}_d x_d} + 1 - \frac{1-e^{-2r}}{2r}}\right) \tag{3-30}$$

According to Eqs. (3-10) and (3-28), an asymptotic expression for the modal damping ratio can be expressed as:

$$\zeta_n = \frac{\mathrm{Im}[\beta_n]}{|\beta_n|} \cong \frac{\mathrm{Im}[\Delta\beta_n]}{\beta_{0n}^s} = \left(\frac{x_d}{L}\right) R_{sn}\,\mathrm{Im}\left[\frac{1}{\frac{\widetilde{w}_d H}{\tilde{F}_d x_d} + 1 - \frac{1-e^{-2r}}{2r}}\right] \tag{3-31}$$

By replacing $\widetilde{w}_d/\tilde{F}_d = (k_s + k_d + ic\sqrt{H/m}\,\beta_n)/[k_s(k_d + ic\sqrt{H/m}\,\beta_n)]$, considering $\beta_n \cong \beta_{0n}^s$, and calculating the imaginary part of the right-hand expression in Eq. (3-31), it becomes:

$$\frac{\zeta_n}{x_d/L} = R_{sn}\left\{\frac{\eta_{sn}\eta_n}{\left[\bar{k}_d\left(1 - \frac{1-e^{-2r}}{2r}\right) + \left(1 + \frac{\bar{k}_d}{\bar{k}_s}\right)\right]^2 + \left[\left(1 - \frac{1-e^{-2r}}{2r}\right) + \frac{1}{\bar{k}_s}\right]^2 \eta_{sn}^2\eta_n^2}\right\} \tag{3-32}$$

By adopting the same notation used for the refined damper design formula in Section 3.3.1, Eq. (3-32) can be further simplified in the form of damper design formula for a hinged-hinged cable:

$$\frac{\zeta_n}{x_d/L} = \tilde{R}_k \tilde{R}_f R_{sn} \frac{\tilde{\eta}_k \eta_{sn} \eta_n}{1 + (\tilde{\eta}_k \eta_{sn} \eta_n)^2} \tag{3-33}$$

where $\tilde{R}_f = 1/\tilde{\eta}_f$ and $\tilde{\eta}_f = 1 - q + 0.5rq^2$ reflect the effect of cable bending stiffness, and $\tilde{R}_k = C_k[\tilde{\eta}_f/(\tilde{\eta}_f + \frac{1}{\bar{k}_s})]$ and $\tilde{\eta}_k = C_k(\tilde{\eta}_f + 1/\bar{k}_s)$ are factors that represent the combined effects of cable bending stiffness, damper stiffness, and damper support stiffness.

It is observed that the damper design formula presented by Eq. (3-33) has the same form as the one for a fixed-fixed cable, i.e. Eq. (3-15). However, the $\tilde{R}_f$ and $\tilde{\eta}_f$ factors, which exert a reduction in the achievable modal damping ratio due to the cable bending stiffness, have been modified. In general, the factors related to the effect of cable bending stiffness can be expressed in a unified form for the studied boundary conditions as follows:

$$\begin{gathered} \eta_f = 1 - q + (0.5 - \alpha_{BC}) rq^2 \\ R_f = (1 - \alpha_{BC} q)^2 / \tilde{\eta}_f \end{gathered} \tag{3-34}$$

where $0 \leq \alpha_{BC} \leq 1$ is the boundary condition factor and is defined as:

$$\begin{gathered} \text{Fixed-fixed: } \alpha_{BC} = 1 \\ \text{Hinged-hinged: } \alpha_{BC} = 0 \end{gathered} \tag{3-35}$$

In other words, the damping ratio of the cable-damper system with a hinged-hinged boundary condition is less affected by the flexural rigidity of the cable than the fixed-fixed case. Given that the support condition of a real stay cable is in between these the two extreme end conditions, α_{BC} can be determined approximately by applying linear interpolation. For example, for a cable anchorage with 90% rotational fixity compared to

an ideal fixed-fixed condition, a value of $\alpha_{BC} = 0.9$ can be used in Eq. (3-34) to compute η_f and R_f.

3.4. Performance comparison between NSD, PSD and ZSD

To investigate the effect of damper stiffness on its performance, a parametric study is presented in this section. For this purpose, Eq. (3-15) is rewritten in the following form:

$$Y_n = \frac{X_n}{\left(\frac{1}{C_k}\right)^2 + \left(1 + \frac{1}{\bar{k}_s \eta_f}\right)^2 X_n^2} \tag{3-36}$$

where $Y_n = \zeta_n / [(x_d/L) R_f R_{sn}]$ is the normalized modal damping ratio which depends on the modified damping parameter $X_n = \eta_f \eta_{sn} \eta_n$, the ratio between the damper support stiffness and the damper stiffness $\bar{k}_s/\bar{k}_d$, and the product $\bar{k}_s \eta_f$. As can be seen from Eq. (3-17), the latter two are the governing parameters of the integrated stiffness coefficient C_k. It is noteworthy that for the special case of zero damper stiffness, $C_k = 1$ and Eq. (3-36) would reduce to $Y_n = X_n / \{1 + [1 + 1/(\bar{k}_s \eta_f)]^2 X_n^2\}$. The maximum value of Y_n is determined by differentiating Y_n in Eq. (3-36) with respect to X_n, which is:

$$Y_n^{max} = \frac{|C_k|}{2\left(1 + \frac{1}{\bar{k}_s \eta_f}\right)} \frac{|\Psi/(\Psi+1)|}{2\left(1 + \frac{1}{\bar{k}_s \eta_f}\right)} \; at \; X_n^{opt} = \frac{1}{|C_k|\left(1 + \frac{1}{\bar{k}_s \eta_f}\right)} \tag{3-37}$$

where $|\cdot|$ denotes the absolute value.

Figure 3-5 illustrates the variation of the normalized modal damping ratio Y_n as a function of X_n at four different values of $\bar{k}_s \eta_f$ when the damper stiffness is either positive or negative. The case of ZSD is also shown in the figure for reference. These curves depict

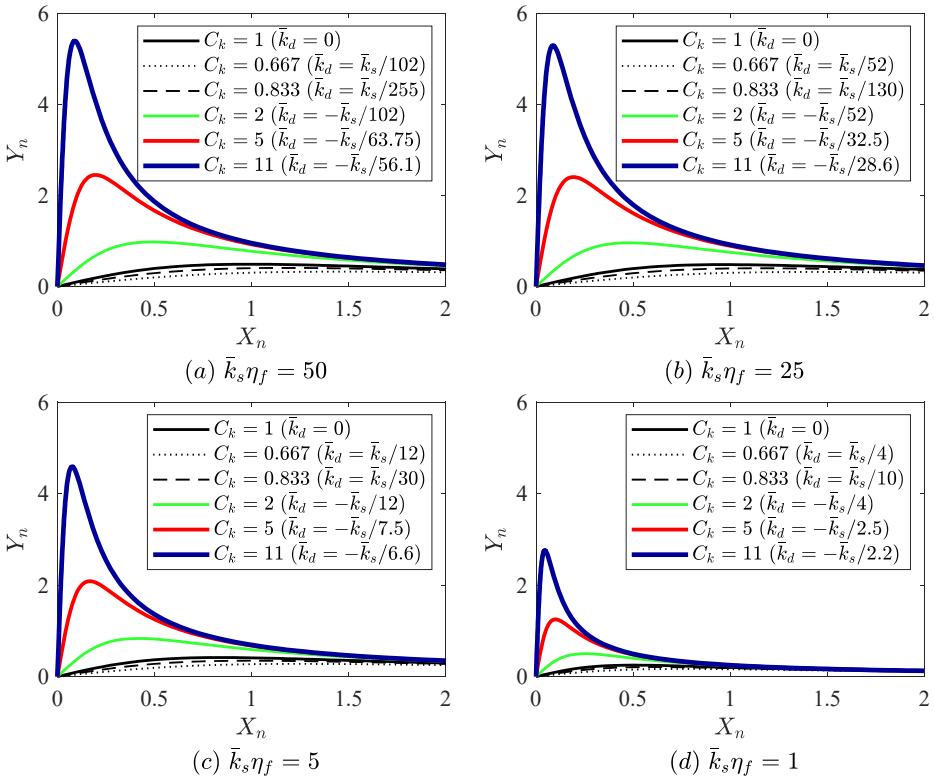

Fig. 3-5. Performance of viscous dampers with negative, zero and positive damper stiffness for different $\bar{k}_s\eta_f$ and C_k values based on normalized parameters X_n and Y_n.

the isolated role of damper stiffness (either positive or negative) in the n^{th} modal damping ratio of a cable-damper system. The optimum damper capacity, in terms of the damping coefficient c_{opt}, as well as the corresponding maximum achievable damping ratio ζ_n^{max} of a specific cable-damper system can be identified from the apex of the $Y_n - X_n$ curves. They can also be used to compare the efficiency of cable-damper systems as a function of their different mechanical properties. In Figs. 3-5(a-d), four representative $\bar{k}_s\eta_f$ values (i.e. 50, 25, 5 and 1) are selected whereas in each subplot, three NSD cases with $C_k = 11$, 5 and 2, two PSD cases with $C_k = 0.833$ and 0.667, and the ZSD case ($C_k = 1$) are considered for comparison. It should also be noted that the influences of the damper support stiffness k_s,

the damper location x_d and the cable length L, the cable chord tension H and the cable flexural rigidity EI are all present in the term $\bar{k}_s\eta_f$.

From Fig. 3-5, it is observed that the cable modal damping ratio in the two PSD cases is slightly smaller than that in the idealized ZSD case. As shown in Fig. 3-4, in the case of PSD, the integrated stiffness coefficient $0 < C_k < 1$, which, based on Eq. (3-37), would lead to a reduction of the maximum normalized modal damping ratio Y_n^{max}. Nevertheless, this reduction effect is not significant and may be neglected in practical applications. On the other hand, the cable modal damping ratio of all three NSD cases is substantially higher than that of the ZSD case. According to Eq. (3-17) and Fig. 3-4, for $\Psi < -1$, it would yield $C_k > 1$. Further, a more negative damper stiffness would correspond to a larger value of C_k, which, as reflected in Fig. 3-5, is the achievement of higher damping ratio (represented by Y_n) with a lower damping coefficient (represented by X_n).

It is learned from Eq. (3-37) that the maximum achievable damping of a damped cable is a function of $\bar{k}_d/\bar{k}_s$ as well as $\bar{k}_s\eta_f$. Therefore, the impact of these two parameters on the optimum performance of PSD and NSD, in terms of the maximum normalized modal damping ratio Y_n^{max}, is further studied in Figs. 3-6 and 3-7, respectively.

Figure 3-6 shows the variation of Y_n^{max} against $\bar{k}_s\eta_f$ for a PSD with $\bar{k}_d/\bar{k}_s = 0.005, 0.05$ and 0.2. The ZSD case is also shown for reference. It can be observed from Fig. 3-6(a) that the presence of a positive damper stiffness would decrease the amount of maximum achievable damping. For a given cable and a given damper support (both η_f and $\bar{k}_s$ remain as constants), using a PSD having more flexible stiffness (smaller $\bar{k}_d/\bar{k}_s$) would enhance the damper efficiency, which is consistent with the findings reported by Fournier and

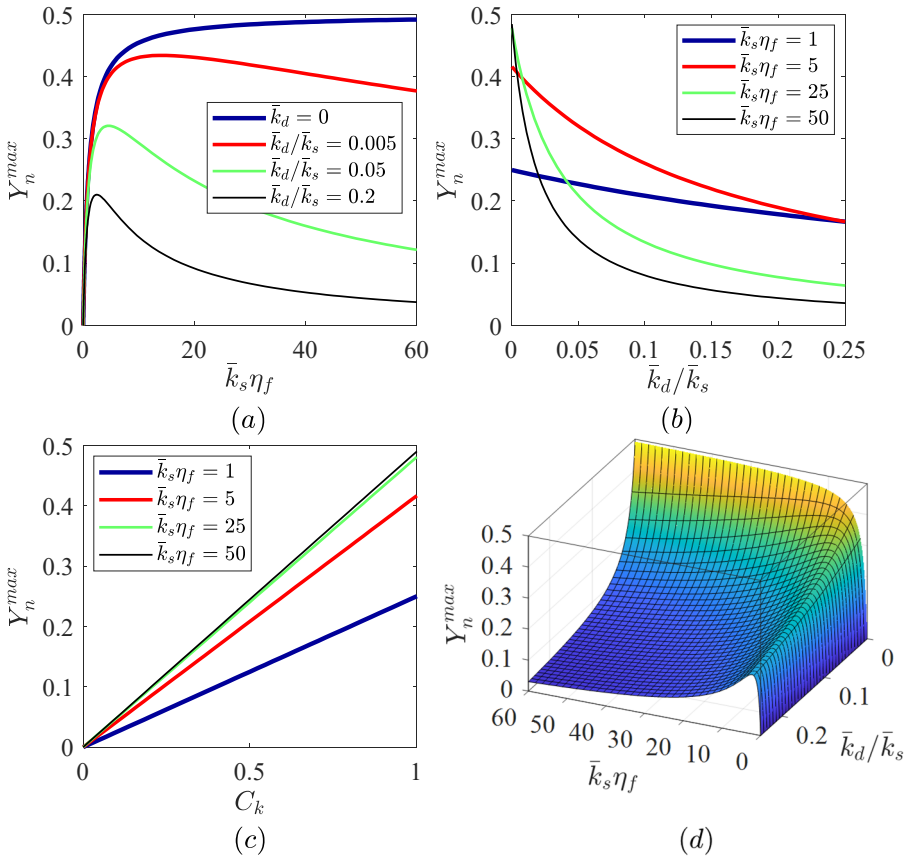

Fig. 3-6. Optimum performance of PSD and ZSD as a function of (a) $\bar{k}_s\eta_f$, (b) $\bar{k}_d/\bar{k}_s$, (c) C_k and (d) both $\bar{k}_s\eta_f$ and $\bar{k}_d/\bar{k}_s$.

Cheng [46]. In addition, it is interesting to note that the support stiffness $\bar{k}_s$ plays different roles in how $\bar{k}_d/\bar{k}_s$ and $\bar{k}_s\eta_f$ would influence the optimum performance of a PSD. If a damper support needs to be designed for a given damped cable (both η_f and $\bar{k}_d$ remain as constants), the pattern of the curves in Fig. 3-6(a) suggests that a more rigid damper support would yield a larger $\bar{k}_s\eta_f$ but a smaller $\bar{k}_d/\bar{k}_s$, which would either reduce or increase the maximum normalized modal damping ratio Y_n^{max}, with the effect of the latter being more dominant. Therefore, using a more rigid damper support would, overall, enhance the efficiency of PSD, which agrees with existing literature [46]. When the ratio between the damper stiffness and its support stiffness remains unchanged ($\bar{k}_d/\bar{k}_s$ remains constant),

there exists an optimum value of $\bar{k}_s\eta_f$, beyond which a further increase of $\bar{k}_s\eta_f$ would degrade the performance of a PSD. The optimum damper performance becomes less sensitive to $\bar{k}_s\eta_f$ if the stiffness of the damper support is much more rigid than that of the damper, i.e. smaller value of $\bar{k}_d/\bar{k}_s$.

Figure 3-6(b) describes how the optimum performance of a PSD would be influenced by the stiffness ratio $\bar{k}_d/\bar{k}_s$ at four different levels of $\bar{k}_s\eta_f$. Results show that for a given cable and a given damper support (both η_f and $\bar{k}_s$ remain constants), a PSD with more rigid damper stiffness, i.e. larger $\bar{k}_d/\bar{k}_s$, would decrease the efficiency of the damper. Again, this confirms the findings reported in [46]. Such an adverse effect becomes more obvious when $\bar{k}_s\eta_f$ increases.

The dependence of the maximum normalized modal damping ratio Y_n^{max} on the integrated stiffness coefficient C_k is portrayed in Fig. 3-6(c) for $\bar{k}_s\eta_f = 1, 5, 25$ and 50. For a given cable and a given damper support (both η_f and $\bar{k}_s$ remain as constants), a C_k range of 0 to 1 covers the variation of the damper stiffness from rigid to 0. It can be seen from the figure that for a PSD, Y_n^{max} would increase linearly with respect to C_k until it reaches $Y_n^{max} = 0.5/[1 + 1/(\bar{k}_s\eta_f)]$ at $C_k = 1$, which corresponds to the ZSD case. In addition, it is also found that the benefit of choosing larger $\bar{k}_s\eta_f$ to promote damper performance would fade out when $\bar{k}_s\eta_f$ is sufficiently large, say, greater than 25, as reflected in Fig. 3-6(c) that the two $Y_n^{max} - C_k$ curves corresponding respectively to $\bar{k}_s\eta_f = 25$ and $\bar{k}_s\eta_f = 50$ almost coincide with each other. The combined effect of the two governing parameters, $\bar{k}_s\eta_f$ and $\bar{k}_d/\bar{k}_s$, on the optimum performance of a PSD is shown as a performance surface in Fig. 3-6(d). The pattern of the surface clearly suggests that more flexible damper stiffness and

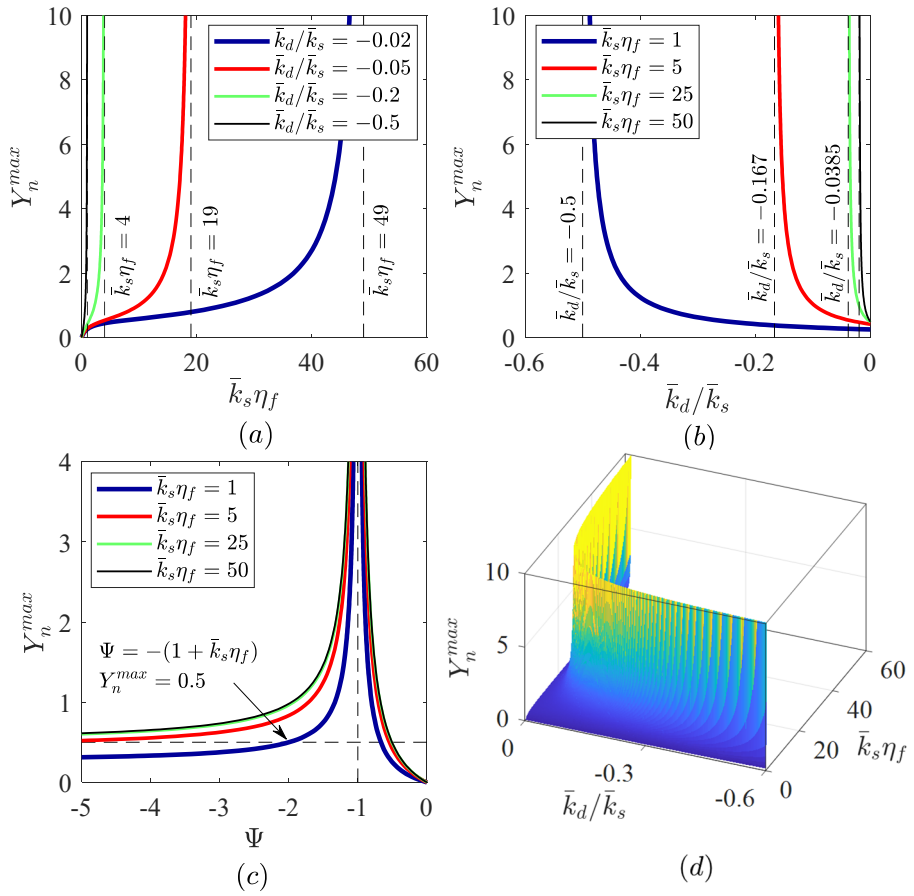

Fig. 3-7. Optimum performance of NSD as a function of (a) $\bar{k}_s\eta_f$, (b) $\bar{k}_d/\bar{k}_s$, (c) Ψ and (d) both $\bar{k}_s\eta_f$ and $\bar{k}_d/\bar{k}_s$.

more rigid damper support stiffness would enhance the energy dissipation capacity of a PSD.

The optimum performance of NSD is illustrated in Fig. 3-7. Figure 3-7(a) portrays the effect of $\bar{k}_s\eta_f$ on the maximum normalized modal damping ratio Y_n^{max} for four different stiffness ratios of $\bar{k}_d/\bar{k}_s = -0.02, -0.05, -0.2$ and -0.5, of which only the portion of the curves that satisfies $\Psi < -1$ are shown (refer to Fig. 3-4). The pattern of the curves in the figure indicates that for a given cable and a given damper support (both η_f and $\bar{k}_s$ remain constants), a smaller stiffness ratio $\bar{k}_d/\bar{k}_s$ resulted from a more negative damper stiffness

would lead to a larger Y_n^{max}. This suggests that using a NSD having more negative damper stiffness would be beneficial for the damper efficiency, on the condition that the stability requirement of the NSD holds. Based on Eq. (3-37), should $\bar{k}_s\eta_f = -1 - 1/(\bar{k}_d/\bar{k}_s)$, NSD would lose its stability and Y_n^{max} would approach to infinity. The margin of stability for the four studied stiffness ratios is shown in Fig. 3-7(a) as dotted lines. They occur respectively at $\bar{k}_s\eta_f = 49$, 19, 4 and 1 for $\bar{k}_d/\bar{k}_s = -0.02$, -0.05, -0.2 and -0.5. On the other hand, for a given cable (η_f remains as a constant), a more rigid damper support would correspond to larger $\bar{k}_s\eta_f$ and $\bar{k}_d/\bar{k}_s$. Although the effect of the former would promote the damper efficiency and that of the latter would degrade the damper performance, with the latter being dominant, using a more rigid damper support would thus have an adverse impact on the NSD performance, which is, interestingly, opposite to the PSD case.

Similarly, the benefit of using NSD with more negative damper stiffness can be observed from Fig. 3-7(b). For a given cable and a given damper support (both η_f and $\bar{k}_s$ remain constants), with the decrease of $\bar{k}_d$ value, i.e. the damper stiffness becomes more negative, Y_n^{max} would increase until when $\bar{k}_d$ reaches the stability bound defined by $\bar{k}_d/\bar{k}_s = -1/(1 + \bar{k}_s\eta_f)$, where the damper performance is unstable and Y_n^{max} approaches infinity. The four dotted lines at $\bar{k}_d/\bar{k}_s = -0.5$, -0.167, -0.0385 and -0.0196 in Fig. 3-7(b) define respectively the margin of stability for the cases of $\bar{k}_s\eta_f = 1$, 5, 25 and 50. The stability requirement of NSD will be discussed further in Chapter 5.

Figure 3-7(c) depicts the variation of Y_n^{max} with Ψ at $\bar{k}_s\eta_f = 1$, 5, 25 and 50. As discussed earlier, $\Psi = -1$ would induce instability of a NSD, which, as reflected in the figure, Y_n^{max}

would approach to infinity as Ψ tends to -1. The fact that there always exist two different Ψ values for the same optimum damper performance Y_n^{max}, i.e. one in the region of $\Psi < -1$ and the other in $-1 < \Psi < 0$, suggests two possible choices of negative damper stiffness in the NSD design. However, since the one associated to the region of $-1 < \Psi < 0$ would corresponding to a more negative damper stiffness, to avoid potential instability issue, it is recommended to choose that in the region of $\Psi < -1$. For a given Ψ (or in other words, C_k) value, a NSD is observed to have better performance at larger $\bar{k}_s\eta_f$. However, similar to the PSD case, Y_n^{max} becomes saturated once $\bar{k}_s\eta_f$ increases beyond a certain level, say $\bar{k}_s\eta_f > 25$. In addition, a lower bound for Ψ can be defined to ensure Y_n^{max}, which is $\Psi \geq -(1 + \bar{k}_s\eta_f)$. It is noteworthy that Y_n^{max} corresponds to the scenario of a ZSD with a rigid damper support. The combined effect of $\bar{k}_s\eta_f$ and $\bar{k}_d/\bar{k}_s$ on the effectiveness of NSD is shown as a performance surface for $\Psi < -1$ in Fig. 3-7(d). Clearly, in the case of NSD, using a damper with more negative damper stiffness and a more flexible support would enhance its performance.

The performance of PSD, ZSD and NSD devices has been demonstrated in Figs. 3-5 to 3-7. Results show that for a given cable and damper capacity (i.e. damping coefficient remains the same), the efficiency of the damper in controlling cable vibration would be governed by the damper stiffness and the damper support stiffness. While a combination of flexible damper stiffness and rigid support is preferred in the design of PSD; a more flexible support and more negative damper stiffness should be selected to promote the NSD efficiency as long as the stability requirement is satisfied. In addition, the maximum achievable damping ratio of the idealized ZSD case represents the performance upper bound of a PSD with the same damper capacity.

3.5. Evaluation of the asymptotic solution

In order to evaluate the accuracy of the proposed asymptotic solution to Eq. (3-6a), Eq. (3-15) is applied to predict the damping property of a cable-damper system studied by Fournier and Cheng [46]. The cable was set up horizontally and fixed at both ends. It had a length of $L = 9.33$ m, a unit mass of $m = 0.2$ kg/m, a diameter of $D = 4.65$ mm and a chord tension of $H = 3200$ N. A passive linear viscous damper with a damping coefficient of $c_d = 32.2$ N.s/m was designed to have variable damper stiffness (0, 280 N/m, and 600 N/m) and support stiffness (47300 N/m, 82000 N/m, and rigid). The efficiency of the damper was evaluated for a number of installation locations via experimental test and numerical simulation. In the current study, only the case of $x_d/\mathrm{L} = 0.06$ is selected for analysis. The system damping obtained from Eq. (3-15) is compared with the experimental and numerical results reported in [46], as well as with the numerical solution to Eq. (3-6a).

Figures 3-8(a) and 3-8(b) portray respectively the first modal damping ratio of the studied cable-damper system with and without the consideration of cable sag and bending stiffness effects. In both figures, the solid and the dashed line correspond to the asymptotic and the numerical solution to Eq. (3-6a), respectively, whereas the experimental and the numerical results by Fournier and Cheng [46] are shown by the markers. It can be seen from Fig. 3-8(a) that the first modal damping ratio of the damped cable yielded from the refined design formula, Eq. (3-15), is about 2% lower than the numerical solution and always lower than the experimental results. This implies that the proposed refined damper design formula would provide a relatively conservative and safe design which is desirable in engineering practice. On the other hand, the taut cable idealization is applied by assuming $\varepsilon = 10^{-7}$ and $\lambda^2 = 0.001$ (small cable bending stiffness and sag-extensibility) and the first modal

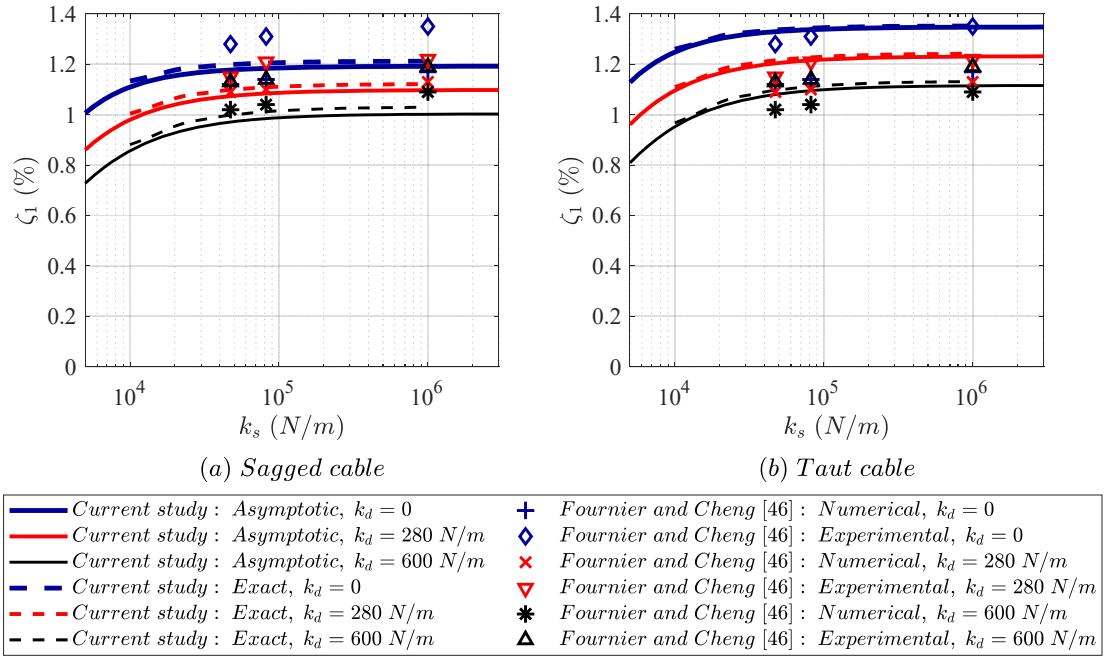

Fig. 3-8. Comparison of first modal damping ratio of a damped cable for equipped with a PSD of $c_d = 32.2$ N·s/m.

damping ratio of this system is shown in Fig. 3-8(b). In this case, although the damping ratio predicted by Eq. (3-15) is found to agree well with the experimental results when the damper stiffness is relatively small, i.e. $k_d \leq 280$ N/m, it could overestimate the experimental data when the damper is installed on more flexible support ($k_s \leq 47.3$ kN/m). Therefore, when applying the refined design formula to predict the damping property of a damped cable, the actual cable sag and bending stiffness should be considered to avoid the potential risk of unsafe design.

Figure 3-9 demonstrates how the introduction of negative damper stiffness could enhance the energy dissipation capacity of the above studied cable-damper system. The first modal damping ratio of the system obtained from the asymptotic (Eq. (3-15)) and the numerical solution to Eq. (3-6) is portrayed in Fig. 3-9(a) for three different levels of damper support stiffness, i.e. $k_s = 47.3$ kN/m, 82 kN/m and rigid. The k_d value corresponding to the

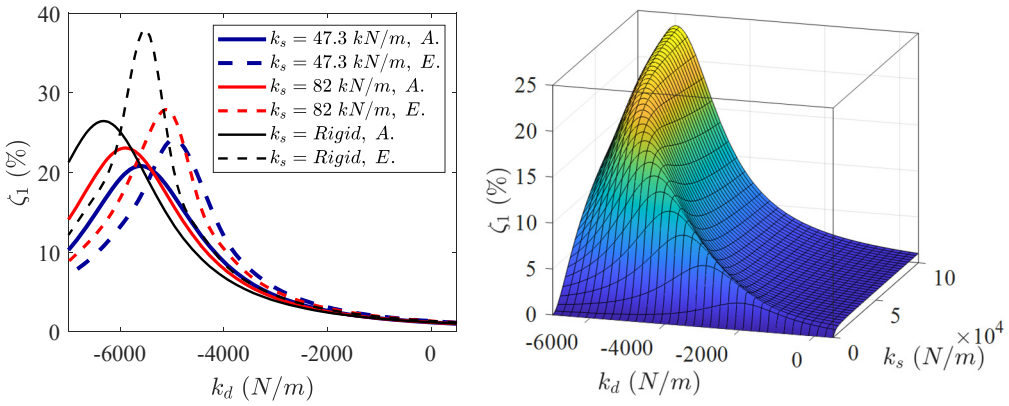

Fig. 3-9. Effect of damper stiffness on the damping property of a cable-damper system studied by Fournier and Cheng [46] for different damper support cases (PSD with $c_d = 32.2$ N·s/m) (A: Asymptotic, E: Exact).

apex of each $\zeta_1 - k_d$ curve defines the NSD stability requirement of the associated case. It is worth pointing out that since the damping coefficient $c_d = 32.2$ N.s/m is not close to zero, the maximum modal damping ratio is thus finite. It can be seen from Fig. 3-9(a) that for a given damper support stiffness, as far as the damper stiffness satisfies the stability requirement defined by the numerical solution, the first modal damping ratio predicted by the asymptotic solution is always less than that by the numerical solution. This implies that Eq. (3-15) can be safely used in the design of NSD having negative damper stiffness within the stable range. To have a clearer picture on how the damping property of the studied cable would be affected when equipped with a PSD or a NSD resting on a finite stiffness support, the variation trend of its first modal damping ratio with respect to the damper stiffness and the damper support stiffness is shown in Fig. 3-9(b) based on Eq. (3-15). It is evident that the presence of negative damper stiffness would significantly enhance the energy dissipation capacity of the system.

3.6. Design example

In this section, a design example is presented to further illustrate the application of the proposed refined design formula for designing viscous dampers with positive stiffness. An empirical formula for designing viscous damper to suppress cable vibrations was proposed by Fournier and Cheng [46] based on experimental test and numerical simulation, which took into account the effect of the damper stiffness and damper support stiffness. One of the application examples in that study considered the AS18 stay cable on the Fred Hartman Bridge [27], in which a viscous damper was needed to control rain-wind-induced vibrations. The cable had a length of $L = 112.28$ m, a diameter of $D = 160$ mm, a unit mass of $m = 52.9$ kg/m and a chord tension of $H = 2732$ kN.

It was assumed that the damper would be installed at $x_d = 0.02L$ from the cable lower anchorage with its size being selected based on its optimum performance associated with the first mode of the cable. If after installing the damper, the bridge owner further requested the damper to be concealed in a tube for aesthetic reasons, what should be the requirement of the tube stiffness? What if the damper itself was measured to have a stiffness of $k_d = 25$ kN/m? Investigate the respective optimum damper capacity for these two scenarios. In the current example, the design will be revisited by applying the proposed refined damping estimation formula.

In practice, to suppress rain-wind-induced cable vibrations, it is recommended that the Scruton number S_c should satisfy the condition $S_c = [m\zeta/(\rho D^2)] > 10$ [93], where m is the cable mass per unit length, ζ is the cable damping ratio, ρ is the air density, and D is the cable diameter. By assuming $\rho = 1.29$ kg/m^3, the minimum required cable damping

ratio would be 0.624%. In other words, it requires the first modal damping ratio of the cable to be $\zeta_1 \geq 0.624\%$.

If the proposed refined damping estimation formula, Eq. (3-16), is applied to conduct the design, the reduction factors in this equation can be calculated through the following steps:

1. For an elastic modulus $E = 200$ GPa [27] and an inclination angle $\theta = 35.3°$ [94], the non-dimensional cable bending stiffness parameter ε and the sag parameter λ^2 of the cable can be computed as $\varepsilon = EI/(HL^2) = 1.87 \times 10^{-4}$ and $\lambda^2 = (8d/L)^2[LEA/(HL_e)] \approx (8d/L)^2(EA/H) = 0.446$.
2. The auxiliary bending stiffness coefficients are $r = (x_d/L)/\sqrt{\varepsilon} = 1.46$ and $q = (1 - e^{-r})/r = 0.525$, so the modification factor of the non-dimensional damper parameter η_n (here, $n = 1$) due to the effect of cable flexural rigidity is $\eta_f = 1 - q - 0.5rq^2 = 0.273$.
3. The wave number of a sagged, non-flexural cable without damper can be determined from Fig. 3-2(a), which is $\beta_{01}^s = 0.0284$.
4. Based on Fig. 3-2(b), the reduction factor reflecting the influence of the cable sag on the maximum achievable damping ratio of the cable-damper system is $R_{s1} = 0.963$.
5. The reduction factors representing the combined stiffness effects of the cable, the damper and the support, as well as the cable bending stiffness on the maximum achievable damping ratio respectively are $\bar{R}_k = 0.273C_k/(0.273 + 1/\bar{k}_s)$ and $R_f = (1 - q)^2/\eta_f = 0.826$.

Since the minimum required cable modal damping ratio for the first mode is 0.624%, Eq. (3-16) can be used to determine the required tube stiffness for the two specified scenarios.

3.6.1. Zero damper stiffness ($k_d = 0$)

Application of Eq. (3-16) would yield $\bar{k}_s \geq 13.4$. Therefore, the minimum required axial stiffness for the damper tube is determined as $k_{s,min} = \bar{k}_s H/x_d = 16.3$ MN/m. If a tube with an outside diameter of 160 mm, a thickness of 10 mm and an elastic modulus of 2.5 GPa is to be used, the maximum allowable tube length would be $L_{max} = AE_{tube}/k_{s,min} = 0.72$ m. Finally, the optimum damping coefficient of the damper is computed as ${\eta_1}^{opt} = 1/(\bar{\eta}_k \eta_{s1}) = 1/[C_k(\eta_f + 1/\bar{k}_s)\beta_{01}^s L/\pi] = 2.833$, which gives $c_{d,opt} = 542$ kN·s/m.

The design formula provided by Huang and Jones [45], based on a taut cable assumption, a zero damper stiffness and a linear damper support stiffness in the mechanical model of the damped cable, can also be utilized to obtain the required tube stiffness. By using $[\zeta_n/(x_d/L)]_{max} = 1/[2(1 + 1/\bar{k}_s)]$, it is found that $\bar{k}_s \geq 1.66$. This is about 12% of the calculated value from the refined design formula ($\bar{k}_s \geq 13.4$). Therefore, neglecting the bending stiffness effect in particular can result in an unsatisfactory design.

3.6.2. Positive damper stiffness ($k_d = 25$ kN/m)

The normalized damper stiffness $\bar{k}_d$ and the integrated stiffness coefficient C_k are calculated as $\bar{k}_d = k_d x_c/H = 0.021$ and $C_k = 1 - 1/[1 + (\bar{k}_s/0.021)/(1 + 0.273\bar{k}_s)]$. After substituting into Eq. (3-16), it gives:

$$\frac{{\zeta_1}^{max}}{x_d/L} = 0.5\bar{R}_k R_f R_{s1} \geq 0.0312$$

which yields $\bar{k}_s \geq 13.8$. Therefore, the minimum required axial stiffness of the tube and the optimum damping coefficient of the damper in this case can be determined respectively as $k_{s,min} = 16.8$ MN/m and $c_{d,opt} = 549.4$ kN·s/m.

To assess the impact of the cable bending stiffness and sag on the damper performance, the minimum required damper support stiffness and the optimum damper capacity of the above two scenarios are re-analyzed by neglecting the cable bending stiffness and sag. Assume small values of ε and λ^2, i.e., $\varepsilon = 10^{-7}$ and $\lambda^2 = 0.001$, the reduction factors in Eq. (3-16) are recalculated as $R_{s1} = 1$, $R_f = 0.992$ and $\bar{R}_k = 0.976C_k/(0.976 + 1/\bar{k}_s)$. To satisfy the minimum required first modal damping ratio of 0.624%, Eq. (3-16) will give $\bar{k}_s \geq 1.74$, i.e. $k_{s,min} = 2.12$ MN/m and $c_{d,opt} = 123.4$ kN·s/m for the case of ZSD; and $\bar{k}_s \geq 1.89$, or $k_{s,min} = 2.30$ MN/m and $c_{d,opt} = 131$ kN·s/m for the case of $k_d = 25$ kN/m.

Table 3-1 summarizes the results of the current design example. For comparison, the design based on the empirical formula by Fournier and Cheng [46] are also presented in the table. The data in the two rightmost columns of Table 3-1 give the first modal damping ratio ζ_1 of the damped cable, which are obtained by plugging respectively the designed values of $k_{s,min}$ and c_{opt} yielded from the current study and Fournier and Cheng [46] into Eq. (3-6a) and numerically solve it for the complex wave number β_1, and then using Eq. (3-10) to obtain the ζ_1. For example, in the case of a sagged cable with $k_d = 0$, the current study requires $k_{s,min} = 16.3$ MN/m and $c_{d,opt} = 542$ kN·s/m, based on which the numerical first modal damping ratio is determined to be 0.644%. Compared to the target damping

Table 3-1. Summary of the design example results.

Deign case	Minimum required damper support stiffness $k_{s,min}$ (MN/m)		Optimum damping coefficient $c_{d,opt}$ (kN · s/m)		Modal damping ratio ζ_1 based on Eq. (3-6)	
	Current study	Fournier and Cheng [46]	Current study	Fournier and Cheng [46]	Design by current study	Design by Fournier and Cheng [46]
Actual ε and λ^2 $k_d = 0$	16.3	-	542	-	0.644% (3.21%)	-
Actual ε and λ^2 $k_d = 25$ kN/m	16.8	-	549.4	-	0.644% (3.21%)	-
ε and $\lambda^2 \ll 1$ $k_d = 0$	2.12	6.93	123.4	189.3	0.633% (1.44%)	0.849% (36.1%)
ε and $\lambda^2 \ll 1$ $k_d = 25$ kN/m	2.30	7.21	131	190.3	0.633% (1.44%)	0.837% (34.1%)

ratio of 0.624%, the current design would result in a damping ratio 3.21% higher than that required. This percentage difference between the numerical and the target first modal damping ratio is shown in the parentheses below the corresponding numerical solution in the table. As can be seen from Table 3-1, the error is as low as 1.44% when the cable sag and bending stiffness are neglected, and 3.21% when the actual sag and bending stiffness parameters are considered. In both cases, the design based on the proposed refined damping estimation formula is slightly conservative and on the safe side. The design based on the empirical formula proposed by Fournier and Cheng [46] is much more conservative. The selected damper support stiffness and optimum damper capacity could yield a cable first modal damping ratio up to 36.1% higher than that required. This is believed to be mainly due to the fact that the empirical damper design formula in [46] was developed based on the taut and non-flexible cable assumption.

Therefore, results in Table 3-1 confirm the importance of including the cable bending stiffness and sag effects in evaluating the performance of a damped cable and providing a more cost-effective design [43]. It should be noted that according to Tabatabai and Mehrabi [24], more than 95% of the stay cables on site have a sag parameter $\lambda^2 < 1$. Thus, the impact of the cable sag effect on the attainable damping ratio of a damped cable is negligible when compared to that of the cable bending stiffness. On the other hand, if Fujino and Hoang's design formula [71] is applied to the PSD ($k_d = 25$ kN/m) case, it would lead to an underestimation of the required damper support stiffness by up to 3%, i.e. 16.3 MN/m instead of 16.8 MN/m, which is not desirable. It is worth mentioning that the damper design formula developed by Fujino and Hoang [71] does not address the effect of damper stiffness and is equivalent to set $C_k = 1$ in Eq. (3-16).

3.6. Summary

In this chapter, an analytical study has been conducted to refine existing viscous damper design formulas for cable vibration control, where the effect of the damper stiffness has been considered in the selection of optimum damper size and the prediction of the corresponding maximum achievable damping of a damped cable by introducing the integrated stiffness coefficient C_k. Both the fixed-fixed and the hinged-hinged boundary conditions have been considered. Besides allowing the evaluation of the damper stiffness' influence, the term C_k enables studying the combined effects of the damper stiffness, damper support stiffness and cable bending stiffness on the damper performance. This refinement not only leads to a more accurate design of conventional passive viscous dampers having positive damper stiffness (PSD), but more importantly, extends its application to the design of negative stiffness dampers (NSD). An analytical model of a

general cable-damper system has been developed, of which the effect of cable sag and cable flexural stiffness are considered in modeling the cable behaviour, and the mechanical model of the viscous damper takes into account the effect of both the damper stiffness and damper support stiffness. Besides seeking a numerical solution to the system equation of motion, an asymptotic solution has also been derived to predict the damping property of a damped cable. One design example has been presented to illustrate the application of the proposed refined damper design tool in designing passive viscous dampers having positive stiffness. Compared to the numerical solution, the proposed refined damper design tool would give a slightly conservative prediction of the optimum damper size and the maximum achievable system damping ratio, which would yield a safe design in practice.

Chapter 4 Numerical Study on the Dynamic Response of a Damped Cable

4.1. Introduction

In this chapter, a control-oriented numerical model is developed to obtain the dynamic response of a stay cable equipped with a transverse damper/actuator for both fixed-fixed and hinged-hinged cable end conditions. The basis of this model is the improvement of the Mode Superposition Method (MSM) using the static correction technique. A new shape function set that consists of two parts was developed. The first part would be a static correction term and defined as the exact static displacement profile of a horizontal sagged cable subjected to a point load at the damper location, and the second part would be a series of sinusoidal functions, which, in the case of fixed-fixed ends, would be modified to be conformable to the boundary conditions. The effects of the cable sag and bending stiffness are included, and the exact expression of the cable self-weight profile corresponding to the fixed-fixed boundary condition is used in the formulation. This would provide a more efficient and accurate computational model that is not only applicable to conventional passive damper design, but also to the semi-active/active control design. The accuracy and numerical efficiency of the proposed control-oriented model are evaluated through numerical design examples of both passive and semi-active/active control. The performance of and the results obtained from the proposed model are compared with those of other existing models.

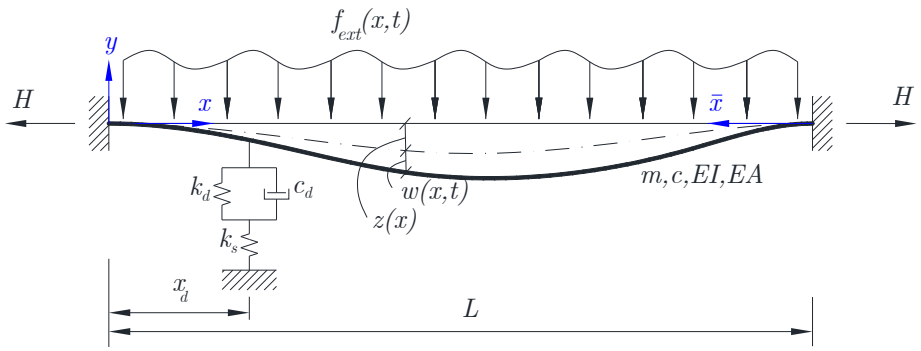

Fig. 4-1. Mechanical model of a shallow-flexural cable equipped with a transverse viscous damper.

4.2. Dynamic response of a uniform cable equipped with a transverse damper

4.2.1. Equation of motion

Figure 4-1 illustrates a horizontal uniform stay cable equipped with a transverse external damper. The x-axis is along the cable chord direction and the y-axis is in the vertical (in-plane) direction. In this figure, $z(x)$ and $w(x,t)$ represent the cable static displacement due to its self-weight and the cable dynamic in-plane motion, respectively. The cable boundary condition can be either hinged-hinged or fixed-fixed with the latter case shown. In this figure, L denotes the cable length, m is the mass per unit cable length, c is the inherent damping coefficient per unit cable length, EI is the cable flexural rigidity and H is the horizontal component of the static cable tension. The damper is located at a distance of x_d from the left support and its behaviour follows the illustrated mechanical model, with a damping coefficient c_d, a damper stiffness k_d and a damper support stiffness k_s.

After dropping the second order terms in the equilibrium equation of a cable element [79], the dynamic in-plane motion, $w(x,t)$, of a damper-equipped cable is governed by the following partial integro-differential equation:

$$m\ddot{w} + c\dot{w} + EIw^{(IV)} - Hw'' - h(t)z'' = f_{ext}(x,t) - F_d(t)\delta(x - x_d) \qquad (4\text{-}1)$$

where $h(t)$ is the additional cable tension due to its dynamic motion; $f_{ext}(x,t)$ is the external distributed force applied at position x, at a given time t; $F_d(t)$ is the damper force; and $\delta(\cdot)$ denotes the Dirac delta function. For this cable, the static displacement due to its self-weight, denoted as $z(x)$, is governed by the following ordinary differential equation, which is obtained by dropping all the time-dependent terms in Eq. (4-1):

$$EI\frac{d^4z}{dx^4} - H\frac{d^2z}{dx^2} = -mg \qquad (4\text{-}2)$$

By solving Eq. (4-2), $z(x)$ is obtained as:

$$z(x) = c_1e^{bx} + c_2e^{-bx} + c_3x^2 + c_4x + c_5 \qquad (4\text{-}3)$$

where coefficients c_1 to c_5 are functions of the cable characteristics $a = mg/(EI)$, $b = \sqrt{H/(EI)}$ and L. Table 4-1 lists these coefficients for the hinged-hinged and the fixed-fixed boundary conditions. For the hinged-hinged case, Eq. (4-3) can be accurately approximated by the parabolic profile $z(x) = c_3x^2 + c_4x = [mgL/(2H)]x(x/L - 1)$, since $c_1e^{bx} + c_2e^{-bx} + c_5 \approx 0$ for typical values of H and EI in the case of full scale bridge stay cables. Therefore, this approximated parabolic self-weight profile will be used in the current study to evaluate the dynamic response of a damped hinged-hinged cable. On the other hand, the exponential terms $c_1e^{bx} + c_2e^{-bx}$ are essential to portray the self-weight profile of a fixed-fixed cable and hence shall be considered in the formulation.

The additional cable tension, $h(t)$, due to the dynamic motion is derived based on the geometric and elastic properties of the cable and is expressed to the first order as:

Table 4-1. Coefficients of the cable self-weight profile $z(x)$ in Eq. (4-3).

Coefficient	End condition	
	hinged-hinged	fixed-fixed
c_1	$-a/[b^4(1+e^{bL})]$ *	$aL/[2b^3(1-e^{bL})]$
c_2	$-a/[b^4(1+e^{-bL})]$	$-aL/[2b^3(1-e^{-bL})]$
c_3	$a/(2b^2)$	$a/(2b^2)$
c_4	$-aL/(2b^2)$	$-aL/(2b^2)$
c_5	a/b^4	$aL\,coth(\,bL/2)/(2b^3)$

* $a = mg/(EI)$; $b = \sqrt{H/(EI)}$

$$h(t) = -\lambda^2[(H/L)^3/(mg)^2]\int_0^L z''w(x,t)dx \tag{4-4}$$

where λ^2 is the non-dimensional Irvine's parameter defined as $\lambda^2 = (mgL/H)^2 LEA/(HL_e)$, and $L_e = \int_0^L [1+(dz/dx)^2]^{3/2}dx \approx L$ is the cable stretched length [79]. Equations (4-3) and (4-4) are then substituted into Eq. (4-1) to form the governing partial integro-differential equation of the cable. In the following sections, different approaches for solving this equation are discussed.

4.2.2. Enhanced shape functions

The Mode Superposition Method (MSM) is an efficient method for evaluating the dynamic response of continuous linear systems. In this method, the transverse cable displacement, $w(x,t)$, is approximated by the following finite series:

$$w(x,t) = \sum_{i=1}^{n} \phi_i(x)\, q_i(t) \tag{4-5}$$

where $\phi_i(x)$ $(i = 1 \text{ to } n)$ are the shape functions that satisfy all the kinematic boundary conditions and are typically the mode shapes of the studied system; $q_i(t)$ $(i = 1 \text{ to } n)$ are the generalized coordinates and n is the number of considered shape function terms (or modes). Since only a limited number of vibrational modes are used in MSM, and the effect of the truncated higher modes on the system dynamic response is assumed to be negligible, the truncation induces error in the analysis results by MSM. However, this error can be compensated by introducing a static correction term into Eq. (4-5) [83].

Johnson et al. [57,95] adopted the static correction technique to improve the convergence rate of the MSM in determining the dynamic response of a damped hinged-hinged cable. The authors considered the static displacement profile of the cable, when subjected to a point load at the damper location, as one of the shape function terms (the static correction term). Results showed that by adding this term, the number of modes (n) required to achieve a desired accuracy in the cable dynamic response would be substantially reduced. This static correction term not only accounts for the effect of the truncated higher modes, but also reflects the presence of the damper and thus substantially increases the convergence rate. In their study on a hinged-hinged cable, combining this static profile term with 20 sine terms, i.e. a total of 21 terms, Johnson et al. [57] showed that an accuracy comparable to the case of using several hundreds of sine-only terms can be achieved. The authors derived an approximate expression for the cable static displacement profile, the effect of such an approximation needs to be assessed. In the current study, the same methodology is utilized by deriving the exact static displacement profile of a cable in the form of analytical solution of the governing integro-differential equation. Furthermore, in the case of a fixed-fixed cable, the sine function terms would be modified to adapt to the

boundary conditions. The static correction term and the adapted sine function terms will be derived in the next subsections.

4.2.2.1. Static correction term

The static correction term used in the current study is the static displacement profile of a cable subjected to a point load at the damper location. Assume the cable in Fig. 4-1 is subjected to a point load, P, at the damper location $x = x_d$. By neglecting the temporal terms in Eq. (4-1), the resulted static displacement, $v(x)$, is governed by the following ordinary integro-differential equation:

$$EI\frac{d^4v}{dx^4} - H\frac{d^2v}{dx^2} + \Psi\frac{d^2z}{dx^2} = P\delta(x - x_d) \tag{4-6}$$

where $\Psi = \lambda^2[(H/L)^3/(mg)^2]\left[\int_0^L z''v(x)dx\right]$ and $z(x)$ is the self-weight profile of the cable defined in Eq. (4-3). By dividing the cable into two parts on the left and right side of the point load (damper location), the general solution to Eq. (4-6) can be expressed by two terms for each side of the cable as follows:

$$v_L(x) = (c_{1L} + c_{2L}x)e^{bx} + (c_{3L} + c_{4L}x)e^{-bx} + c_{5L}x^2 + c_{6L}x + c_{7L} \tag{4-7a}$$

$$v_R(\bar{x}) = (c_{1R} + c_{2R}\bar{x})e^{b\bar{x}} + (c_{3R} + c_{4R}\bar{x})e^{-b\bar{x}} + c_{5R}\bar{x}^2 + c_{6R}\bar{x} + c_{7R} \tag{4-7b}$$

where $\bar{x} = L - x$ and $b = \sqrt{H/(EI)}$. The coefficients c_{1L} to c_{7L} (left side) and c_{1R} to c_{7R} (right side) contain a total of eight unknowns and are functions of m, L, H, λ^2, EI, x_d, the magnitude of the applied load, P, and the boundary conditions. The coefficients are explicitly determined through the following steps:

Table 4-2. Conditions of the static cable displacement profile.

Condition type	Expression
Boundary condition	$v_L(0) = 0$, $v_R(0) = 0$ $v_L^{'}(0) = 0$, $v_R^{'}(0) = 0$ (fixed-fixed cable) $v_L^{''}(0) = 0$, $v_R^{''}(0) = 0$ (hinged-hinged cable)
Compatibility condition	$v_L(x_d) = v_R(\bar{x}_d)$ $v_L^{'}(x_d) = v_R^{'}(\bar{x}_d)$ $v_L^{''}(x_d) = v_R^{''}(\bar{x}_d)$
Equilibrium condition	$EI[v_L^{'''}(x_d) - v_R^{'''}(\bar{x}_d)] = P$

1. Determine the coefficients ($c_{1L} - c_{7L}$ and $c_{1R} - c_{7R}$) as a function of Ψ by applying the kinematic and equilibrium conditions to both cable parts. These conditions are summarized in Table 4-2.
2. Substitute the coefficients determined in step 1 into Eqs. (4-7a) and (4-7b) to obtain $v_L(x)$ and $v_R(x)$ as a function of Ψ. Evaluate the expression $\Psi = \lambda^2[(H/L)^3/(mg)^2]\left[\int_0^L z^{''}v(x)dx\right]$ and expand the integral, it yields:

$$\Psi = \lambda^2[(H/L)^3/(mg)^2]\left[\int_0^{x_d} z^{''}v_L(x)dx + \int_0^{\bar{x}_d} z^{''}v_R(\bar{x})d\bar{x}\right] = f(\Psi)$$

3. Find Ψ by solving $f(\Psi) - \Psi = 0$.
4. Substitute Ψ into the coefficients to determine their explicit expression.

After determining all the coefficients in Eqs. (4-7a) and (4-7b) for a fixed-fixed or a hinged-hinged cable, the exact static displacement profile is used to define the static correction term as follows:

$$\phi_0(x) = \begin{cases} v_L(x) & x \le x_d \\ v_R(L-x) & x > x_d \end{cases} \tag{4-8}$$

4.2.2.2. Adapted sinusoidal terms

The conventional sinusoidal terms can be used as shape functions in the MSM for a hinged-hinged cable since they satisfy the kinematic boundary condition. However, in the case of a fixed-fixed cable, each of the outer ends of the sine functions needs to be replaced with a proper polynomial to adapt to the end constraints. Therefore, the following set of shape functions is proposed:

$$\begin{matrix} \phi_i(x) = \\ (i = 1,2,\dots) \end{matrix} \begin{cases} \tilde{c}_1 x^6 + \tilde{c}_2 x^5 + \tilde{c}_3 x^4 + \tilde{c}_4 x^3 + \tilde{c}_5 x^2 & x \le \underset{\sim}{L} \\ \sin(ax) & \underset{\sim}{L} < x \le L - \underset{\sim}{L} \\ (-1)^{i-1}(\tilde{c}_1 \bar{x}^6 + \tilde{c}_2 \bar{x}^5 + \tilde{c}_3 \bar{x}^4 + \tilde{c}_4 \bar{x}^3 + \tilde{c}_5 \bar{x}^2) & x > L - \underset{\sim}{L} \end{cases} \tag{4-9}$$

where $\bar{x} = L - x$, $a(i) = -i\pi/L$, $\underset{\sim}{L}(i) = L/(2i)$ and the polynomial coefficients are determined to maintain the consistency at the boundaries:

$$\tilde{c}_1 = -(\underset{\sim}{L}^4 a^4 - 36\underset{\sim}{L}^2 a^2 + 120)/(24\underset{\sim}{L}^6) \qquad \tilde{c}_2 = (\underset{\sim}{L}^4 a^4 - 42\underset{\sim}{L}^2 a^2 + 144)/(6\underset{\sim}{L}^5)$$

$$\tilde{c}_3 = -(\underset{\sim}{L}^4 a^4 - 50\underset{\sim}{L}^2 a^2 + 180)/(4\underset{\sim}{L}^4) \qquad \tilde{c}_4 = (\underset{\sim}{L}^4 a^4 - 60\underset{\sim}{L}^2 a^2 + 240)/(6\underset{\sim}{L}^3)$$

$$\tilde{c}_5 = -(\underset{\sim}{L}^4 a^4 - 72\underset{\sim}{L}^2 a^2 + 360)/(24\underset{\sim}{L}^2)$$

In Eq. (4-9), the two outer boundaries of the sine function are substituted by polynomial functions that satisfy both the fixed-fixed boundary condition and the continuity condition at $x = \underset{\sim}{L}$ and $x = L - \underset{\sim}{L}$. For the hinged-hinged case, the conventional sine functions $\phi_i(x)\sin(ax)$ with $(i = 1,2,\dots)$ can be directly used as shape functions without any

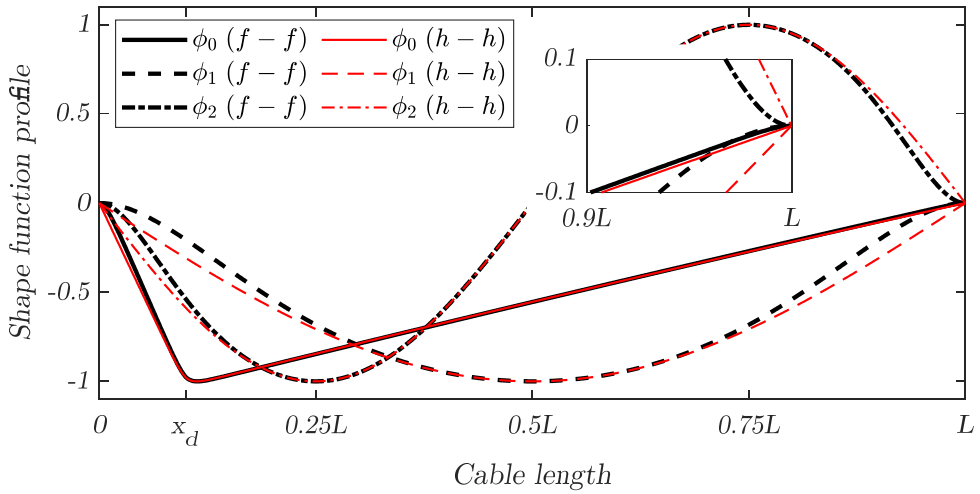

Fig. 4-2. Proposed shape functions for a damped cable (f-f: fixed-fixed; h-h: hinged-hinged).

modification. The static correction term and the conventional/adapted sinusoidal terms are then combined to construct the final shape function vector which can be used in the alternative form of Eq. (4-5), as given below:

$$\{\phi(x)\}_{n\times 1} = \left\{ \underbrace{\phi_0(x)}_{\substack{\text{static}\\ \text{correction}\\ \text{term}}} \quad \underbrace{\phi_1(x) \ \cdots \ \phi_{n-1}(x)}_{\substack{\text{conventional/adapted}\\ \text{sinusoidal}\\ \text{terms}}} \right\}^T \tag{4-10a}$$

$$w(x,t) = \sum_{i=0}^{n-1} \phi_i(x)\, q_i(t) \tag{4-10b}$$

where $\phi_0(x)$ and $q_0(t)$ are the static correction term and its corresponding generalized coordinate, respectively. Figure 4-2 illustrates the proposed shape function, where the normalized static displacement profile $\phi_0(x)$ and the first two sine terms $\phi_1(x)$ and $\phi_2(x)$ are shown for both the fixed-fixed and the hinged-hinged cases of a sample cable.

4.2.3. Mode Superposition Method (MSM) for a damped cable

The matrix form of the equation of motion is derived by substituting Eq. (4-5) into Eq. (4-1), then multiplying all terms by $\phi_j(x)$ and integrating over the cable length:

$$\boldsymbol{M}\{\ddot{q}\} + \boldsymbol{C}\{\dot{q}\} + \boldsymbol{K}\{q\} = \{F_{ext}\} - F_d(t)\{\phi(x_d)\} \tag{4-11}$$

where $\boldsymbol{M} = [m_{ij}]_{n\times n} = m[\int_0^L \phi_i(x)\phi_j(x)dx]$ is the modal mass matrix; $\boldsymbol{C} = [c_{ij}]_{n\times n} = (c/m)\boldsymbol{M}$ is the modal damping matrix; $\boldsymbol{K} = \boldsymbol{K}^s + \boldsymbol{K}^t + \boldsymbol{K}^b$ is the modal stiffness matrix, which consists of three stiffness sources, namely $\boldsymbol{K}^s = [k_{ij}^s]_{n\times n} = \lambda^2\,((H/L)^3/(mg)^2)[\int_0^L z''(x)\phi_i(x)dx \int_0^L z''(x)\phi_j(x)dx]$ as the contribution from the additional cable tension due to its sag, $\boldsymbol{K}^t = [k_{ij}^t]_{n\times n} = -H[\int_0^L \phi_i''(x)\phi_j(x)dx] = H[\int_0^L \phi_i'(x)\phi_j'(x)dx]$ as the contribution from the cable tension and $\boldsymbol{K}^b = [k_{ij}^b]_{n\times n} = EI[\int_0^L \phi_i^{(iv)}(x)\phi_j(x)dx] = EI[\int_0^L \phi_i''(x)\phi_j''(x)dx]$ as the contribution from the cable bending stiffness; $\{F_{ext}\} = \{f_j\}_{n\times 1} = \{\int_0^L f_{ext}(x,t)\phi_j(x)dx\}$ is the generalized external force; $F_d(t)$ is the time-dependent force in the damper; $\{\phi(x_d)\} = \{\phi_j(x_d)\}_{n\times 1}$ is the vector of shape function amplitudes at the damper location; and $\{\ddot{q}\} = \{\ddot{q}_i\}_{n\times 1}$, $\{\dot{q}\} = \{\dot{q}_i\}_{n\times 1}$ and $\{q\} = \{q_i\}_{n\times 1}$ are the generalized modal acceleration, velocity and displacement vectors, respectively. To maintain the symmetry of the stiffness matrix, the order of differentiation of the integrands in $\boldsymbol{K}^t$ and $\boldsymbol{K}^b$ have been equalized by integration by parts and application of the corresponding boundary conditions (i.e. $\phi(0) = \phi(L) = 0$, $\phi'(0) = \phi'(L) = 0$ (fixed-fixed) and $\phi''(0) = \phi''(L) = 0$ (hinged-hinged)). This ensures the convergence of the MSM [96].

The dynamic response of a damped cable can be determined using different approaches, with the damper being treated either as an external control device, or as an inherent element of the cable-damper system. In the former, the focus would be on the behaviour of the cable itself, and the effect of the damper is represented by a concentrated force acting on the cable at the damper location, which is the second term on the right-hand side of Eq. (4-11). This approach is applicable to the semi-active control devices, as well as to passive dampers when not only the damping and stiffness properties but also other nonlinearities and complexities, such as the damper support stiffness, need to be considered in the analysis. On the other hand, the inherent damper approach integrates the cable and the damper into a full system. By considering the mechanical model shown in Fig. 4-1 for the damper and its support, the time-dependent force generated by the damper can be expressed as:

$$F_d(t) = k_d[w(x_d,t) - u_s(t)] + c_d[\dot{w}(x_d,t) - \dot{u}_s(t)] \tag{4-12}$$

Also, it is noticed that:

$$F_d(t) = k_s u_s(t) \tag{4-13}$$

which gives $u_s(t) = F_d(t)/k_s$ and $\dot{u}_s(t) = \dot{F}_d(t)/k_s$. Substituting these two expressions into Eq. (4-12) yields:

$$F_d(t) = \tilde{k}_d w(x_d,t) + \tilde{c}_d \dot{w}(x_d,t) - \alpha \dot{F}_d(t) \tag{4-14}$$

where $\tilde{k}_d = k_d/(1 + k_d/k_s)$ is the modified damper stiffness, $\tilde{c}_d = c_d/(1 + k_d/k_s)$ is the modified damper size, and $\alpha = c_d/(k_d + k_s)$ is the time constant of the damper force. It is evident that for a rigid damper support with $k_s \to \infty$, Eq. (4-14) reduces to the explicit force-displacement relationship for NSD, i.e. $F_d(t) = k_d w(x_d,t) + c_d \dot{w}(x_d,t)$.

The mode superposition method can be used to obtain $w(x,t)$ by utilizing a numerical time-domain differential equation solver and the modal damping ratio can be estimated based on the free vibration response time history. However, the calculated damping ratio depends on the type and location of the external load, the location of the cable response measurement since the damping ratio is amplitude-dependent, and the method used for filtering the cable response for a specific mode. To avoid these dependencies and accelerate the process, an eigenvalue problem that governs the free vibration of the studied cable-damper system can be solved directly to find the modal damping ratio. However, this approach requires the damper force to be explicitly defined as a function of the displacement field and its derivatives, whereas the damper force given by Eq. (4-14) is implicit. To find an explicit expression for the damper force, the term $\dot{F}_d(t)$ on the right-hand side can be replaced by the time derivative of the equation itself. Therefore, Eq. (4-14) can be rewritten as:

$$F_d(t) = \tilde{k}_d w(x_d,t) + (\tilde{c}_d - \alpha\tilde{k}_d)\dot{w}(x_d,t) - \alpha\tilde{c}_d\ddot{w}(x_d,t) + \alpha^2\ddot{F}_d(t) \quad (4\text{-}15)$$

Based on the practical ranges of the damping coefficient and damper support stiffness values in passive dampers, the time constant $\alpha = c_d/(k_d + k_s)$ would be relatively small. Consequently, the term $\alpha^2\ddot{F}_d(t)$ would also become negligible as $\ddot{F}_d(t)$ is not expected to be too large. By substituting Eq. (4-10b) into Eq. (4-15) and dropping $\alpha^2\ddot{F}_d(t)$, an approximate explicit form of Eq. (4-15) can be expressed as:

$$F_d(t) \approx \boldsymbol{\phi}_{\boldsymbol{d}}^T[\tilde{k}_d\boldsymbol{q} + (\tilde{c}_d - \alpha\tilde{k}_d)\dot{\boldsymbol{q}} - \alpha\tilde{c}_d\ddot{\boldsymbol{q}}] \quad (4\text{-}16)$$

The equation of motion of the cable-damper system can now be derived by substituting Eq. (4-16) into Eq. (4-11), which gives:

$$\widetilde{\boldsymbol{M}}\ddot{\boldsymbol{q}} + \widetilde{\boldsymbol{C}}\dot{\boldsymbol{q}} + \widetilde{\boldsymbol{K}}\boldsymbol{q} = \boldsymbol{f} \tag{4-17}$$

where $\widetilde{\boldsymbol{M}} = [\tilde{m}_{ij}] = \boldsymbol{M} - \alpha\tilde{c}_d[\phi_i(x_d)\phi_j(x_d)]$, $\widetilde{\boldsymbol{C}} = \left[\tilde{c}_{ij}\right] = \boldsymbol{C} + (\tilde{c}_d - \alpha\tilde{k}_d)[\phi_i(x_d)\phi_j(x_d)]$, and $\widetilde{\boldsymbol{K}} = [\tilde{k}_{ij}] = \boldsymbol{K} + \tilde{k}_d[\phi_i(x_d)\phi_j(x_d)]$ are the effective mass, damping and stiffness matrices, respectively, and $\boldsymbol{f} = \{f_j\} = \{\int_0^L f_e(x,t)\phi_j(x)dx\}$ is the vector of generalized external force. If the damper is mounted on a rigid support (i.e. $k_s \to \infty$), the effective matrices reduce to $\widetilde{\boldsymbol{M}} = \boldsymbol{M}$, $\widetilde{\boldsymbol{C}} = \boldsymbol{C} + c_d[\phi_i(x_d)\phi_j(x_d)]$, and $\widetilde{\boldsymbol{K}} = \boldsymbol{K} + k_d[\phi_i(x_d)\phi_j(x_d)]$.

The modal damping ratio and the natural frequency of the damped cable can be determined by applying the logarithmic decrement method to the free vibration response of the damped cable. In this approach, the model can be numerically excited by a simple harmonic load at a frequency in the proximity of that of the cable mode of interest. Upon removal of the excitation force, the cable vibrates freely. The forced and then free vibration response of the damped cable can be determined from Eq. (4-10b) using the MSM, where the proposed new set of shape functions are implemented either in Eq. (4-11) or if applicable, Eq. (4-12), to find the generalized modal vector $\{q\}$ at each time step, followed by the subsequent substitution of shape functions and $\{q\}$ into Eq. (4-10b). The logarithmic decrement method can then be utilized to calculate the modal parameters. However, the modal damping ratio obtained in this method depends slightly on the excitation frequency and the location of the applied harmonic load. The excitation frequency can be updated iteratively to match the calculated natural frequency of the target mode.

An alternative approach to find the modal parameters of a cable-damper system governed by Eq. (4-12) is to solve a complex eigenvalue problem. A linearized state-space form of

the eigenvalue problem would be more convenient for finding the complex eigenvalues using available numerical procedures. Assume $\{q\} = \{\varphi\}e^{\eta t}$ for the free vibration response and substitute into the homogeneous form of Eq. (4-12). It yields the following complex eigenvalue equation with $2n$ solutions [96]:

$$\eta \boldsymbol{A}\{\kappa\} = \boldsymbol{B}\{\kappa\} \tag{4-18a}$$

$$\boldsymbol{A} = \begin{bmatrix} \boldsymbol{0} & \widetilde{\boldsymbol{M}} \\ \widetilde{\boldsymbol{M}} & \widetilde{\boldsymbol{C}} \end{bmatrix}_{2n\times 2n} \quad \boldsymbol{B} = \begin{bmatrix} \widetilde{\boldsymbol{M}} & \boldsymbol{0} \\ \boldsymbol{0} & -\widetilde{\boldsymbol{K}} \end{bmatrix}_{2n\times 2n} \tag{4-18b}$$

where $\eta = -\zeta\omega_n \pm i\omega_n\sqrt{1-\zeta^2}$ is the complex eigenvalue pair and $\{\kappa\}_{2n\times 1} = \{\eta\varphi^T \quad \varphi^T\}^T$ is the corresponding eigenvector. The modal frequency and the modal damping ratio of the cable-damper system can be obtained by directly solving the complex eigenvalue problem described by Eq. (4-18), which are $\omega_n = |\eta|$ and $\zeta = -Re(\eta)/|\eta|$, respectively. The application of the Cholesky decomposition is a common approach to obtain the system eigenvalues [97].

4.2.4. Brief review of existing approaches for analyzing cable dynamics

Several numerical and analytical approaches have been proposed for evaluating the dynamic behaviour of a damped stay cable. Among these, the finite difference formulation (FD) by Mehrabi and Tabatabai [73] and the generalized analytical solution by Fujino and Hoang [71], both of which include the cable bending stiffness and cable sag effects, have been selected in this study for comparison purposes and will be briefly reviewed in this section.

4.2.4.1. Cable discretization using FD method

Mehrabi and Tabatabai [73] developed a FD formulation for evaluating the modal properties of a damped cable considering the effects of cable sag and cable bending

stiffness. For a discretized cable with n internal nodes and $N = n + 1$ segments, assume the nodal free vibration response is in the form of $\{w\} = \{u\}e^{pt}$ in the homogeneous form of Eq. (4-1). The matrix form of the discretized cable can be expressed as the following eigenvalue equation:

$$(p^2\boldsymbol{M} + p\boldsymbol{C} + \boldsymbol{K})\{u\} = \{0\} \tag{4-19}$$

where $p = -\zeta\omega_n \pm i\omega_n\sqrt{1-\zeta^2}$ is the complex eigenvalue pair and $\{u\}_{n\times 1}$ is the corresponding eigenvector. It should be noted that Eq. (4-19) is the original second-order form of the eigenvalue problem which was presented earlier in a linearized state-space form by Eq. (4-18). By assuming a parabolic self-weight profile and utilizing the central finite difference formulation, the stiffness matrix $\boldsymbol{K}$ becomes:

$$\boldsymbol{K} = \begin{bmatrix} Q & U & W & & & 0 \\ & S & U & W & & \\ & & S & U & & \\ & & & S & U & \\ & \text{sym} & & \vdots & \ddots & \\ & & & & & Q \end{bmatrix}_{n\times n} + \frac{\lambda^2 H l^2}{L^3}\boldsymbol{J} \tag{4-20}$$

where $Q = 7EI/l^3 + 2H/l$ for the fixed-fixed cable and $Q = 5EI/l^3 + 2H/l$ for the hinged-hinged cable, $U = -4EI/l^3 - H/l$, $W = EI/l^3$, $S = 6EI/l^3 + 2H/l$, $l = L/N$ and $\boldsymbol{J} = [1]_{n\times n}$ is the all-ones matrix. The mass and damping matrices are defined as $\boldsymbol{M} = diag([m_1 l, \cdots, m_i l, \cdots, m_n l])$ and $\boldsymbol{C} = diag([c_1 l, \cdots, c_i l, \cdots, c_n l])$, respectively, of which m_i is the mass per unit length at node i, and c_i is the damping coefficient of a damper attached to the i^{th} node. The magnitude of the damping coefficient and the stiffness of a viscous damper attached to a specific cable node can also be respectively added to the diagonal elements of $\boldsymbol{C}$ and $\boldsymbol{K}$ matrices that correspond to that node. Equation (4-19) is a complex eigenvalue problem that can be solved to obtain the modal frequencies and

damping ratios of the cable-damper system. The accuracy and computational cost of the FD method highly depends on the spatial discretization size and will be investigated in Section 4.3.

4.2.4.2. Analytical solution for free vibration

Two analytical models for the dynamic response of a damped cable were presented in Chapter 3 by considering a fixed-fixed (Eq. 3-6) and a hinged-hinged (Eq. 3-11) boundary condition for the cable. These equations can be numerically solved to obtain the complex wave number $\beta_n = \omega_n\sqrt{m/H}$ and subsequently, the modal damping ratio $\zeta_n = \text{Imag}[\beta_n]/|\beta_n|$.

4.3. Evaluation of the proposed MSM framework

In the previous section, the MSM based on an enhanced set of shape functions was proposed for a damped cable with fixed-fixed or hinged-hinged boundary conditions. These shape functions consist of two parts, the first being the static correction term defined as the static displacement profile of a cable under a point load at the damper location, and the second part being the conventional/adapted sine functions depending on the boundary conditions. The objective is to provide an efficient control-oriented model for the dynamic response of a damped cable, which is required for the design and evaluation of passive or semi-active/active control schemes. In order to evaluate the performance of the proposed shape functions and compare with the available methods, a numerical example is presented in this section.

A sample full-scale cable which has a length of $L = 122\,\text{m}$, a unit mass of $m = 51.8\,\text{kg/m}$, a chord tension of $H = 3150\,\text{kN}$, a flexural stiffness property of $EI =$

2×10^6 N $\cdot m^2$ and an axial stiffness property of $EA = 2.44 \times 10^9$ N is considered. A viscous damper which has a damping coefficient of $c_d = 50$ kN $\cdot$ s/m is attached at $x_d = 0.05L = 6.1$ m. It is also assumed that $k_d = 0$ and $k_s \to \infty$ (rigid damper support). First, the effect of static correction term on the computational efficiency of the MSM is studied for both the fixed-fixed and hinged-hinged end conditions. Next, the performances of the three different solution techniques, namely the MSM, the FD and the analytical approach, are compared in terms of their accuracy and efficiency.

4.3.1. Dynamic response based on the proposed shape functions

4.3.1.1. Effect of static correction

The effect of including the cable static displacement profile (static correction) on the computational efficiency of the proposed dynamic model is studied in this section. A convergence criterion is required to compare the efficiency of different computational models in terms of their convergence rate. The following criterion is defined based on the relative error between the current and the target response values:

$$Er = \frac{|Y - Y_{target}|}{|Y_{target}|} \leq Er_{max} \tag{4-21}$$

where Y is the response value at the current discretization size (the number of mode shapes or cable nodes considered in the simulation), Y_{target} is the asymptotic response value obtained from a sufficiently large discretization, Er is the relative error between the current and the asymptotic values and Er_{max} is the acceptable error limit. Equation (4-21) is defined on the basis that in the MSM, the measured response would converge to an asymptotic value as the number of modes (shape function terms) included in the analysis increases. The same trend is also observed in the FD method with an increased

discretization (i.e. more internal nodes). To observe more sizeable difference between the studied methods in terms of accuracy and computational cost, the error limit in the current example is taken as $Er_{max} = 5 \times 10^{-4}$.

The complex eigenvalue problem defined in Eq. (4-18) is solved using MATLAB to calculate the first modal damping ratio and the fundamental frequency of the sample damped cable with and without including the static correction. Figures 4-3 and 4-4 show the convergence rate of the fixed-fixed and the hinged-hinged cable, respectively. As illustrated in Fig. 4-3(a) and 4-3(b), for a fixed-fixed cable, when the static correction is included in the MSM, the required number of sine terms to meet the convergence criterion ($Er \leq 5 \times 10^{-4}$) reduces from 128 to 23 terms for the first modal damping ratio and remains unchanged as 19 terms for the fundamental frequency. In this case, the target values of the first modal damping ratio and the fundamental frequency to the third decimal points are 1.923% and 1.045 Hz, respectively.

Figure 4-4 shows the results obtained for the hinged-hinged cable, of which the target values of the first modal damping ratio and the fundamental frequency to the third decimal points are 2.340% and 1.036 Hz, respectively. It is observed that by considering the static correction, the required number of sine terms to satisfy the convergence criterion reduces from 113 to 3 terms for the first modal damping ratio and from 16 to 1 term for the fundamental frequency. Therefore, the static correction can substantially improve the convergence rate, especially in the case of the hinged-hinged cable. The number of considered shape function terms (or equivalently, the size of the system matrices, $\boldsymbol{M}$, $\boldsymbol{C}$ and $\boldsymbol{K}$) is a dominant factor for the computational efficiency of dynamic simulations.

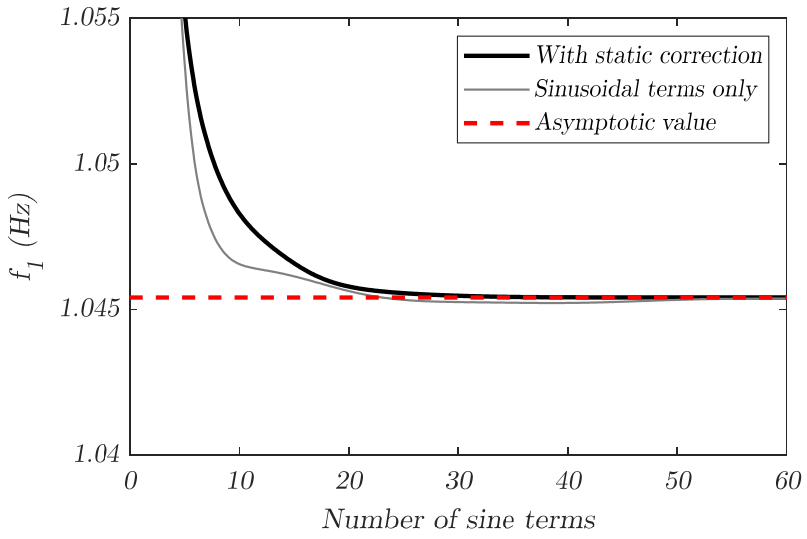

(a)

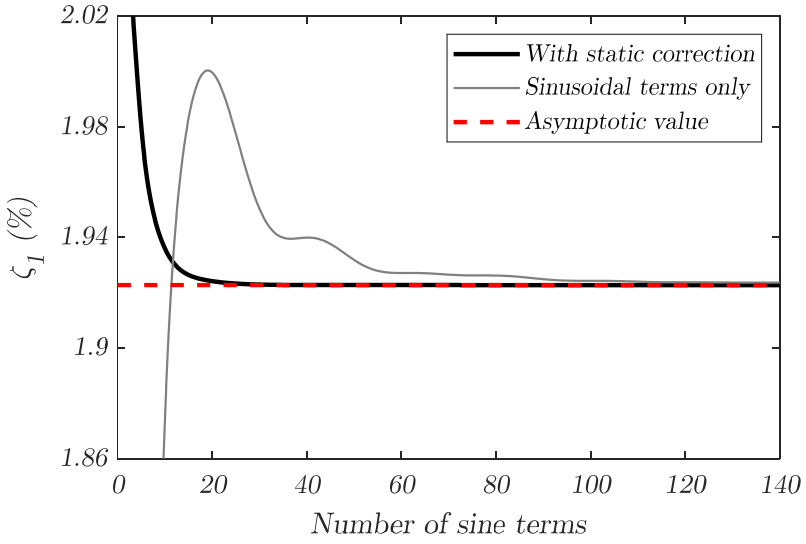

(b)

Fig. 4-3. Effect of static correction term on the convergence rate of the first modal properties of a fixed-fixed cable. (a) Fundamental frequency, (b) First modal damping ratio.

4.3.1.2. Comparison between different solution techniques

As discussed earlier, the dynamic behaviour of a damped cable can be evaluated by either applying the logarithmic decrement method to its free vibration time history, which is obtained from the MSM; or directly solving the complex eigenvalue problem associated

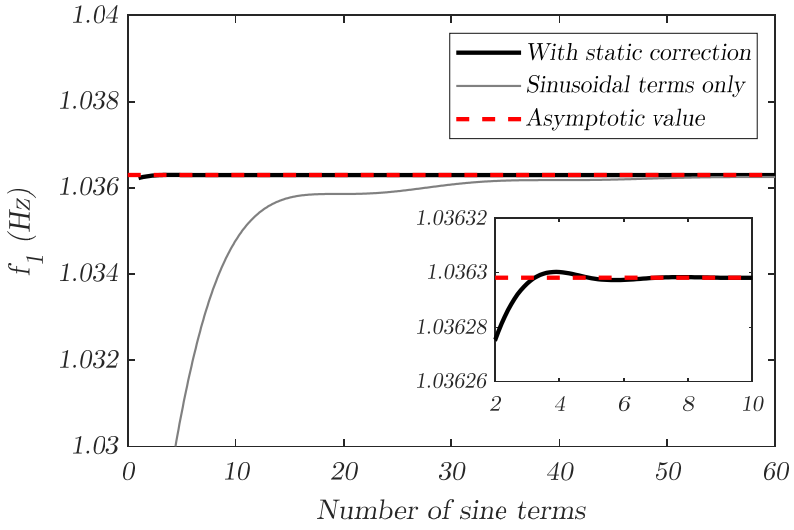

(a)

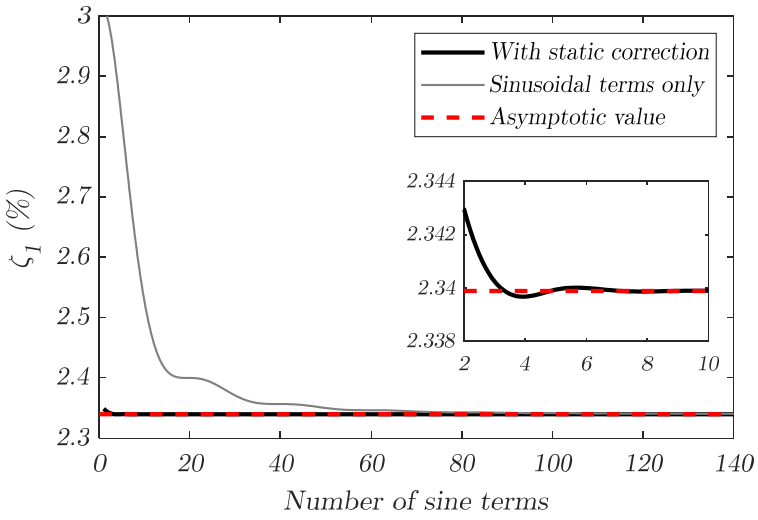

(b)

Fig. 4-4. Effect of static correction term on the convergence rate of the first modal properties of a hinged-hinged cable. (a) Fundamental frequency, (b) First modal damping ratio.

with the cable-damper system. The accuracy and efficiency of these two different solution techniques are compared in this section.

To generate the free vibration time history of the fixed-fixed sample cable, a harmonic load with an amplitude of $P = 1$ kN and a frequency of $f = 1.05$ Hz is applied at $L/10$ (L is

the cable length) for 100 seconds and then removed. The subsequent cable free vibration response at mid-span is captured for 50 seconds. Since the excitation frequency of the harmonic load is chosen to be close to the first modal frequency of the fixed-fixed cable, the obtained modal parameters would pertain to the first mode. Figure 4-5 shows the response time history of a fixed-fixed damped cable. The simulation is performed in the MATLAB/Simulink environment using a fixed integration time step of 1 millisecond. The envelope of the free vibration response is obtained by fitting an exponential curve to the displacement peaks. The logarithmic decrement method is then applied to determine the damping ratio of the excited mode, and the corresponding modal frequency can be computed from the response time history.

Figure 4-6 shows a scatter plot of the fundamental frequency and the first modal damping ratio obtained from the logarithmic decrement method ($x - axis$) and the complex eigenvalue equation ($y - axis$) for the studied fixed-fixed damped cable. The results show that as the number of shape function terms increases, the logarithmic decrement method yields a slightly higher first modal damping ratio since the points eventually fall slightly below the 45° line, possibly due to the presence of numerical damping and frequency distortion [98], while the fundamental frequencies calculated from these two methods are almost the same. This set of results suggest that both approaches can be used to determine the modal properties of the studied cable with the same level of accuracy. Thus, the selection of the solution technique would mainly depend on the mechanical model of the damper. If factors other than the damping property and stiffness of the damper need to be considered in describing the damper effect, such as the damper support stiffness, the MSM combined with the logarithmic decrement method would be preferred. Otherwise, solving

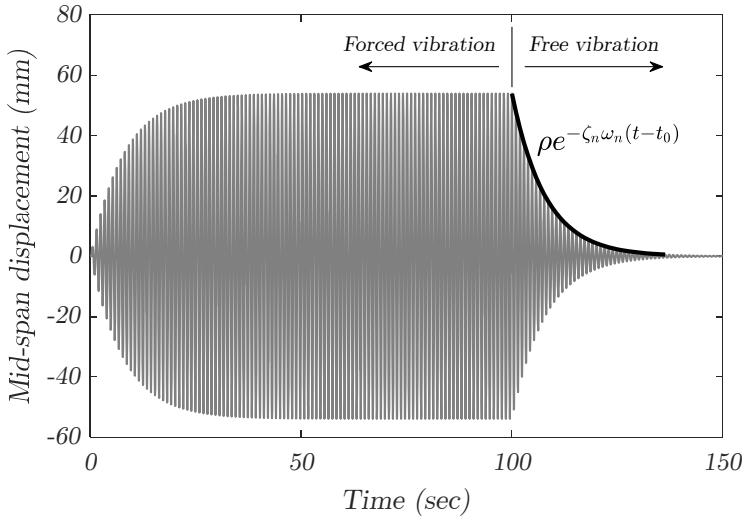

Fig. 4-5. Response time history of a fixed-fixed damped cable excited by a harmonic load.

the complex eigenvalue problem would be a suitable choice, since it would be computationally more efficient without performing the full response time-history simulation. In addition, since there would be no need to introduce external excitations, the possible discrepancies in the predicted modal parameters due to differences in the excitation force characteristics could be avoided. Due to its closed-form nature, the eigenvalue solution is advantageous compared to the numerical integration as the latter may introduce approximation errors depending on the time step size. In the current example, if a total of 60 shape function terms are used in the analysis, the computation time would increase from 0.2 second to 14 second if the MSM plus the logarithmic decrement methods are used instead of the complex eigenvalue approach. Nonetheless, a time history simulation would be inevitable for the scenario of complicated passive damper models such as the one shown in Fig. 4-1 or in the case of semi-active/active dampers.

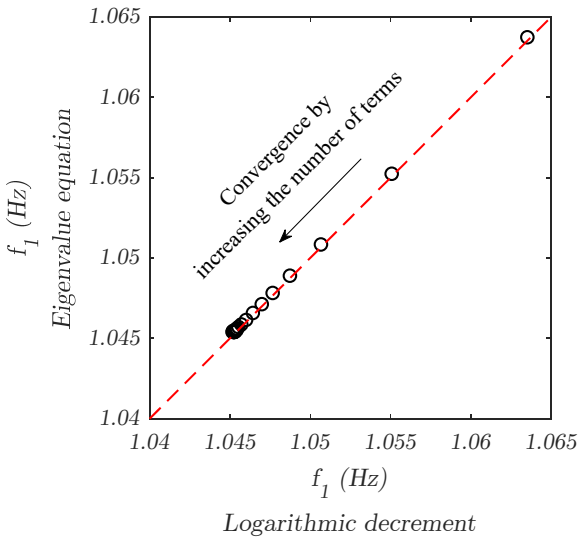

(a)

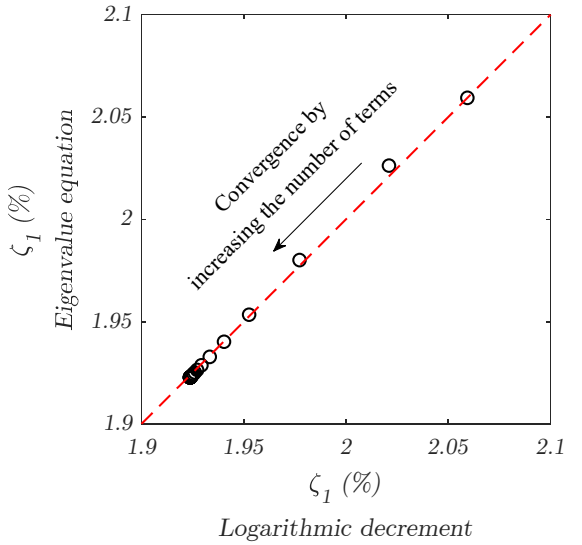

(b)

Fig. 4-6. Comparison of the modal parameters of a fixed-fixed damped cable obtained from logarithmic decrement method and complex eigenvalue equation: (a) Fundamental frequency, (b) First modal damping ratio.

4.3.2. Comparison with existing methods

Figure 4-7 depicts the numerical efficiency of different methods for evaluating the modal parameters of a fixed-fixed damped cable, including the MSM with the shape functions proposed in this study, the FD method by Mehrabi and Tabatabai [73] and the analytical

model by Fujino and Hoang [71]. In Fig. 4-7(a), the fundamental frequency obtained from the FD method converges to the analytical value when the cable is discretized by a relatively large number of nodes, i.e. 260 nodes. It should be noted that both the FD method and the analytical model assume a parabolic self-weight profile for the fixed-fixed cable. Thus, it is observed that the result obtained from the FD method would eventually coincide with the analytical value of $f_1 = 1.0458$ Hz after including sufficiently large number of nodes. On the other hand, the result of the MSM using the proposed shape functions converges with only 20 terms, as mentioned earlier in Section 4.3.1.1, to a slightly lower fundamental frequency of $f_1 = 1.0454$ Hz. This minor difference is believed to stem from the parabolic self-weight profile assumption adopted in the analytical model. To evaluate this assumption, the stiffness property of the cable can be considered. By substituting Eq. (4-4) into Eq. (4-1) and grouping the terms representing the cable stiffness, the total cable stiffness, K_{tot}, is defined as :

$$K_{total} = EI\frac{d^4w}{dx^4} - H\frac{d^2w}{dx^2} + \frac{EA}{L_e}\left[\int_0^L z''wdx\right]z'' \tag{4-22}$$

In the case of a parabolic shape of the self-weight profile $z(x)$, $z''(x)$ would always be positive, whereas for the actual self-weight profile of a fixed-fixed profile, $z''(x)$ would be negative near the cable supports and positive elsewhere. According to Eq. (4-22), the total stiffness property of the cable would be lower in the latter case and therefore, the modal frequency would be slightly lower. As can be observed from Fig. 4-7(a), the amount of such discrepancy is only 0.04%. Thus, the error induced by assuming a parabolic self-weight profile is negligible.

Besides, it can also be seen from Fig. 4-7(a) that the convergence trend in the FD method and the MSM is different. The FD method converges ascendingly to the analytical value, whereas the MSM converges in a descending manner. This phenomenon is related to how the system mass matrix is defined and formed. If a lumped mass model is used, as in the case of the FD method, the obtained frequency tends to converge ascendingly; whereas if a consistent mass model is used, as in the case of the MSM, it converges in a descending mode. This phenomenon has been reported and investigated analytically by Meirovitch and Baruh [99] and Chan et al. [100].

Figure 4-7(b) depicts the convergence rate of the first modal damping ratio of the studied cable. It is observed that the results yielded from the FD method converges very slowly to the analytical result. If the analytical result is considered as the target value, the convergence criterion defined in Eq. (4-21) cannot be satisfied even for a discretization of 2000 nodes. Furthermore, the difference between the first modal damping ratio determined by the MSM (1.923%) and the analytical approach (1.914%), which arises from the assumption of the parabolic self-weight profile in the latter, is about 0.45% of the analytical value. This suggests that the assumption of the parabolic self-weight profile made in the analytical model by Fujino and Hoang [71] is acceptable for design applications since it results in a slightly lower cable damping ratio and is thus conservative.

Figure 4-8 shows the convergence rate of the modal parameters of a hinged-hinged damped cable based on the studied methods. The results show that the MSM using the proposed shape functions manifests a superior performance in determining both the fundamental frequency and the first modal damping ratio (ζ_1) compared to the FD method. The fundamental frequency (f_1) converges to the asymptotic value of 1.0363 Hz by using only

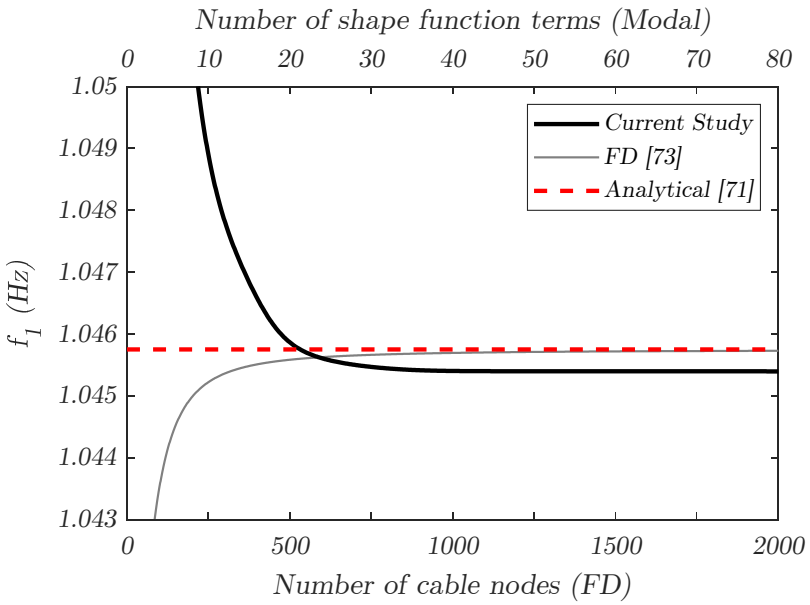

(a)

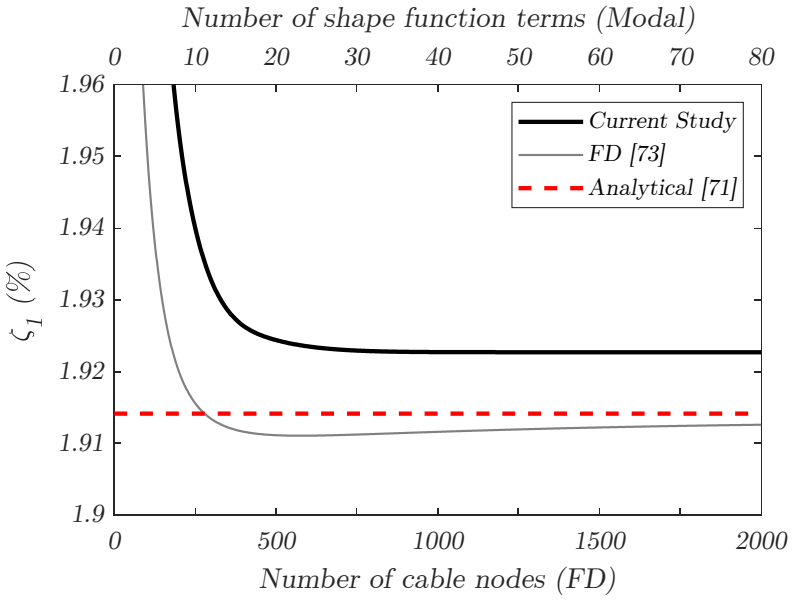

(b)

Fig. 4-7. Convergence rate of the modal parameters of a fixed-fixed damped cable based on different methods. (a) Fundamental frequency, (b) First modal damping ratio.

2 shape function terms in the MSM while the convergence criterion is satisfied with 60 nodes in the FD method. Likewise, ζ_1 converges to its asymptotic value (2.340%) by using

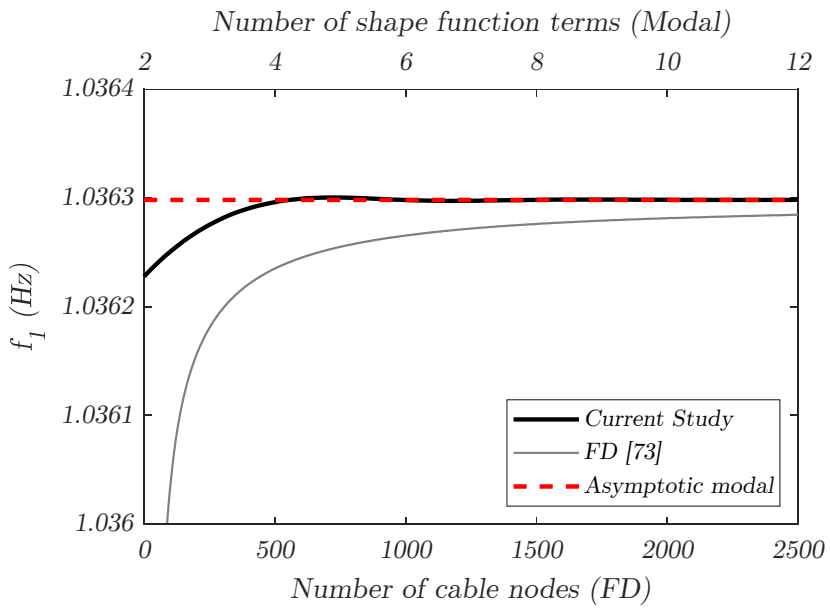

(a)

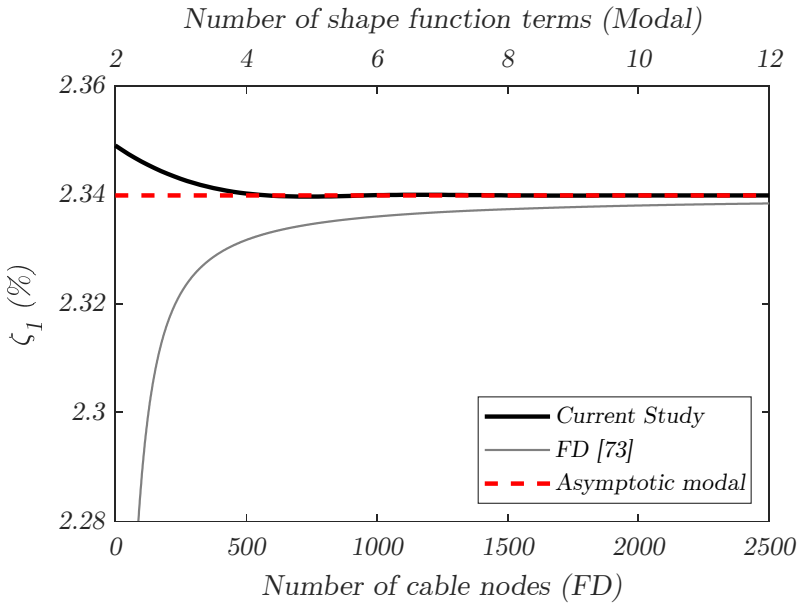

(b)

Fig. 4-8. Convergence rate of the modal parameters of a hinged-hinged damped cable based on different methods: (a) Fundamental frequency (b) Damping ratio.

only 4 shape function terms in the MSM, whereas in the FD method, the convergence criterion would not be satisfied even for an extremely fine mesh (2500 nodes).

Table 4-3. Computational efficiency of different methods for calculating the first modal damping ratio of a fixed-fixed damped cable.

(a) Current study

Number of terms	Critical time step (second)	Relative simulation time	Damping ratio ζ_1 (%)	Er (%) [Eq. (4-21)]
5	0.03	0.32	2.010	4.53
10	0.01	0.64	1.940	0.91
24	**0.009**	**1 (0.35 second)**	**1.924**	**0.04 (conv.)**
60	0.002	6.8	1.923	0

(b) FD method

Number of nodes	Critical time step (second)	Relative simulation time	Damping ratio ζ_1 (%)	Er (%) [Eq. (4-21)]
100	0.002	12	1.952	1.97
180	0.0008	59	1.923	0.46
380	0.0001	1943	1.912	0.12
600	0.00008	9009	1.911	0.16
2000	N/A	N/A	1.913	0.08

Tables 4-3 and 4-4 list the details of the numerical simulation performed in this section for the fixed-fixed and the hinged-hinged cables, respectively. The number of included terms/nodes, the critical time step, the simulation time and the level of accuracy obtained in each simulation case are given. The computational efficiency of the proposed shape functions and the FD method is evaluated based on the results of a forced vibration simulation, of which a harmonic force is applied to the studied cable at $L/10$ for 100 seconds with an amplitude of $P = 1$ kN and a frequency of $f = 1.05$ Hz. As described in 4.2.1.1, the acceptable error limit is defined as $Er_{max} = 5 \times 10^{-4}$. The maximum allowable time step to prevent the instability of the computations (i.e. the critical time step) is listed in the second column of Tables 4-3 and 4-4. The critical time step decreases as the number of terms/nodes increases [101].

As can be seen from Table 4-3(a), for the studied fixed-fixed damped cable, the first modal damping ratio would satisfy the convergence criterion if 24 terms of the proposed shape

Table 4-4. Computational efficiency of different methods for calculating the first modal damping ratio of a hinged-hinged damped cable.

(a) Current study

Number of terms	Critical time step (second)	Relative simulation time	Damping ratio ζ_1 (%)	Er (%) [Eq. (4-21)]
2	0.05	0.84	2.349	0.39
3	0.05	0.88	2.342	0.10
4	**0.04**	**1 (0.23 second)**	**2.340**	**0.02 (conv.)**
20	0.01	4	2.340	0

(b) FD method

Number of nodes	Critical time step (second)	Relative simulation time	Damping ratio ζ_1 (%)	Er (%) [Eq. (4-21)]
100	0.002	35	2.288	2.24
180	0.0008	131	2.313	1.13
520	0.0001	6896	2.332	0.34
600	0.00008	13804	2.333	0.29
2500	N/A	N/A	2.338	0.06

functions are considered, and the simulation can be completed in 0.35 second. For a clearer comparison, the simulation time of the rest of the cases in Tables 4-3(a) and 4-3(b) are normalized to this reference computational time of 0.35 second, and shown in the third column of both tables as the "relative simulation time". To calculate the relative error according to Eq. (4-21), which is given in the last column, the asymptotic first modal damping ratio is used as the target value. Table 4-3(b) lists the numerical simulation information of the FD method in five different discretization meshes. In this case, the target value is the damping ratio obtained from the analytical model. Based on these results, even for a space discretization of 2000 nodes the error is still higher than 5×10^{-4}.

Table 4-4 presents a comparison of the simulation results for the hinged-hinged damped cable. The target value in both methods is the asymptotic value of the first modal damping ratio obtained from the MSM. Results show that only 4 terms of the proposed shape functions are needed in the MSM to achieve the convergence and the simulation took only

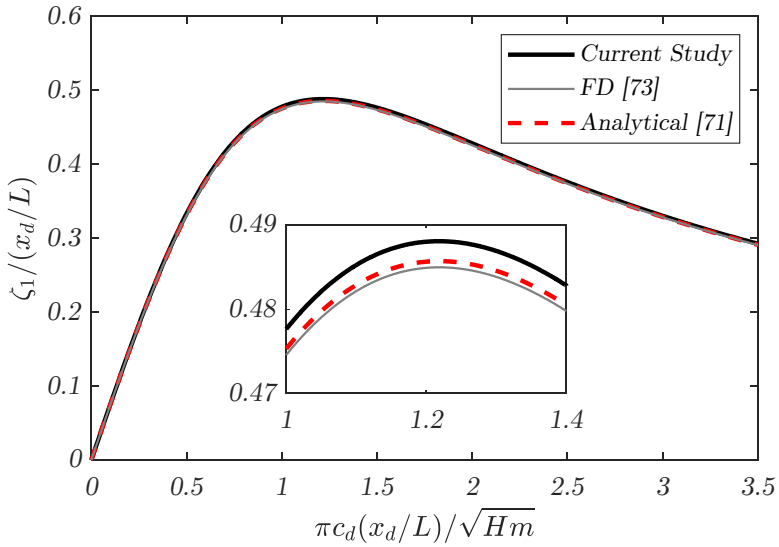

Fig. 4-9. Prediction of damper performance for a fixed-fixed damped cable.

0.23 second. In the FD method, convergence did not occur even if 2500 nodes were used for cable discretization. By increasing the acceptable error margin to $Er_{max} = 0.004$, ζ_1 would converge with only 2 terms of the proposed shape function in the MSM while it needs 460 nodes to converge in the FD method.

Figures 4-9 and 4-10 portray the relation between the viscous damping coefficient, c, and the first modal damping ratio, ζ_1, of a fixed-fixed damped cable and a hinged-hinged damped cable by different approaches, respectively. For the fixed-fixed case in Fig. 4-9, such a relation is predicted by three methods, i.e. the MSM with 24 terms of the shape functions proposed in the current study, the FD formulation by Mehrabi and Tabatabai [73] using 600 nodes in cable discretization, and the analytical approach by Fujino and Hoang [71]. It can be observed from Fig. 4-9 that the $\zeta_1 - c_d$ curves obtained from these three different approaches agree well with each other, with ζ_1 predicted by the current study slightly higher than the other two. This is consistent with the finding in Fig. 4-7(b). In

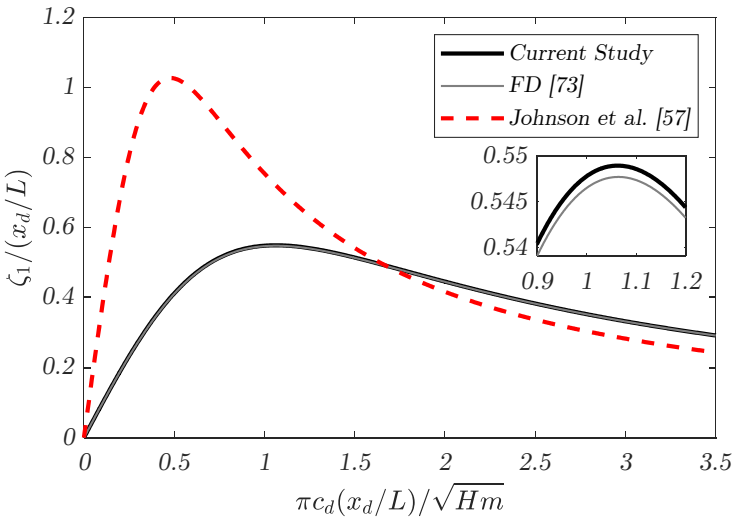

Fig. 4-10. Prediction of damper performance for a hinged-hinged damped cable.

particular, the minor discrepancy between the current result and the analytical approach is believed to be attributed to the parabolic self-weight cable profile assumed in the latter. Further, it is noteworthy that the analytical method [71] can only be used to determine the modal damping ratios and the frequencies of the studied damped cable, but not its dynamic response.

Similarly, Fig. 4-10 illustrates the $\zeta_1 - c_d$ relation for a hinged-hinged cable determined by two different methodologies, namely the MSM and the FD method [73]. In the MSM, either 4 terms of the proposed shape functions or 100 terms of those introduced by Johnson et al. [57] were used, whereas 600 nodes were considered for cable discretization in the FD method. Results show that while the predictions by the current study and the FD method agree well, with the MSM results slightly higher than the FD's, the $\zeta_1 - c$ curve determined from the Johnson's formulation deviates considerably from the other two in terms of the pattern and the magnitude. The maximum first modal damping ratio yielded by this method, i.e. $\zeta_{1,max} = 5.13\%$ at $c = 38.9$ kN · s/m, is almost 1.9 times the value obtained

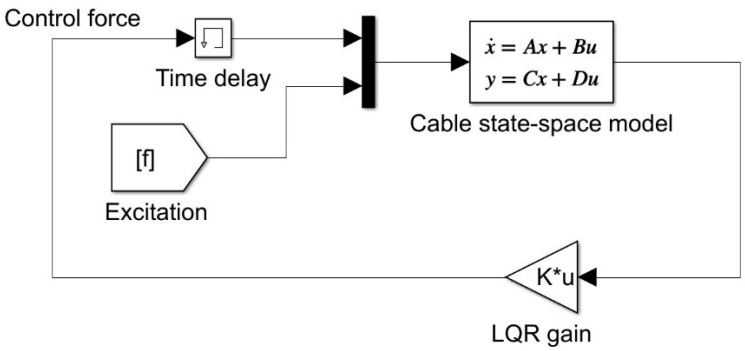

Fig. 4-11. Block diagram of the LQR controller.

by the current study, which is $\zeta_{1,max} = 2.75\%$ and occurs at a smaller damping coefficient of $c = 86.4\ \mathrm{kN \cdot s/m}$. The formulation used in [57] ignores the effect of cable bending stiffness and it may explain this discrepancy. Besides, by comparing Fig. 4-10 with Fig. 4-9, it is found that the maximum achievable first modal damping ratio of a hinged-hinged cable ($\zeta_{1,max} = 2.75\%$) is approximately 13% higher than its fixed-fixed counterpart ($\zeta_{1,max} = 2.44\%$). Experimental studies show that the behaviour of a real stay cable on site is generally more agreeable with that of a fixed-fixed cable [66]. Therefore, if no adequate information is available regarding the actual constraints at the cable anchorage, it is recommended to assume a fixed-fixed boundary condition when designing an external damper to suppress cable vibration in order to ensure a conservative and safe design.

4.3.3. Application to semi-active/active control

In this section, the performance of the proposed dynamic model for application in semi-active/active control is examined. The case study in Section 4.3.2 is extended to design an optimal linear-quadratic regulator (LQR) for mitigating the vibrations of the sample hinged-hinged cable subjected to a harmonic excitation. The LQR scheme is an inherently stable closed-loop optimal gain which regulates the controlled plant based on full state

feedback. In this example, the $\boldsymbol{Q}$ and $\boldsymbol{R}$ matrices of the LQR controller [68] are defined as $\boldsymbol{Q} = diag([\boldsymbol{K} \quad \boldsymbol{M}])$ and $R = 10^{-5}$, where $\boldsymbol{M}$ and $\boldsymbol{K}$ are respectively the cable mass and stiffness matrices defined by Eq. (4-11), and the actuator is assumed to be ideal (i.e. able to exactly generate the required control force) and placed at $0.05L$ from the cable anchorage. Figure 4-11 shows the block diagram of the LQR controller. The effect of time delay is included in the control system by passing the control force through a unit step delay block, as shown in the figure. The hinged-hinged cable is subjected to a harmonic point load with an amplitude of $P = 1$ kN and a frequency of $f = 1.02$ Hz at $L/10$ for 20 seconds. Then the load is released so that the cable vibrates freely for another 20 seconds. The logarithmic decrement method is then utilized to calculate the first modal damping ratio of the controlled cable, based on the free vibration time history. In addition, the integration time step of the simulations is limited to 1 millisecond to meet the requirements of digital control implementation [102]. Therefore, the above simulation with a time step of 1 millisecond would perform 40,000 loops of computation within 40 seconds.

As before, the performance of the computational models can be assessed based on the accuracy of the first modal damping ratio obtained from each one, namely the MSM and the FD method. The convergence rate of the first modal damping ratio is evaluated similar to the previous section. The MSM runtime is selected as the normalization time reference, i.e. $t_{sim,MSM} = 1.09$ s=1 unit. It is found that the convergence ($Er < 5 \times 10^{-4}$) is achieved by using 10 shape function terms in the MSM while each simulation loop takes relatively $t_{loop,MSM} = 2.5 \times 10^{-5}$ unit to complete. The maximum discretization size that can be defined in the FD method without violating the integration time step limit (0.001 second), however, is 80. By using 80 nodes in the FD method, there would be a 1.3% error

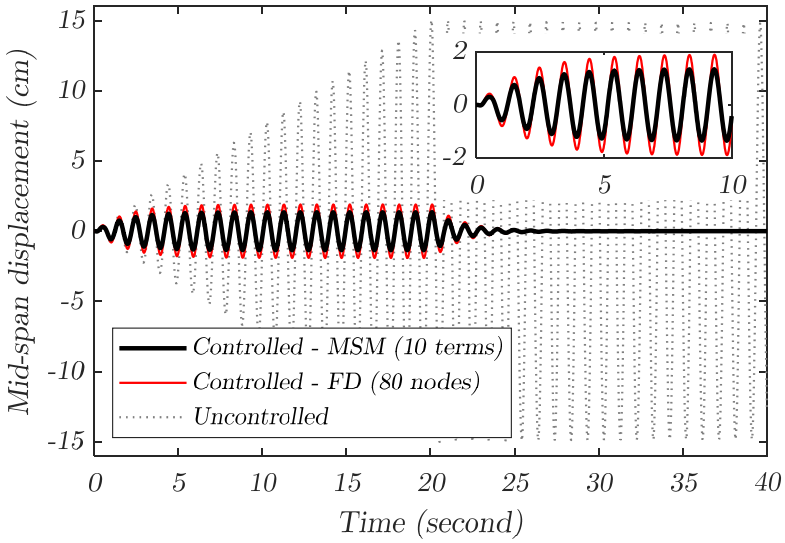

Fig. 4-12. Time history of cable displacement at the mid-span.

in estimation of the first modal damping ratio and also, the time required to perform each simulation loop would increase to $t_{loop,FD} = 2.68 \times 10^{-4}$ unit which is approximately 10 times higher than the MSM. Figure 4-12 shows the time history of the cable displacement at the mid-span with and without the LQR control, where the results of both MSM and FD method are shown for the controlled response. It is observed that the control efficiency in the FD method is affected by a less accurate prediction of the cable states required for the LQR.

4.4. Summary

In this chapter, a control-oriented model for simulating the dynamic response of a stay cable equipped with a transverse damper/actuator has been developed based on the mode superposition method with enhanced shape functions. These shape functions deal with both the hinged-hinged and the fixed-fixed boundary condition and incorporate the effects of cable sag and cable bending stiffness. They consist of two parts: the static correction term,

which is the static displacement of a cable subjected to a point load at the damper location and explicitly derived from the solution of the governing integro-differential equation; and sinusoidal terms which are modified for the fixed-fixed cable to adapt to the boundary conditions. The accuracy and computational efficiency of the proposed model have been evaluated through numerical examples for both passive and semi-active/active control schemes and compared to other existing approaches, namely the FD method by Mehrabi and Tabatabai [73], and the analytical approach by Fujino and Hoang [71]. The main findings of the current chapter are summarized as:

1. The enhanced shape functions, which consist of the static correction term (the exact static displacement profile of the damped cable) and the adapted sinusoidal terms, significantly improve the accuracy and efficiency of the mode superposition method in determining the dynamic response of a damped cable with both the fixed-fixed and hinged-hinged boundary conditions.
2. The proposed computational model based on MSM does not require spatial discretization and is therefore, more efficient and robust in comparison with the FD method in terms of the necessary number of modes to achieve good convergence rate at a reduced computational cost. This superior performance is confirmed in both the passive and the semi-active/active control schemes. Results show that the MSM with enhanced shape functions is more adapted for the design of semi-active and active dampers.
3. The modal properties of a damped/controlled cable can be found either by using the logarithmic decrement method or by solving the complex eigenvalue equation of

the system. It is found that both methods yield agreeable results and hence can be used accordingly based on their applicability.

4. Compared to the exact self-weight profile, the parabolic profile assumption made for a fixed-fixed cable would result in a slightly higher modal frequency estimation but lower damping ratio. However, the discrepancies are negligible. Thus, the parabolic self-weight profile assumption is deemed acceptable for design purposes, even in the case of a fixed-fixed cable.
5. It is recommended to consider a fixed-fixed end condition for predicting the damping of a damped/controlled cable when no reliable information is available regarding the level of rotational fixity in the cable anchorage, since the achievable damping ratio of a fixed-fixed cable is lower than its hinged-hinged counterpart.

Chapter 5 Passive Negative Stiffness Dampers

5.1. Introduction

The urgent need of efficient, robust and cost-effective passive damping devices has led to the recent development of negative stiffness dampers (NSD). As reviewed in Chapter 2, the beneficial effect brought by the negative stiffness was initially observed in building vibration control systems. In particular, the negative stiffness in the force-displacement response of the base isolators optimized by active controllers resulted in improved system behaviour [58]. Iemura and Pradono [103] demonstrated that the existence of pseudo-negative stiffness in the hysteresis loop of variable-orifice dampers would enhance their effectiveness to mitigate seismic response of full-size cable-stayed bridges. The idea of negative stiffness damper was also adopted in stay cable vibration control systems. Li et al. [104] investigated the negative stiffness characteristics of active and semi-active cable control schemes both analytically and numerically by introducing a pseudo-viscoelastic (P-VE) damper with negative stiffness attached to a taut cable. Weber and Distl [77] approximated the control force characteristics of a semi-active clipped linear-quadratic regulator (LQR) by using collocated viscous damping with negative stiffness (VDNS) for controlling multi-mode cable vibrations. In parallel, several passive NSD specimens were created for stay cable vibration control by using compressed springs [64,65] and a combination of static and moving magnets [63], where the efficiency of the latter was experimentally confirmed [66] and showed to be comparable to that of an active control scheme [68].

To improve the current understanding of NSD features and characteristics, this chapter will first provide a physical interpretation for the observed superior damping performance of NSD compared to conventional passive viscous dampers. Next, the problem of NSD stability will be investigated in more detail by extending the discussion presented in Chapter 3. Finally, analytical design relationships and practical design aids will be developed to optimize NSD for controlling single-mode cable vibrations and to design NSD for providing a specified modal damping ratio. In the current chapter, the discussion will be focused on the rigid damper support condition. The effect of the damper support stiffness on the performance of a NSD will be examined in more detail in the next chapter.

5.2. NSD performance

To better understand the superior performance of a negative stiffness damper, the characteristics of the control forces generated by a NSD and a PSD are compared. Figure 5-1 illustrates the variation of the damper force, which consists of the dashpot force and the spring force, within one cable oscillation cycle and the corresponding hysteresis loops of a NSD and a PSD. The hysteresis loop of a ZSD is also shown in the figure for comparison. A complete vibration cycle of a cable can be divided into four zones (I to IV) based on the direction of the cable displacement and velocity at the damper location, namely $u(t)$ and $\dot{u}(t)$. In zones I and III, the cable moves away from the static equilibrium position, while in zones II and IV, it moves backwards toward its original position. Assume a rigid damper support, the direction of the dashpot and spring forces generated by the damper in each zone are given in Fig. 5-1. The dashpot force, F_{cd}, resists the cable motion and is thus always in the opposite direction of $\dot{u}(t)$ for both the NSD and PSD. The direction of the spring force, F_{kd}, is the same as that of the cable displacement $u(t)$ for

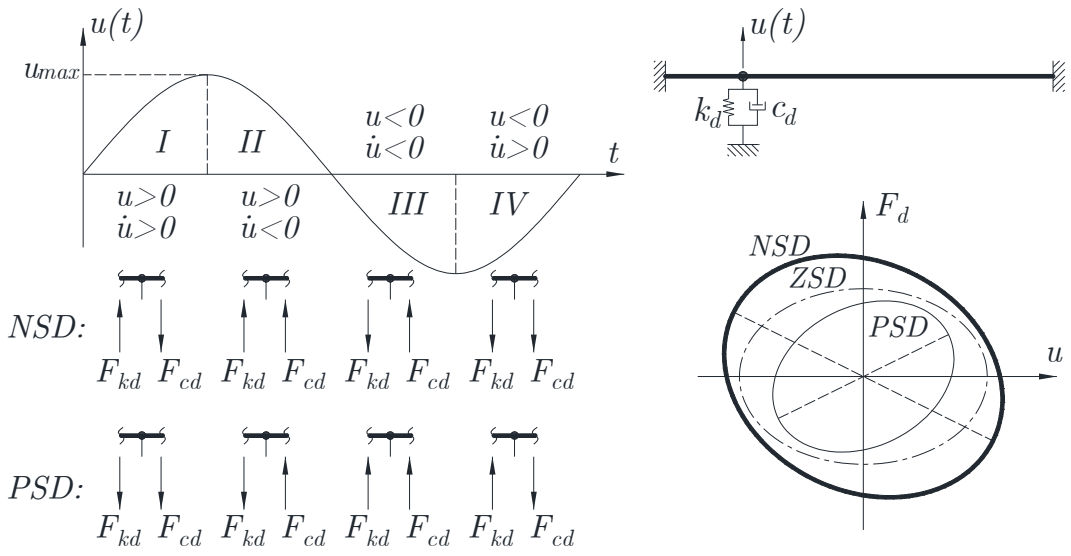

Fig. 5-1. Control force generated by typical positive and negative stiffness dampers during a cable vibration cycle.

NSD but opposite for PSD. The total resistive force, F_d, is the resultant of the dashpot and spring forces.

In zones I and III, the total NSD and PSD resisting forces are equal to $F_d^{NSD} = F_{cd} - F_{kd}$ and $F_d^{PSD} = F_{cd} + F_{kd}$, respectively, whereas in zones II and IV, the total NSD and PSD forces respectively become $F_d^{NSD} = F_{cd} + F_{kd}$ and $F_d^{PSD} = F_{cd} - F_{kd}$. Thus, the NSD would produce less total resisting force in zones I and III during which the cable moves away from the static equilibrium position and therefore, allows the cable to move further away from this position. In contrast, the PSD would impose greater resistance to the cable motion in zones I and III due to a larger F_d and thus results in a smaller cable displacement at the damper location than the NSD case. This behaviour can be observed in the hysteresis loop of the NSD and PSD. As shown in Fig. 5-1, the area enclosed by the NSD hysteresis loop is greater than those of the other two cases due to the increased cable displacement at the damper installation location (i.e. damper stroke). Therefore, a NSD is able to absorb more

kinetic energy from an oscillating cable and offer better control performance in comparison with a PSD and a ZSD. In the case of non-rigid damper support with finite stiffness, the impact of the support flexibility on the damper behaviour requires further investigation and will be discussed in Chapter 6.

5.3. NSD stability

An asymptotic design formula was derived in Chapter 3 (Eq. (3-15)) for estimating the modal damping ratio provided by a passive viscous damper attached to a stay cable. By assuming a rigid damper support, this equation can be rewritten by defining the auxiliary normalized parameters as follows:

$$\sigma_n = \left[\frac{(1-\alpha_{BC}q)^2}{\eta_f^2}\right]\frac{R_{sn}(n\pi\eta_{sn}\hat{X})}{(\bar{k}_d + 1/\eta_f)^2 + (n\pi\eta_{sn}\hat{X})^2} \tag{5-1}$$

where $\sigma_n = \zeta_n/(x_d/L)$ is the normalized cable damping ratio of mode n; $\hat{X} = (x_d/L)\, c_d/\sqrt{Hm}$ is the dimensionless damper size; $\eta_f = 1 - q + (0.5 - \alpha_{BC})rq^2$ is the factor associated with cable bending stiffness, with $q = (1 - e^{-r})/r$, $r = (x_d/L)/\sqrt{EI/(HL^2)}$ and α_{BC} is the boundary condition factor defined by Eq. (3-35). According to Eq. (5-1), σ_n is not only a function of the mechanical and geometric characteristics of the cable, which includes mass, length, chord tension, inclination angle, flexural rigidity, and sag, but also that of the engineering parameters associated with the NSD, i.e. installation location, damper size, and damper stiffness. Therefore, for a given cable, the desired NSD performance can be achieved by properly selecting these NSD parameters.

Observing the term $(\bar{k}_d + 1/\eta_f)^2$ in the denominator of Eq. (5-1), it is clear that the damping ratio is a function of $\bar{k}_d$ and would be considerably affected by its sign. When $\bar{k}_d$ is positive, the damping ratio would decrease if $\bar{k}_d$ increases and therefore, a positive stiffness damper (PSD) would yield a lower damping ratio compared to a zero-stiffness damper (ZSD). In contrast, the presence of a negative $\bar{k}_d$ would result in an increase in the damping ratio. The stronger the negative damper stiffness is, the more it would help to dissipate system energy, which is reflected by a higher damping ratio. This trend continues until $\bar{k}_d$ reduces to $-1/\eta_f$, of which the damping ratio would become a function of $1/\hat{X}$ and approach to infinity when $\hat{X}$ tends to zero, i.e. $\hat{X} \to 0$. Based on the definition of the dimensionless damper size $\hat{X}$ given by $\hat{X} = (x_d/L)c_d/\sqrt{Hm}$, since the damper installation location x_d cannot be zero, and the cable length L, the chord tension H, and the unit mass m all have definite values, $\hat{X}$ would become zero only when the damper damping coefficient c_d is zero. Physically, it indicates that the presence of negative damper stiffness tends to reduce the overall stiffness of the cable-damper system. If the stiffness of a NSD is selected to be $\bar{k}_d = -1/\eta_f$ and its damping capacity is fully removed (i.e. $c_d = 0$), then the negative damper stiffness would fully counteract the inherent positive stiffness of the cable at the damper location and lead to an instability of the damped cable. In other words, the condition $\bar{k}_d = -1/\eta_f$ would cause a system instability only if $c_d = 0$. Otherwise, it would result in a system with no damping ($\zeta_n = 0$). Therefore, $\bar{k}_d = -1/\eta_f$ is a necessary condition for the occurrence of NSD instability and has been used to express the allowable negative stiffness of a NSD as [61,67]:

$$\bar{k}_d^{min} = -\frac{1}{\eta_f} \tag{5-2}$$

The NSD stability criterion defined by Eq. (5-2) takes into account the effect of the cable bending stiffness. Therefore, it can be considered as a generalized form of the theoretical NSD stability limit previously introduced by Li et al. [61] and revisited in [67,105] for the special case of a taut non-flexural cable. If we assume a case of taut cable, i.e. $\eta_f = 1$, Eq. (5-2) would reduce to $k_d > -H/x_d$, which is equivalent to the criterion derived in [61]. For a given cable, the minimum allowable negative stiffness of a NSD depends on the damper installation location x_d, the cable bending stiffness EI, the cable length L and the cable chord tension H. Here, "minimum" means the most negative value allowed for damper stiffness (i.e. farthest from zero on the negative side).

5.4. NSD design for single-mode cable vibration control

5.4.1. Three-dimensional damper performance surface

The dynamic behaviour of a damped cable system has been studied in Chapter 3. It was shown that by assuming low cable bending stiffness and linear cable behaviour, the n^{th} modal damping ratio of the damped cable, ζ_n, is governed by Eqs. (3-15) and (3-33). These equations take into account the stiffness of the damper and can be used to either design a new NSD or to evaluate the efficiency of an existing one. When designing a NSD mounted on a rigid damper support, the modal damping ratio defined in Eq. (3-15) can be rewritten by isolating the sag effect in the following form:

$$Y_n = \frac{R_{sn} n\pi\eta_{sn} X}{(1-\tau)^2 + (n\pi\eta_{sn} X)^2} \tag{5-3}$$

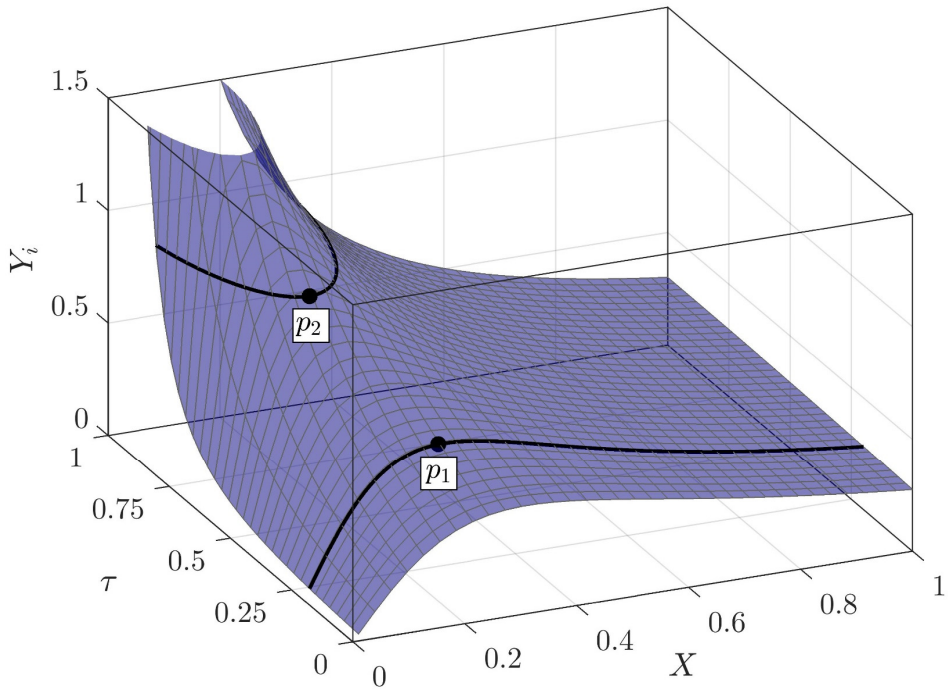

Fig. 5-2. Three-dimensional damper performance surface for an arbitrary mode.

where $Y_n = \zeta_n / \left[(x_d/L) R_{fs}\right]$ is the normalized n^{th} cable modal damping ratio; $X = \eta_f (x_d/L)\, c_d/\sqrt{Hm}$ is the modified damping parameter; $R_{fs} = (1 - \alpha_{BC} q)^2/\eta_f$; and $\tau = k_d/k_d^{min}$ is the NSD stiffness ratio; k_d is the stiffness of a NSD; $k_d^{min} = -H/(x_d \eta_f)$ is the pole of the integrated stiffness coefficient, C_k, and is the lowest negative stiffness of the NSD that defines its stability limit (Eq. (5-2)). In the case of a NSD, τ varies between 0 (zero-stiffness damper) and 1 (stiffness of a NSD reaches its stability limit).

In Fig. 5-2, the variation of the normalized cable modal damping ratio of an arbitrary mode i, Y_i, as a function of the modified damping parameter, X, and the NSD stiffness ratio, τ, is portrayed in the form of a three-dimensional damper performance surface. In this figure, the two horizontal axes τ and X define the NSD design domain, which describes respectively the damper stiffness and the damper size; the vertical axis indicates the

damping capacity of a NSD. For small values of X the damping ratio increases with increasing τ and approaches infinity at $\tau \to 1$. This suggests that although introducing more negative stiffness into a NSD would enhance its performance, when the stiffness reaches the stability limit k_d^{min}, a NSD would manifest an unstable behaviour. As X increases, the sensitivity of the modal damping ratio to the NSD stiffness ratio, τ, would gradually decrease. Referring to Fig. 5-2, when $X > 0.6$, the maximum achievable normalized damping ratio, $Y_{i,max}$, is less than 0.5 independently of τ.

An interesting feature of the damper performance surface is its smoothness and continuity. The first derivatives of Y_i with respect to X and τ are continuous in the design domain, except for the instability point at $\tau \to 1$ and $X \to 0$. This important property ensures the damper behaviour to be consistent and its optimization is feasible. Besides, the intersection of the damper performance surface with any τ-plane would result in a curve defining the relation between the modified damping parameter and damping ratio of a NSD at a given stiffness ratio τ; whereas, its intersection with any Y_i-plane would yield a curve describing the stiffness and size combination of a NSD to achieve a required damping ratio of Y_i. It is worth to note that these two types of curves have only one single extremum point. All these unique attributes associated with the damper performance surface allow the possibility to develop a systematic design approach for NSD to suppress single-mode cable vibrations. The NSD performance surface is illustrated in Fig. 5-2 for the i^{th} mode over the ranges of $0 \leq Y_i \leq 1.5$, $0 \leq \tau \leq 1$ and $0 \leq X \leq 1$. This surface can be applied to two typical design scenarios of a damper. The first common design scenario is to choose the size of a damper to maximize the energy dissipation capacity of the damped cable when the NSD stiffness ratio, τ, is determined by other factors such as the manufacturing requirements (point p_1).

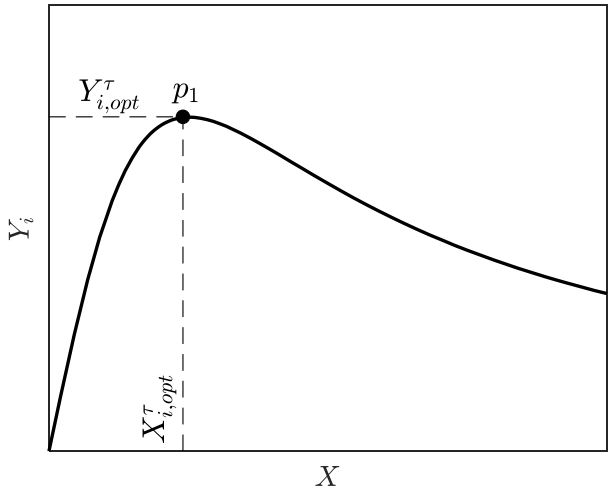

Fig. 5-3. NSD performance on an arbitrary τ-plane.

The second scenario is to find a suitable damper (both damper size and damper stiffness) for a given cable to achieve the specified level of modal damping ratio (point p_2). A systematic approach to address these two design schemes based on the NSD performance surface will be illustrated in the following subsections.

5.4.2. Design scenario 1: Given the damper stiffness, choose damper size

When the NSD stiffness ratio τ is specified, the performance of a NSD in suppressing cable vibrations dominated by a specific mode i can be described by a $Y_i - X$ curve resulted from the intersection of the 3D damper performance surface associated with this mode (Fig. 5-2) and the corresponding τ-plane (Fig. 5-3).

As it can be seen from Fig. 5-3, for a specific NSD stiffness ratio τ, there always exists one optimum damper size for a particular vibration mode, showed by point p_1, which would yield the highest damping ratio in that mode for a given damper location. This approach is similar to the common practice for optimizing conventional positive stiffness (PSD) or zero stiffness dampers (ZSD) in controlling single-mode cable vibration [21–23, 26–28]. In

general, for the i^{th} mode, this optimum design point can be determined by identifying the peak point on the $Y_i - X$ curve, i.e. $dY_i/dX = 0$, where Y_i is given by Eq. (5-3). This leads to:

$$X_{i,opt}^{\tau} = \frac{1-\tau}{i\pi\eta_{sn}} \tag{5-4a}$$

$$Y_{i,opt}^{\tau} = \frac{R_{si}}{2(1-\tau)} \tag{5-4b}$$

Equation (5-4) indicates that if a NSD needs to be used to suppress vibrations of a stay cable in its i^{th} mode for a given NSD stiffness ratio, τ, and if the damper is installed at x_d from one cable end, the optimum damper size can be determined by the following expression:

$$c_{d_{i,opt}}^{\tau} = \frac{X_{i,opt}^{\tau}\sqrt{Hm}}{\eta_f(x_d/L)} \tag{5-5a}$$

and the corresponding maximum achievable n^{th} cable modal damping ratio is:

$$\zeta_{i,max}^{\tau} = Y_{i,opt}^{\tau}\left[\left(\frac{x_d}{L}\right)R_{fs}\right] \tag{5-5b}$$

5.4.3. Design scenario 2: Given a required cable damping ratio, choose NSD stiffness and size

This design scenario is often encountered in practice. Based on the loading condition on the site, especially the potential wind loads predicted from historical data, vulnerable cables and the respective dominant modes associated with these cables can be obtained from dynamic analyses. This information is then used to determine the required damping ratio to mitigate vibration of these cables. Therefore, in this design scenario, the damper is designed to achieve a target damping ratio in a single mode.

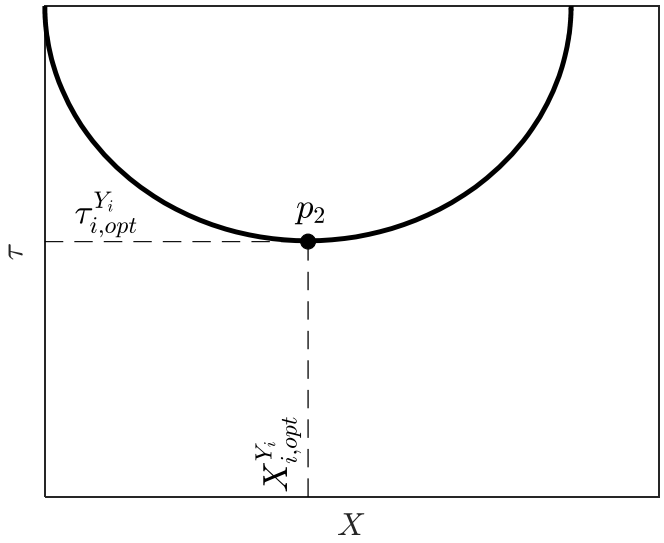

Fig. 5-4. NSD performance on an arbitrary Y_i-plane.

The damper curve $\tau - X$ in an arbitrary Y_i-plane is illustrated in Fig. 5-4. The vertical axis is the NSD stiffness ratio and the horizontal axis is the normalized damping parameter of the NSD. They represent the stiffness and the size of a NSD, respectively. Thus, any point located on the i^{th} modal damper property curve would give a NSD with the corresponding k_d and c_d deduced from the τ- and X-coordinates of the point, to allow the damped cable to achieve a normalized n^{th} modal damping ratio of Y_i. As shown in Fig. 5-4, the $\tau - X$ curve for a particular cable mode has a concave shape. Among all the points located on the same damper property curve, the lowest point corresponds to a combination of k_d and c_d with the smallest NSD stiffness ratio to achieve Y_i. This would yield a NSD design of the least amount of negative stiffness to satisfy the modal damping ratio requirement. Since the negative stiffness generation mechanism is an important component in a NSD, having less negative stiffness would not only enhance the stability of a NSD, but can also be beneficial to the manufacturing process and save cost. Therefore, this lowest point p_2 can

be considered as the optimum damper design point for the i^{th} mode in the second design scenario.

The coordinates of the optimum design point p_2, ($X_{i,opt}^{Y_i}$, $\tau_{i,opt}^{Y_i}$), can be derived by rewriting Eq. (5-3) and express τ as a function of X (note that Y_i in this case is a predefined constant). By taking $dX/d\tau = 0$, it gives:

$$X_{i,opt}^{Y_i} = \frac{R_{si}}{2i\pi\eta_{si}Y_i} \tag{5-6a}$$

Substitute Eq. (5-6a) into Eq. (5-3), $\tau_{i,opt}^{Y_i}$ can be determined, which is:

$$\tau_{i,opt}^{Y_i} = 1 - \frac{R_{si}}{2Y_i} \tag{5-6b}$$

Therefore, the corresponding damper size can be determined from Eq. (5-5a), whereas the damper stiffness can be computed from:

$$k_{d_{i,opt}}^{Y_i} = \tau_{i,opt}^{Y_i} k_d^{min} \tag{5-7}$$

where $k_d^{min} = -H/(x_d\eta_f)$ is the NSD stability limit defined by Eq. (5-2).

Equations (5-6a) and (5-6b) can be applied to design a NSD for a single-mode cable vibration control when the required modal damping ratio is given.

5.5 Verification of the proposed NSD design equations

5.5.1. Sample cables

To verify the validity of the NSD design approach proposed in Section 5.4, the developed NSD design equations are applied to select a NSD for real bridge stay cables in this section. The effectiveness of the selected NSD in mitigating cable vibrations is then evaluated. Fifteen sample cables are used for this purpose. They are chosen from the stay cable

Table 5-1. Properties of the sample stay cables used in numerical simulation.

L (m)	θ (deg.)	m (kg/m)	H (kN)	EI (kN · m^2)	EA (MN)	λ^2	D (m)	f_1 (Hz)
43.7	49.4	72.3	2240.2	1229.1	1282.0	0.05	0.18	2.10
61.7	58.9	103.0	5738.0	2775.3	1974.8	0.01	0.20	1.97
83.0	27.0	214.7	8554.9	17859.1	4733.6	0.18	0.24	1.27
101.8	27.8	52.8	2813.0	555.1	1064.8	0.10	0.14	1.13
135.9	24.4	89.2	5081.3	1702.5	1941.5	0.17	0.17	0.90
168.7	25.5	167.1	8346.2	9497.0	3508.1	0.38	0.23	0.67
200.5	25.3	136.3	7772.0	4013.8	2691.0	0.34	0.23	0.60
245.0	23.6	188.3	9493.8	9010.2	3466.3	0.70	0.28	0.47
276.6	35.2	94.8	5062.9	2411.3	2226.0	0.76	0.15	0.45
293.0	33.7	100.7	5335.7	2712.9	2361.9	0.90	0.16	0.43
327.1	34.4	94.8	4916.8	2411.3	2226.0	1.18	0.15	0.39
363.0	26.9	89.3	4537.1	2231.1	2135.5	1.84	0.15	0.35
401.6	25.0	93.0	4774.5	2411.3	2226.0	2.26	0.15	0.31
421.1	24.1	98.6	4947.2	2712.9	2361.9	2.69	0.16	0.30
460.1	22.6	118.9	6665.9	3983.3	2859.9	2.37	0.17	0.29

database compiled by Tabatabai et. al. [106], which contains engineering specifications of 1406 stay cables on 16 cable-stayed bridges. The properties of the 15 sample cables are listed in Table 5-1. The boundary condition of these cables is assumed to be fixed-fixed.

5.5.2. Applicability of the proposed NSD design equations

The NSD design equations in Section 5.4 are developed based on the assumption of low cable bending stiffness and linear cable behaviour. To assess their applicability, they are applied to design NSD for each of the 15 sample cables by varying the NSD stiffness ratio, τ, from 0 to 0.9. For each specific τ value, the optimum damper size for suppressing cable vibrations dominated by mode i ($i = 1 - 4$) and the corresponding maximum achievable modal damping ratio are predicted by Eqs. (5-4) and (5-5). Meanwhile, for each design

case a numerical simulation is conducted, of which the optimum damper determined by Eqs. (5-4a) and (5-5a) is attached to the cable at $x_d = 0.05L$. The cable is then excited by a harmonic point load applied at $x_p = 0.9L$ to trigger resonant cable vibration in the i^{th} mode ($i = 1 - 4$). The load is removed after 80 seconds and the cable vibrates freely for another 80 seconds. The i^{th} modal damping ratio of the damped cable is computed by fitting an exponential envelope to the free vibration time-history of the cable. This numerically obtained cable modal damping ratio is then compared with that calculated from Eqs. (5-4b) and (5-5b).

The analytically and numerically obtained maximum normalized damping ratio $Y_{i,opt}^{\tau}$ for the symmetric modes (mode 1 and mode 3) and the antisymmetric modes (mode 2 and mode 4) are shown respectively in Figs. 5-5(a) and 5-5(b). To eliminate the effect of mode number, in Fig. 5-5, the vertical axis in both subplots is defined as $Y_{max} = Y_{i,opt}^{\tau}/R_{si}$. The maximum normalized modal damping ratio predicted by the proposed NSD design equations over the range of τ from 0 to 0.9 is shown as a solid line, whereas the numerical results for all 15 sample cables are portrayed as a shaded region. Results show that in the case of mode 1, the analytically predicted and numerically obtained $Y_{max} - \tau$ relation agree well in both pattern and magnitude till $\tau = 0.74$. Beyond this point, the proposed equation would give an over-estimated maximum achievable damping ratio. Note that $\tau = 0.74$ is determined based on the minimum envelope of the shaded region and defines the applicability limit of the proposed NSD design equations to ensure a safe design to suppress mode 1. Thus, this point is defined as the allowable NSD stiffness ratio, τ_{all}. Similarly, for modes 2, 3, and 4, the applicability limit can be identified from Figs. 5-5(a) and 5-5(b) as $\tau_{all} = 0.73,\ 0.62$, and 0.53, respectively. This clearly implies that with the increase of

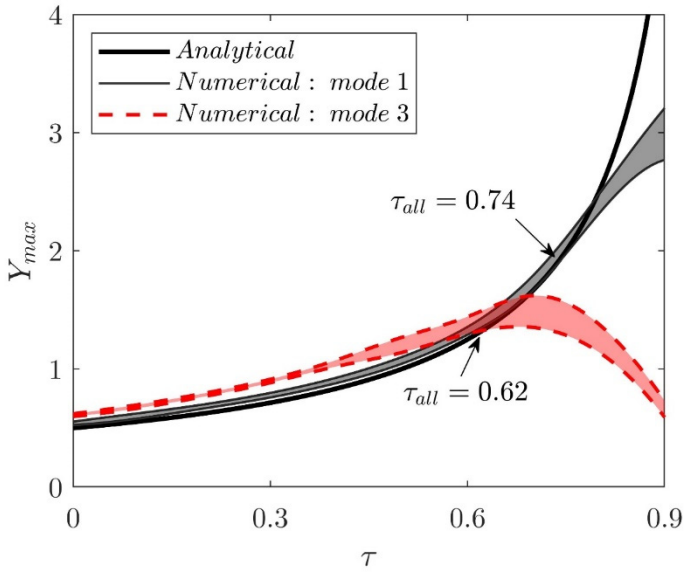

(a)

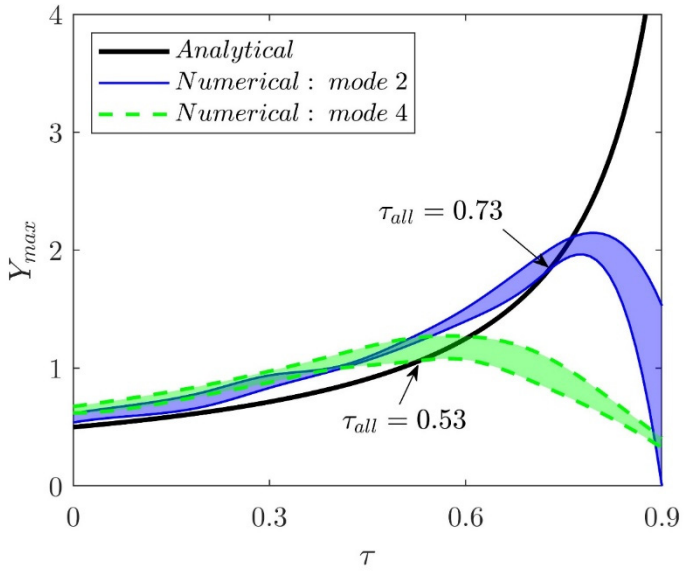

(b)

Fig. 5-5. Maximum damping ratio of an optimized negative stiffness damper. (a) Symmetric modes, and (b) Antisymmetric modes.

mode number, the applicability of the proposed NSD design equations, in terms of the allowable NSD stiffness ratio τ_{all}, would decrease.

Beyond the identified τ -limit, the optimum damper size predicted by Eqs. (5-4a) and (5-5a) will no longer be valid and a full numerical calibration is necessary. In addition, unlike

mode 1, of which both the analytical and numerical results show that the maximum modal damping ratio of a damped cable would increase with greater amount of negative stiffness in the NSD even beyond the applicable τ-limit, for the other three modes, as soon as τ is beyond the applicability limit, a sudden change in the trend of the $Y_{max} - \tau$ relation can be observed from the numerical results where the maximum damping ratio decreases rapidly with the introduction of additional negative stiffness in the NSD. Due to the sensitivity of higher modes to τ, therefore, more caution should be exercised when applying the proposed NSD design equations.

The τ_{all} values shown in Fig. 5-5, though are obtained based on single-mode cable vibration control, are also applicable to NSD design for multi-mode cable vibration control. In this case, the NSD stiffness ratio, either designed or predetermined, shall be limited to τ_{all} for all the modes contributing to the cable vibration (i.e. $\tau < \tau_{all}$).

5.6. Design example

A fixed-fixed stay cable with a length of 122 m, a unit mass of 51.8 kg/m, a chord tension of 3150 kN, and a diameter of 119 mm was studied by Shi et al. [67], of which a NSD device was installed at 5% cable length from the lower end on a rigid damper support. The objective is to determine: (a) the minimum allowable negative stiffness of the NSD and the maximum 1st modal damping ratio for a factor of safety of 1.5, and (b) the NSD parameters for achieving a damping ratio of 5% in the second mode of cable vibration.

5.6.1. Design scenario (a): Select damper size

By assuming an elastic modulus $E = 200$ GPa and an inclination angle $\theta = 0°$ (horizontal cable), the sag and the bending stiffness parameters of this cable are determined as $\lambda^2 =$

0.274 and $\varepsilon = 4.2 \times 10^{-5}$, respectively. The modification and reduction factors due to cable bending stiffness and cable sag are then determined as $\eta_f = 0.806$, $\eta_{s1} = 1.01$, $R_f = 0.940$, $R_{fs} = R_f$ and $R_{s1} = 0.97$, respectively.

The minimum allowable negative stiffness of the damper that would ensure its stability can be obtained using Eq. (5-2), i.e.

$$\bar{k}_d > \frac{-1}{\eta_f} = -1.241$$

which leads to the minimum allowable negative stiffness equal to $k_d^{min} = -640.9$ kN/m. By considering a factor of safety of 1.5 is applied to the above theoretical stability limit, the practical negative damper stiffness would be $k_{d,prac} = -640.9/1.5 = -427.3$ kN/m ($\bar{k}_{d,prac} = -0.827$).

The optimum non-dimensional NSD damper size and the corresponding maximum 1st modal damping ratio are determined using Eqs. (5-4) by substituting $\tau = -427.3/-640.9 = 0.67$:

$$X_{1,opt}^{\tau} = \frac{1-\tau}{(1)\pi\eta_{s1}} = \frac{1-0.67}{1 \times \pi \times 1.01} = 0.104$$

$$Y_{1,opt}^{\tau} = \frac{R_{s1}}{2(1-\tau)} = \frac{0.97}{2(1-0.67)} = 1.47$$

The values of the optimum damper size and maximum damping ratio are obtained from Eq. (5-5) as:

$$c_{d_{1,opt}}^{\tau} = \frac{X_{1,opt}^{\tau}\sqrt{Hm}}{\eta_f(x_d/L)} = \frac{0.104\sqrt{3150 \times 10^3 \times 51.8}}{0.806 \times 0.05} = 33.0 \text{ kN} \cdot \text{s/m}$$

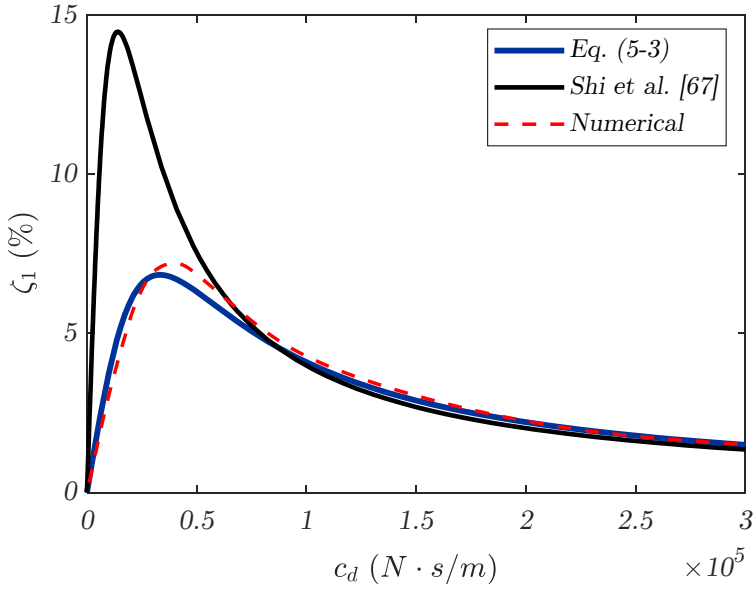

Fig. 5-6. NSD performance prediction by different methods.

$$\zeta_{1,max}^{\tau} = Y_{1,opt}^{\tau}\left[(x_d/L)R_{fs}\right] = 1.47 \times 0.05 \times 0.94 = 0.069 = 6.9\%$$

Figure 5-6 illustrates the variation of the first modal damping ratio ζ_1 with respect to the damping coefficient c_d determined from three different approaches, including the work of Shi et. al. [67], the design Eq. (5-3) and the numerical simulation, for the rigid support case. It is noteworthy to mention that Shi et. al. [67] have neglected the effects of cable sag and cable bending stiffness. Therefore, their model over-estimates the damping capacity of the system. It can be seen from the figure that the asymptotic solution is in good agreement with the numerical one. In addition, the asymptotic solution gives a slightly conservative prediction of the optimum performance of the NSD and therefore, it leads to safe design in practical applications. The maximum achievable first modal damping ratio obtained by Eq. (5-3) is $\zeta_1^{max} = 6.9\%$; which shows an error of 5.1% when compared to the numerical value $\zeta_1^{max} = 7.2\%$. The higher maximum damping ratio reported in [67], i.e. $\zeta_1^{max} = 14.5\%$, is believed to be mainly caused by ignoring the effects of cable sag and bending

Table 5-2. Effect of cable sag and bending stiffness on higher modal damping ratios

Cable model	First mode		Second mode		Third mode	
	ζ_1^{max}	$c_{d,opt}$	ζ_2^{max}	$c_{d,opt}$	ζ_3^{max}	$c_{d,opt}$
Current cable	6.9	33.3	7.1	22.4	7.1	20.2
Flexural non-sagged	7.1	33.6	7.1	22.4	7.1	20.2
Sagged non-flexural	14.1	13.9	14.5	9.4	14.5	8.4
Taut	14.5	14	14.5	9.4	14.5	8.4

stiffness in the analytical model. Therefore, the consideration of cable sag and bending stiffness effects would be crucial in designing cable-NSD systems.

In order to investigate the effect of cable sag and bending stiffness on the damping ratios of higher modes, ζ_2^{max} and ζ_3^{max} are also computed for the current example by considering four scenarios, namely, the actual cable, the sagged non-flexural cable, the flexural non-sagged cable and the taut cable, as summarized in Table 5-2. It can be concluded that the 1st modal damping ratio is affected by both the cable bending stiffness and the cable sag effects, while the influence of the cable sag on the damping ratio is negligible in the higher modes (namely the 2nd and the 3rd modes) and they are only sensitive to the cable bending stiffness effect.

5.6.2. Design scenario (b): Select damper size and damper stiffness

In this section, the NSD design parameters, c_d and k_d, for achieving a damping ratio of 5% in the second mode of cable vibration are determined. It should be noted that the sag-related parameters are equal to one in the 2nd mode. For achieving a normalized second modal

damping ratio of $Y_2 = \zeta_2/\left[(x_d/L)R_{fs}\right] = 0.05/(0.05 \times 0.94) = 1.06$, the non-dimensional NSD parameters are obtained from Eq. (5-6) as ($i = 2$):

$$X_{i,opt}^{Y_i} = \frac{R_{si}}{2i\pi\eta_{si}Y_i} = \frac{1}{2(2)\pi(1)(1.06)} = 0.075$$

$$\tau_{i,opt}^{Y_i} = 1 - \frac{R_{si}}{2Y_i} = 1 - \frac{1}{2(1.06)} = 0.528$$

which are then converted to the dimensional form as:

$$c_{d_{i,opt}}^{Y_i} = \frac{X_{i,opt}^{Y_i}\sqrt{Hm}}{\eta_f(x_d/L)} = \frac{0.075\sqrt{3150 \times 10^3 \times 51.8}}{0.806 \times 0.05} = 23.8\ \text{kN} \cdot \text{s/m}$$

$$k_{d_{i,opt}}^{Y_i} = \tau_{i,opt}^{Y_i} k_d^{min} = 0.528 \times (-640.9) = -338.4\ \text{kN/m}$$

Since the NSD stiffness ratio is smaller than the allowable limit given in Fig. 5-5(b), i.e. $\tau = 0.528 < \tau_{all} = 0.73$, the design is acceptable.

5.7. Summary

In this chapter, a physical explanation for the superior damping performance of NSD compared to conventional passive viscous dampers, with either zero or positive damper stiffness, is presented. It is shown that a reduced total resisting force in NSD against the cable moving away from its neutral position allows a higher damper stroke and consequently, causes a higher capability in absorbing the kinetic energy. This phenomenon increases the damping ratio at the cost of an increased cable displacement, especially at the damper installation location. The issue of NSD stability is then investigated in detail. Based on the analytical model developed in previous chapters, theoretical and practical NSD stability limits are obtained. It is observed that for a given cable, the minimum allowable

negative stiffness of a NSD depends on the damper installation location, the cable bending stiffness, the cable length and the cable chord tension.

Next, an innovative approach for designing NSDs to control single-mode stay cable vibration is proposed based on the three-dimensional NSD performance surface. Two design scenarios are considered. In the first scenario, the NSD negative damper stiffness is given and the optimum damper size needs to be selected to achieve the maximum damping ratio; whereas in the second scheme, both the size and the negative damper stiffness of the NSD are optimized to satisfy the damping requirement for the target cable mode. The applicability of the proposed NSD design equations is verified by conducting an extensive numerical study on fifteen representative full-size stay cables. The allowable limits of the NSD stiffness ratio for different cable modes are identified. The effectiveness of the proposed NSD design approach is evaluated by presenting two design examples whereby a NSD is designed to suppress vibration of a 122 m long stay cable. It is shown that the design equations can efficiently determine the NSD parameters in both scenarios. It is concluded that while the damping ratio in the first mode is affected by both the cable bending stiffness and the cable sag effects, the influence of cable sag on the damping ratio is negligible for the higher modes (namely modes 2 and 3), both of which are only sensitive to the effect of cable bending stiffness.

Chapter 6 Impact of Support Stiffness on the NSD Performance

6.1. Introduction

In this chapter, the impact of damper support stiffness on the NSD performance in controlling cable vibration is investigated. The numerical and analytical approaches for evaluating the performance of a NSD when mounted on a flexible damper support are presented first. By utilizing existing analytical damper design formula, the NSD design for a target damping ratio is addressed in three typical design scenarios. The first scenario considers the NSD design for a given support condition. The second scenario deals with the design of the damper support by optimizing the support stiffness for a given NSD. The third scenario addresses the design of the entire NSD-support system by proposing an algorithm to identify the optimum combination of NSD parameters (damper size and stiffness) and damper support stiffness. In parallel, the NSD design is refined iteratively to minimize the influence of the assumptions considered in developing the analytical damper design formulation and improve the accuracy of the design. To evaluate the effectiveness of the proposed design schemes for a NSD mounted on rigid or flexible supports, a numerical example is conducted on a 325 m long stay cable installed on the Tatara bridge in Japan. The cable is equipped with an optimized NSD and subjected to harmonic excitation. The dynamic behaviour of the damped cable and the control performance of the optimized NSD are evaluated based on the displacement time-history at certain locations on the cable. To assess the performance of the NSD optimized for a flexible support, its

control effectiveness is compared with that of an optimal active linear-quadratic regulator (LQR) controller which is considered as the reference for cable vibration control.

6.2. Dynamic response of a damped cable

6.2.1. Formulation of the equation of motion

Figure 6-1 shows the mechanical model of a cable-damper system. The cable chord direction and the in-plane transverse direction are along the x- and y-axes, respectively. The static cable profile due to its self-weight and the dynamic in-plane transverse cable displacement caused by an arbitrary external force $f_e(x,t)$ are denoted by $z(x)$ and $w(x,t)$, respectively. The cable is inclined at an angle θ with respect to the horizontal axis and has a chord length L, a mass per unit length m, a chord tension H, a finite flexural rigidity EI and an axial rigidity EA. A transverse NSD is installed at the position $x = x_d$ from the lower end of the cable and is modeled by a linear dashpot with size c_d and a linear spring with stiffness k_d connected in parallel. The flexibility of the damper support is represented by a linear spring with stiffness k_s connected between the damper and the fixed base. In Fig. 6-1, $u_s(t)$ denotes the displacement at the top of the damper support spring.

By neglecting the inherent damping of the cable, its in-plane transverse dynamic response $w(x,t)$ is governed by the following integro-differential equation [79]:

$$m\ddot{w} + EIw^{(IV)} - Hw'' - \left(\frac{EA}{L_e}\right)z'' \int_0^L z'w'dx = f_e - F_d\delta(x - x_d) \qquad (6\text{-}1)$$

where $L_e = \int_0^L \{1 + [z'(x)]^2\}^{3/2}dx \approx L[1 + (8mgL\cos\theta/H)^2]$ is the effective cable length, $F_d(t)$ is the damper force, and $\delta(\cdot)$ is the Dirac delta function.

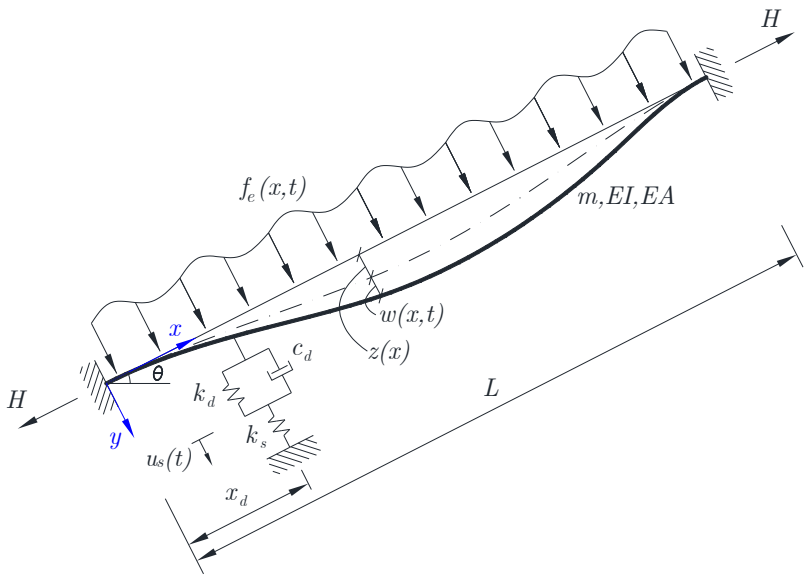

Fig. 6-1. Mechanical model of a cable-damper system.

6.2.2. Damping ratio of a cable equipped with a NSD mounted on a damper support

Analytical and numerical approaches are available to determine the damping ratio of a NSD-equipped cable based on Eq. (6-1). In the analytical approach, the free vibration response of the cable-damper system is derived as a function of the system complex modal frequency and the modal damping ratio is then extracted from this solution. Using a numerical technique, the free vibration displacement time-history of the damped cable is calculated from standard numerical methods (such as the mode superposition method (MSM)); the modal damping ratio is obtained by applying the logarithmic decrement method to the cable displacement time-history. Alternatively, the damping ratio can also be calculated numerically from system complex eigenvalues. This approach allows the independence of the evaluated cable damping ratio on the loading characteristics and the response measurement location. Furthermore, this approach can replace the time-consuming time-domain analysis for control implementation purposes and is

computationally more efficient. Both analytical and numerical approaches will be reviewed in this section to provide a framework for investigating the effect of damper support stiffness on the NSD performance.

6.2.2.1. Analytical approach

A refined asymptotic expression was developed in Chapter 3 for the modal damping ratio of a cable equipped with a passive damper by using the NSD mechanical model shown in Fig. 6-1. First, by assuming $w(x,t) = \bar{w}(x)e^{i\omega t}$ and $F_d(t) = \bar{F}_d e^{i\omega t}$ in Eq. (6-1), a transcendental equation was obtained to represent the free vibration response of the cable as a function of the complex modal frequency, ω. Next, an asymptotic solution to the transcendental equation was derived and further simplified to express the modal damping ratio of the damped cable as

$$\sigma_n = \left[\frac{(1-\alpha_{BC}q)^2}{\eta_k^2}\right]\frac{R_{sn}(n\pi\eta_{sn}X)}{(\bar{k}_d + 1/\eta_k)^2 + (n\pi\eta_{sn}X)^2} \tag{6-2}$$

where $\sigma_n = \zeta_n/(x_d/L)$ is the normalized cable damping ratio of mode n; $X = (x_d/L)\, c_d/\sqrt{Hm}$ is the dimensionless damper size, and $\eta_k = \eta_f + 1/\bar{k}_s$. The rest of the parameters have been defined in Section 3.3.

Equation (6-2) reveals that when a NSD is attached to a given cable at a specified location, the damping ratio achieved by the damped cable is a function of the damping coefficient c_d, the stiffness k_d of the damper, as well as the support stiffness k_s. For a given damper location of $0.02L$, Fig. 6-2(a) portrays the relationship between the normalized damping ratio σ_n of a damped cable and these three damper parameters in their dimensionless form, with the non-dimensional damping coefficient X, the non-dimensional damper stiffness $\bar{k}_d$,

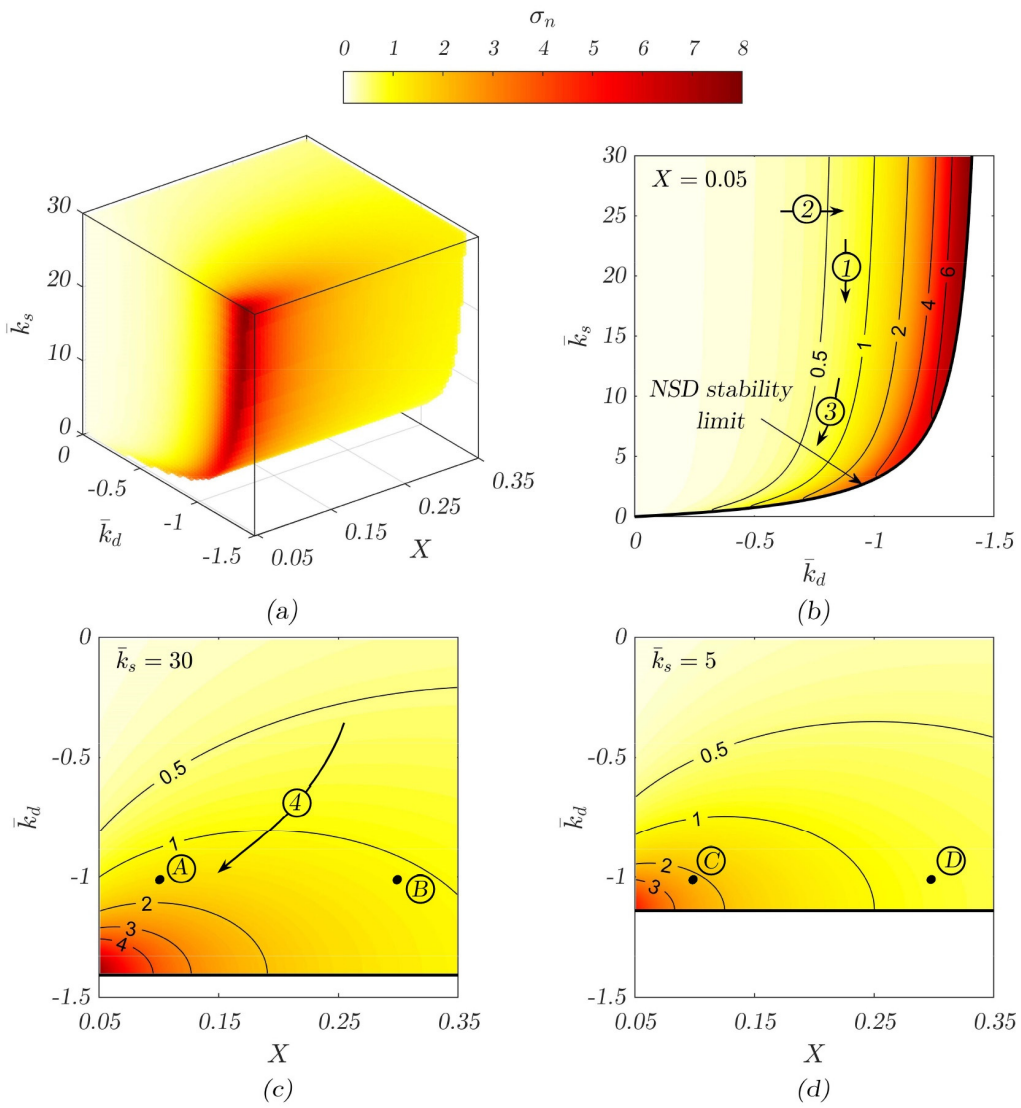

Fig. 6-2. Effect of non-dimensional damper size X, damper stiffness $\bar{k}_d$ and support stiffness $\bar{k}_s$ on the normalized damping ratio of a NSD. (a) Simultaneous effects of X, $\bar{k}_d$ and $\bar{k}_s$, (b) Effects of $\bar{k}_d$ and $\bar{k}_s$ for a given $X = 0.05$, (c) Effects of X and $\bar{k}_d$ for a given $\bar{k}_s = 30$, and (d) Effects of X and $\bar{k}_d$ for a given $\bar{k}_s = 5$.

and the non-dimensional damper support stiffness $\bar{k}_s$ represented respectively by the three axes, while the magnitude of the normalized damping ratio σ_n by the color defined in the color map. This non-dimensional plot is constructed based on a typical full-size stay cable in the cable database compiled by Tabatabai et al. [106]. The cable has a unit mass $m =$

$52.8\ \mathrm{kg/m}$, a length $L = 101.8\ \mathrm{m}$, a pre-tension $H = 2813\ \mathrm{kN}$, a bending stiffness $EI = 555.1\ \mathrm{kN \cdot m^2}$, an axial stiffness $EA = 1064.8\ \mathrm{MN}$, and is inclined at $\theta = 27.8°$ with respect to the horizontal. It can be observed from Fig. 6-2(a) that larger σ_n values occur at the anterior corner of the plot where X approaches the minimum value of 0.05 considered in the plot, and the combination of $\bar{k}_d$ and $\bar{k}_s$ advances toward the NSD stability limit governed by Eq. (5-2).

Figure 6-2(b) illustrates the variation of σ_n with respect to $\bar{k}_s$ and $\bar{k}_d$ when $X = 0.05$. In particular, the contours of $\sigma_n = 0.5$, 1, 2, 4, 6, and 7.5 are illustrated in the figure, of which $\sigma_n = 0.5$ corresponds to the maximum possible normalized damping ratio provided by an ideal ZSD [70], whereas $\sigma_n = 7.5$ represents the stability limit of a NSD at $X = 0.05$. The region between the contours of $\sigma_n = 0.5$ and $\sigma_n = 7.5$ describes the performance of a stable NSD under different combinations of damper stiffness and support stiffness when $X = 0.05$. The pattern of the σ_n contours suggests that for a given NSD, i.e. both X and $\bar{k}_d$ are known constants, choosing a more flexible damper support would increase the damping ratio of the cable. This trend is reflected by arrow 1 in Fig. 6-2(b), which indicates a lower $\bar{k}_s$ value would lead to a larger σ_n. On the other hand, arrow 2 in the figure shows that when the support stiffness and the damper size of a NSD are given, introducing stronger negative stiffness into the damper would be more effective in dissipating the energy. In the case that the required damping ratio and damper size are specified, i.e. σ_n and X are constants, the choice of a more flexible damper support would reduce the demand on the negative damper stiffness. This phenomenon can be clearly seen by following arrow 3 in Fig. 6-2(b).

Figures 6-2(c) and 6-2(d) depict the influence of the non-dimensional damper size X and the non-dimensional damper stiffness $\bar{k}_d$ on the normalized damping ratio σ_n of a damped cable when the non-dimensional damper support stiffness $\bar{k}_s$ equals to 30 and 5, respectively. These two $\bar{k}_s$ values represent respectively a relatively rigid or a relatively flexible damper support conditions. Based on Eq. (5-2), the stability requirement of the NSD for these two stiffness values are $\bar{k}_d^{min} = -1.41$ and -1.14, respectively, which are shown as horizontal lines at the bottom of Figs. 6-2(c) and 6-2(d). The variation pattern of σ_n in both plots show that a higher damping ratio can be achieved if $\bar{k}_d$ and X become smaller, as indicated by arrow 4 in Fig. 6-2(c). The maximum damping ratio is achieved when both $\bar{k}_d$ and X reach their minimum allowable values, which is reflected by the darkest color at the lower-left corner of Figs. 6-2(c) and 6-2(d). Further, it can be seen from these two plots that for a given damper support stiffness, various combinations of damper size and stiffness are possible to satisfy a specific damping ratio requirement. This observed feature will be exploited to optimize the NSD design, as will be discussed further in Section 6.3.

The effect of the damper support stiffness on the NSD performance is further evaluated by referring to the design points A, B, C, and D in Figs. 6-2(c) and 6-2(d). Points A and C represent the performance of a NSD with a non-dimensional damper size $X = 0.1$ and a negative damper stiffness $\bar{k}_d = -1$ when mounted respectively on a damper support having non-dimensional stiffness $\bar{k}_s$ of 30 and 5. The normalized damping ratio that corresponds to these two cases are 1.5 and 2.1, respectively, which implies that for such a case installing a NSD on a more flexible damper support would be beneficial for its performance. Nevertheless, if the damper stiffness of the NSD remains the same at $\bar{k}_d =$

-1, but the non-dimensional damper size increases to modify $X = 0.1$ to $X = 0.3$, the same reduction of $\bar{k}_s$ from 30 to 5 would result in a decrease in the normalized damping ratio from 1.1 to 0.8 and thus has an adverse effect on the damper performance. This suggests that the effect of damper support stiffness depends on the damper size. This feature will be discussed in detail in Section 6.3.2.

As indicated in the previous studies (e.g. [71]), it is expected that the damping ratio determined by Eq. (6-2) would be slightly conservative due to the assumptions made in its derivation, i.e. $x_d \ll L$ and $4EI(\beta_{0n}^s)^2/H \ll 1$. On the other hand, a numerical method can also be used to calculate the damping ratio of the studied cable-damper system. Since such assumptions are not needed in the numerical approach, it is expected to yield more accurate results, and could, therefore, be used to refine a NSD designed in accordance with Eq. (6-2).

6.2.2.2. Numerical approach

The damping ratio of a cable-damper system can be predicted from the decay rate of the cable dynamic displacement time-history. Equation (6-1), which governs the in-plane transverse dynamic response of the cable, can be solved by the mode superposition method (MSM). The cable displacement, $w(x,t)$, is approximated by the following finite series

$$w(x,t) = \sum_{i=1}^{n} \phi_i(x) q_i(t) \tag{6-3}$$

where $\phi_i(x)$ is the i^{th} mode shape function, $q_i(t)$ is the i^{th} mode generalized coordinate, and n is the number of considered modes. Referring to Section 4.2.3, the matrix form of the equation of motion of a damped cable can be expressed as:

$$\boldsymbol{M}\ddot{\boldsymbol{q}} + \boldsymbol{K}\boldsymbol{q} = \boldsymbol{f} - \boldsymbol{\phi_d} F_d(t) \tag{6-4}$$

where $\boldsymbol{q} = \{q_i(t)\}_{n\times 1}$ is the generalized displacement vector, $\boldsymbol{M} = \left[m_{ij}\right]_{n\times n} = m[\int_0^L \phi_i(x)\phi_j(x)dx]$ is the modal mass matrix, $\boldsymbol{K} = \left[k_{ij}\right]_{n\times n} = H[\int_0^L \phi_i^{'}(x)\phi_j^{'}(x)dx] + EI[\int_0^L \phi_i^{''}(x)\phi_j^{''}(x)dx] + (EA/L_e)[\int_0^L z^{''}(x)\phi_i(x)dx \int_0^L z^{''}(x)\phi_j(x)dx]$ is the modal stiffness matrix, $z(x)$ is the static cable profile due to its self-weight, $\boldsymbol{f} = \left\{f_j\right\}_{n\times 1} = \{\int_0^L f_e(x,t)\phi_j(x)dx\}$ is the generalized external force vector, $\boldsymbol{\phi_d} = \left\{\phi_j(x_d)\right\}_{n\times 1}$ is the shape function vector at the damper location, $F_d(t)$ is the time-dependent force in the damper defined in Section 4.2.3, and $j = 1,2,\dots,n$. Based on the mechanical model considered in Fig. 6-1 for the NSD, a slightly approximate linearized form of Eq. (6-4) can be derived as:

$$\widetilde{\boldsymbol{M}}\ddot{\boldsymbol{q}} + \widetilde{\boldsymbol{C}}\dot{\boldsymbol{q}} + \widetilde{\boldsymbol{K}}\boldsymbol{q} = \boldsymbol{f} \tag{6-5}$$

where $\widetilde{\boldsymbol{M}} = [\tilde{m}_{ij}] = \boldsymbol{M} - \alpha\tilde{c}_d[\phi_i(x_d)\phi_j(x_d)]$, $\widetilde{\boldsymbol{C}} = [\tilde{c}_{ij}] = (\tilde{c}_d - \alpha\tilde{k}_d)[\phi_i(x_d)\phi_j(x_d)]$, and $\widetilde{\boldsymbol{K}} = [\tilde{k}_{ij}] = \boldsymbol{K} + \tilde{k}_d[\phi_i(x_d)\phi_j(x_d)]$ are the effective mass, damping and stiffness matrices, respectively, $\tilde{k}_d = k_d/(1 + k_d/k_s)$ is the modified damper stiffness, $\tilde{c}_d = c_d/(1 + k_d/k_s)$ is the modified damper size, $\alpha = c_d/(k_d + k_s)$ is the time constant of the damper force, and $\boldsymbol{f} = \{f_j\} = \{\int_0^L f_e(x,t)\phi_j(x)dx\}$ is the vector of generalized external force. The subsequent steps for calculating the modal damping ratio from the complex eigenvalues of the homogenous form of Eq. (6-5) have already been presented in Section 4.2.3.

6.2.3. NSD stability

The NSD stability issue was addressed in Section 5.3 for a NSD installed on a rigid damper support. In a more general case where the damper is supported by a flexible base, the stability limit defined by Eq. (5-2) would no longer be valid. In this case, and referring to the term $(\bar{k}_d + 1/\eta_k)^2$ in the denominator of Eq. (6-2), the NSD stability criterion can be extended to a more general form by including the effect of damper support stiffness to define the damper stiffness limit as:

$$\bar{k}_d^{min} = -\frac{1}{\eta_k} \tag{6-6}$$

where $\eta_k = \eta_f + 1/\bar{k}_s$. Equation (6-6) takes into account the effects of damper support stiffness and cable bending stiffness, it can be considered as the generalized form of the theoretical NSD stability limit previously introduced by Eq. (5-2). The NSD instability phenomenon was first observed in Fig. 3-4 where the integrated stiffness coefficient $C_k = \Psi/(1+\Psi)$ approaches to positive infinity as $\Psi = 1/(\bar{k}_d\eta_k)$ tends toward to -1. In practical applications, it is recommended to consider a safety margin when determining the minimum allowable negative damper stiffness, k_d, in order to prevent possible damage to the cable and/or the NSD, i.e.$\Psi < -1 \times \Omega_{st}$, where $\Omega_{st} > 1$ is the factor of safety which may be chosen based on engineering judgement. In addition, it was observed in Sections 3.4 and 3.5 that the efficiency of a NSD would be better than that of the ZSD with the same damper size when $\Psi \geq -(1 + \bar{k}_s\eta_f)$. By considering both conditions, the practical range for the negative stiffness of a NSD device can be expressed as:

$$-\frac{1}{\eta_k}\frac{1}{\Omega_{st}} < \bar{k}_{d,prac}^{min} < -\frac{1}{\bar{k}_s\eta_k^2} \tag{6-7}$$

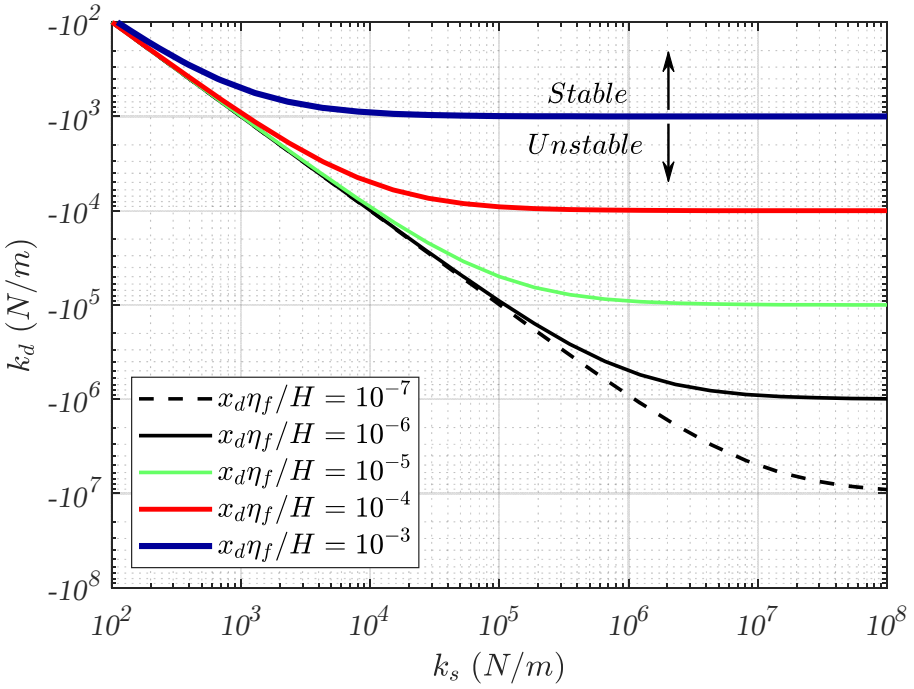

Fig. 6-3. Stability limit of NSD mounted on a flexible support.

The stability requirement of a NSD under different installation conditions is studied in Fig. 6.3. The damper installation conditions include properties of the attached cable and the damper location, which can be described by $x_d\eta_f/H$. The relation between the minimum allowable negative damper stiffness, k_d, and the damper support stiffness, k_s, under $x_c\eta_f/H = 10^{-3}$, 10^{-4}, 10^{-5}, 10^{-6} and 10^{-7} are portrayed in this figure, with each curve corresponds to one specific installation condition. For each installation condition, the stable performance of a NSD can be ensured should its stiffness falls within the zone above the $k_d - k_s$ curve. The NSD would lose its stability if the negative damper stiffness is less than the limit defined by the curve. As an example, the stable and unstable zones associated with the installation condition of $x_d\eta_f/H = 10^{-3}$ are shown in Fig. 6-3, of which the former is defined by the shaded area above the $k_d - k_s$ curve. In addition, it can be observed from Fig. 6-3 that as the damper support becomes stiff enough, the threshold of

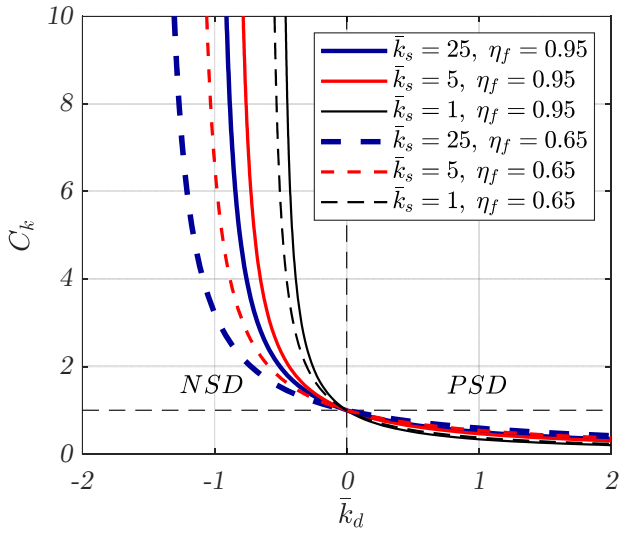

(a)

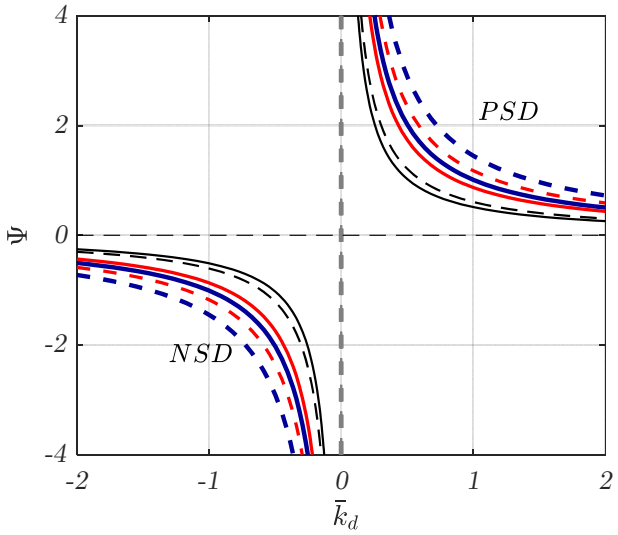

(b)

Fig. 6-4. Variation of C_k and Ψ with respect to the nondimensional damper stiffness $\bar{k}_d$ for different values of $\bar{k}_s$ and η_f.

minimum allowable negative damper stiffness to ensure stable performance of a NSD approaches to a constant value of $-1/\eta_f$.

Figures 6-4(a) and 6-4(b) show the variation of C_k and Ψ with respect to the non-dimensional damper stiffness $\bar{k}_d$, respectively. Three levels of damper support stiffness $\bar{k}_s$, i.e. $\bar{k}_s = 25$, 5 and 1, and two η_f values of 0.95 and 0.65 are considered. Based on Fig. 6-

4(a), for a constant negative value of $\bar{k}_d$, C_k will increase when the damper support becomes more flexible. This phenomenon agrees with the observations made from Figs. 3-7(a) and 3-7(b), and is also confirmed by the results in Fig. 6-3, where the minimum permissible negative damper stiffness increases when k_s is reduced. In other words, if the damper stiffness of a NSD remains constant, as the support becomes more flexible, it will approach to the stability limit and therefore C_k will increase. As illustrated in figure 6-4(a), for a stable NSD with constant damper stiffness and support conditions, the integrated stiffness coefficient C_k increases with an increase in η_f. Therefore, it is concluded that placing the damper further from the cable anchorage and/or lowering the flexural rigidity will increase both η_f and C_k for NSD (see also Fig. 3-3(a)). Results in Fig. 6-4(b) reveal that an increase in $\bar{k}_s$ or a reduction in η_f would increase Ψ for a PSD device with constant $\bar{k}_d$. Based on Eq. (3-17), this would lead to an increase in C_k, as already been observed in Fig. 6-4(a). On the other hand, in the case of NSD, the pattern is opposite. For a given NSD, Ψ would increase for smaller $\bar{k}_s$ and/or larger η_f.

6.3. Impact of damper support stiffness on NSD design

It can be seen from Eq. (6-2) that the normalized damping ratio of a cable equipped with a NSD can be influenced by various factors, some of which are associated with the cable, while others are related to the NSD and its support. Therefore, if a NSD is needed to suppress excessive vibrations of a particular cable and the damper installation location has been specified, then the NSD design would typically include the design of the entire NSD system, i.e. the NSD itself and the support, or part of the system such as the damper or the support if other features of the NSD system have already been selected. How the damper

support stiffness would affect the NSD design in these typical scenarios will be discussed in the following sub-sections.

6.3.1. Design scenario 1: Damper design

In the first scenario, it is assumed that the damper installation location, x_d, has been determined and the damper support has been fabricated, i.e. the support stiffness, k_s, is known. The design objective is to select the size and the stiffness of a NSD to achieve the desired damping ratio for a particular mode. It has been observed in Figs. 6-2(c) and 6-2(d) that for a given support stiffness, various combinations of c_d and k_d are possible for a NSD to achieve the same damping ratio. These combinations form a damping ratio contour which is concave downward and has a peak point representing a NSD with the least amount of negative stiffness to satisfy the specified damping requirement. Since among all the design points on the same damping ratio contour line, the peak point corresponds to the NSD design that is the farthest from the NSD stability limit, it is considered as the optimum design in this scenario.

The c_d and k_d values corresponding to the above design point can be obtained for an arbitrary k_s based on Eq. (6-2). The equation is first rewritten in the form of $\bar{k}_d = f(X)$. Then, by solving for the extremum, $\partial f(X)/\partial X = 0$, and substituting the root back into $\bar{k}_d = f(X)$, the optimum non-dimensional damper size and damper stiffness that provide the n^{th} modal damping ratio of ζ_n can be obtained as follows:

$$X^{opt} = \frac{R_{sn}}{2n\pi\eta_{sn}Y_n} \tag{6-8}$$

$$\bar{k}_d^{opt} = \frac{R_{sn}}{2Y_n} - \frac{1}{\eta_k} \tag{6-9}$$

where $Y_n = \zeta_n/[(x_d/L)(1-q)^2/\eta_k^2]$ is an auxiliary damping ratio parameter. The following expressions can then be used to determine the optimum damper size and damper stiffness values, which are:

$$c_d^{opt} = \frac{X^{opt}\sqrt{Hm}}{x_d/L} \tag{6-10}$$

$$k_d^{opt} = \frac{\bar{k}_d^{opt} H}{x_d} \tag{6-11}$$

The impact of support stiffness on the optimum NSD design parameters c_d^{opt} and k_d^{opt} is investigated in Fig. 6-5. In this figure, the variation of the normalized damping ratio σ_n with X and $\bar{k}_d$ is illustrated for three damper support stiffness cases, namely $\bar{k}_s = \infty$, 10 and 3. Figure 6-5(a) shows the three-dimensional damping ratio surfaces and their intersection with the plane of $\sigma_n = 2$. In this plane, the NSD design curves can be identified for achieving a constant damping ratio of $\zeta_n = 2(x_d/L)$. Figure 6-5(b) depicts the NSD design curves corresponding to the three studied support stiffness cases in the plane of $\sigma_n = 2$, as well as the optimal design points p_1, p_2 and p_3 in each case. The respective NSD stability limits are also shown in Fig. 6-5(b) as dashed lines. To achieve the same damping requirement, the change in the design points while the support stiffness reduces can be clearly observed from the three $\bar{k}_d - X$ curves in the figure, i.e. both the damper size and the absolute value of the damper stiffness decreases as the support becomes more flexible. Therefore, by considering the manufacturing and maintenance costs of a NSD, using more flexible damper support would also help to improve its cost-efficiency.

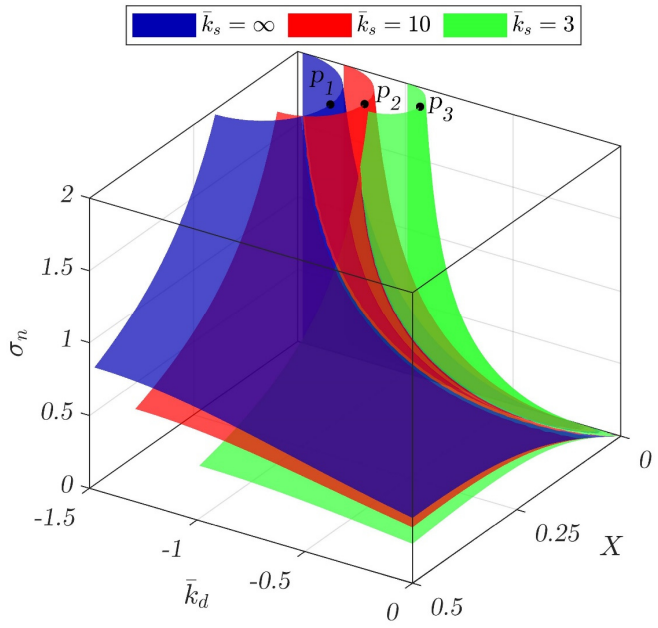

(a)

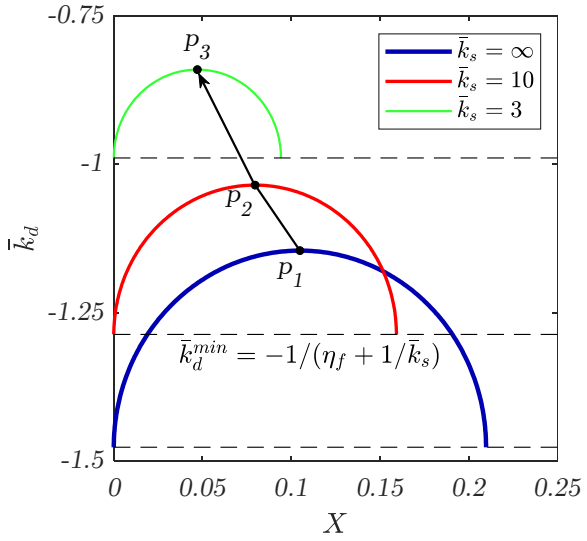

(b)

Fig. 6-5. NSD design for single-mode cable vibration control. (a) Effects of X and $\bar{k}_d$ on the normalized damping ratio of NSD for three given values of $\bar{k}_s = \infty, 10$ and 3. (b) Impact of damper support stiffness on the NSD design points.

6.3.2. Design scenario 2: Damper support design

In this scenario, the damper installation location has been specified and both the size c_d and the stiffness, k_d, of the NSD have been selected in advance. The goal is to choose an

optimum damper support stiffness to attain the best vibration control performance, i.e. to maximize the damping ratio of the damped cable.

The optimum value of the normalized damper support stiffness, $\bar{k}_s^{opt}$, can be found by solving $\partial\sigma_n/\partial\bar{k}_s = 0$ based on Eq. (6-2). The solution is a function of $\bar{k}_d$ and X, which can be expressed as:

$$\bar{k}_s^{opt} = -\frac{1}{\eta_f + \dfrac{1}{\bar{k}_d + (n\pi\eta_{sn}X)^2/\bar{k}_d}} \tag{6-12}$$

On the other hand, the minimum allowable support stiffness can be determined from the NSD stability limit (Eq. (6-6)) and expressed as:

$$\bar{k}_s^{min} = -\frac{1}{\eta_f + 1/\bar{k}_d} \tag{6-13}$$

For an optimum support stiffness to exist, the $\bar{k}_s^{opt}$ value obtained from Eq. (6-12) must be greater than the minimum allowable support stiffness. Compare Eq. (6-13) with Eq. (6-12), it can be observed that for a NSD which has negative damper stiffness, the condition $\bar{k}_s^{opt} > \bar{k}_s^{min}$ always holds. It should be noted that $\bar{k}_s^{min}$ is the minimum support stiffness needed to prevent NSD instability and $\bar{k}_s^{opt}$ is the optimum support stiffness that would allow an existing NSD to achieve its best performance. According to Eq. (6-13), the minimum allowable support stiffness, $\bar{k}_s^{min}$, can be either positive or negative. The positive $\bar{k}_s^{min}$ occurs when $\bar{k}_d > -1/\eta_f$ and $\bar{k}_d < 0$, while the negative $\bar{k}_s^{min}$ requires either $\bar{k}_d > 0$ (i.e. PSD) or $\bar{k}_d < -1/\eta_f$. Hence, the negative $\bar{k}_s^{min}$ would result in a NSD with a stronger negative damper stiffness compared to the positive $\bar{k}_s^{min}$ case. Since a stronger negative damper stiffness is not a preferable choice in terms of not only the fabrication and

cost, but also in terms of system stability, a positive $\bar{k}_s^{min}$ should be used. Hence, by combining the above two conditions of $\bar{k}_s^{opt} > \bar{k}_s^{min}$ and $\bar{k}_s^{min} > 0$, it is concluded that the optimum damper support stiffness $\bar{k}_s^{opt}$ should also be positive. This condition can be satisfied when the denominator of the term on the right-hand side of Eq. (6-12) is negative. Therefore, any combination of X and $\bar{k}_d$ that can yield $\{\eta_f + 1/[\bar{k}_d + (n\pi\eta_{sn}X)^2/\bar{k}_d]\} < 0$ would meet this requirement. The critical non-dimensional damper size required to ensure the presence of a positive $\bar{k}_s^{opt}$ can thus be derived as:

$$X^{cr} = \frac{\sqrt{(-\bar{k}_d)(\bar{k}_d + 1/\eta_f)}}{n\pi\eta_{sn}} \tag{6-14}$$

Therefore, $c_d < X^{cr}\sqrt{Hm}/(x_d/L)$ would be a sufficient condition to ensure a positive $\bar{k}_s^{opt}$ exists. Otherwise, a reduction in $\bar{k}_s$ would not help to increase the NSD damping ratio. By substituting Eq. (6-12) into Eq. (6-2), the maximum achievable damping ratio of a NSD after optimizing its support stiffness can be derived as:

$$\sigma_n^{max} = \frac{(1-q)^2 R_{sn}[\bar{k}_d{}^2 + (n\pi\eta_{sn}X)^2]}{n\pi\eta_{sn}X} \tag{6-15a}$$

or

$$\zeta_n^{max} = (\frac{x_d}{L})\sigma_n^{max} \tag{6-15b}$$

Figure 6-6 illustrates the effect of the damper support stiffness on the modal damping ratio in three different damper size cases, i.e. $X < X^{cr}$, $X = X^{cr}$ and $X > X^{cr}$. It can be observed that when $X < X^{cr}$, a reduction in $\bar{k}_s$ would enhance the damping ratio until it reaches the maximum value σ_n^{max} at $\bar{k}_s^{opt}$ (Eq. (6-15)). However, in the latter two cases, the usage of

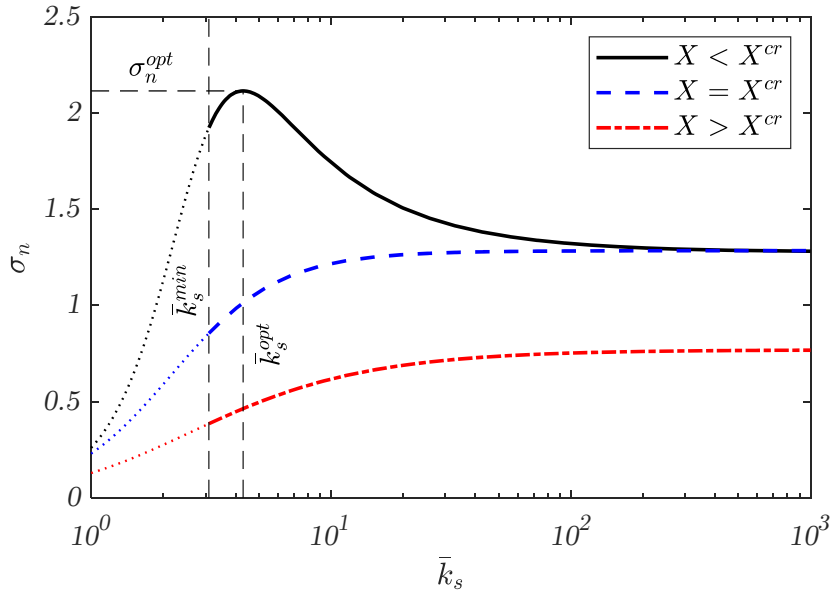

Fig. 6-6. Impact of damper support stiffness on the modal damping ratio of a NSD-equipped cable.

a flexible support for a NSD has no advantage since the damping ratio of the damped cable would decrease monotonically with the reduction of $\bar{k}_s$.

6.3.3. Design scenario 3: Design of the entire NSD system (damper and support)

The design of an entire NSD system for a given damper location to satisfy a specified cable damping requirement is also a commonly encountered scenario. The purpose of such design is to determine the optimum combination of c_d, k_d and k_s for a given ζ_n and x_d. As shown in Fig. 6-6, the damping ratio increases with the decrease of the support stiffness to reach its maximum value at $\bar{k}_s^{opt}$ provided that $X < X^{cr}$. Besides, it has been shown in the previous section that the optimized damper support stiffness would always be larger than the positive minimum allowable support stiffness, i.e. $\bar{k}_s^{opt} > \bar{k}_s^{min} > 0$. Although in theory, the choice of $\bar{k}_s^{opt}$ as the NSD support stiffness seems to be an obvious solution, the stiffness of the NSD support must be sufficiently larger than $\bar{k}_s^{min}$ to avoid instability

of the cable-damper system. It is then necessary to find an appropriate support stiffness that is as close as possible to $\bar{k}_s^{opt}$ and at the same time, sufficiently larger than $\bar{k}_s^{min}$. For this purpose, a safety factor, $SF > 1$, is introduced to ensure the selected damper support stiffness satisfies $\bar{k}_s \geq \bar{k}_s^{min} \times SF$. Based on these considerations, an algorithm for obtaining an optimum combination of damper size, damper stiffness, and damper support stiffness is proposed as follows:

1. Initialize the design by setting a counter for the iteration number as $i = 1$ and assuming a rigid damper support condition (a large $\bar{k}_{s,i}$ value such as $\bar{k}_{s,i} = 1000$ can be used to represent rigid support).
2. Use $\bar{k}_{s,i}$ to determine the non-dimensional damper size X_i and damper stiffness $\bar{k}_{d,i}$ in accordance with Scenario 1 for the given cable parameters, damper location and the required damping ratio (Eqs. (6-10) and (6-11)).
3. Based on the NSD parameters obtained in Step 2, calculate $\bar{k}_{s,i}^{min}$, $\bar{k}_{s,i}^{opt}$ and X_i^{cr} using Eqs. (6-12) to (6-14).
4. If $X_i < X_i^{cr}$, calculate $\bar{k}_{s,new} = (\bar{k}_{s,i} + \bar{k}_{s,i}^{opt})/2$ where $\bar{k}_{s,i}$ is the support stiffness used in Step 2. Otherwise, continue with Step 6.
5. If $\bar{k}_{s,new} > \bar{k}_{s,i}^{min} \times SF$, increase the counter i by 1, update $\bar{k}_{s,i}$ as $\bar{k}_{s,i} = \bar{k}_{s,new}$ and go back to Step 2.
6. Calculate the dimensional values of the damper size, damper stiffness and damper support stiffness obtained in Step 2 ($c_{d,i}$, $k_{d,i}$ and $k_{s,i}$) and report them as the final design parameters of NSD and its support.

The above optimization algorithm for NSD system design is summarized in the flowchart shown in Fig. 6-7. Based on this algorithm, the selected damper support stiffness would be as close to $\bar{k}_s^{opt}$ as possible to maximize the NSD control efficiency and also sufficiently larger than $\bar{k}_s^{min}$ to ensure the stability of the NSD. Since $\bar{k}_s$ decreases monotonically towards $\bar{k}_s^{opt}$ and both $\bar{k}_s$ and $\bar{k}_s^{opt}$values are always positive, the proposed algorithm is robust and will converge after a few iterations.

6.4. Refinement of NSD design

It was indicated earlier that Eq. (6-2) is derived for a damped cable under the assumptions of a fixed-fixed boundary conditions, and small values of x_d/L and $4EI(\beta_{0n}^s)^2/H$. As detailed in Chapter 3 for PSD- and NSD-controlled cables and reported in [71] for ZSD-controlled cables, these assumptions would cause Eq. (6-2) to underestimate the attainable damping ratio of a damped cable. Although Eq. (6-2) provides a conservative damper design in all cases which is safe, the underestimation of the actual achievable damping ratio would be more considerable for longer cables. This stems from the fact that due to the high in-plane flexibility of a longer stay cable ($L > 250\ m$), its end anchorage condition is more agreeable with a hinged-hinged boundary condition rather than a fixed-fixed condition [90]. Therefore, the actual energy dissipation capability is greater than that predicted by the asymptotic damping ratio equation, Eq. (6-2). On the other hand, accurate numerical models are available to analyze the dynamic response of a cable-damper system, such as the MSM-based control-oriented model proposed in Chapter 4. This model relaxes the aforementioned assumptions and can thus accurately evaluate the NSD performance. Hence, it is possible to refine the NSD design by combining the analytical and the numerical approaches. The numerical model is adopted to calculate the damping ratio of

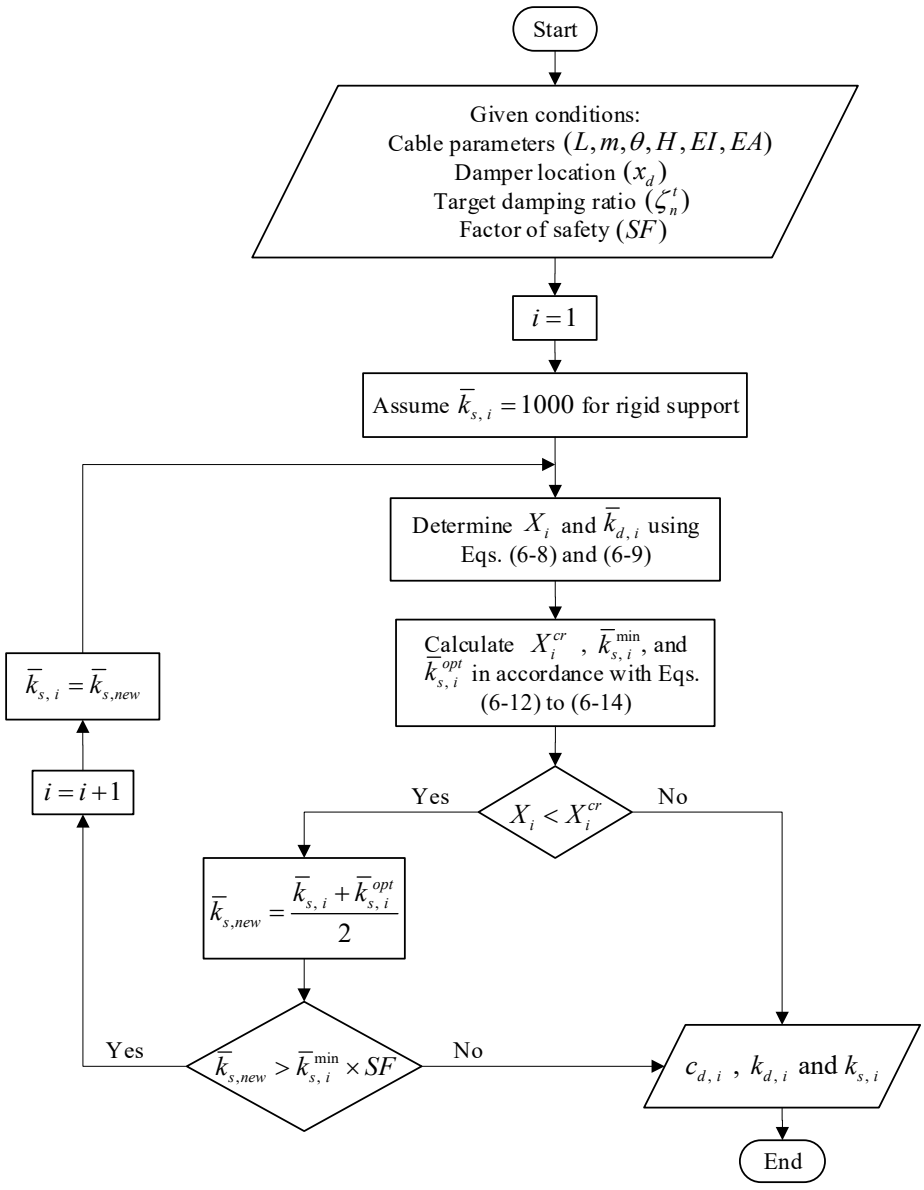

Fig. 6-7. Design optimization of a NSD system for cable vibration control in design scenario 3.

the cable equipped with an analytically designed NSD. Then, the numerically-calculated damping ratio is compared with the required damping ratio. Based on the observed discrepancy between the numerical and the target damping ratio, the NSD design process is repeated with the modified design input. The accuracy of the refinement is controlled by

the tolerance parameter, e_{tol}, which shall be selected sufficiently small to minimize the error in the design. The proposed refinement algorithm is as follows:

1. The process is initialized by defining $\zeta_n^d = \zeta_n^t$, where ζ_n^d is the design damping ratio used in the analytical design formulas to determine the NSD parameters, and ζ_n^t is the specified target damping ratio to be provided by the NSD.
2. For the given cable properties and damper installation location, the unknown parameters of the NSD and its support are determined analytically for the design damping ratio, ζ_n^d, by using the design procedures presented in Section 6.3.
3. The obtained NSD parameters are taken as input to the numerical model (Section 6.2.2.2) to construct the modal matrices of the cable-damper system. The modal damping ratio, ζ_n^r, is calculated numerically by finding the complex eigenvalues of the damped cable. The numerically-obtained damping ratio is expected to be larger than the input damping ratio, i.e. $\zeta_n^r > \zeta_n^d$.
4. Compare ζ_n^r with ζ_n^t and calculate the error $e = (\zeta_n^r - \zeta_n^t)/\zeta_n^t$. If $|e| < e_{tol}$, the refinement process of the NSD design is completed and the resulted NSD would provide the required damping ratio accurately. Otherwise, multiply the design damping ratio by $1/(1+e)$ and return to Step 2 to redesign the NSD for the updated design damping ratio of $\zeta_n^d/(1+e)$.

6.5. Numerical example

In this section, a numerical example is presented to illustrate the NSD design procedures outlined in Sections 6.3 and 6.4 and evaluate the impact of the damper support stiffness on

Table 6-1. Properties of the cable used in the numerical example.

L (m)	m (kg/m)	D (m)	θ (deg.)	H (kN)	EI (kN · m^2)	EA (MN)	f_1 (Hz)	λ^2
324.9	83.9	0.145	29.3	4175.1	2011.2	1999.7	0.378	1.49

the NSD performance. The dynamic behaviour of a full-size cable equipped with a NSD mounted on either a rigid or a flexible damper support is studied. The effectiveness of the NSD yielded from the refined and non-refined design will be compared. Finally, the performance of a NSD system, with its parameters optimized by the proposed approach, is compared with that of an optimal LQR controller.

6.5.1. Problem description

A 324.9-meter long stay cable is selected from the cable database compiled by Tabatabai et al. [106] for the numerical example. The mechanical and geometric properties of this cable are listed in Table 6-1. It is required to design a damper system which can provide a damping ratio of 4% in the first mode to suppress potential cable vibrations. The damper is restricted to be installed at 2% of the cable length from the cable-deck anchorage. The objective is to determine the parameters of the damper and its support for the prescribed conditions (design scenario 3). It is worth noting that for the specified damper location, should an ideal passive ZSD be used, it could provide a maximum damping ratio of $0.5(x_d/L) = 1\%$ [70]. Hence, to satisfy the design requirement, a NSD system will be designed following the algorithm for design scenario 3 presented in Section 6.3.3.

6.5.2. Design of the NSD system

The detailed design of the NSD system is illustrated below. The safety factor SF is taken as 3. The optimum non-dimensional damper size and stiffness of the NSD are first

estimated using Eqs. (6-8) and (6-9) based on the assumption of rigid damper support, i.e. $\bar{k}_s = 1000$ ($k_s = 642$ MN/m).

1. The cable-related parameters are calculated as: $R_{s1} = 0.842$, η_{s1}=1.059, $\eta_f = 0.84$, $q = 0.107$, and $\eta_k = \eta_f = 0.84$.
2. For the required damping ratio of 4% and the specified damper location of 2%. The corresponding auxiliary damping ratio parameter is calculated as $Y_1 = (0.04/0.02)/[(1-0.107)^2/0.84^2] = 1.77$.

$$X^{opt} = \frac{R_{s1}}{2(1)\pi\eta_{s1}Y_1} = \frac{0.842}{2 \times 1 \times \pi \times 1.059 \times 1.77} = 0.0715$$

$$\bar{k}_d^{opt} = \frac{R_{s1}}{2Y_1} - \frac{1}{\eta_k} = \frac{0.842}{2 \times 1.77} - \frac{1}{0.84} = -0.953$$

The optimum damper size and damper stiffness are then calculated using Eqs. (6-10) and (6-11), which are:

$$c_d = \frac{X^{opt}\sqrt{Hm}}{(x_d/L)} = \frac{0.0715\sqrt{4175.1 \times 10^3 \times 83.9}}{0.02} = 66.9 \text{ kN} \cdot \text{s/m}$$

$$k_d = \frac{\bar{k}_d^{opt} H}{x_d} = \frac{-0.953 \times 4175.1 \times 10^3}{0.02 \times 324.9} = -612.2 \text{ kN/m}$$

3. To determine the possibility of optimizing the damper support stiffness, the non-dimensional optimum and minimum support stiffness, as well as the critical non-dimensional damper size are first calculated using Eqs. (6-12) to (6-14):

$$\bar{k}_s^{opt} = -\frac{1}{0.84 + 1/[-0.953 + (\pi \times 1.059 \times 0.0715)^2/(-0.953)]} = 6.8$$

Table 6-2. Optimization of the NSD and its support in the numerical example.

Iteration	$\bar{k}_s$ (a)	X (b)	$\bar{k}_d$ (c)	X^{cr} (d)	$\bar{k}_s^{min}$ (e)	$\bar{k}_s^{opt}$ (f)	$\frac{\bar{k}_s + \bar{k}_s^{opt}}{2}$ (g)	$\bar{k}_s^{min} \times SF$ (h)	Check (b) < (d)?	Check (g) > (h)?
1	1000	0.071	-0.953	0.143	4.8	6.8	503.4	14.4	True	True
2	503.4	0.071	-0.951	0.143	4.7	6.7	255.0	14.2	True	True
3	255.0	0.071	-0.949	0.144	4.7	6.6	130.8	14.0	True	True
4	130.8	0.070	-0.946	0.145	4.6	6.4	68.6	13.8	True	True
5	68.6	0.069	-0.940	0.146	4.5	6.1	37.4	13.4	True	True
6	37.4	0.067	-0.930	0.148	4.3	5.7	21.5	12.8	True	True
7	21.5	0.064	-0.915	0.151	3.9	5.1	13.3	11.8	True	True
8	**13.3**[a]	**0.060**[b]	**-0.892**[c]	0.155	3.6	4.4	8.8	10.7	True	**False**
9	8.8	0.056	-0.865	0.160	3.2	3.8	6.3	9.5	True	False

[a] $k_s = 8542$ kN/m;
[b] $c_d = 56.4$ kN · s/m;
[c] $k_d = -573.4$ kN/m.

$$\bar{k}_s^{min} = -\frac{1}{0.84 + 1/(-0.953)} = 4.77$$

$$X^{cr} = \frac{\sqrt{(0.953)(-0.953 + 1/0.84)}}{\pi \times 1.059} = 0.143$$

4. The conditions required for a possible optimization of the damper support stiffness are checked as below

   a) $X_1 = 0.0715$ (Step 2) and $X_1^{cr} = 0.143$ (Step 3). Therefore, the condition $X_1 < X_1^{cr}$ holds which ensures a reduction in the damper support stiffness can improve the maximum achievable damping ratio.

   b) $\bar{k}_{s,1} = 1000$ (initial assumption for a rigid support, $k_s = 642.5$ MN/m), $\bar{k}_{s,1}^{opt} = 6.8$ (Step 3), $\bar{k}_{s,1}^{min} = 4.77$ (Step 3) and $SF = 3$. Hence,

$\bar{k}_{s,new} = (\bar{k}_{s,1} + \bar{k}_{s,1}^{opt})/2 = 503.4$, $\bar{k}_{s,1}^{min} \times SF = 14.4$, and the condition $\bar{k}_{s,new} > \bar{k}_{s,1}^{min} \times SF$ is also satisfied.

5. Steps 1 to 4 are repeated with the updated non-dimensional support stiffness of $\bar{k}_{s,2} = \bar{k}_{s,new} = 503.4$. The iteration continues until either the condition of $X_i < X_i^{cr}$ or $(\bar{k}_{s,i} + \bar{k}_{s,i}^{opt})/2 > \bar{k}_{s,i}^{min} \times SF$ cannot be satisfied. In this case, the latest $c_{d,i}$, $k_{d,i}$, and $k_{s,i}$ values will be the selected values for the NSD system. Table 6-2 summarizes the iterations of optimizing the design of the NSD system. The final design is concluded in eight iterations which yields $c_d = 56.4\ \text{kN} \cdot \text{s/m}$, $k_d = -573.4\ \text{kN/m}$, and $k_s = 8542.7\ \text{kN/m}$. It can be seen from this table that compared to the case of rigid damper support, the size and the absolute value of the stiffness of the NSD have been respectively reduced by 15.6% and 6.3% when an optimized support stiffness is determined based on the proposed approach.

6.5.3. Refinement of the NSD design

As mentioned earlier, Eq. (6-2) leads to a conservative NSD design, especially for longer cables. Considering the length of the stay cable studied in this example ($L = 324.9$ m) and the values of $x_d/L = 0.02$ and $4EI(\beta_{0n}^s)^2/H \approx 0.0002$, the NSD design refinement would be suggested. The refinement algorithm proposed in Section 6.4 is applied herein with a tolerance of $e_{tol} = 0.1\%$ to improve the NSD system designed in Section 6.5.2. As illustrated in Section 6.3.3, the support stiffness optimization in design scenario 3 is an iterative process, where, in each iteration, the size and stiffness of a NSD are determined for a given k_s. The design refinement described in Section 6.4 can be applied either at the end of each iteration step or when the entire optimization process is completed. In this example, the latter approach is used.

Table 6-3. Refinement of the NSD design in the numerical example ($e_{tol} = 0.1\%$).

Iteration	k_s (kN/m)	c_d (kN · s/m)	k_d (kN/m)	ζ_1^d	ζ_1^r	e	$\frac{\zeta_1^d}{1+e}$	$\lvert e\rvert < e_{tol}$
1	8542.7	56.4	-573.4	4.000%	5.249%	31.23%	3.048%	False
2	8096.2	73.4	-531.5	3.048%	3.845%	-3.87%	3.171%	False
3	8140.4	70.6	-538.2	3.171%	4.020%	0.51%	3.155%	False
4	**8134.2**	**70.9**	**-537.3**	3.155%	3.997%	-0.07%	3.157%	**True**
5	8135.0	70.9	-537.4	3.157%	4.000%	0.01%	3.156%	True

The first modal damping ratio of the studied cable equipped with the NSD system optimized in the 8th iteration of Table 6-2, i.e. $c_d = 56.4$ kN · s/m, $k_d = -573.4$ kN/m, and $k_s = 8542.7$ kN/m, can be numerically calculated from the first complex eigenvalue of Eq. (6-5), i.e. $\lambda_1 = -0.117 + 2.224i$. In this case, $\zeta_1^r = -\text{Imag}[\lambda_1]/|\lambda_1| = 0.117/\sqrt{(-0.117)^2 + 2.224^2} = 5.25\%$. Hence, the error between ζ_1^r and the target first modal damping ratio $\zeta_1^t = 4\%$ is $e = (5.25 - 4)/4 = 31.2\%$. In the second iteration, the design of the NSD system is optimized for the damping ratio of $\zeta_1^d/(1+e) = 4\%/(1 + 0.312) = 3.05\%$, which yields $c_d = 73.4$ kN · s/m, $k_d = -531.5$ kN/m, and $k_s = 8096.2$ kN/m. By attaching this updated NSD system to the studied cable, the numerically obtained first modal damping ratio of the damped cable is obtained as $\zeta_1^r = 3.85\%$ and the error between the achieved and the required damping ratio becomes $e = -3.87\%$. The refinement continues until the tolerance $e < 0.1\%$ is satisfied after four iterations. Table 6-3 gives a summary of the refinement process. The parameters of the refined NSD system are determined to be $c_d = 70.9$ kN · s/m, $k_d = -537.3$ kN/m, and $k_s = 8134.2$ kN/m, of which the first modal damping ratio of the damped cable is 3.997%. The rate of convergence of the proposed refinement algorithm is shown in Fig. 6-8. It can

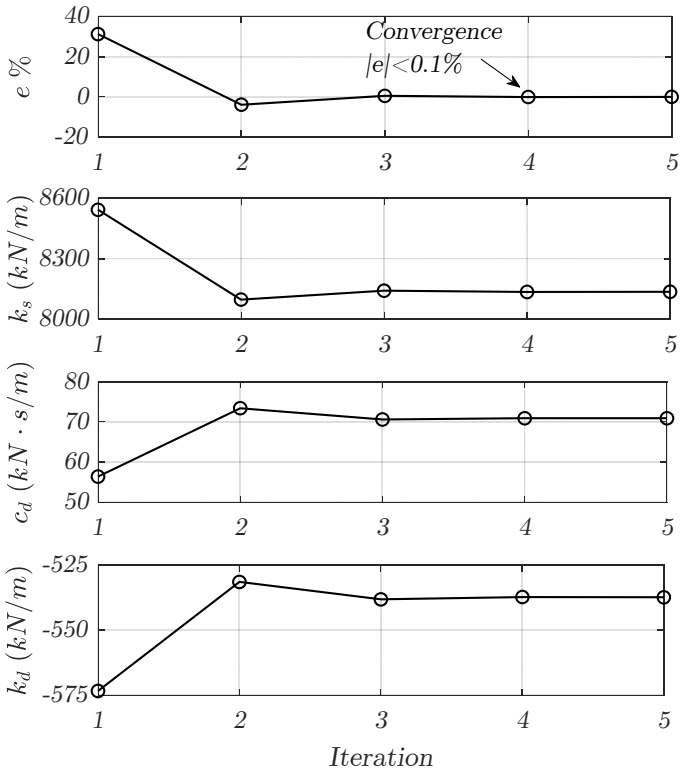

Fig. 6-8. Convergence of the NSD design refinement algorithm.

be observed that the error between the achieved and the required damping ratio reduces substantially in only one iteration and the NSD design parameters rapidly converge to their refined values. It is worth mentioning that if the refinement is applied at the end of each iteration in the optimization process of the NSD design, the results will be almost identical ($c_d = 70.9\ \text{kN} \cdot \text{s/m}$, $k_d = -537.3\ \text{kN/m}$, and $k_s = 8137.6\ \text{kN/m}$). This demonstrates the robustness and stability of the proposed refinement algorithm. However, applying refinement at the end of each iteration is not advantageous in terms of computational efficiency.

A numerical simulation is conducted by solving Eq. (6-4) to evaluate the control performance of the designed NSD. In this simulation, the cable-damper system is subjected to a uniformly distributed harmonic load with a frequency of $f_1 = 0.36$ Hz for 50 seconds.

The excitation is then removed to allow the cable to vibrate freely for another 50 seconds. To excite the damped cable in the first mode, the frequency of the harmonic excitation is selected to be the same as the first modal frequency of the cable-damper system. A static load component is also added to the dynamic excitation to simulate the effect of the mean wind load and generate a more realistic wind effect on the stay cable.

To evaluate the effect of NSD design refinement on the performance of a cable-NSD system, the free vibration response of the studied cable equipped respectively with a non-refined NSD (row 1 in Table 6-3) and a refined NSD (row 4 in Table 6-3) are examined. The modal damping ratio of the damped cable is obtained by fitting an exponential curve to its free vibration displacement time history. In Fig. 6-9, the displacement time history of the damped cable at its mid-span is considered for calculating its first modal damping ratio based on the exponential envelope of the peak displacement. As can be observed in this figure, the maximum free vibration response at the cable mid-span for the non-refined NSD ($w_{max} = 0.92D$) is 15.2% larger than that of the refined NSD ($w_{max} = 0.8D$). This increased cable displacement is due to the presence of greater negative stiffness in the non-refined NSD. Besides, the maximum cable displacement at the damper location is increased by 33% (from $0.27D$ to $0.36D$) when the NSD design refinement is not applied. On the other hand, the first modal damping ratio provided by the refined and the non-refined NSD systems are $\zeta_1 = 4\%$ and 5.3%, respectively. Therefore, the non-refined NSD can provide an additional 1.3% damping ratio at the cost of increasing the cable displacement. Hence, it is necessary to refine the NSD design to prevent an unnecessary, yet significant, increase in the cable response.

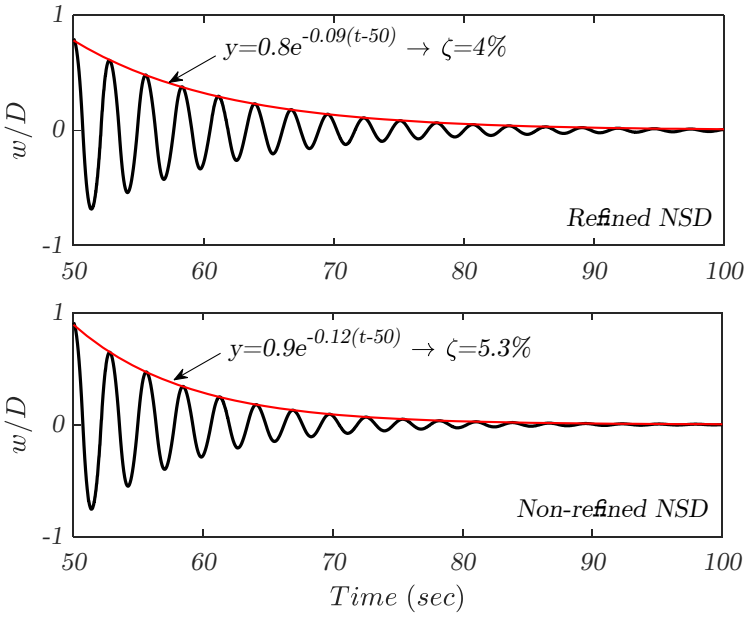

Fig. 6-9. Free vibration displacement time history of the studied cable at the mid-span and the corresponding 1st modal damping ratio when equipped respectively with a refined and a non-refined NSD.

6.5.4. Effect of damper support flexibility

To investigate the impact of damper support flexibility on the NSD performance, three cases are considered for the same cable and damper design requirements discussed in Section 6.5.1 (i.e. provide a damping ratio of 4% in the 1st mode). These NSD design cases are:

Case 1) NSD-R: The damper is designed and refined for a rigid support. The selected NSD parameters are $c_d = 84.5$ kN · s/m and $k_d = -572.2$ kN/m.

Case 2) NSD-RF: The damper designed in Case 1 (NSD-R), which is optimized for a rigid support, is mounted on a flexible support with $k_s = 8134.2$ kN/m (4th iteration in Table 6-3).

Case 3) NSD-F: The damper is optimized and refined for a flexible support. The NSD parameters are $c_d = 70.9\ \text{kN} \cdot \text{s/m}$, $k_d = -537.3\ \text{kN/m}$, and $k_s = 8134.2\ \text{kN/m}$ (4^{th} iteration in Table 6-3).

In three separate simulations, the studied cable is equipped with one of the above NSD systems and subjected to a uniformly distributed load with a load intensity of $f(t) = 15.4 + 0.31\sin(0.72\pi t)\ \text{N/m}$ for 50 seconds. The loading parameters are selected to generate a predefined response amplitude in the uncontrolled cable. The excitation is then removed to capture the free vibration of the cable for another 50 seconds. The time-history of the cable response at the damper location and the NSD hysteresis loop is shown in Fig. 6-10 for the three NSD systems defined above. As can be observed in Fig. 6-10(a), using the NSD-RF would increase the cable displacement amplification at the damper location during the forced vibration phase as compared to the case where the NSD-R is used. The hysteresis loop of the NSD-RF shown in Fig. 6-10(b) has a higher negative slope than the NSD-R. In other words, mounting a NSD on a flexible support is equivalent to a decrease in the negative damper stiffness. In this case, the NSD-RF could generate a control force 21.7% larger than that by the NSD-R, and the attached cable would undergo a displacement 13.8% larger at the damper location. As a result, mounting a NSD optimized for a rigid support on a flexible support would provide a higher damping ratio ($\zeta_1 = 4.6\%$) than the target value at the cost of amplifying the cable response during the forced vibration phase. In the case of NSD-F, the dynamic behaviour of the cable-damper system is similar to the NSD-R and both dampers provide the required damping ratio ($\zeta_1 = 4\%$). It should be noted that the NSD-F is designed with smaller damper size and less strong negative stiffness than the NSD-R. The optimized and refined NSD-F can effectively mitigate cable vibrations

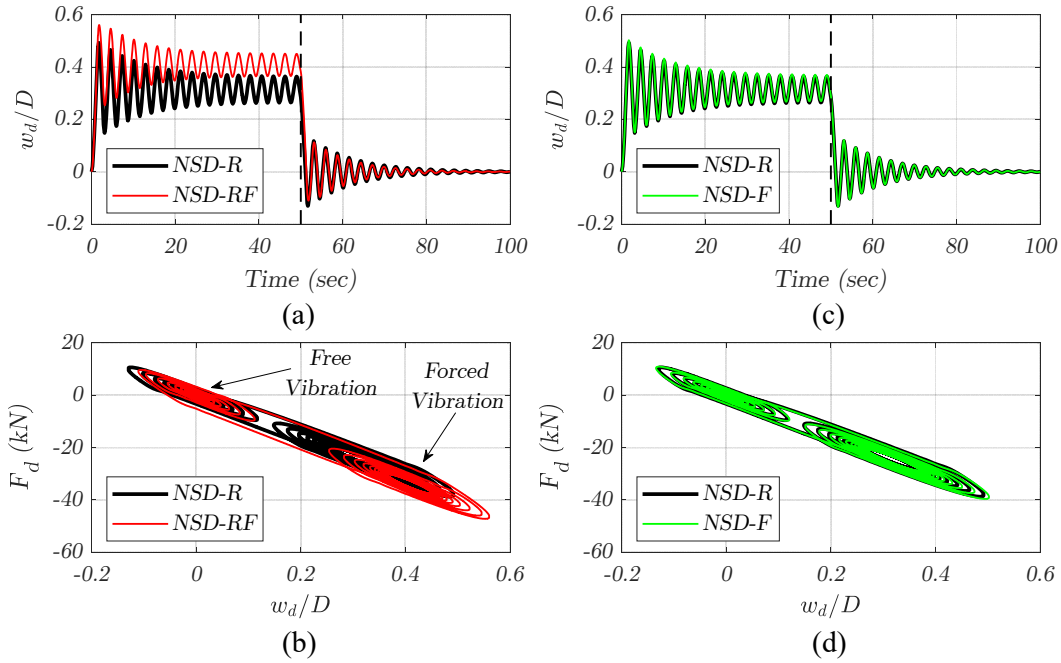

Fig. 6-10. Impact of damper support stiffness on the performance of NSD. (a) Cable displacement at the damper location controlled by NSD-R and NSD-RF, (b) Hysteresis loop of NSD-R and NSD-RF, (c) Cable displacement at the damper location controlled by NSD-R and NSD-F, (d) Hysteresis loop of NSD-R and NSD-F.

when installed on a flexible support. This design is also cost-efficient as it leads to smaller damper size, c_d, and less negative damper stiffness. k_d.

6.5.5. Performance comparison between NSD and LQR

To further evaluate the performance of a NSD, the control efficiency of the damper designed in Case 3, i.e. NSD-F, is compared with that of an optimal LQR controller. The loading condition of the damped cable is similar to the preceding sections. An LQR controller has been adopted by Shi et al. [68] for mitigating stay cable vibration. The classical $\boldsymbol{Q}$ matrix in the LQR controller is defined as:

$$\boldsymbol{Q} = \begin{bmatrix} \boldsymbol{K} & 0 \\ 0 & \boldsymbol{M} \end{bmatrix} \tag{6-16}$$

where $\boldsymbol{M}$ and $\boldsymbol{K}$ are the modal mass and stiffness matrices of the cable, respectively (in accordance with Section 6.2.2.2), and the R parameter in the LQR controller is selected as 1.8×10^{-6} to ensure the peak control force generated by the LQR is comparable to that by the NSD-F. To evaluate the overall vibration control effectiveness of the NSD-F along the cable length and take into account the local response amplification near the damper location due to the negative damper stiffness, the RMS cable response in the uncontrolled and controlled state will be compared. For this purpose, the mean square of the cable displacement integrated along the cable length (IMS) can be used to capture the overall NSD-F and LQR control performance as well as the localized effect of NSD-F near the damper installation location. The IMS is defined as:

$$\mathrm{IMS} = \mathrm{mean}\left(\int_0^L w^2(x,t)dx\right) \tag{6-17}$$

where $\mathrm{mean}(\cdot)$ denotes the arithmetic mean over time. The IMS for the uncontrolled and controlled cable is calculated for the forced and the free vibration phases of the damped cable when equipped with the NSD-F and the LQR. The evaluation criteria are defined as follows:

$$\delta_P = \left(\frac{\mathrm{IMS_C}}{\mathrm{IMS_U}}\right)_{\mathrm{forced}} \tag{6-18}$$

$$\delta_F = \left(\frac{\mathrm{IMS_C}}{\mathrm{IMS_U}}\right)_{\mathrm{free}} \tag{6-19}$$

where δ_P and δ_F are the displacement reduction indices of the forced and the free vibration phases, respectively; $\mathrm{IMS_C}$ and $\mathrm{IMS_U}$ are the IMS of the controlled and the uncontrolled cable, respectively.

Table 6-4. Comparison of the performance of NSD-F and LQR in cable vibration control.

Controller	c_d (kN · s/m)	k_d (kN/m)	k_s (kN/m)	ζ_1	δ_P	δ_F	F_d^{max} (kN)
NSD-F	70.9	-537.3	8134.2	4.0%	67.6%	2.6%	39.6
LQR	N/A	N/A	∞	8.6%	58.8%	1.7%	39.3

Table 6-4 presents the numerical simulation results of the control efficiency provided by the NSD-F and the LQR. The NSD-F optimized and refined by the proposed design approach has successfully provided the target damping ratio of 4% by generating a maximum control force of 39.6 kN, while the LQR produced a damping ratio of 8.6% with the same level of control force. The displacement reduction indices of the forced and the free vibration phases are also provided in the table. During the forced vibration stage, the IMS has been reduced by 32.4% when the cable is equipped with the NSD-F. Also, the LQR controller can reduce IMS more effectively and its displacement reduction index during the forced vibration is $\delta_P = 58.8\%$. On the other hand, both control schemes are substantially effective in suppressing free vibration, with the optimized NSD (NSD-F) and the LQR controller offer respectively a 97.4% and 98.3% reduction in the IMS during the free vibration phase.

Figure 6-11 shows the displacement time history of the cable at its mid-span when equipped with the NSD-F or the LQR. As can be seen in this figure, the effectiveness of the NSD-F in reducing cable displacement is satisfactory as the peak cable displacement at the mid-span is reduced by 55% in the free vibration phase. The NSD-controlled and uncontrolled cable response at the cable mid-span are respectively $w_{max}^C = 2.2D$ and $w_{max}^U = 3.1D$ in the forced vibration phase, and $w_{max}^C = 0.86D$ and $w_{max}^U = 1.9D$ in the

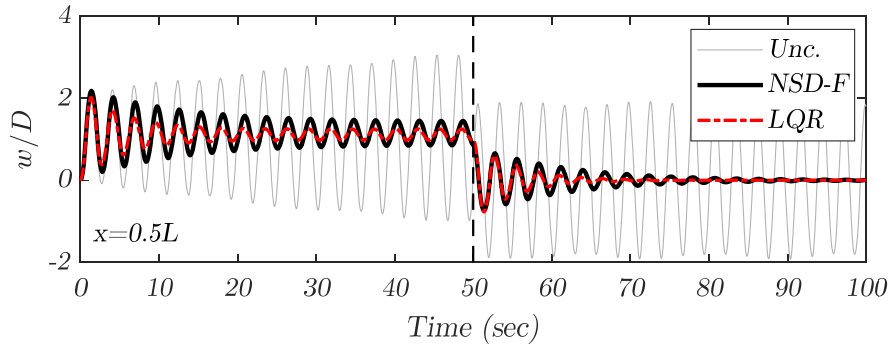

Fig. 6-11. Uncontrolled and controlled cable displacement at the mid-span when the cable is equipped with NSD-F and LQR.

free vibration phase. It can also be seen that the LQR performs better in both vibration phases. However, if LQR would be used to offer such a control efficiency, it would require full system identification and availability of the system states at any time during the cable vibration, both of which are challenging for practical application. Figure 6-12 shows the displacement of the NSD-equipped cable along three cable segments of $0.9L < x < L$, $0.4L < x < 0.6L$ and $0 < x < 0.1L$, where the last segment includes the damper installation location. By comparing the cable response in the two boundary zones, namely $0.9L < x < L$ and $0 < x < 0.1L$, the effect of negative damper stiffness on the cable displacement is portrayed. Besides, the overall NSD performance will be reflected in the cable mid-region, $0.4L < x < 0.6L$, where the largest displacement occurs in the first mode of cable vibration. As can be seen in Figs. 6-12(a) and 6-12(c), the cable undergoes larger displacements in the left end where NSD is installed (i.e. $0 < x < 0.1L$) as compared to the right boundary region. The maximum cable displacement in these two zones are respectively $w_{max} = 1.1D$ and $w_{max} = 0.75D$. Therefore, there is a 47% increase in the maximum cable response in the cable boundary zones as a result of NSD attachment. Besides, Fig. 6-12(b) shows that the maximum controlled cable displacement at the cable

mid-span is $w_{max} = 2.2D$. It is effectively suppressed by the optimized and refined NSD system. By comparing the performance of NSD-F and LQR in this section, it was found that the negative stiffness damper can effectively control the cable displacement in both free and forced vibration phases and provide the required damping ratio when installed on a flexible support. However, due to the presence of negative stiffness in the damper, the cable displacement is amplified near the damper installation location. The amount of such cable response amplification can be limited by applying the proposed optimization and refinement algorithms in the NSD design process.

6.6. Summary

The impact of damper support stiffness on the NSD performance in controlling stay cable vibrations has been investigated in this chapter. The existing analytical and numerical approaches for evaluating the control performance of a NSD mounted on a flexible support have been reviewed. The NSD stability limit has been extended to the case of flexible support condition and a practical value for the allowable negative damper stiffness is recommended by introducing a safety factor. Three typical NSD design scenarios have been addressed, which target respectively the NSD design for a given support condition, the support design for a given NSD, and the design of the entire NSD-support system. The last scenario was tackled by proposing an optimization algorithm to identify the optimum combination of NSD parameters (damper size and stiffness) and damper support stiffness. In parallel, to minimize the impact of the assumptions made in the analytical damper design formulation and improve the accuracy of the NSD design, refinement of the NSD design has been proposed. To further evaluate the effectiveness of the proposed design scheme for a NSD mounted on a flexible support, a numerical example has been presented, of which

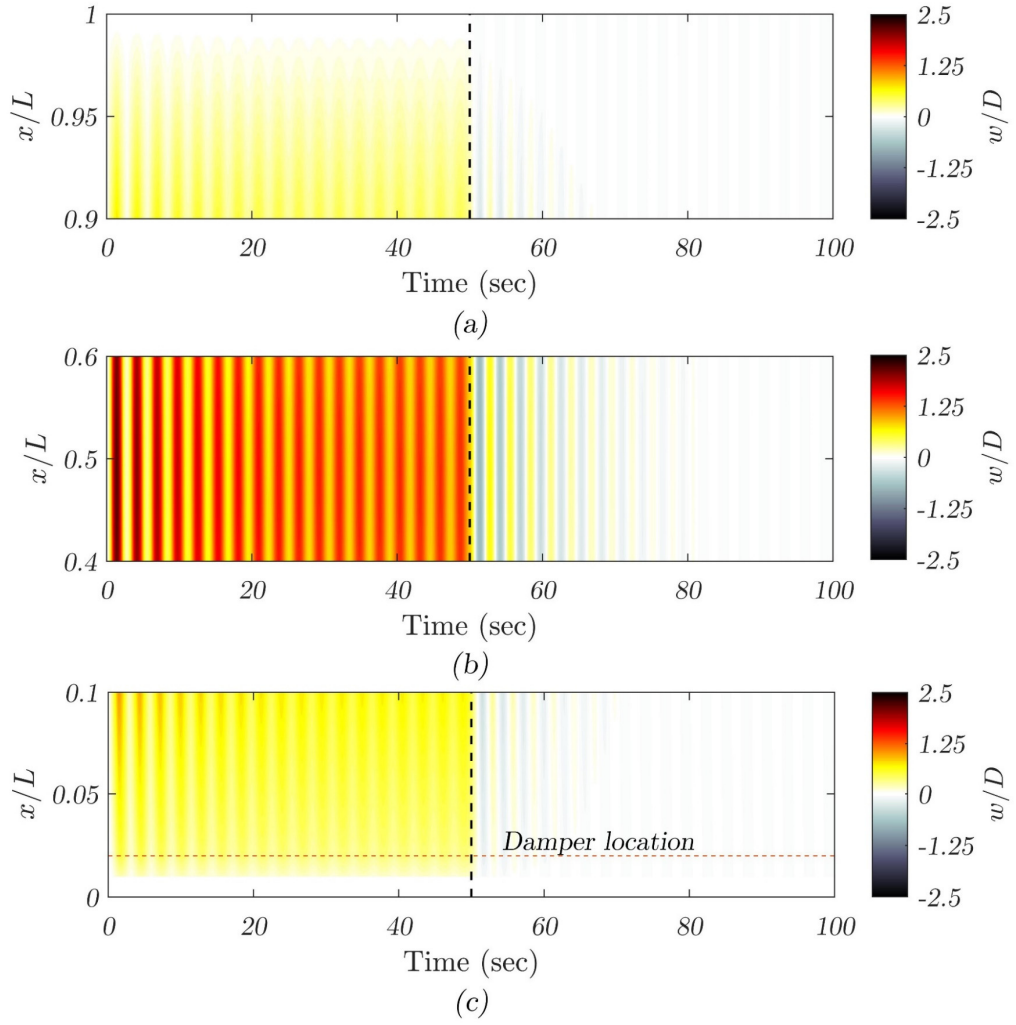

Fig. 6-12. Displacement of the cable equipped with NSD-F at (a) $0.9L < x < L$, (b) $0.4L < x < 0.6L$, and (c) $0 < x < 0.1L$.

the dynamic response of a 324.9 m long stay cable was analyzed when it was equipped with an optimized and refined NSD and subjected to harmonic excitation. First, the effect of damper support stiffness on the NSD performance has been evaluated by comparing three NSD design cases with different support conditions and design approaches. Then, the control effectiveness of the optimized and refined NSD has been compared with an optimal LQR controller. Besides, the problem of cable response amplification near the damper

installation location due to the presence of negative damper stiffness has also been investigated. The main findings of the current study are summarized as follows:

1. Depending on the damper size of a NSD, mounting it on a flexible damper support can have different effects on its control performance. A critical damper size has been identified such that if the damper size is smaller than this critical value, using a more flexible damper support would enhance the performance of the NSD by increasing the damping ratio of the cable-NSD system. Otherwise, depending on the stiffness of the damper support, using a flexible support would have either a negative or neutral impact on the effectiveness of a NSD.
2. If the damper size of a NSD is smaller than the identified critical value, an optimum damper support stiffness exists which would allow a given NSD to achieve the best vibration control effect.
3. For a given negative stiffness damper, there exists a minimum damper support stiffness which ensures the stability of the entire cable-NSD system. At this minimum support stiffness, if the damping coefficient of the NSD is zero, the negative damper stiffness would fully offset the inherent positive stiffness of the cable at the damper location and lead to instability of the damped cable. It has been found that this minimum damper support stiffness must be positive and is always smaller than the optimum support stiffness.
4. By optimizing a NSD for a flexible support condition, it is possible to reduce the damper size and the amount of negative damper stiffness to achieve the desired control performance. This would reduce the fabrication and maintenance cost of the NSD. In addition, the optimization would reduce the amplification of cable

response, in particular, at the damper installation location, which is a main drawback in the NSD application.

5. The control effectiveness of an optimized and refined NSD mounted on a flexible support is comparable to that of an optimal LQR controller and hence, NSD can be considered as a feasible alternative to the more complicated active and semi-active control schemes.
6. The proposed NSD design optimization and refinement algorithms are robust and computationally efficient. This feature ensures that their application would practicably improve the accuracy and efficiency of the NSD design.

Chapter 7 Multi-mode Vibration Control of Cables Using Optimized NSD

7.1. Introduction

As discussed in previous chapters, all the existing NSD design methods target damper optimization for controlling cable vibration dominated by a specific mode. However, on-site records show that vibrations of stay cables are usually influenced by more than a single mode. For example, it was observed that under rain-wind induced vibration the first few cable modes are often excited [10,38,49]. On the other hand, the dominant cable modes during a vibration incidence highly depend on the excitation source and may vary. Hence, using a single-mode-based approaches to optimize passive viscous damper design, including NSDs, may result in suboptimal damper performance. In order to address this concern, multi-mode vibration control techniques have been studied by a number of researchers for both passive and semi-active dampers of linear or nonlinear nature. Wang et al. [75] proposed a method to optimize the performance of viscous dampers in mitigating multi-mode cable vibrations. Weber et al. [48] developed an analytical method for the optimization of linear viscous dampers. Hoang and Fujino [76] studied the behaviour of nonlinear dampers and obtained their equivalent damping ratio by using energy-based arguments. More recently, Weber and Distl [77] introduced a semi-active control scheme for multi-mode cable vibration mitigation. On the other hand, the passive NSD has shown high damping capability which is comparable to smart semi-active systems. As a linear passive device, NSD would be a better choice for designing a less-complicated and

measurement-free controller. However, existing NSD design tools only address single-mode cable vibration control and the potential of NSD in mitigating multi-mode cable vibrations is still unknown.

In this chapter, a novel approach for optimizing NSD for controlling multi-mode stay cable vibrations is proposed. An asymptotic design formula which includes the effect of damper stiffness is adopted to develop NSD design equations for controlling not only a single-mode, but also multi-mode cable vibrations. The validity of the proposed NSD design approach for multi-mode cable vibration control is verified by the dynamic response of a group of representative real stay cables which undergo multi-mode vibrations when equipped with NSD designed based on the proposed approach. To further evaluate the effectiveness of the proposed NSD design scheme for multi-mode vibration control, a numerical example is conducted on a 460 m long stay cable subjected to wind excitation and equipped with a NSD designed by the proposed approach. The performance of the NSD is also compared with an optimal LQR controller.

7.2. Formulation of NSD design approach to suppress multi-mode cable vibrations

7.2.1. In-plane dynamic response of a damped cable

Figure 7-1 shows the mechanical model of a stay cable with a transverse damper installed near its lower end on a flexible support. The x- and y-axes represent the cable chord direction and the transverse (in-plane) direction, respectively. The cable is subjected to an external load $f_{ext}(x,t)$ and undergoes an in-plane dynamic displacement $w(x,t)$ at location x and time instant t. In this model, m is the cable mass per unit length, L is the cable length, H is the cable tension in the direction of its chord, EI and EA represent the cable flexural and axial rigidity, respectively, θ is the inclination angle, and $z(x)$ is the

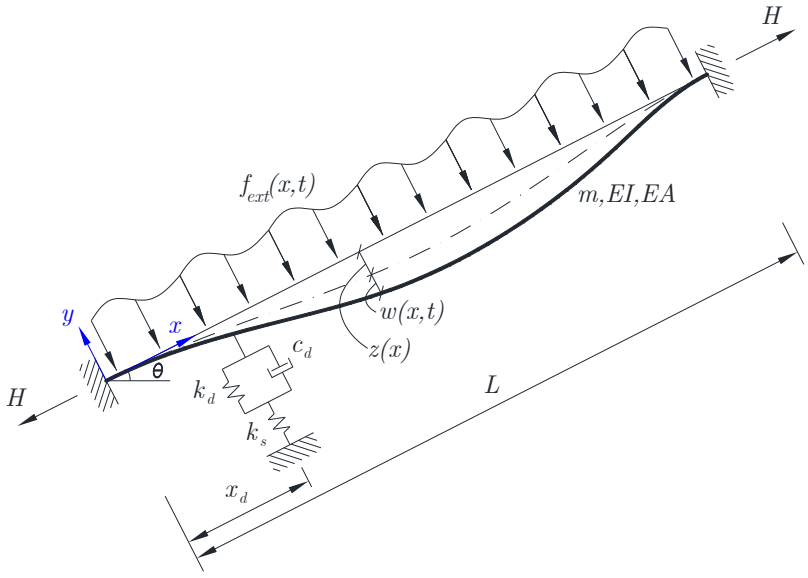

Fig. 7-1. Sagged-flexural stay cable equipped with a transverse damper.

static cable displacement due to its self-weight. The cable is equipped with a viscous damper of size c_d located at a distance x_d from the lower end. In the damper model, the damper stiffness, k_d, is simulated by a linear spring parallel to the dashpot. The flexibility of the damper support is represented by a linear spring with stiffness k_s connected between the damper and the fixed base.

By adopting the mode superposition method, it is possible to approximate the in-plane dynamic displacement of the cable, $w(x,t)$, by the following finite series:

$$w(x,t) = \sum_{i=1}^{n} \phi_i(x) q_i(t) \tag{7-1}$$

where $\phi_i(x)$ and $q_i(t)$ are the shape function and the generalized coordinate of the i^{th} mode, respectively; and n is the number of modes considered in the approximation. The accuracy of this approximation will, obviously, depend on how well the shape functions could represent the actual dynamic behaviour of the damped cable and the number of the

modes included. A conventional approach to enhance the performance of the mode superposition method is to include a static correction in the mode shapes [57]. It was shown in Chapter 4 that the accuracy and computational efficiency can be greatly improved by considering the static displacement of the cable under a point load at the damper location as one of the shape functions. Thus, in the current discussion, the shape function vector is defined as:

$$\{\Phi(x)\} = \left\{ \underbrace{\phi_0(x)}_{\text{static correction term}} \quad \underbrace{\phi_1(x) \dots \phi_{n-1}(x)}_{\text{conventional shape functions}} \right\} \tag{7-2}$$

By ignoring the inherent cable damping, the equation of motion of a damped cable based on the generalized coordinates can be expressed as:

$$\mathbf{M}\{\ddot{q}(t)\} + \mathbf{K}\{q(t)\} = \{F_{ext}(t)\} + F_d(t)\{\boldsymbol{\phi}(x_d)\} \tag{7-3}$$

where $\boldsymbol{M} = [m_{ij}] = m\int_0^L \phi_i(x)\phi_j(x)dx$ is the modal mass matrix; $\boldsymbol{K} = \boldsymbol{K_s} + \boldsymbol{K_t} + \boldsymbol{K_b}$ is the modal stiffness matrix which consists of three parts and each represents a distinct source of stiffness in the system, i.e. $\boldsymbol{K_s} = [k_{ij}^s] = (EA/L_e)\int_0^L z''(x)\phi_i(x)dx \int_0^L z''(x)\phi_j(x)dx$ is the stiffness due to the additional dynamic cable tension which is governed by the cable sag and $z(x)$ is the displacement of the cable under its own weight; $\boldsymbol{K}_t = [k_{ij}^t] = H\int_0^L \phi_i'(x)\phi_j'(x)dx$ is the stiffness due to the static cable tension; and finally, $\boldsymbol{K}_b = [k_{ij}^b] = EI\int_0^L \phi_i''(x)\phi_j''(x)dx$ results from the cable flexural rigidity; $\{F_{ext}(t)\} = \{f_j\} = \left\{\int_0^L f_{ext}(x,t)\phi_j(x)dx\right\}$ is the generalized external force; $F_d(t)$ is the time-dependent damper force; and $\{\ddot{q}(t)\}$ and $\{q(t)\}$ are the vectors of generalized modal acceleration and displacement, respectively. Based on Eq. (7-3), the in-

plane dynamic response of a damped cable subjected to an arbitrary external load can be obtained numerically.

7.2.2. Design optimization of a NSD

As an extension to Fig. 5-5, Fig. 7-2 illustrates the damping ratio surfaces for three successive modes i, j, and k ($i < j < k$) over the ranges of $0 \leq Y_n \leq 1$, $0 \leq \tau \leq 1$ and $0 \leq X_n \leq 0.6$. It is worth to point out that modes i, j, and k do not need to be consecutive. Figure 7-2 can be applied to two typical design scenarios of a damper. The first common design scenario is to choose the size of a damper to maximize the energy dissipation capacity of the damped cable when the NSD stiffness ratio, τ, is determined by other factors such as manufacturing requirements. Whereas the second scenario is to find a suitable damper (both damper size and damper stiffness) for a given cable to achieve the specified level of modal damping ratio. A systematic approach to address these two design issues based on the damper performance surfaces shown in Fig. 7-2 will be illustrated in the following sub-sections.

7.2.2.1. Design scenario 1: Given the damper stiffness, choose damper size

The NSD optimization for controlling single-mode cable vibration was addressed in Section 5.4 where practical analytical formulation was derived for a similar design scenario in Section 5.4.2. The NSD design point for single-mode cable vibration control in this scenario (point p_1) was shown in Fig. 5-5 for an arbitrary mode. Similar design points are illustrated in Fig. 7-2 for two successive modes i and j, namely points i' and j'. It can be observed from this figure that the optimum damper size for a particular cable mode would not be the most effective one for the other modes. Therefore, when the cable motion is dominated by more than one mode, Eq. (5-5) will not lead to an optimum design for NSD

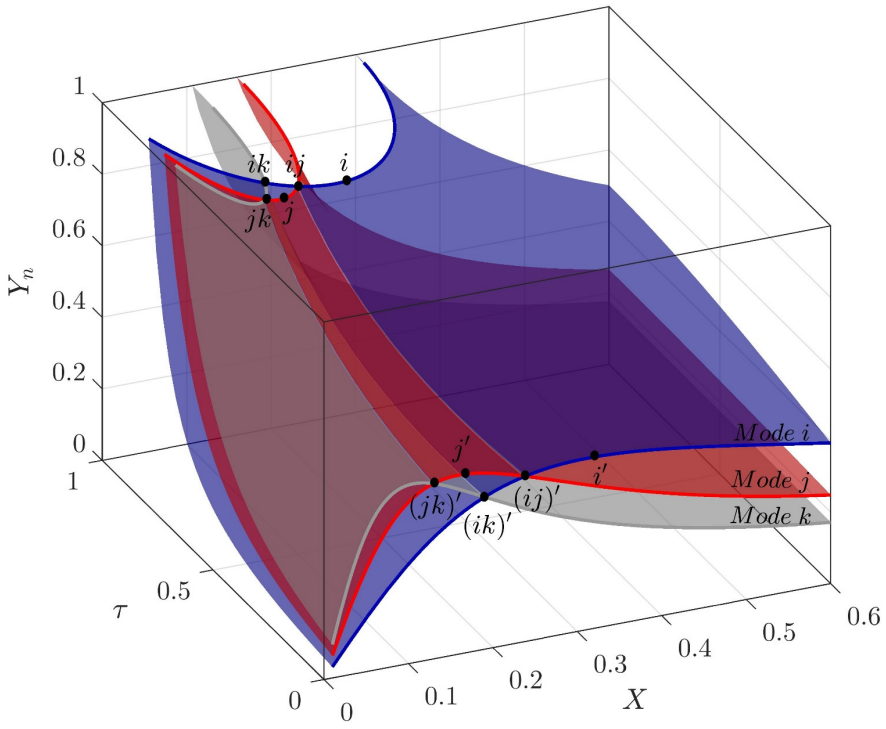

Fig. 7-2. Three-dimensional damper performance surfaces for three successive modes i, j, and k.

and a method is required to optimize it for all the governing modes. Figure 7-3 shows a generalized form of Fig. 5-6 by including additional design points that correspond to the case of multi-mode cable vibration.

Take two arbitrary cable modes i and k as an example and assume, for design purpose, that they are the dominant modes of cable vibration. It can be seen from Fig. 7-3(a) that the performance curves of these two modes intersect at point $(ik)'$. If the size of the NSD is chosen based on $X^{\tau}_{ik,opt}$, it would allow the damped cable to achieve the same modal damping ratio in the i^{th} and the k^{th} modes, i.e. $Y^{\tau}_{ik,opt}$. Although such a damper would not be optimum for either modes as compared to a damper design targeting for only the i^{th} or the k^{th} mode, this damper would have a better performance in mitigating both modes

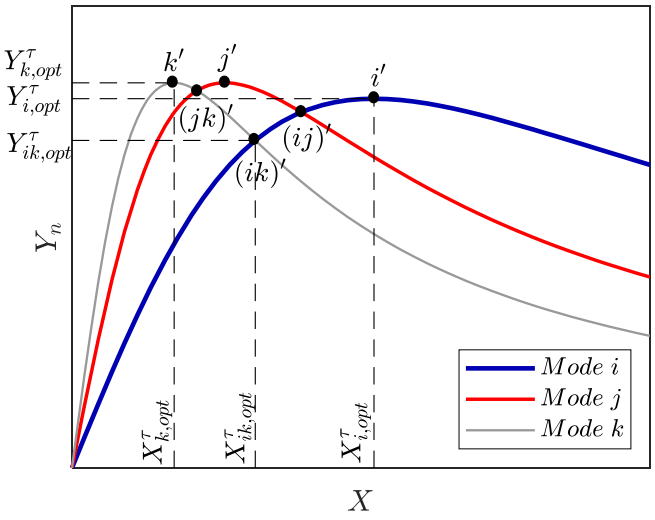

(a)

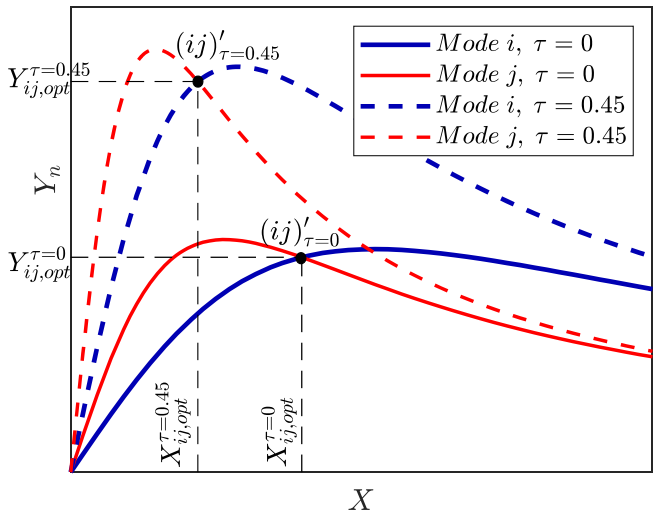

(b)

Fig. 7-3. NSD performance on arbitrary τ-planes. (a) An arbitrary τ-plane, (b) planes $\tau = 0$ and $\tau = 0.45$.

simultaneously. By applying Eq. (5-4) respectively to the i^{th} and the k^{th} modes, and setting $Y_i = Y_k$, it yields:

$$X^{\tau}_{ik,opt} = \left(\frac{1-\tau}{\pi}\right)\sqrt{\frac{kR_{sk}\eta_{sk} - iR_{si}\eta_{si}}{ik\eta_{si}\eta_{sk}(kR_{si}\eta_{sk} - iR_{sk}\eta_{si})}} \tag{7-4a}$$

where $\tau = k_d/k_d^{min}$ is the NSD stiffness ratio; k_d is the stiffness of a NSD; $k_d^{min} = -H/(x_d\eta_k)$ is the lowest negative stiffness of the NSD that ensures its stability. Further, by substituting Eq. (7-4a) into Eq. (5-4), we can obtain:

$$Y_{ik,opt}^{\tau} = \frac{\sqrt{ik\eta_{si}\eta_{sk}(iR_{si}\eta_{si} - kR_{sk}\eta_{sk})(iR_{sk}\eta_{si} - kR_{si}\eta_{sk})}}{(1-\tau)(k\eta_{sk} - i\eta_{si})(k\eta_{sk} + i\eta_{si})} \tag{7-4b}$$

Therefore, for a given NSD stiffness ratio, τ, and damper installation location, x_d, the damper size selected based on Eq. (7-4a) would be most effective in controlling cable motions dominated by both modes i and k. The optimal damper size can be obtained from:

$$c_{d_{ik,opt}}^{\tau} = \frac{X_{ik,opt}^{\tau}\sqrt{Hm}}{\eta_k(x_d/L)} \tag{7-5a}$$

whereas the corresponding cable damping ratio is:

$$\zeta_{ik,max}^{\tau} = Y_{ik,opt}^{\tau}\left[(x_d/L)R_{fs}\right] \tag{7-5b}$$

where $R_{fs} = (1-\alpha_{BC}q)^2/\eta_k$. Besides, Fig. 7-3(a) suggests that if the two targeted modes i and k are not consecutive, then the damper size determined by Eq. (7-5a) would also perform satisfactorily in suppressing cable modes between i and k. For instance, it can be seen from Fig. 7-3(a) that for any mode j lying between mode i and mode k, the optimum damper size for controlling both modes i and k, $X_{ik,opt}^{\tau}$, would allow to achieve a j^{th} modal damping ratio higher than the optimized value for the two target modes, i.e. $Y_j^{\tau} > Y_{ik,opt}^{\tau}$. On the other hand, the damper size selected to optimize the controlling effect for the two target modes would be suboptimal for any mode that is beyond that range. For the three successive modes shown in Fig. 7-3(a), i.e. $i < j < k$, if mode i and mode j are the two target modes, the optimum design point would be $(ij)'$ and the optimum damper size could

be deduced from $X_{ij,opt}^{\tau}$. However, if such a damper is installed, the k^{th} modal damping ratio of the damped cable , namely Y_k^{τ}, would be less than the optimum damping ratio of the two target modes, $Y_{ij,opt}^{\tau}$. This implies that to design a NSD which could most efficiently suppress cable vibrations dominated by a number of modes for a given NSD stiffness ratio τ, the designer only needs to choose the lowest and the highest dominating modes as the two target modes, then determine the optimum modified damping parameter for these two modes using Eq. (7-4a). If the damper installation location is also specified, the optimum damper size can be obtained from Eq. (7-5a). By using this damper, the modal damping ratio for the intermediate modes would be higher than that of the two target modes predicted from Eqs. (7-4b) and (7-5b). Similar phenomenon was reported by Weber et al. [48] when optimizing linear viscous damper for multi-mode cable vibration control. A formal theoretical proof of this finding is presented as follows.

First, consider design scenario 1 for three successive modes i, j and k. For a given negative stiffness ratio, use Eq. (7-4a) to optimize a NSD based on modes i and k, i.e. $Y_i = Y_k$. The optimum damper size, $X_{ik,opt}^{\tau}$, is then substituted into Eq. (5-4) to obtain the normalized damping ratio in mode j. Two cases can be considered:

1. Modes i, j and k with $i > 1$. In this case, the sag effect in these three modes is minor. Thus, $\eta_{si} = \eta_{sj} = \eta_{sk} \approx 1$, $R_{si} = R_{sj} = R_{sk} \approx 1$, and Eq. (5-4) will yield:

$$Y_j - Y_i = \frac{ik(j-i)(k-j)\sqrt{1/(ik)}}{(1-\tau)(i+k)(ik+j^2)} \tag{7-6}$$

It is evident that the right-hand side of Eq. (7-6) is positive. Therefore, $Y_j - Y_i > 0$, which suggests that the damping ratio of the j^{th} mode is higher than the target damping ratio in modes i and k.

2. Modes i, j, and k with $i = 1$. In this case, the values of η_{s1} and R_{s1} will be functions of λ^2 and it can be shown that for $\lambda^2 \leq 8$, $Y_j - Y_i > 0$ holds. This λ^2 requirement is met for majority of the stay cables on cable-stayed bridges, for which the λ^2 is typically less than 1.

Another noteworthy phenomenon is the effect of NSD stiffness ratio in the multi-mode cable vibration mitigation. By reducing the stiffness of a NSD, the stiffness ratio τ would increase, which would subsequently lead to a smaller damper size and larger achievable damping ratio, as reflected respectively in Eqs. (7-4a) and (7-4b). This phenomenon is also shown in Fig. 7-3(b) where the damper performance curves of the two target modes, namely i and j, in the planes of $\tau = 0$ (solid line) and $\tau = 0.45$ (dashed line) are shown together in terms of their projection on an arbitrary τ-plane. By comparing the optimum damper design for these two NSD stiffness ratio cases, it can be clearly seen that $X_{ij,opt}^{\tau=0.45} < X_{ij,opt}^{\tau=0}$, i.e. when the damper installation location remains the same, increasing τ would help reducing the optimum size of NSD to most effectively suppress cable vibration dominated by mode i and mode j; whereas $Y_{ij,opt}^{\tau=0.45} > Y_{ij,opt}^{\tau=0}$ indicates that if the installation location and the size of a NSD remains the same, using a larger damper stiffness ratio in the design would increase the maximum achievable damping ratio for all the target modes, and thus enhance the performance of the NSD in the multi-mode cable vibration control.

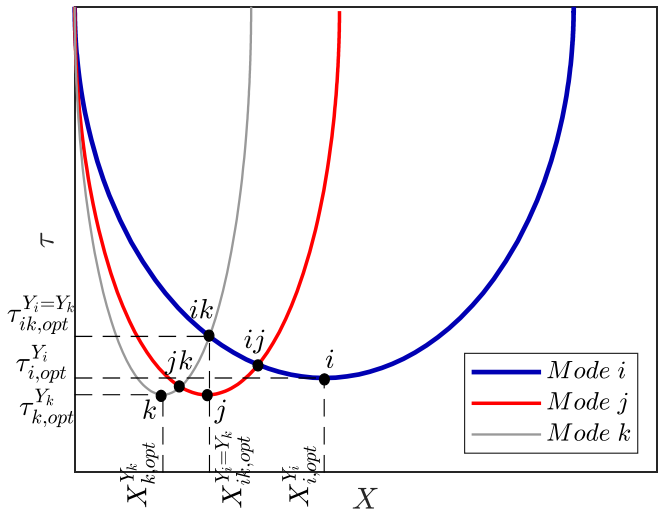

(a)

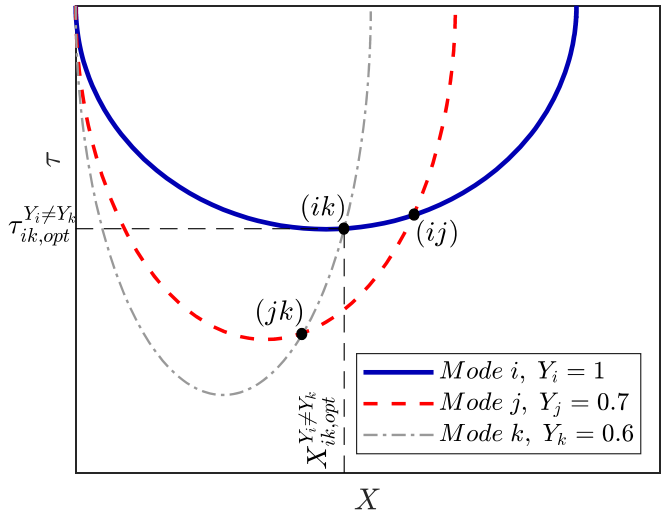

(b)

Fig. 7-4. NSD performance on arbitrary Y_n-planes. (a) An arbitrary Y_n-plane, (b) planes $Y_i = 1$ and $Y_j = 0.7$ and $Y_k = 0.6$.

7.2.2.2. Design scenario 2: Given a required damping ratio, choose NSD stiffness and size

The damper property curves $\tau - X$ associated with three successive modes i, j, and k (where $i < j < k$ and they are not necessarily consecutive) are illustrated in Fig. 7-4. When there are more than one dominant modes, optimizing NSD design for multiple modes is necessary to ensure the modal damping ratio of all these modes satisfy the design

requirement. Take mode i and mode k as an example. As can be seen from Fig. 7-4(a), the intersection point of the damper property curves for mode i and mode k, i.e. point ik, would correspond to a NSD design which allows the modal damping ratio of both target modes reach the specified damping level. Noticing that point ik is above the damper property curve associated with mode j, which, based on the slope of the damper performance surfaces shown in Fig. 7-2, indicates that a NSD with the size and stiffness determined respectively from $X_{ik,opt}^{Y_n}$ and $\tau_{ik,opt}^{Y_n}$ would yield a higher j^{th} modal damping ratio than the specified value for modes i and k. This implies that designing a NSD to satisfy a specific damping requirement for a number of dominant modes, the designer only needs to find the optimum damper design for the lowest and the highest order dominant modes, and the so selected NSD would ensure the damping ratio of other dominant modes within this range to be higher than the specified design value. This observation is an important feature of the NSD multi-mode design. A formal proof of this finding will be presented later.

Since the required damping ratio of different vibrational modes may not be required to be the same, a more general NSD optimization task could be to specify different damping requirement for each of the dominant modes. Here, assume the three target cable modes being i, j and k ($i < j < k$ and they are not necessarily consecutive), and the specified damping ratio requirement represented respectively by Y_i, Y_j and Y_k ($Y_i \neq Y_j \neq Y_k$). The damper performance curves corresponding to these three modes on the planes of $Y_i = 1$, $Y_j = 0.7$ and $Y_k = 0.6$ are portrayed together in Fig. 7-4(b), in the form of their projection on an arbitrary Y_n-plane. It can be observed from Fig. 7-4(b) that point (ik) is the intersection point of the projected $\tau - X$ curve of mode i on plane $Y_i = 1$ and that of mode

k on plane $Y_k = 0.6$. The coordinates of this point can be derived by rewriting Eq. (5-4) respectively for mode i and mode k, i.e.

$$(1-\tau)^2 = \frac{R_{si} i\pi\eta_{si} X}{Y_i} - (i\pi\eta_{si})^2 \tag{7-7a}$$

$$(1-\tau)^2 = \frac{R_{sk} k\pi\eta_{sk} X}{Y_k} - (k\pi\eta_{sk} X)^2 \tag{7-7b}$$

Equate the right-hand side of Eqs. (7-7a) and (7-7b), it yields:

$$X_{ik,opt}^{Y_i,Y_k} = \frac{kR_{sk}\eta_{sk}Y_i - iR_{si}\eta_{si}Y_k}{Y_i Y_k \pi(k\eta_{sk} - i\eta_{si})(k\eta_{sk} + i\eta_{si})} \tag{7-8a}$$

Then substitute Eq. (7-8a) into Eq. (7-7a) to obtain:

$$\tau_{ik,opt}^{Y_i,Y_k} = 1 - \sqrt{\frac{i\pi R_{si}\eta_{si} X_{ik,opt}^{Y_i,Y_k}}{Y_i} - \left(i\pi\eta_{si} X_{ik,opt}^{Y_i,Y_k}\right)^2} \tag{7-8b}$$

Finally, the damper size and damper stiffness corresponding to this optimum design point (ik) can be computed based on Eqs. (7-5a) and (5-8), respectively. From Fig. 7-4(b), we observe that the optimum NSD design point (ik) is located above the projection of the j^{th} mode damper property curve. Based on the slope of the damper performance surface of the j^{th} mode shown in Fig. 7-2, the NSD designed to optimize the vibration suppression for modes i and k will results in a Y_j value greater than the specified value of 0.7. Therefore, if different damping requirements are specified for each of the dominant cable mode in the NSD design, it is recommended to choose the size and stiffness of an optimum NSD based on the respective control requirement of the lowest and the highest order dominant modes. The resulted NSD is expected to effectively mitigate all other dominant modes within this range.

The optimum NSD for achieving a damping ratio of Y in modes i and k can be calculated using Eq. (7-8), i.e. $Y_i = Y_k = Y$. The optimum modified damping parameter, $X_{ik,opt}^{Y}$, and the optimum NSD stiffness ratio, $\tau_{ik,opt}^{Y}$, are substituted into Eq. (5-4) to obtain normalized damping ratio of mode j. Again, two cases can be considered:

1. Modes i, j, and k with $i > 1$. In this case, $\eta_{si} = \eta_{sj} = \eta_{sk} \approx 1$, $R_{si} = R_{sj} = R_{sk} \approx 1$, and Eq. (5-4) will yield:

$$Y_j - Y_i = \frac{(j-i)(k-j)Y}{ik + j^2} \tag{7-9}$$

   Since the right-hand side of Eq. (7-9) is greater than 0, so $Y_j - Y_i > 0$, which suggests the damping ratio of the j^{th} mode is higher than the target damping ratio in modes i and k, namely $Y_j > Y$.

2. Modes i, j, and k with $i = 1$. In this case, η_{s1} and R_{s1} depend on the value of λ^2. It can be shown that for $\lambda^2 \leq 39$, $Y_j - Y_i > 0$. Since majority of the stay cables have $\lambda^2 < 1$, so $Y_j > Y_i$.

Nevertheless, it is worthy to note that optimizing the design of a NSD to suppress a wider range of modes would lead to a higher value of negative stiffness ratio τ, i.e. a NSD with a greater amount of negative stiffness. This would not be a preferred choice due to safety concerns related to its stability and cost efficiency. The proposed NSD design optimizations for single-mode (Chapter 5) and multi-mode cable vibration control have been summarized in the flowchart shown in Fig. 7-5.

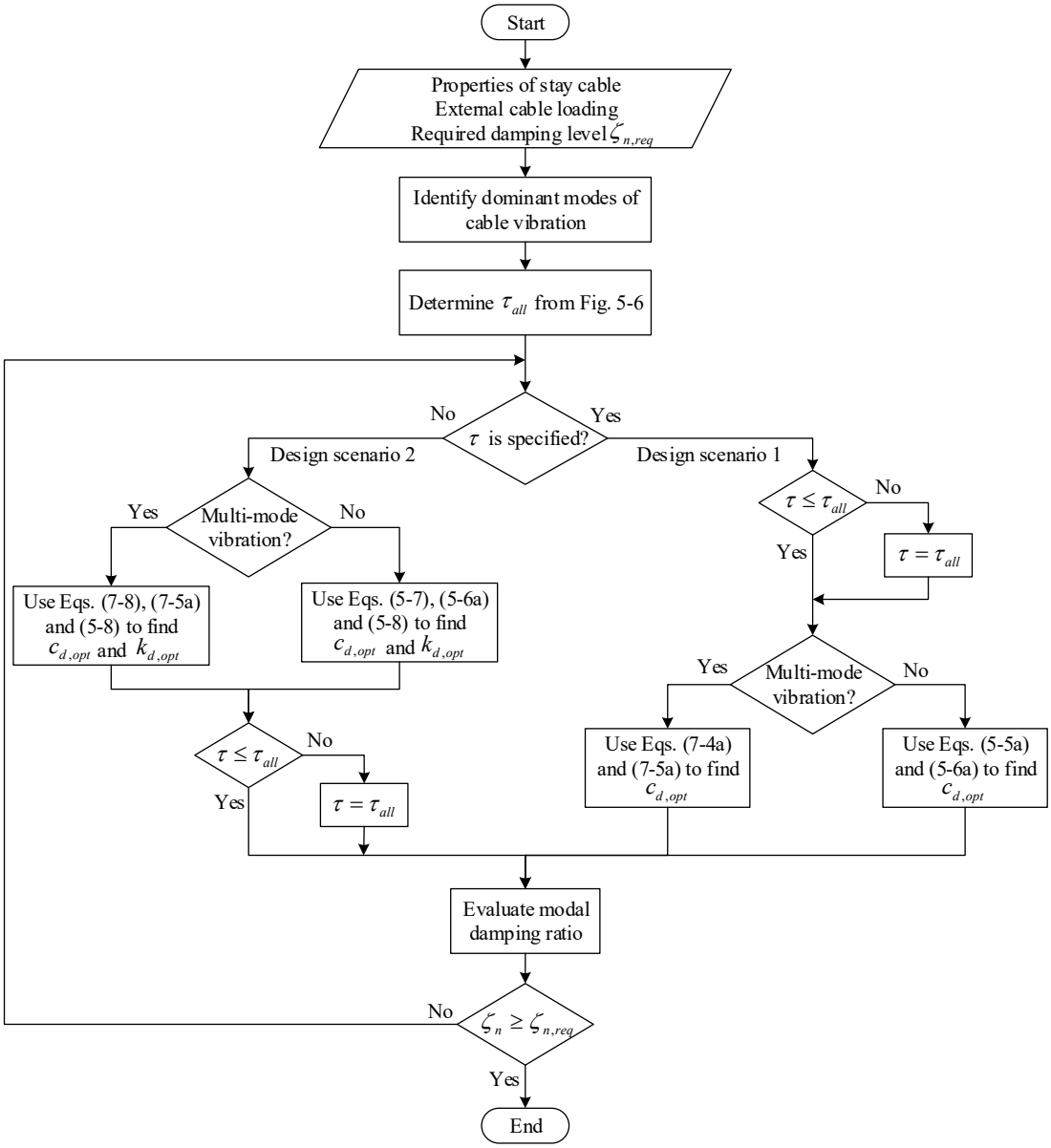

Fig. 7-5. Negative stiffness damper design optimization for single-mode and multimode stay cable vibration control.

7.3. Verification of proposed NSD design equations

7.3.1. Sample cables

To verify the validity of the NSD design approach proposed in Section 7.2.2, the developed NSD design equations will be applied to select a NSD for real bridge stay cables. The effectiveness of the selected NSD in mitigating cable vibrations is then evaluated. Fifteen

sample cables which have been previously introduced in Section 5.5.1, are adopted herein for verification purposes. The properties of these cables are listed in Table 5-1.

7.3.2. Verification of NSD design equations for design scenario 1

In the design scenario 1, the size of the NSD needs to be determined based on the given damper stiffness. Equations (5-5) and (5-6) are developed to design NSD for single-mode vibration control, whereas Eqs. (7-4) and (7-5) for multi-mode vibration control.

To verify their validity and effectiveness, in particular the NSD design equations for multi-mode vibration control, NSD's are designed for the 15 selected sample cables for a given stiffness ratio of $\tau = 0.3$ to suppress vibrations dominated respectively by their first four modes. Three different NSD's are designed for each cable, with the first two dampers designed to control respectively only the 1st or the 4th mode, and the third NSD designed to control both the 1st and the 4th modes. These three dampers are denoted as d1, d4, and d14, respectively. Each damper is then attached to the cable at a location $0.05L$ and the cable is subjected to a harmonic load with the same frequency as the first four cable modes for 80 seconds and then removed. The damped cable continues with free vibration for another 80 seconds. The damping ratio of the damped cable is computed using the free vibration displacement time-history.

Figure 7-6 shows the box-whisker plot of the first four modal damping ratios of the 15 sample cables when equipped respectively with d1, d4, and d14, with the median marked by a horizontal line in the box. It can be observed from Fig. 7-6 that compared to d4 and d14, d1 has the best performance in suppressing mode 1. However, its effectiveness gradually degrades in the control of higher order modes. The median modal damping ratio decreases from 3.6% for mode 1 to 1.8% for mode 4. Similarly, in the case of d4, the

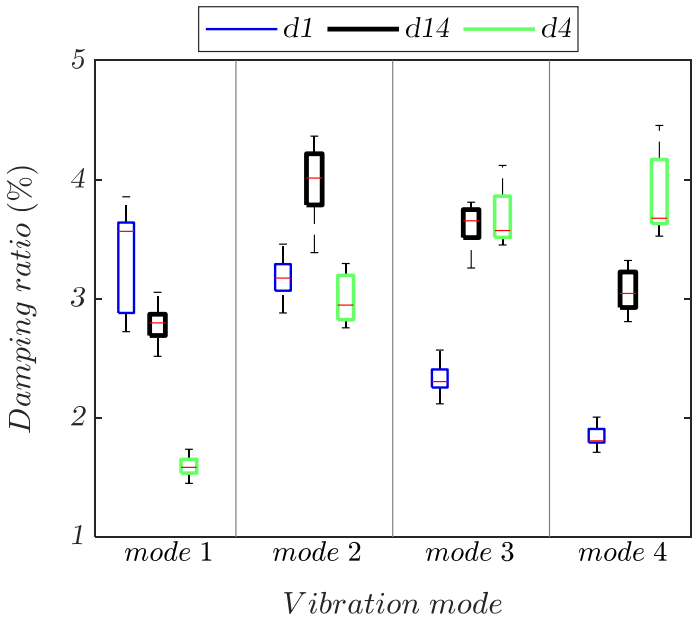

Fig. 7-6. Statistical performance of the negative stiffness damper designed with $\tau = 0.3$ for modes 1 and 4.

damper out-performs d1 and d14 in mitigating mode 4, but becomes less effective in suppressing lower order modes. This clearly reflects the limitation of damper design based on single-mode vibration control. On the other hand, for d14, which is designed based on multi-mode vibration control, although it is not as effective as d1 in suppressing mode 1 and d4 in suppressing mode 4, it out-performs d1 in controlling mode 2, 3, and 4, and has a better performance than d4 in mitigating modes 1, 2, and 3. This phenomenon was also reflected in Fig. 7-3(a). The results presented in Fig. 7-6 clearly demonstrates the validity and effectiveness of the proposed NSD design equations for multi-mode cable vibration control in design scenario 1.

7.3.3. Verification of NSD design equations for design scenario 2

Design scenario 2 aims at selecting the proper size and stiffness for a NSD to satisfy the specified damping requirement of a cable. Equations (5-7) and (7-8) can be used to address

single-mode and multi-mode cable vibration control, respectively. To verify these two sets NSD design equations, three dampers are designed for each of the 15 sample cables. The first two dampers are required to supplement respectively the modal damping ratio of mode 1 or mode 3 to at least 3%, whereas the third damper is expected to increase the modal ratio of both mode 1 and mode 3 to at least 3%. They are denoted as d1-3, d3-3, and d13-3, respectively. Dampers d1-3 and d3-3 are designed for a single-mode vibration control, of which the size and stiffness of the damper can be determined respectively from Eqs. (5-7a) and (5-7b). The design of damper d13-3 should follow the multi-mode vibration control approach, i.e. using Eqs. (7-8a) and (7-8b) to select its size and stiffness. Numerical simulations are then conducted, of which each of the 15 sample cables is equipped respectively with the three designed dampers at $x_d = 0.05L$. These cables are excited respectively by a harmonic load of the same frequency as the modal frequency of its 1st to 4th modes for 80 seconds in four separate simulations. Upon removal of the harmonic load, the cable undergoes 80 seconds of free vibration. The damping ratio of the damped cable is determined from the free vibration displacement time history.

The numerically obtained 1st to 4th modal damping ratio of all 15 sample cables are presented in Fig. 7-7. in the form of a box-whisker plot. The required minimum damping ratio of 3% is shown as a horizontal dotted line. Results clearly show that d1-3 and d3-3, which are designed based on the single-mode vibration control respectively for mode 1 and mode 3, all ensure the median of the modal damping ratio of the targeted mode reaches 3%. In this case, d1-3 is more effective than d13-3 and d3-3 for the 1st mode and d3-3 shows a better performance compared to d1-3 and d13-3 for the 3rd mode. However, these dampers would lose efficiency in mitigating other higher or lower order modes. For

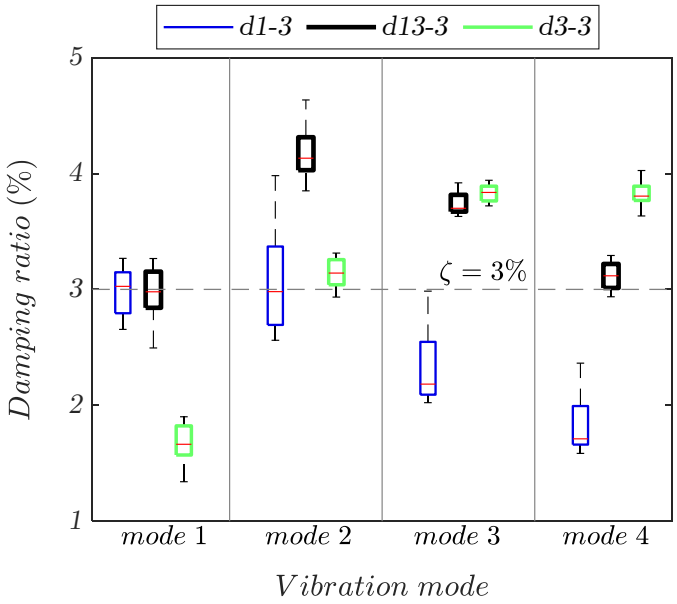

Fig. 7-7. Statistical performance of the negative stiffness damper designed for a target damping ratio of 3% for modes 1 and 3.

example, when d1-3 is installed to suppress cable vibration, the median of the modal damping ratio of the 15 sample cables gradually decreases from 3.0% for mode 1 to 1.7% for mode 4. Similar phenomenon is observed in d3-3, of which the median of the modal damping ratio for mode 3 is 3.8%, but drops to 3.1% for mode 2 and 1.7% for mode 1. This behaviour is expected for the damper designed for single-mode vibration control, i.e. it would have an optimum performance for the targeted mode, but show suboptimal performance in mitigating other modes. This drawback can be addressed by d13-3, which is designed to control simultaneously mode 1 and mode 3. It can be observed from Fig. 7-7 that by installing d13-3, the median of both the 1st and 3rd modal damping ratio of all 15 sample cables can satisfy the specified 3% requirement, which compensates the inadequacy of d1-3 in mode 3 and d3-3 in mode 1. Further, d13-3 out-performs d1-3 and d3-3 in controlling the intermediate mode, mode 2, with the median of the modal damping ratio reaching 4.1%, i.e. a NSD which is designed for the lowest and highest order modes in a

group of dominant modes can also effectively control vibrations of all the intermediate modes. This confirms the same phenomenon that has been observed earlier in Fig. 7-4. Interestingly, it is found in Fig. 7-7 that mode 4, which is beyond the range of the targeted modes, can also be effectively mitigated by d13-3 with the median of the modal damping ratio being 3.1%. Therefore, the validity of using the proposed NSD design equations for multi-mode cable vibration control to address design scenario 2 can be verified.

7.4. Numerical example

7.4.1. Problem definition

In this section, a numerical example is presented to illustrate the application of the proposed NSD design approach to a wind-induced multi-mode vibration control of a real bridge stay cable. The performance of the selected NSD is then compared with an optimal active controller.

The longest cable among the 15 samples is used in this example as it is vulnerable to multi-mode rain-wind induced vibration due to its very low fundamental frequency. This cable has a length of 460.1 m and is the longest one on the Tatara Bridge. The main parameters of this cable are given in Table 7-1. In this numerical example, a NSD is designed for this cable to resist wind-induced cable vibrations. It is required that the dominant cable modes should all reach a modal damping ratio of 2%. The damper is assumed to be installed at

Table 7-1. Properties of the sample stay cables used in numerical simulation.

L (m)	θ (deg.)	m (kg/m)	H (kN)	EI (kN · m^2)	EA (MN)	λ^2	D (m)	f_1 (Hz)
460.1	22.6	118.9	6665.9	3983.3	2859.9	2.37	0.17	0.29

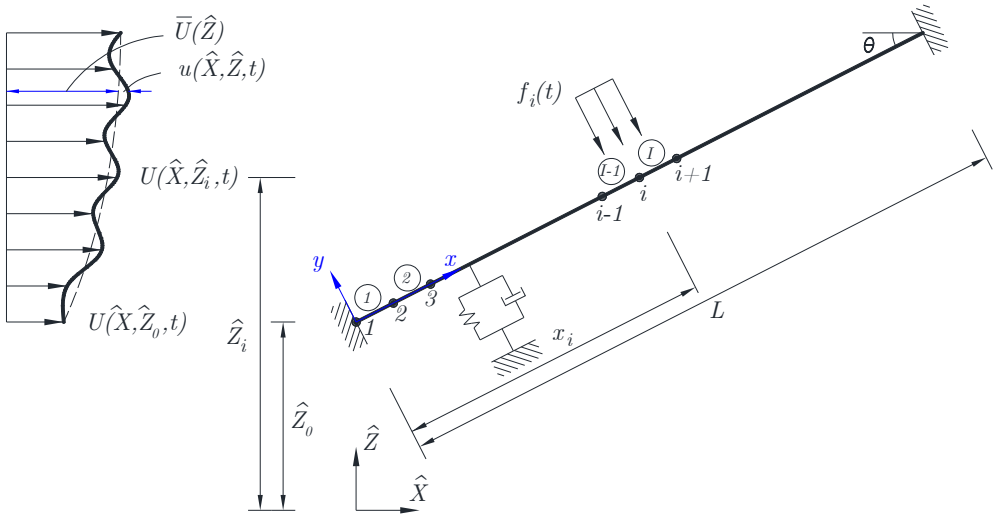

Fig. 7-8. Uniform transverse wind load acting on the i^{th} node of the discretized cable.

2% of the cable length from its cable-deck anchorage and mounted on a rigid damper support.

7.4.2. Wind load

Wind is turbulent in nature. It varies randomly both in time and space. In engineering practice, wind in the atmospheric boundary layer is often characterized by the mean wind velocity profile and an additional turbulence. Figure 7-8 depicts the wind-induced load acting on a stay cable with a length L, a diameter D and an inclination angle θ. A global and a local coordinate system are introduced to define the wind direction and the cable orientation, respectively. In the global coordinate system $\hat{X}\hat{Z}$, the mean wind velocity is along the $\hat{X}$-axis and the vertical direction is along the $\hat{Z}$-axis; whereas in the local coordinate system xy, the cable chord is along the x-axis and in-plane transverse direction is along the y-axis. The along-wind velocity component at a specific time instant t and location $(\hat{X},\hat{Z})$ can be described as:

$$U(\hat{X},\hat{Z},t) = \bar{U}(\hat{Z}) + u(\hat{X},\hat{Z},t) \tag{7-10}$$

where the mean wind velocity $\bar{U}$ is only a function of the height $\hat{Z}$ above the ground, and u is the along-wind turbulence component, which is assumed as a stationary, stochastic process with a zero mean value. In the present study, $\bar{U}$ is modeled by the power law wind profile [107], whereas u is simulated by the spectral representation method (SRM) [108].

The cable is discretized into a number of elements and the adjacent elements are connected by nodes. Three consecutive nodes, namely $i-1$, i and $i+1$, are shown in Fig. 7-8 whereas node i is at a distance x_i from the lower cable end and connects elements $(I-1)$ and I. The coordinates of the i^{th} node in the global coordinate system, $(\hat{X}_i, \hat{Z}_i)$, can be expressed as:

$$\hat{X}_i = x_i \cos\theta \tag{7-11a}$$

$$\hat{Z}_i = \hat{Z}_0 + x_i \sin\theta \tag{7-11b}$$

where $\hat{Z}_0$ is the deck height above the ground and is assumed to be 44.5 m in this example. At an arbitrary time instant t, the along-wind velocity component at the i^{th} node can be expressed as:

$$U(\hat{X}_i,\hat{Z}_i,t) = \bar{U}(\hat{Z}_i) + u(\hat{X}_i,\hat{Z}_i,t) \tag{7-12a}$$

$$\bar{U}(\hat{Z}_i) = \bar{U}_0 \left(\frac{\hat{Z}_i}{\hat{Z}_0}\right)^{\alpha} \tag{7-12b}$$

where $\bar{U}_0$ is the wind speed at the deck level and is assumed to be 20 m/s; α is the power law exponent which depends on the terrain condition and is selected as 0.143 to represent an open terrain condition [109]; and u is obtained based on the spectral representation method [108] in accordance with the Kaimal model [110] and the Davenport model [111].

Table 7-2. NSD design parameters.

R_{s1}	η_{s1}	R_{s2}	η_{s2}	R_{fs}	η_f	η_k	k_d^{min} (kN/m)
0.765	1.093	1	1	0.960	0.874	0.874	-828.8

The transverse component of the along-wind load intensity at the i^{th} cable node, $f_i(t)$, can be computed from:

$$f_i(t) = \frac{1}{2}\rho C_D D U^2(\hat{X}_i, \hat{Z}_i, t)[sin(\theta)]^2 \tag{7-13}$$

where C_D is the drag coefficient and is assumed to be 1.2 [93], D is the cable outer diameter, and $\rho = 1.25$ kg/m^3 is the air density. It is assumed that half of the load acting respectively on elements $(I-1)$ and I is imposed on node i with a uniform load intensity, $f_i(t)$. Thus, the total amount of wind load acting on node i is $f_i(t)$ times the distribution length. The stochastic wind field is simulated for a duration of 80 seconds. Figure 7-9 illustrates the spatial and temporal distribution of the simulated wind velocity along the cable. As an example, the time-history of the wind speed at $x = 0.1L$, $x = 0.5L$, and $x = 0.9L$ are shown in Fig. 7-9(b). It can be seen that the wind speed gradually increases toward the cable upper end (relative length of 1). This is due to an increase of the mean wind velocity along the height resulted from the atmospheric boundary layer effect.

7.4.3. Wind-induced response of the uncontrolled cable

The 80-second wind velocity time-history simulated in Section 7.4.2 is applied to all the nodes of the discretized cable model. Afterwards, the cable vibrates freely for another 80 seconds. The dominant modes of wind-induced cable vibration are identified by conducting a power spectrum analysis for the free vibration displacement time-history of the uncontrolled cable at $x = 0.15L$, as portrayed in Fig. 7-10. Since this point is not associated

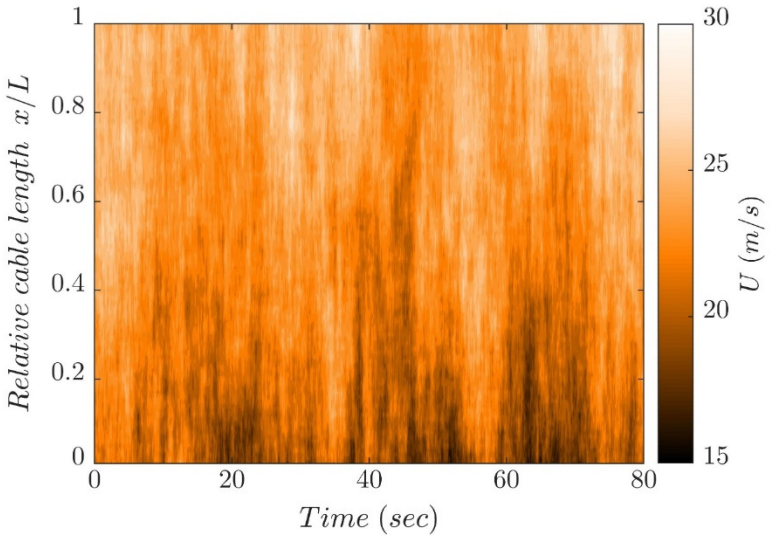

(a)

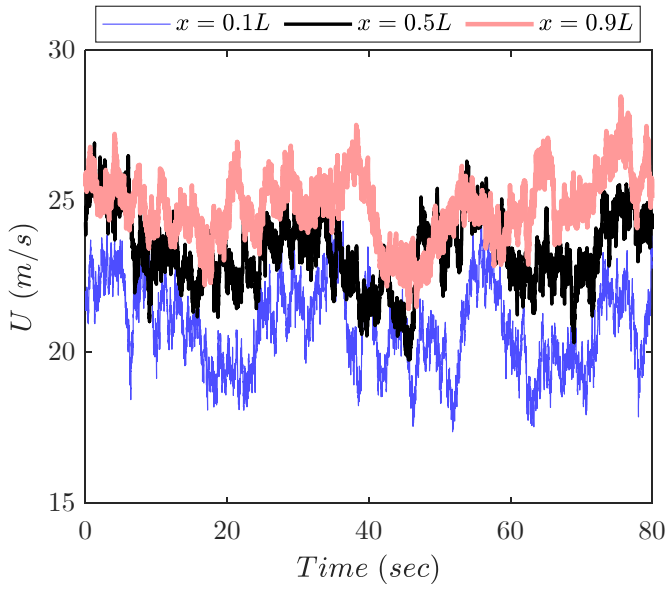

(b)

Fig. 7-9. Stochastic wind field simulated for 80 seconds along the cable.

with any modal node, analyzing cable free vibration response at this point would ensure to represent all the excited modes. Results show that the dominant modes are mode 1 and mode 2. Thus, a NSD will be designed to achieve a target modal damping ratio of 2% for these two modes.

7.4.4. NSD design

Since the current design problem belongs to design scenario 2, Eq. (7-8) is applied to choose the NSD size and stiffness. The associated modification and reduction factors are computed first and listed in Table 7-2. It should be noted that the sag-dependent factors, namely η_{sn} and R_{sn}, are both equal to one for the 2nd mode due to its antisymmetric nature. By following the NSD design procedures outlined in Fig. 7-5 and applying Eq. (7-8), the optimum damper size and damper stiffness for the NSD to suppress the two dominant cable modes, i.e., mode 1 and mode 2, are determined to be $c_d = 204.5\ \text{kN}\cdot\text{s/m}$ and $k_d = -529.6\ \text{kN/m}$. The detailed design calculations are presented below:

Calculate the normalized damping ratio parameter for each target mode (Eq. (7-5b)):

$$Y_1 = Y_2 = \frac{\zeta_1}{(x_d/L)R_{fs}} = \frac{0.02}{0.02(0.960)} = 1.042$$

Determine the optimized modified damping parameter for the target modes (Eq. (7-8a)):

$$X_{12,opt}^{Y_1,Y_2} = \frac{kR_{sk}\eta_{sk}Y_i - iR_{si}\eta_{si}Y_k}{Y_iY_k\pi(k\eta_{sk} - i\eta_{si})(k\eta_{sk} + i\eta_{si})}$$

$$= \frac{2(1)(1)(1.042) - 1(0.765)(1.093)(1.042)}{(1.042)^2\pi[2(1) - 1(1.093)][2(1) + 1(1.093)]}$$

$$= 0.127$$

Determine the optimized NSD stiffness ratio for the target modes (Eq. (7-8b)):

$$\tau_{12,opt}^{Y_1,Y_2} = 1 - \sqrt{\frac{i\pi R_{si}\eta_{si}X_{12,opt}^{Y_1,Y_2}}{Y_i} - \left(i\pi\eta_{si}X_{12,opt}^{Y_1,Y_2}\right)^2}$$

$$= 1 - \sqrt{\frac{(1)\pi(1.093)(0.765)(0.127)}{1.042} - [(1)\pi(1.093)(0.127)]^2} = 0.639$$

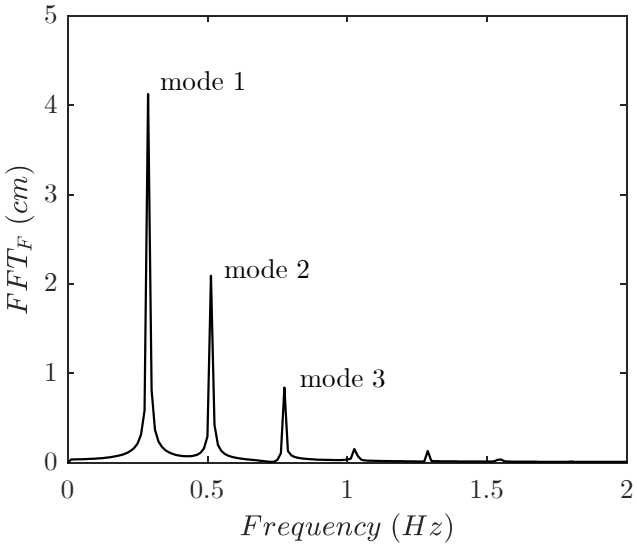

Fig. 7-10. Identification of the dominant modes of wind-induced cable vibration.

This optimum NSD stiffness ratio is less than the allowable limits proposed in Section 5.5.2, i.e. $\tau_{all} = 0.74$ for mode 1 and $\tau_{all} = 0.73$ for mode 2, and is therefore acceptable.

Calculate the damping coefficient and damper stiffness of the NSD (Eqs. (7-5a) and (5-8)):

$$c_d = \frac{X_{12,opt}^{Y_1,Y_2}\sqrt{Hm}}{\eta_k(x_d/L)} = \frac{0.127\sqrt{6665.9 \times 10^3(118.9)}}{0.874(0.02)} = 204.5\ \text{kN} \cdot \text{s/m}$$

$$k_d = \tau_{12,opt}^{Y_1,Y_2} k_d^{min}\ \text{kN/m}$$

This NSD is attached to the studied cable at $x_d = 0.02L$. Its performance in mitigating mode 1 and mode 2 of the sample cable is evaluated in the next section.

7.4.5. Design evaluation

7.4.5.1. Evaluation criteria

To evaluate the effectiveness of the selected NSD, it is reasonable to compare the uncontrolled cable response with the controlled one. The mean square of the cable

displacement integrated along the cable length [57] would not only reflect the dynamic response of the entire cable but also considers the localized impact of the control device on the cable behaviour. This parameter, which was first defined by Eq. (6-15), is expressed as:

$$\mathrm{IMS} = \mathrm{mean}\left(\int_0^L w^2(x,t)dx\right) \tag{7-14}$$

where $\mathrm{mean}(\cdot)$ denotes the arithmetic mean over time. The integrated mean square of the cable displacement can be applied to the uncontrolled and controlled cable response during the forced and free vibration phases. Hence, the following evaluation criteria, first defined in Section 6.5.5, can be defined:

$$\delta_P = \left(\frac{\mathrm{IMS_c}}{\mathrm{IMS_u}}\right)_{\mathrm{forced}} \tag{7-15a}$$

$$\delta_F = \left(\frac{\mathrm{IMS_c}}{\mathrm{IMS_u}}\right)_{\mathrm{free}} \tag{7-15b}$$

where δ_P and δ_F are the response reduction index of the forced and free vibration phase, respectively; $\mathrm{IMS_c}$ is the integrated mean square displacement of the controlled cable; and $\mathrm{IMS_u}$ is the integrated mean square displacement of the uncontrolled cable. It is obvious that the lower the values of δ_P and δ_F, the higher the performance of the control device is.

7.4.5.2. Effectiveness of the designed NSD

Numerical simulations are conducted to evaluate the dynamic response of the cable with a NSD attached at $x_d = 0.02L$ subjected to multi-mode wind-induced vibration. The simulation is continued for 160 seconds in two phases, the first phase includes 80 seconds of wind-induced vibration and the second phase is 80 seconds of cable free vibration. Table

Table 7-3. Control performance of NSD and LQR schemes.

Control device	ζ_1	ζ_2	ζ_3	f_1 (Hz)	f_2 (Hz)	f_3 (Hz)	δ_p	δ_F	F_d^{max} (kN)
NSD	2.44%	3.74%	1.58%	0.290	0.523	0.802	79.33%	45.91%	32.3
LQR	6.03%	4.64%	2.76%	0.290	0.529	0.794	70.39%	22.23%	33.3

7-3 presents the numerical simulation results in terms of the modal damping ratio, the response reduction indices, and the maximum control force of the NSD. First, it can be observed that the designed NSD can provide a damping ratio of more than 2% for both the first and the second modes and hence, satisfies the design requirement. In this case, the 1st and the 2nd modal damping ratios are 2.44% and 3.74%, respectively. In terms of the response reduction indices, the values of δ_P and δ_F are respectively 79.3% and 45.9%. The fact that both response reduction indices are less than 1 indicates that the cable displacement in both the forced and free vibration stages has been effectively controlled. The maximum control force generated in the NSD is 32.3 kN.

Figures 7-11(a) to 7-11(c) illustrate the time-history of the cable displacement at $x = 0.02L$ (i.e. the damper location), $x = 0.25L$, and $x = 0.5L$, respectively. A deviation of the cable displacement from its static equilibrium position during the forced-vibration phase can be observed in these three subplots. This deviation is caused by the wind load from the mean wind speed component $\bar{U}(z)$. At the onset of free vibration, however, the cable returns back to the neutral position and vibrates around the static equilibrium point. From Fig. 7-11(a), it can be seen that the installation of NSD has amplified the cable displacement at the damper location during the wind excitation. This phenomenon is due to the presence of negative stiffness in the damper. From the frequency response of the free vibration, it can

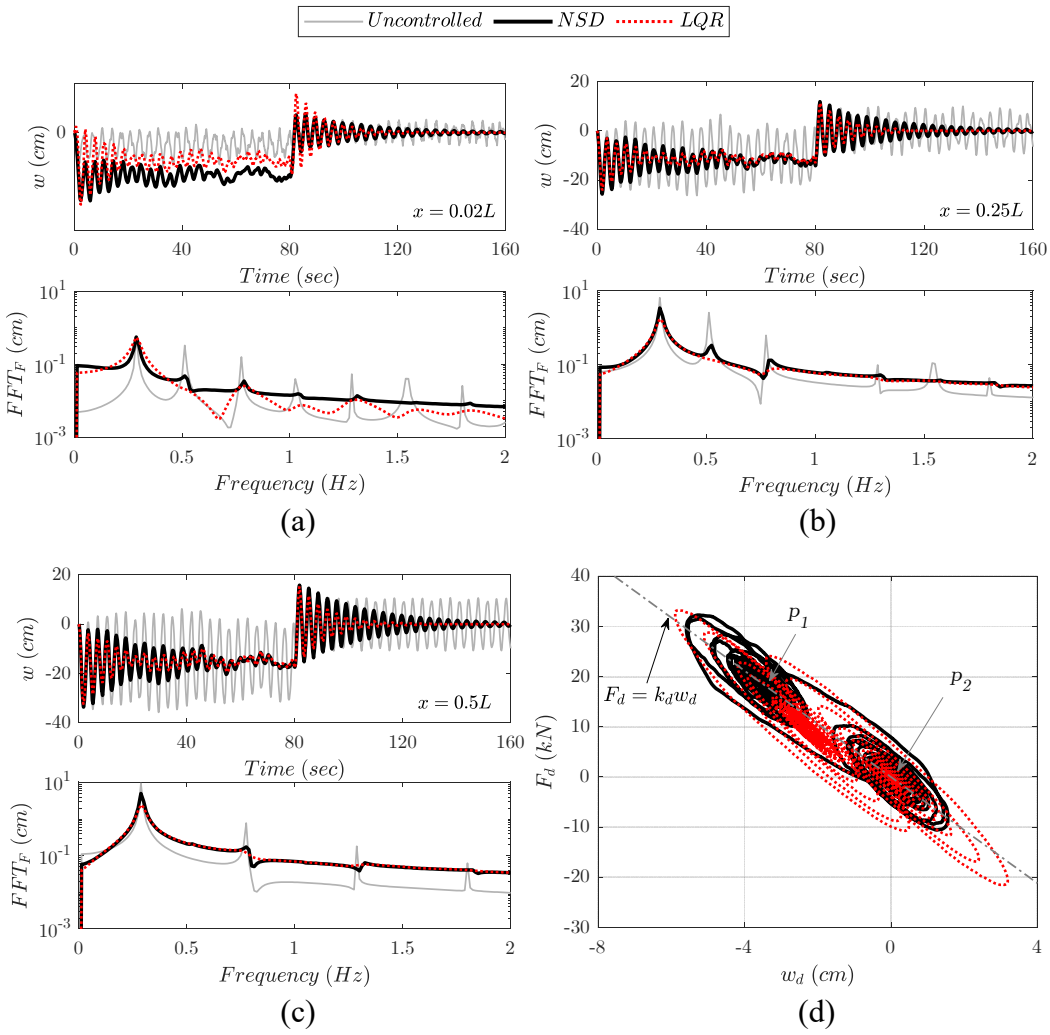

Fig. 7-11. Effectiveness of NSD in controlling wind-induced cable vibrations. (a) Time-history and FFT amplitude of cable displacement at $x = x_d = 0.02L$; (b) Time-history and FFT amplitude of cable displacement at $x = 0.25L$; (c) Time-history and FFT amplitude of cable displacement at $x = 0.5L$; (d) Hysteresis loop of the control devices.

be observed that the 2nd and higher modes are effectively controlled by the NSD. Figure 7-11(b) shows the cable response at $x = 0.25L$ where the cable vibration is mainly governed by the 1st and the 2nd modes and to a lower degree, by the 3rd mode. The 2nd modal damping ratio ($\zeta_2 = 3.74\%$) is calculated by applying a band-pass filter at the 2nd modal frequency, i.e. 0.51 Hz, to the free vibration response. The frequency response of the free vibration

shows that the optimized NSD is able to mitigate the cable displacement dominated by the first three modes. The FFT amplitude corresponding to the first three modal frequencies (i.e. 0.29, 0.51 and 0.78 Hz) are reduced by 45%, 87% and 79%, respectively. The cable response at the mid-span is illustrated in Fig. 7-11(c). At this location, the NSD controlling effect in both forced and free vibration phases is significant. The FFT amplitude at the first and the third modal frequencies is reduced respectively by 46% and 78% after installing the NSD. Figure 7-11(d) provides the hysteresis loop of the NSD. The figure shows that the maximum damper force is generated when the cable displacement is 5.3 cm below the static equilibrium profile at the damper location. From this figure, it is observed that the NSD oscillates around two points p_1 and p_2, which correspond respectively to the forced and the free vibration phases. These two points are connected by the line $F_d = -5.296 w_d$, the slope of which denotes the negative stiffness of the damper, i.e. $k_d = -529.6$ kN/m.

7.4.5.3. Comparison with active control

To compare the performance of the designed NSD with other vibration control schemes for long stay cables, the optimal LQR controller introduced by Shi et al. [68] is adopted. LQR requires the full system states to generate the control force and is considered to be an ideal reference control solution. The **Q** matrix of the LQR controller is selected as:

$$\boldsymbol{Q} = \begin{bmatrix} \boldsymbol{K} & 0 \\ 0 & \boldsymbol{M} \end{bmatrix} \tag{7-16}$$

where **M** and **K** are the mass and stiffness matrix of the cable obtained from Eq. (7-3). The R parameter of the LQR controller defines the intensity of the control action and can be selected to generate the desired control force. In this example, the R parameter is selected in such a way that both the NSD and LQR would generate similar peak for the control

force. The peak of the control force provided by NSD is 32.3 kN. It was found by trial and error that for a R value of 6×10^{-6}, the LQR would generate a peak control force of 33.3 kN. Thus, $\mathrm{R} = 6 \times 10^{-6}$ will be used in this example.

Table 7-3 also lists the main performance parameters of the LQR controller. The modal damping ratio for the first three cable modes are 6.03%, 4.64%, and 2.76%, respectively. They are higher than those of the NSD case. With a similar control force peak as that of the NSD, by installing the LQR, the first modal damping ratio of the damped cable would be 2.5 times that of the NSD case. In the case of the LQR, the response reduction indices δ_F and δ_P are respectively 52% and 11% lower than those of the NSD case. Thus, with a similar control force peak, the LQR is more effective than the NSD in suppressing both free and forced cable vibrations.

The performance of the NSD and the LQR can be further compared in Fig. 7-11. Figure 7-11(a) shows the cable response at the installation location of the controller. It is observed from the figure that the LQR case has larger cable displacement at the controller installation location during the early stage of both the forced and free vibration phases. The maximum peak-to-peak cable displacement at the LQR installation location are respectively 15.3% and 30% larger than that of the NSD case during forced and free vibration phases. In this regard, the NSD performs better than the LQR. Comparisons of the LQR and NSD performance in suppressing cable vibrations at the quarter- and mid-span are shown in Figs. 7-11(b) and 7-10(c), respectively, of which the LQR manifests superior vibration control efficiency. Based on the hysteresis loops of the NSD and the LQR shown in Fig. 7-11(d), both controllers produce pseudo-negative stiffness and result in higher positive cable displacements at the installation location.

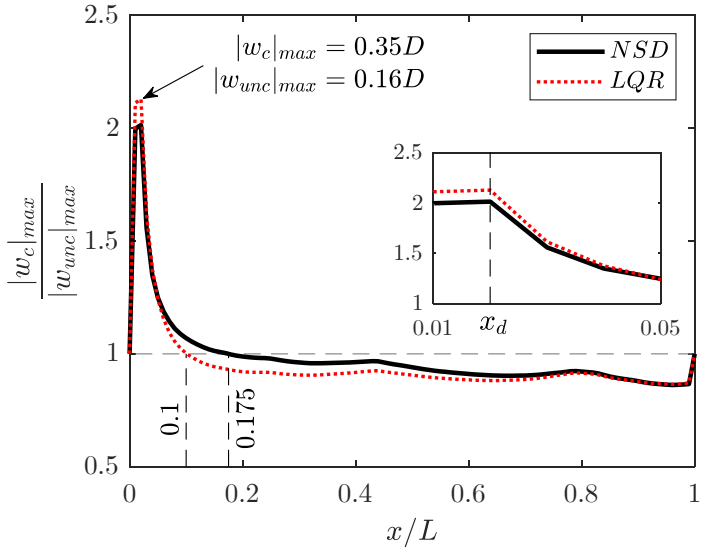

Fig. 7-12. NSD-induced amplification of the cable response.

As discussed earlier, the main drawback of the NSD is that it would amplify the cable displacement around the damper installation location. This behaviour is further investigated in Fig. 7-12. In this figure, the ratio between the maximum controlled cable displacement, $|\mathrm{w_c}|_{max}$, and the maximum uncontrolled cable displacement, $|\mathrm{w_{unc}}|_{max}$, is illustrated along the cable for both the NSD and the LQR cases. The horizontal line at $|\mathrm{w_c}|_{max}/|\mathrm{w_{unc}}|_{max} = 1$ represents the uncontrolled cable response. The effect of the NSD on the cable response can be characterized by two key parameters: the displacement amplification factor and the affected length of the cable. It can be observed in Fig. 7-12 that the amplification of the cable response due to the NSD covers about 17.5% of the cable length from the lower anchorage with the maximum amplification factor being 2.06. At the damper location, the maximum controlled and uncontrolled cable response are $0.33D$ and $0.16D$, respectively, where D is the cable outer diameter. In the case of the LQR, the displacement amplification covers 10% of the cable length with the maximum amplification factor being 2.19. Therefore, under the condition of similar peak control

force, although the LQR can provide a higher damping ratio to the attached cable than the NSD, it would induce larger cable displacement at the its installation location.

For the sample cable considered in this example, if an ideal conventional passive damper (no reduction due to cable sag, cable bending stiffness, and damper stiffness) is used instead, then the maximum achievable damping ratio can be obtained from Eqs. (5-5b) and (5-6b), which is $\zeta_{max} = 0.5(x_d/L) = 0.5 \times 0.02 = 0.01$. Therefore, it cannot reach the required level of damping ratio, i.e. 2%. In other words, the NSD is able to achieve the same control level as the LQR and can suppress multi-mode cable vibrations more effectively than other conventional passive dampers such as PSD and ZSD.

7.5. Summary

A novel NSD optimization approach for multi-mode stay cable vibration control has been proposed based on the three-dimensional NSD performance surface. Two design scenarios have been considered. In the first scenario, the NSD negative stiffness is predetermined and the optimum damper size is selected to reach the maximum damping ratio; whereas in the second one, both the size and negative stiffness of the NSD are optimized to satisfy the damping requirement for the targeted dominant modes. The applicability of the proposed NSD design equations has been verified using 15 sample representative real stay cables. To further assess the effectiveness of the proposed NSD design approach, a design example has been presented, of which a NSD has been designed based on the proposed approach to suppress wind-induced multi-mode cable vibration of a 460.1 m stay cable. The performance of the designed NSD has been evaluated and compared to the optimal linear-quadratic regulator (LQR) control. The main findings of the current chapter can be summarized as follows:

1- The proposed NSD optimization approach can be used for designing a NSD to effectively control both single-mode and multi-mode cable vibrations and provide required damping ratio for the targeted dominant mode(s).

2- The NSD designed using the proposed optimization approach is found not only to have superior performance than conventional PSD and ZSD, but also have better performance than the LQR, having comparable peak control force at the installation location.

3- When there exist more than two dominant modes in vibration, designing a NSD for the lowest and the highest dominant modes would also adequately control the mid-range modes. This unique feature can greatly facilitate NSD design in more complex loading conditions and/or cable behaviour.

4- Compared to other cable vibration control schemes, the main drawback of using a NSD is the localized amplification of cable response around the damper location.

Chapter 8 Conclusions and Recommendations

Different aspects of controlling the vibrations of bridge stay cables using passive negative stiffness dampers have been studied comprehensively in the present work. This chapter provides a summary of the main contributions and conclusions of this study. In addition, recommendations are made to extend the research in the future.

8.1. Conclusions

The performance and safety of cable-stayed bridges are adversely affected by the frequent and sometimes excessive vibrations of stay cables. Therefore, it is necessary to provide an effective method to control these harmful oscillations. Among various existing countermeasures, the passive cable vibration control using NSD is the focus of this study due to its high control performance and cost efficiency.

An extensive literature review was conducted in Chapter 2 not only to understand the theoretical background of the cable vibration problem, but also to investigate the recent advances in the field of cable vibration control and identify the areas that need further development. By reviewing the recently emerged cable vibration control schemes, it was found that passive NSD had attracted much attention due to their high damping performance. However, the knowledge associated with the dynamic behaviour of a cable-NSD system and its design requirements were still limited. Furthermore, the literature review indicated that the combined effects of cable sag, cable bending stiffness, damper stiffness, and damper support stiffness could significantly affect the damping capacity of a

cable-damper system. Therefore, existing analytical and numerical models were required to be further refined to reflect these effects.

Chapter 3 presented an analytical study to refine an existing viscous damper design formula, developed by Fujino and Hoang [71], by including the effect of damper stiffness in the mechanical model of a clamped or pinned cable-damper system. This will generalize Fujino and Hoang's model to address the behaviour of a cable equipped with a passive viscous damper having either zero (ZSD), positive (PSD) or negative stiffness (NSD). The latter is of particular importance to study the performance of a NSD. The refined design formula was obtained by finding an asymptotic solution to the governing transcendental equation and validated by the results of an existing experimental study [46]. The superior performance of the NSD compared to zero- and positive stiffness dampers was confirmed. A threshold for the negative stiffness was identified in NSD which ensured the stability of the system.

In Chapter 4, a control-oriented numerical framework was developed based on the mode superposition method (MSM) to analyze the dynamic response of a damped stay cable. The efficiency of the MSM-based framework was substantially improved by applying the static correction technique, in which a special shape function is introduced to reflect the damper presence. The static shape function was defined as the cable's static displacement when subjected to an arbitrary point load at the damper location and was explicitly derived by solving the associated governing integro-differential equation. Furthermore, the other shape functions were conventional sinusoidal terms which were modified to be consistent with the boundary conditions of a clamped cable.

With the development of analytical and numerical models capable of explaining the behaviour of a cable equipped with a negative stiffness damper, Chapter 5 was devoted to investigate and evaluate the control performance of a NSD when mounted on a rigid damper support. The superior damping performance of NSD compared to conventional ZSD and PSD was explained based on the damper's force generation mechanism. The issue of NSD stability was revisited and a stability limit was formulated based on the asymptotic damper design formula. An innovative approach for designing a NSD to control single-mode stay cable vibration was proposed based on the three-dimensional NSD performance surface obtained from the asymptotic design formula. This surface represents the modal damping ratio of a cable-NSD system as a function of damper size and damper stiffness.

In practice, the damping ratio of a cable equipped with a passive viscous damper can be increased by mounting the damper on a non-rigid support to move its installation location towards the cable mid-span. Therefore, the assumption of rigid damper support is released in Chapter 6 to study the impact of damper support flexibility on the NSD control performance. The NSD stability limit derived in Chapter 3 was extended to be applicable to the flexible support condition. In Chapter 6, different NSD design scenarios were considered and an optimization algorithm was proposed to identify the optimum combination of NSD parameters (i.e. damper size and stiffness) and damper support stiffness. In parallel, the NSD design was refined to minimize the difference between the damping ratio predictions obtained from the analytical and numerical frameworks.

An innovative approach for optimizing a NSD to control multi-mode stay cable vibrations was proposed in Chapter 7. Analytical design relationships were developed to determine NSD parameters which allow the cable-NSD system to satisfy the damping requirement

for the targeted dominant modes. We have provided evidence that the proposed design approach was not only able to target the two dominant modes but also to control all the intermediate modes between the lowest and the highest modes for which the design is based.

Based on the above summary of various aspects that have been addressed in the dissertation, the key findings and conclusions drawn from this study are presented in the following main categories:

8.1.1. NSD behaviour and design

1- The superior control performance of NSD is due to a reduced total resisting force in NSD against the cable motion when it moves away from the neutral position. This would increase the cable displacement and thus, enhance the capacity of NSD in absorbing kinetic energy. The higher damping ratio of a NSD comes at the cost of increased cable displacement, especially at the damper installation location.

2- The NSD stability limit defines the minimum allowable negative damper stiffness and depends on the various design parameters including damper installation location, the cable bending stiffness, cable length, cable chord tension and damper support stiffness. At the stability limit, when damping in a NSD is absent, the negative damper stiffness would fully counteract the inherent positive stiffness of the cable at the damper location and lead to an instability of the damped cable.

3- The negative damper stiffness ratio, τ, is defined as k_d/k_d^{min} . Beyond an identified limit of τ, denoted as τ_{all}, the analytical design equation overestimates the modal damping ratio for a group of full-size NSD-equipped cables. Hence, a safe NSD

design requires the negative damper stiffness to satisfy $\tau < \tau_{all}$ for all the targeted modes.

4- The first modal damping ratio of a NSD-equipped cable is affected by both the cable bending stiffness and the cable sag. However, the damping ratio in the higher modes is only sensitive to the effect of cable bending stiffness but the influence of cable sag is negligible.

5- The impact of damper support stiffness on the NSD control performance depends on the damper size. If the damper size is smaller than an identified critical value, a more flexible damper support can raise the damping ratio of a NSD-equipped cable. Otherwise, using a more flexible support would not have a beneficial effect on the NSD performance. Optimizing the damper support stiffness by using the proposed algorithms not only reduces the size and the stiffness of a NSD but also mitigates the cable response amplification along its length. This would reduce the fabrication and maintenance costs of the NSD. The control effectiveness of an optimized/refined NSD mounted on a flexible support is comparable to that of an optimal LQR controller. Hence, NSD is a feasible alternative to the active and semi-active control schemes for mitigating cable vibrations.

6- Using the proposed analytical equations, a NSD can be designed to effectively control multi-mode cable vibrations by providing the required damping ratio in two dominant modes. Besides, the NSD can be optimized for a given negative damper stiffness to provide equal damping ratio in two modes. A cable vibration with more than two dominant modes can be controlled by designing a NSD for the lowest and the highest target modes. The analytical design equations are validated by

conducting a numerical study on a large set of representative full-size cables. The control performance of NSD in mitigating multi-mode cable vibrations is comparable to that of an optimal LQR controller having a similar peak control force.

8.1.2. Damping ratio of a damped cable

1- The effect of the damper stiffness on the damping ratio of a cable-damper system is integrated with the cable flexural rigidity and the damper support stiffness.
2- The proposed asymptotic design relationships for the fixed-fixed and the hinged-hinged cables are found to have the same form. The effect of the cable boundary condition can be represented by a coefficient α_{BC} in the factors related to the cable bending stiffness, namely η_f and R_f.
3- The asymptotic design formula tends to provide a conservative estimation of the maximum achievable damping ratio of a cable-damper system. Therefore, this approximation would yield a safe damper design in practice and is deemed acceptable.
4- In the absence of reliable information on the level of rotational rigidity in the cable anchorage, it is recommended to assume a fixed-fixed boundary condition to achieve a conservative damper design. However, a hinged-hinged assumption would generally lead to a more realistic design for long stay cables with length $L > 250\ m$.

8.1.3. Dynamic analysis of a damped cable

1- By including the static correction term for both the fixed-fixed and the hinged-hinged cables and modifying the sinusoidal terms for the fixed-fixed cable, the

number of modes required for convergence is substantially reduced in the MSM. This correction improves the computational efficiency of the proposed numerical framework by reducing the size of the modal matrix equations which need to be solved numerically in the time domain.

2- It is deemed acceptable to assume a parabolic self-weight profile for a damped cable. The error in the modal parameters resulted from this assumption is found to be negligible for both the fixed-fixed and hinged-hinged cases.

3- The modal frequency tends to converge ascendingly to the analytical value in the Finite Difference method which uses a lumped mass model. However, it converges in a descending mode in the MSM which is based on a consistent mass model.

8.2. Recommendations

This study has deepened the understanding of the behaviour and control performance of negative stiffness dampers by developing adapted analytical and numerical solutions in cable dynamics. However, a few issues in this field still deserve close attention and they are recommended for future research as follows:

8.2.1. Cable boundary conditions

In this study, idealized fixed-fixed or hinged-hinged boundary conditions were considered in the analytical model. However, the actual boundary condition for a real stay cable lies between these two extreme cases. Thus, it is recommended to obtain a more realistic prediction of the cable dynamic response by conducting an analytical study in which the cable end conditions are modeled as rotational springs, with the spring stiffness representing the fixity of the cable-deck and the cable-pylon anchorages.

8.2.2. Three-dimensional cable motion

In the current study, only the in-plane motion of the cable is considered. However, the actual motion of the cables might include both in-plane and out-of-plane components. Therefore, it is recommended for future research to consider the interaction between both in-plane and out-of-plane motions in the analytical model and study the damper performance in suppressing coupled cable motions along those two directions.

8.2.3. Mechanical model of a damper

In this study, both the springs and the dashpot were assumed to behave linearly in the mechanical model of a NSD. It is recommended to include the effect of possible nonlinearity in the mechanical representation of a NSD and derive new design relationships accordingly to ensure the applicability of the design tools under nonlinear damper behaviour.

References

1. Virlogeux M. Recent evolution of cable-stayed bridges. *Engineering Structures* 1999; **21**(8): 737–755. DOI: 10.1016/S0141-0296(98)00028-5.

2. Gimsing NJ, Georgakis CT. *Cable supported bridges : concept and design*. John Wiley & Sons; 2012.

3. Svensson H. The Development of Cable-Stayed Bridges since John Röbling. *IABSE Symposium Report* 2007; **93**(26): 1–8. DOI: 10.2749/222137807796119825.

4. Bimson DTO. A critical analysis of the pont de Normandie cable-stayed bridge. *Proceedings of Bridge Engineering* 2007; **2**.

5. Chen EW fah, Duan L. *Bridge Engineering Handbook*. CRC Press; 2014.

6. Yamaguchi H, Adhikari R. Energy-based evaluation of modal damping in structural cables with and without damping treatment. *Journal of Sound and Vibration* 1995; **181**(1): 71–83. DOI: 10.1006/JSVI.1995.0126.

7. Mehrabi AB. In-Service Evaluation of Cable-Stayed Bridges, Overview of Available Methods and Findings. *Journal of Bridge Engineering* 2006; **11**(6): 716–724. DOI: 10.1061/(ASCE)1084-0702(2006)11:6(716).

8. Abdel-Ghaffar AM, Khalifa MA. Importance of Cable Vibration in Dynamics of Cable Stayed Bridges. *Journal of Engineering Mechanics* 1991; **117**(11): 2571–2589. DOI: 10.1061/(ASCE)0733-9399(1991)117:11(2571).

9. Virlogeux M. State-of-the-art in cable vibrations of cable-stayed bridges. *Bridge Structures* 2005; **1**(3): 133–168. DOI: 10.1080/15732480500301004.

10. Kumarasena S, Jones NP, Irwin P, Taylor P, Corporation H. *Wind-induced vibration of stay cables*. United States. Federal Highway Administration; 2007.

11. Matsumoto M, Daito Y, Kanamura T, Shigemura Y, Sakuma S, Ishizaki H. Wind-induced vibration of cables of cable-stayed bridges. *Journal of Wind Engineering and Industrial Aerodynamics* 1998; **74**–**76**: 1015–1027. DOI: 10.1016/S0167-6105(98)00093-2.

12. Ozkan E, Main JA, Jones NP. Full-scale measurements on the Fred Hartman Bridge. *Proc. 5th Asia-Pacific Conf. on Wind Engrg*, 2001.

13. Savor Z, Radic J, Hrelja G. Cable vibrations at Dubrovnik bridge. *Bridge Structures* 2006; **2**(2): 97–106. DOI: 10.1080/15732480600855800.

14. Ni YQ, Wang XY, Chen ZQ, Ko JM. Field observations of rain-wind-induced cable vibration in cable-stayed Dongting Lake Bridge. *Journal of Wind Engineering and Industrial Aerodynamics* 2007; **95**(5): 303–328. DOI:

10.1016/J.JWEIA.2006.07.001.

15. Johnson EA, Christenson RE, Spencer Jr BF. Flat-Sag Cables with Semiactive Damping. *Computer-Aided Civil and Infrastructure Engineering* 2002.

16. Caetano E de S. *Cable Vibrations in Cable-stayed Bridges*. IABSE; 2007.

17. Christiansen H, Jakobsen JB, Macdonald JHG, Larose GL, Bosch HR. Aerodynamics of a stay cable with helical fillets - Part I: Stability and load characteristics. *Journal of Wind Engineering and Industrial Aerodynamics* 2018; **177**: 376–391. DOI: 10.1016/j.jweia.2018.01.045.

18. Bi JH, Qiao HY, Nikitas N, Guan J, Wang J, Lu P. Numerical modelling for rain wind induced vibration of cables with longitudinal ribs. *Journal of Wind Engineering and Industrial Aerodynamics* 2018; **178**: 69–79. DOI: 10.1016/J.JWEIA.2018.05.002.

19. Flamand O. Rain-wind induced vibration of cables. *Journal of Wind Engineering and Industrial Aerodynamics* 1995; **57**(2–3): 353–362. DOI: 10.1016/0167-6105(94)00113-R.

20. Kleissl K, Georgakis CT. Comparison of the aerodynamics of bridge cables with helical fillets and a pattern-indented surface. *Journal of Wind Engineering and Industrial Aerodynamics* 2012; **104**–**106**: 166–175. DOI: 10.1016/j.jweia.2012.02.031.

21. Fujino Y, Kimura K, Tanaka H. *Wind Resistant Design of Bridges in Japan*. Tokyo: Springer Japan; 2012. DOI: 10.1007/978-4-431-54046-5.

22. Caracoglia L, Jones NP. In-plane dynamic behaviour of cable networks. Part 1: formulation and basic solutions. *Journal of Sound and Vibration* 2005; **279**(3–5): 969–991. DOI: 10.1016/J.JSV.2003.11.058.

23. Yamaguchi H, Nagahawatta HD. Damping effects of cable cross ties in cable-stayed bridges. *Journal of Wind Engineering and Industrial Aerodynamics* 1995; **54**–**55**(C): 35–43. DOI: 10.1016/0167-6105(94)00027-B.

24. Yamaguchi H, Jayawardena L. Analytical estimation of structural damping in cable structures. *Journal of Wind Engineering and Industrial Aerodynamics* 1992; **43**(1–3): 1961–1972. DOI: 10.1016/0167-6105(92)90620-P.

25. Caracoglia L, Zuo D. Effectiveness of cable networks of various configurations in suppressing stay-cable vibration. *Engineering Structures* 2009; **31**(12): 2851–2864. DOI: 10.1016/j.engstruct.2009.07.012.

26. Yamaguchi H. Control of cable vibrations with secondary cables. *Proceedings of the International Symposium on Cable Dynamics, Liege*, AIM Liege; 1995.

27. Caracoglia L, Jones NP. In-plane dynamic behaviour of cable networks. Part 2: prototype prediction and validation. *Journal of Sound and Vibration* 2005; **279**(3–5): 993–1014. DOI: 10.1016/J.JSV.2003.11.059.

28. Kangas S, Helmicki A, Hunt V, Sexton R, Swanson J. Cable-Stayed Bridges: Case Study for Ambient Vibration-Based Cable Tension Estimation. *Journal of Bridge Engineering* 2012; **17**(6): 839–846. DOI: 10.1061/(ASCE)BE.1943-5592.0000364.

29. Ahmad J, Cheng S. Effect of cross-link stiffness on the in-plane free vibration behaviour of a two-cable network. *Engineering Structures* 2013; **52**: 570–580. DOI: 10.1016/j.engstruct.2013.03.018.

30. Ahmad J, Cheng S, Ghrib F. An analytical approach to evaluate damping property of orthogonal cable networks. *Engineering Structures* 2014; **75**: 225–236. DOI: 10.1016/j.engstruct.2014.06.001.

31. Ahmad J, Cheng S. Analytical study on in-plane free vibration of a cable network with straight alignment rigid cross-ties. *Journal of Vibration and Control* 2015; **21**(7): 1299–1320. DOI: 10.1177/1077546313497245.

32. Ahmad J, Cheng S, Ghrib F. Impact of cross-tie design on the in-plane stiffness and local mode formation of cable networks on cable-stayed bridges. *Journal of Sound and Vibration* 2016; **363**: 141–155. DOI: 10.1016/j.jsv.2015.09.052.

33. Ahmad J, Cheng S, Ghrib F. Effect of the Number of Cross-Tie Lines on the In-Plane Stiffness and Modal Behaviour Classification of Orthogonal Cable Networks with Multiple Lines of Transverse Flexible Cross-Ties. *Journal of Engineering Mechanics* 2016; **142**(4): 04015106. DOI: 10.1061/(ASCE)EM.1943-7889.0001008.

34. Ahmad J, Cheng S, Ghrib F. Efficiency of an External Damper in Two-Cable Hybrid Systems. *Journal of Bridge Engineering* 2018; **23**(2): 04017138. DOI: 10.1061/(ASCE)BE.1943-5592.0001185.

35. Ahmad J, Cheng S, Ghrib F. Generalized Approach for the Formulation of Analytical Model of Hybrid Cable Networks. *Journal of Engineering Mechanics* 2018; **144**(6): 04018035. DOI: 10.1061/(ASCE)EM.1943-7889.0001455.

36. Miyata T, Fujiwara T, Yamada H. Wind-resistant design of cables for the Tatara bridge. *Symposium, Long-span and high-rise structures*, vol. 79, Kobe; Japan: IABSE Reports; 1998. DOI: 10.5169/seals-59830.

37. Tabatabai H, Mehrabi ABA. Design of mechanical viscous dampers for stay cables. *Journal of Bridge Engineering* 2000; **5**(May): 114–123. DOI: 10.1061/(ASCE)1084-0702(2000)5:2(114).

38. Main, JA and Jones N. Evaluation of viscous dampers for stay-cable vibration mitigation. *Journal of Bridge Engineering* 2001; **6**(6): 385–397. DOI: 10.1061/(ASCE)1084-0702(2001)6:6(385).

39. Krenk S, Høgsberg JR. Damping of Cables by a Transverse Force. *Journal of Engineering Mechanics (ASCE)* 2005; **131**(4): 340–348. DOI: 10.1061/(ASCE)0733-9399(2005)131:4(340).

40. Cu VH, Han B. A stay cable with viscous damper and tuned mass damper. *Australian Journal of Structural Engineering* 2015; **16**(4): 316–323. DOI:

10.1080/13287982.2015.1092693.

41. Weber F, Høgsberg J, Krenk S. Optimal Tuning of Amplitude Proportional Coulomb Friction Damper for Maximum Cable Damping. *Journal of Structural Engineering* 2010; **136**(2): 123–134. DOI: 10.1061/(ASCE)0733-9445(2010)136:2(123).

42. Nakamura A, Kasuga A, Arai H. The effects of mechanical dampers on stay cables with high-damping rubber. *Construction and Building Materials* 1998; **12**(2–3): 115–123. DOI: 10.1016/S0950-0618(97)00013-5.

43. Krenk S, Nielsen SRK. Vibrations of a shallow cable with a viscous damper. *Proceedings of the Royal Society A: Mathematical, Physical and Engineering Sciences* 2002; **458**(2018): 339–357. DOI: 10.1098/rspa.2001.0879.

44. Hoang N, Fujino Y. Analytical Study on Bending Effects in a Stay Cable with a Damper. *Journal of Engineering Mechanics* 2007; **133**(11): 1241–1246. DOI: 10.1061/(ASCE)0733-9399(2007)133:11(1241).

45. Huang Z, Jones NP. Damping of Taut-Cable Systems: Effects of Linear Elastic Spring Support. *Journal of Engineering Mechanics* 2011; **137**(7): 512–518. DOI: 10.1061/(ASCE)EM.1943-7889.0000252.

46. Fournier JA, Cheng S. Impact of Damper Stiffness and Damper Support Stiffness on the Efficiency of a Linear Viscous Damper in Controlling Stay Cable Vibrations. *Journal of Bridge Engineering* 2014; **19**(4): 04013022. DOI: 10.1061/(ASCE)BE.1943-5592.0000562.

47. Huang L. Experimental study on bridge stay cable vibration mitigation using external viscous damper. University of Windsor, 2011.

48. Weber F, Feltrin G, Maślanka M, Fobo W, Distl H. Design of viscous dampers targeting multiple cable modes. *Engineering Structures* 2009; **31**(11): 2797–2800. DOI: 10.1016/J.ENGSTRUCT.2009.06.020.

49. Ni Y, Duan YF, Chen Z. Damping identification of MR-damped bridge cables from in-situ monitoring under wind-rain-excited conditions. In: Liu SC, Pines DJ, editors. *SPIE's 9th Annual International Symposium on Smart Structures and Materials*, vol. 4696, San Diego, California: International Society for Optics and Photonics; 2002. DOI: 10.1117/12.472573.

50. Bossens F, Preumont A. Active tendon control of cable-stayed bridges: a large-scale demonstration. *Earthquake Engineering & Structural Dynamics* 2001; **30**(7): 961–979. DOI: 10.1002/eqe.40.

51. Fujino Y, Warnitchai P, Pacheco BM. Active Stiffness Control of Cable Vibration. *Journal of Applied Mechanics* 1993; **60**(4): 948. DOI: 10.1115/1.2901006.

52. Huang P, Wang X, Wen Q, Wang W, Sun H. Active Control of Stay Cable Vibration Using a Giant Magnetostrictive Actuator. *Journal of Aerospace Engineering* 2018; **31**(5): 04018074. DOI: 10.1061/(ASCE)AS.1943-5525.0000905.

53. Duan YF, Ni YQ, Ko JM. Cable Vibration Control using Magnetorheological Dampers. *Journal of Intelligent Material Systems and Structures* 2006; **17**(4): 321–325. DOI: 10.1177/1045389X06054997.

54. Ni YQ, Chen Y, Ko JM, Cao DQ. Neuro-control of cable vibration using semi-active magneto-rheological dampers. *Engineering Structures* 2002; **24**(3): 295–307. DOI: 10.1016/S0141-0296(01)00096-7.

55. Weber F, Distl H. Amplitude and frequency independent cable damping of Sutong bridge and Russky bridge by magnetorheological dampers. *Structural Control and Health Monitoring* 2015; **22**(2): 237–254. DOI: 10.1002/stc.1671.

56. Li H, Liu M, Li J, Guan X, Ou J. Vibration control of stay cables of the Shandong Binzhou Yellow River Highway Bridge using Magnetorheological fluid dampers. *Journal of Bridge Engineering* 2007; **12**(4): 401–409. DOI: 10.1061/(ASCE)1084-0702(2007)12:4(401).

57. Johnson EA, Christenson RE, Spencer BF. Semiactive damping of cables with sag. *Computer-Aided Civil and Infrastructure Engineering* 2003; **18**(2): 132–146. DOI: 10.1111/1467-8667.00305.

58. Iemura H, Igarashi A, Nakata N. Semi-active control of full-scale structures using variable joint damper system. *The Fourteenth KKNN Symposium on Civil Engineering*, 2001.

59. Sarlis AA, Pasala DTR, Constantinou MC, Reinhorn AM, Nagarajaiah S, Taylor DP. Negative Stiffness Device for Seismic Protection of Structures. *Journal of Structural Engineering* 2013; **139**(7): 1124–1133. DOI: 10.1061/(ASCE)ST.1943-541X.0000616.

60. Iemura H, Pradono MH. Advances in the development of pseudo-negative-stiffness dampers for seismic response control. *Structural Control and Health Monitoring* 2009; **16**(7–8): 784–799. DOI: 10.1002/stc.345.

61. Li H, Liu M, Ou J. Negative stiffness characteristics of active and semi-active control systems for stay cables. *Structural Control and Health Monitoring* 2008; **15**(2): 120–142. DOI: 10.1002/stc.200.

62. Weber F, Boston C. Clipped viscous damping with negative stiffness for semi-active cable damping. *Smart Materials and Structures* 2011; **20**(4): 045007. DOI: 10.1088/0964-1726/20/4/045007.

63. Shi X, Zhu S. Magnetic negative stiffness dampers. *Smart Materials and Structures* 2015; **24**(7): 072002. DOI: 10.1088/0964-1726/24/7/072002.

64. Zhou P, Li H. Modeling and control performance of a negative stiffness damper for suppressing stay cable vibrations. *Structural Control and Health Monitoring* 2016; **23**(4): 764–782. DOI: 10.1002/stc.1809.

65. Liu M, Zhou P, Li H. Novel Self-Centering Negative Stiffness Damper Based on Combination of Shape Memory Alloy and Prepressed Springs. *Journal of Aerospace Engineering* 2018; **31**(6): 04018100. DOI: 10.1061/(ASCE)AS.1943-

5525.0000926.

66. Shi X, Zhu S, Spencer BF. Experimental Study on Passive Negative Stiffness Damper for Cable Vibration Mitigation. *Journal of Engineering Mechanics* 2017; **143**(9): 04017070. DOI: 10.1061/(ASCE)EM.1943-7889.0001289.

67. Shi X, Zhu S, Li JY, Spencer BF. Dynamic behaviour of stay cables with passive negative stiffness dampers. *Smart Materials and Structures* 2016; **25**(7): 075044. DOI: 10.1088/0964-1726/25/7/075044.

68. Shi X, Zhu S, Nagarajaiah S. Performance Comparison between Passive Negative-Stiffness Dampers and Active Control in Cable Vibration Mitigation. *Journal of Bridge Engineering* 2017; **22**(9): 04017054. DOI: 10.1061/(ASCE)BE.1943-5592.0001088.

69. Pacheco BMB, Fujino Y, Sulekh A. Estimation curve for modal damping in stay cables with viscous damper. *Journal of Structural Engineering* 1993; **119**(6): 1961–1979. DOI: 10.1061/(ASCE)0733-9445(1993)119:6(1961).

70. Krenk S. Vibrations of a Taut Cable With an External Damper. *Journal of Applied Mechanics* 2000; **67**(4): 772. DOI: 10.1115/1.1322037.

71. Fujino Y, Hoang N. Design Formulas for Damping of a Stay Cable with a Damper. *Journal of Structural Engineering* 2008; **134**(2): 269–278. DOI: 10.1061/(ASCE)0733-9445(2008)134:2(269).

72. Cheng S, Darivandi N, Ghrib F. The design of an optimal viscous damper for a bridge stay cable using energy-based approach. *Journal of Sound and Vibration* 2010; **329**(22): 4689–4704. DOI: 10.1016/J.JSV.2010.05.027.

73. Mehrabi AB, Tabatabai H. Unified Finite Difference Formulation for Free Vibration of Cables. *Journal of Structural Engineering* 1998; **124**(11): 1313–1322. DOI: 10.1061/(ASCE)0733-9445(1998)124:11(1313).

74. Johnson EA, Baker GA, Spencer, Jr. BF, Fujino Y. Mitigating stay cable oscillation using semiactive damping. In: Liu SC, editor. *Smart Structures and Materials 2000: Smart Systems for Bridges, Structures, and Highways*, vol. 3988, Newport Beach, CA, United States: International Society for Optics and Photonics; 2000. DOI: 10.1117/12.383142.

75. Wang XY, Ni YQ, Ko JM, Chen ZQ. Optimal design of viscous dampers for multi-mode vibration control of bridge cables. *Engineering Structures* 2005; **27**(5): 792–800. DOI: 10.1016/j.engstruct.2004.12.013.

76. Hoang N, Fujino Y. Multi-mode control performance of nonlinear dampers in stay cable vibrations. *Structural Control and Health Monitoring* 2009; **16**(7-8): n/a-n/a. DOI: 10.1002/stc.364.

77. Weber F, Distl H. Semi-active damping with negative stiffness for multi-mode cable vibration mitigation: Approximate collocated control solution. *Smart Materials and Structures* 2015; **24**(11): 115015. DOI: 10.1088/0964-1726/24/11/115015.

78. Irvine HM, Caughey TK. The linear theory of free vibrations of a suspended cable. *Proceedings of the Royal Society of London A Mathematical and Physical Sciences* 1974; **341**(1626): 299–315. DOI: 10.1098/rspa.1974.0189.

79. Irvine HM. *Cable structures*. Dover Publications; 1992.

80. Shimada T. Estimating method of cable tension from natural frequency of high mode. *Doboku Gakkai Ronbunshu* 1994; **1994**(501): 163–171.

81. Zui H, Shinke T, Namita Y. Practical Formulas for Estimation of Cable Tension by Vibration Method. *Journal of Structural Engineering* 1996; **122**(6): 651–656. DOI: 10.1061/(ASCE)0733-9445(1996)122:6(651).

82. Carne TG. Guy Cable Design and Damping for Vertical Axis Wind Turbines. *Report No SAND80-2669, Sandia National Laboratory, Albuquerque, NM* 1981.

83. Leger P, Wilson EL. Modal summation methods for structural dynamic computations. *Earthquake Engineering & Structural Dynamics* 1988; **16**(1): 23–27. DOI: 10.1002/eqe.4290160103.

84. Woodard SE, Housner JM. Nonlinear behaviour of a passive zero-spring-rate suspension system. *Journal of Guidance, Control, and Dynamics* 1991; **14**(1): 84–89. DOI: 10.2514/3.20608.

85. Platus DL. Negative-stiffness-mechanism vibration isolation systems. In: Derby EA, Gordon CG, Vukobratovich D, Yoder, Jr. PR, Zweben CH, editors. vol. 3786, International Society for Optics and Photonics; 1999. DOI: 10.1117/12.363841.

86. Lee CM, Goverdovskiy VN, Temnikov AI. Design of springs with “negative” stiffness to improve vehicle driver vibration isolation. *Journal of Sound and Vibration* 2007; **302**(4–5): 865–874. DOI: 10.1016/J.JSV.2006.12.024.

87. Iemura H, Pradono MH. Passive and semi-active seismic response control of a cable-stayed bridge. *Journal of Structural Control* 2002; **9**(3): 189–204. DOI: 10.1002/stc.12.

88. Sarlis AA, Pasala DTR, Constantinou MC, Reinhorn AM, Nagarajaiah S, Taylor DP. Negative Stiffness Device for Seismic Protection of Structures. *Journal of Structural Engineering* 2013; **139**(7): 1124–1133. DOI: 10.1061/(ASCE)ST.1943-541X.0000616.

89. Izzi M, Caracoglia L, Noè S. Investigating the use of Targeted-Energy-Transfer devices for stay-cable vibration mitigation. *Structural Control and Health Monitoring* 2016; **23**(2): 315–332. DOI: 10.1002/stc.1772.

90. Yan B, Chen W, Yu J, Jiang X. Mode shape-aided tension force estimation of cable with arbitrary boundary conditions. *Journal of Sound and Vibration* 2019; **440**: 315–331. DOI: 10.1016/j.jsv.2018.10.018.

91. Sun L, Shi C, Zhou H, Cheng W. A Full-scale Experiment on Vibration Mitigation of Stay Cable. *IABSE Symposium Report* 2004; **88**(6): 31–36. DOI: 10.2749/222137804796291520.

92. Zhou H, Sun L, Xing F. Free vibration of taut cable with a damper and a spring. *Structural Control and Health Monitoring* 2014; **21**(6): 996–1014. DOI: 10.1002/stc.1628.

93. Post-Tensioning Institute. Cable-Stayed Bridge Committee. *Recommendations for stay cable design, testing, and installation*. 6th ed. Farmington Hills MI: Post-Tensioning Institute; 2012.

94. Zuo D, Jones NP. *Stay-Cable Vibration Monitoring of The Fred Hartman Bridge (Houston, Texas) and The Veterans Memorial Bridge (Port Arthur, Texas)*. Center for Transportation Research, Bureau of Engineering Research, University of Texas at Austin; 2005.

95. Johnson EA, Spencer BF, Fujino Y. Semiactive damping of stay cables. *Proceedings of the 1999 17th International Modal Analysis Conference, IMAC*, SEM; 1999.

96. Humar JL. Dynamics of structures, CRC Press - Taylor & Francis Croup; 2012.

97. Davies PI, Higham NJ, Tisseur F. Analysis of the Cholesky Method with Iterative Refinement for Solving the Symmetric Definite Generalized Eigenproblem. *SIAM Journal on Matrix Analysis and Applications* 2001; **23**(2): 472–493. DOI: 10.1137/S0895479800373498.

98. Brusa L, Nigro L. A one-step method for direct integration of structural dynamic equations. *International Journal for Numerical Methods in Engineering* 1980; **15**(5): 685–699. DOI: 10.1002/nme.1620150506.

99. Meirovitch L, Baruh H. On the inclusion principle for the hierarchical finite element method. *International Journal for Numerical Methods in Engineering* 1983; **19**(2): 281–291. DOI: 10.1002/nme.1620190209.

100. Chan HC, Cai CW, Cheung YK. Convergence Studies of Dynamic Analysis by Using the Finite Element Method With Lumped Mass Matrix. *Journal of Sound and Vibration* 1993; **165**(2): 193–207. DOI: 10.1006/JSVI.1993.1253.

101. Hughes TJR, Liu WK. Implicit-Explicit Finite Elements in Transient Analysis: Stability Theory. *Journal of Applied Mechanics* 1978; **45**(2): 371. DOI: 10.1115/1.3424304.

102. Ohtori Y, Christenson RE, Spencer BF, Dyke SJ. Benchmark Control Problems for Seismically Excited Nonlinear Buildings. *Journal of Engineering Mechanics* 2004; **130**(4): 366–385. DOI: 10.1061/(ASCE)0733-9399(2004)130:4(366).

103. Iemura H, Pradono MH. Application of pseudo-negative stiffness control to the benchmark cable-stayed bridge. *Journal of Structural Control*, vol. 10, John Wiley & Sons, Ltd; 2003. DOI: 10.1002/stc.25.

104. Li H, Liu M, Ou J. Vibration mitigation of a stay cable with one shape memory alloy damper. *Structural Control and Health Monitoring* 2004; **11**(1): 21–36. DOI: 10.1002/stc.29.

105. Chen L, Sun L, Nagarajaiah S. Cable with discrete negative stiffness device and viscous damper: passive realization and general characteristics. *Smart Structures and Systems* 2015; **15**(3): 627–643. DOI: 10.12989/sss.2015.15.3.627.

106. Tabatabai H, Mehrabi AB, Morgan BJ, Lotfi HR. Non-destructive bridge evaluation technology: Bridge stay cable condition assessment. *Final Report Submitted to the FHWA, Construction Technology Laboratories, Inc, Skokie, IL* 1998.

107. Holmes JD. *Wind Loading of Structures*. CRC Press; 2018. DOI: 10.1201/b18029.

108. Hu L, Li L, Gu M. Error Assessment for Spectral Representation Method in Wind Velocity Field Simulation. *Journal of Engineering Mechanics* 2010; **136**(9): 1090–1104. DOI: 10.1061/(ASCE)EM.1943-7889.0000058.

109. Davenport AG. Rationale for determining design wind velocities. *Journal of the Strcutural Division* 1960; **86**(5): 39–68.

110. Kaimal JC, Finnigan JJ. Atmospheric boundary layer flows : their structure and measurement 1994: 289.

111. Davenport AG. The spectrum of horizontal gustiness near the ground in high winds. *Quarterly Journal of the Royal Meteorological Society* 1961; **87**(372): 194–211. DOI: 10.1002/qj.49708737208.

Vita Auctoris

Name:	Majd Javanbakht
Place of Birth:	Ahvaz, Iran
Year of Birth:	1986
Education:	Shiraz University, Shiraz, Iran, 2008 Civil Engineering, B.Sc.
	Iran University of Science and Technology, Tehran, Iran, 2014 Earthquake Engineering, M.Sc.
	University of Windsor, Windsor, Canada, 2020 Civil Engineering, Ph.D.